High-throughput screening of kinase siRNAs and small molecule compounds identify novel candidates for the development of Myotonic Dystrophy Type 1 therapies: A step towards therapeutic advancements in DM1

Nafisa Neault

Thesis submitted to the University of Ottawa
in partial Fulfillment of the requirements for the
Doctorate in Philosophy degree in Cellular and Molecular Medicine

Department of Cellular and Molecular Medicine
Faculty of Medicine
University of Ottawa

TABLE OF CONTENT

ACKNOWLEDGEMENT

First and foremost, I would like to express my utmost gratitude to my Ph.D. thesis supervisor, Dr. Alex MacKenzie, a true source of inspiration and motivation for me and many others. Thank you for your selfless mentorship and constant support over the last six years.

To the two people who started me on my research path, my high school biology/biotechnology teachers from Centennial CVI, Ms. Evelyn Brown and Mr. Dough Gajic – I am forever grateful to you both for creating so many extracurricular opportunities for me, from science fair projects to summer internships, for without your encouragement, I may not have discovered my drive and love of scientific research. From those early days, I would also like to thank Drs. Richard Mosser and Manish Raizada from the University of Guelph for taking chance on a high school student and allowing me to learn in your labs. From the University of Ottawa, I would like to thank my undergraduate research supervisors, Drs. Ken Dimock, Reza Nokhbeh, and Laura Trinkle-Mulcahy, for showing me the ins and outs of basic molecular research and helping me gain valuable hands-on experience. From the University of McGill, a special thanks to Dr. Louise Larose and her lab for affording me my summer student research positions. It was at the labs of Dr. Larose and Dr. Trinkle-Mulcahy that I was inspired to pursue graduate studies.

Next, I would like to acknowledge members of my thesis advisory committee (TAC), Drs. Robert Korneluk, Rashmi Kothary and Michael Schlossmacher, for their expert scientific advice and guidance throughout my M.Sc. years, fast-track exam, and Ph.D. projects. A special thanks to Dr. Robert Korneluk for going above and beyond his role as a TAC member and looking out for my best interest beyond the confines of the annual TAC meetings.

I would also like to thank my research family – it goes without saying that without the kind and supportive scientific community at the CHEO research institute, I could not have reached the finish line. Firstly, a special dedication to the late Sandy Boehmer, who surpassed her administrative responsibilities and was always ready with a helping hand – you are gone, but never forgotten. To our lab manager, Lynn Kyte; to our secretary, Joycelyn Mmrah; and to all the other staff at the CHEO RI, your work made this research feasible and the workload bearable. To my mentors in the MacKenzie lab - Drs Faraz Farooq, Alan Mears, Jason Vanstone, Sarah Shock, Izabella Pena and Kristin Kernohan, and Sean O'Rielly – thank you for your guidance with the day-to-day projects and for providing me with a productive learning environment. To all my peers in the MacKenzie lab, thank you for helping create an overall fun grad school experience; a special thanks to those who contributed to the DM1 project, at one time or another – Fahad Shamim, Kate Daniel, Mehrdad Azimi, Dr. Jeremiah Hadwen, Kamran Rezai, Sophie LeBlanc,

Stuart Macleod, Emiliyan Staykov, Mathieu Poirier, and Donelda Lahey. Thank you to the Care4Rare collaborators, especially the labs of Drs. Kym Boycott and Dave Dyment, for their constructive feedback and discussion forums. I would further like to thank Dr. Kym Boycott herself, along with Claire Goldsmith, for my clinical exposure to DM1, an experience which was very rewarding and key to my understanding of DM1 genetics and diagnostics. I would also like to express my gratitude to the lab of Dr. Bernard Jasmin, especially Dr. Aymeric Ravel-Chapuis and John Lunde, without whom our *in vivo* trials would not have been possible. Lastly from my research family, I owe a great deal to Dr. Stephen Baird, with whom I worked closely to complete all the high-through put screens; your confidence in my abilities and praise along the way helped instill in me the self-confidence I needed to become independent and successful.

A great thanks to the patients who donated samples to our research initiatives and allowed us the best chance for successful discovery. Thank you also to the funding agencies for their financial support, without which, progress would be halted.

To my friends and family, we did it! Pursuing a Ph.D. in science was not an easy path, but you stood by me with unwavering support. Thank you for putting aside any concerns and trusting me to follow my scientific passion, because in the end, it was worth it.

Last but not least, a special word of thanks to by dear husband, Serge Neault, although words alone cannot express how essential you have been to my success and sanity. No one has been more loving, understanding and unconditionally supportive as you. Not only that, I am also the luckiest to have found in you a partner with whom I can share this passion for science. Let's flip this James Bond script and, together, pursue science for a better world – you and I as Drs. Neault.

LIST OF TABLES

LIST OF FIGURES

LIST OF ABBREVIATIONS

ALS	amyotrophic lateral sclerosis
ANOVA	analysis of variance
ASO	antisense oligonucleotide
ATP	adenosine triphosphate
ATXN	ataxin
BBB	blood-brain barrier
BEAN	brain expressed associated with NEDD4
bFGF	basic fibroblast growth factor
β-Me	betamercaptoetanol
BSA	bovine serum albumin
cAMP	cyclic adenosine monophosphate
cDNA	complimentary DNA
CELF1	CUGBP Elav-Like Family Member
CLCN1	chloride channel
CNBP or ZNF9	CCHC-type zinc finger nucleic acid binding protein
CO_2	carbon dioxide
cTNT	cardiac troponin T
CUGBP	CUG binding protein
DfM	differentiation media or differentiated myoblasts
DM1	dystrophia myotonica type 1
DM2	dystrophia myotonica type 2
DMD	duchenne's muscular dystrophy
DMEM	Dulbecco's Modified Eagle Media
DMPK	dystrophia myotonica protein kinase
DMSO	dimethyl sulfoxide
DNA	deoxyribonucleic acid
dsRNA	double-stranded RNA
ECL	enhanced luminol-based chemiluminescent
ECM	extracellular matrix
EDL	extensor digitorum longus
EDS	excessive daytime sleepiness
EDTA	ethylenediaminetetraacetic acid
EGF	epidermal growth factor
EMG	electromyography
EtOH	ethanol
FBS	fetal bovine serum
FCS	fetal calf serum
FDA	food and drug administration
FECD	fuchs endothelial corneal dystrophy
FGFR	fibroblast growth factor receptor
FISH	fluorescent in situ hybridization
FMR1	fragile X mental retardation 1

FTD	frontotemporal dementia
FWD	forward
FXTAS	fragile X-associated tremor/ataxia syndrome
GAPDH	glyceraldehyde 3-phosphate dehydrogenase
GM	growth media
H_2O	water
HcM	human converted myoblasts
HD	huntington disease
HDAC	histone deacetylase complex
HDL2	huntington disease-like 2
HEK	human embryonic kidney
HF	human fibroblast
HIPK4	homeodomain interacting kinase 4
HPBCD	hydroxypropyl beta cyclodextrin
HPRT	hypoxanthine phosphoribosyltransferase
HRP	horse-radish peroxidase
HSALR	human skeletal actin long-repeat
HSP90	heat-shock protein 90
HTT	huntington
i.p.	intraperitoneal
IR or INSR	insulin receptor
KO	knock out
LF	low fluorescence
MBNL	muscleblind-like
mRNA	messenger RNA
NaAz	sodium azide
NaCl	sodium chloride
NaOH	sodium hydroxide
NOP56	nucleolar protein 56
OCT	optical cutting temperature
PACT	PKR activator
PAGE	polyacrylamide gel electrophoresis
PBS	phosphate buffered saline
PCR	polymerase chain reaction
PEG	polyethylene glycan
PKA2β	cAMP-dependent protein kinase type II beta regulatory chain
PKC	protein kinase C
PKR	protein kinase RNA-activated
PNK	polynucleotide kinase
PRISM-1	patient-reported impact of symptoms in myotonic dystrophy type 1
PRKRA	protein kinase, interferon inducible double stranded RNA dependent activator
PVDF	polyvinylidene difluoride
qPCR	quantitative, real-time PCR
RAN	repeat-associated non-AUG

RBP	RNA binding protein
REV	reverse
RIPA	Radioimmunoprecipitation assay buffer
RNA	ribonucleic acid
RYR1	ryanodine receptor 1
SAHA	suberoyl+anilide+hydroxamic acid
SCA	spinocerebellar ataxia
SCA	spinocerebellar ataxia
SD	standard deviation
SDS	sodium dodecyl sulfate
SEM	standard error of the mean
ser/thr	serine/threonine
SERCA1	sarcoplasmic/endoplasmic reticulum Ca^{2+}-ATPase
siRNA	small interfering RNA
SMA	spinal muscular atrophy
SSC	saline sodium citrate
SSPE	sodium chloride-sodium phosphate-EDTA
TA	tibialis anterior
TBE	tris/borate/EDTA
TBS	tris buffered saline
TK2	Thymidine kinase 2
TRED	trinucleotide repeat expansion disorder
tRNA	transfer RNA
TSA	trichostatin A
UTR	untranslated region
VRC	vanadyl ribonucleoside complex
WT	wild type

ABSTRACT

Myotonic dystrophy type 1 (DM1) is the most common form of adult muscular dystrophy (1:8000) and is caused by an abnormal expansion of CTG repeats in the 3' untranslated region of the dystrophia myotonica protein kinase (DMPK) gene. The expanded repeats of the DMPK mRNA forms hairpin structures which sequester RNA-binding proteins (RBP) in intranuclear foci, such as the splicing regulator muscleblind-like 1 (MBNL1), which results in aberrant splicing of several mRNAs and underlie, at least in part, DM1 pathogenesis. It has been previously shown that disaggregating these RNA foci repletes free and thus functional MBNL1, rescuing DM1 spliceopathy and alleviating associated signs and symptoms such as myotonia. Importantly, the direct upregulation of MBNL1 has comparable beneficial outcomes. The focus of this thesis was to develop novel and practical therapeutic avenues for DM1 by employing high-throughput screening technology to identify key pathways and small molecule candidates which reduce CUG foci in patient cells, and ultimately correct DM1 spliceopathy and associated signs *in vivo*. First, a high-throughput kinome screen using an siRNA library targeting 692 kinase subunits identified PACT, HIPK4, and PKA2β as candidates for reducing CUG foci in patient fibroblasts. Knockdown of each gene resulted in a partial reduction in CUG foci, but ultimately did not correct aberrant splicing of insulin receptor (IR) or sarcoplasmic/endoplasmic reticulum Ca2+-ATPase (SERCA1), two genes which are typically misspliced in DM1. A second set of screens focused on testing small molecules, several of which are FDA-approved for clinical use, in an effort to expedite drug discovery. One approach was to data-mine from a previously completed chemical screen, which used system-wide RNA sequencing to establish drug-gene interactions in mouse neuronal cultures treated with blood brain barrier-penetrant drugs, and specifically look for compounds

which downregulate DMPK mRNA or upregulate MBNL mRNA (MBNL1 and MBNL2). No compounds were found to downregulate DMPK mRNA. However, several compounds upregulated MBNL mRNAs; the activity of one of these, nilotinib, was validated in human DM1 fibroblasts and converted myoblasts, mediating a small correction in SERCA1 spliceopathy. Administration of nilotinib to unaffected mice did not result in *in vivo* MBNL gene upregulation in mouse skeletal muscle, as was seen *in vitro*. Further testing of nilotinib in DM1 *in vivo* models is required. A final set of chemical screens in patient myoblasts using an FDA-approved drug library and a chemogenomic drug library identified several HDAC inhibitors which reduced foci and rescued SERCA1 spliceopathy *in vitro* in DM1 differentiated myoblasts. Of these, vorinostat (SAHA) was further tested in a mouse model of DM1 (HSA^{LR}), proving safe and effective in correcting aberrant muscle pathology as well as splicing defects of RYR1, SERCA1, and CLCN1. Functional validation, such as myotonia, remains to be completed, but given the strong evidence for CUG foci reduction and splicing correction, vorinostat has emerged as a promising novel candidate for DM1 therapy.

CHAPTER 1: INTRODUCTION

1.1 EPIDEMIOLOGY AND ETIOLOGY OF MYOTONIC DYSTROPHY TYPE 1 (DM1)

1.1.1 An epidemiologic overview of DM1.

The rare, inherited Dystrophia Myotonica Type 1 or Myotonic Dystrophy Type 1 (DM1) was first reported by Hans Gustav Wilhelm Steinert, a German neurologist, in 1909 (Mishra et al. 2018); as such, it is also known as Steinert's disease. Over a century past since its initial discovery, DM1 currently affects about 1 in 8000 individuals world-wide, classifying it as the most common form of muscular dystrophy in adults. However, disease prevalence can reach as high as approximately 1 in 500 individuals in the Saguenay-Lac-Saint-Jean region of Quebec due to a founder effect where genetic migration is limited (Mathieu and Prévost 2012).

1.1.2 Clinical presentations of DM1: multisystemic signs and symptoms

Myotonic Dystrophy Type 1 is a type of muscular dystrophy, which are a group of genetic diseases generally characterized by degeneration and thus weakening of skeletal muscle. However, DM1 is a multisystemic and heterogeneous disorder characterised by a diverse array of signs and symptoms which affect a multitude of organs in addition to skeletal muscles. Nonetheless, skeletal muscle manifestations are the most commonly observed findings in DM1 patients, in particular, sustained muscular contractions or myotonia, a hallmark clinical feature of this disease. Other muscular phenotypes include degeneration, weakness and wasting.

Another common trait of this disease is the early development of cataracts (Reardon et al. 1993; Voermans et al. 2015); ptosis (drooping of upper eyelid) is another observable ocular involvement in DM1 (Ikeda et al. 2016; Nguyen and Campbell 2016). Patients can also present with fertility defects, particularly in males, presenting as hypogonadism and erectile dysfunction (Antonini et al. 2009; Peric et al. 2013). Metabolic conditions can also arise in cases of DM1 – insulin resistance leading to impaired glucose metabolism and diabetes are commonly seen (Matsumura et al. 2009; Savkur, Philips, and Cooper 2001); a small-scale study of 66 DM1 patients also revealed a high incidence of dyslipidemia characterized by hypertriglyceridemia (high blood triglycerides) and low HDL cholesterol (Vujnic et al. 2015). Gastro-intestinal clinical presentations may include diarrhea, constipation, abdominal pain, and fecal incontinence. (Nguyen and Campbell 2016).

In addition to significant morbidity, there is also DM1 associated mortality. A 10-year longitudinal study of a 367 patient-cohort identified respiratory insufficiency and cardiac failure as the leading causes of death in patients with DM1 (Mathieu et al. 1999). The latter includes myocardial infarction (heart attack), congestive heart failure, pulmonary embolism (blood clot in lung vasculature), cardiac arrythmia (irregular heartbeat) and cardiac conduction defects.

Peripheral neuropathy and cognitive impairment are also common findings in severe DM1, which affect visuospatial abilities, executive function, reasoning and naming (Caso et al. 2014; Hermans et al. 2011). MRI scans showed white matter hyperintensities, which are lesions

resulting from demyelination and axonal loss, in DM1 brain to correlate with severity of cognitive impairments. Such cognitive impairment can contribute to lower education among DM1 cohorts and extend to impaired social cognition. For example, DM1 patients have reduced ability to recognize facial emotions, particularly anger and disgust (Labayru et al. 2018).

In addition to physician-reported signs, DM1 management is also guided by patient-reported symptoms. PRISM-1 (patient-reported impact of symptoms in myotonic dystrophy type 1), a patient-centred clinical study, summarized feedback from 278 adult DM1 patients and ranked the symptoms based on frequency and significance (Heatwole et al. 2012). The most frequent and debilitating symptoms were related to fatigue and mobility – specific symptoms included myotonia, problems with the hand and arms (in addition to myotonia, hand weakness and difficulty opening jars or bottles), impaired sleep or excessive daytime sleepiness (EDS), and general fatigue associated with decreased energy and tired muscles. Fatigue and sleepiness were also reported in a later study assessing cognitive impairment in DM1 patients (Caso et al. 2014). In summary, different combinations of a wide range of DM1 signs and symptoms arise in patients with varying severity and can be extremely debilitating.

1.1.3 The genetic basis of DM1, a nucleotide repeat expansion disorder

Despite the heterogeneity in clinical presentations, there is a single genetic cause of DM1 – a CTG repeat expansion in the 3' untranslated region (UTR) of the dystrophia myotonica protein kinase (DMPK) gene on chromosome 19q (Brook et al. 1992; Harley et al. 1992; Mahadevan et al. 1992). As such, while DM1 is clinically classified as a multisystemic

neuromuscular disorder, it is classified genetically as a trinucleotide repeat expansion disorder (TRED). This mutation is transmitted in an autosomal dominant manner and affected patients present with expanded CTG repeats on at least one DMPK allele. Molecular verification of the expansion mutation is typically performed using Southern blot analysis of patient genomic DNA identifying expanded CTG tracts detected by radioactive probes against *DMPK*. The greater the number of CTG repeats, the more severe the signs and symptoms are, and the earlier the age of onset.

Individuals with only 5-37 CTG repeats in the DMPK 3' UTR are unaffected, those with 38-50 repeats are said to have a pre-mutation and are generally asymptomatic while patients with more than 50 CTG repeats begin to manifest symptoms. Symptomatic DM1 is further broken down into four categories, primarily determined by CTG repeat size: mild, adult (classical), childhood and congenital (de Die-Smulders C.E. et al. 1994). Patients with mild DM1 often have 50-100 CTG repeats and usually do not show signs and symptoms until later in life (>50 years old); mild DM1 is generally characterised by early development of cataracts and later/progressive development of myotonia and mild muscle weakness. In adult cases of DM1, also known as classical DM1, patients have 100 CTG repeats or more and age of onset is highly variable, ranging from 10 to 50 years of age; these patients initially present with myotonia, muscle weakness, and testicular atrophy in males which can lead to reduced fertility, and can also develop cataracts and cardiac abnormalities. Childhood DM1 is characterized by an early, post-natal age of onset (1-10years old) with additional signs and symptoms relating to delayed or impaired cognitive development, mental retardation, and more severe muscle weakness.

Congenital DM1 is the most severe category, arising in neonates. In fact, this level of disease severity can result in reduced fetal movements. In successful births, these neonatal patients can present with additional physical signs of infantile hypotonia, joint immobility, psychomotor retardation, and respiratory insufficiency which can result in death. CTG trinucleotide repeat expansions in childhood and congenital cases number in the thousands.

The expanded, unstable trinucleotide repeats can undergo inter-generational expansion which leads to earlier age of onset and gives rise to the more severe forms of DM1 in successive generations; this phenomena of earlier age of onset and increased severity of inherited disease down successive generations is known as genetic anticipation (de Die-Smulders C.E. et al. 1994; Harley et al. 1992; Tsilfidis et al. 1992). Anticipation is observed primarily through a maternal transmission of the expansion as demonstrated in a landmark 1992 study which followed an extended family across five generations; eight cases of parents with adult onset DM1 were reported to have children with childhood/congenital DM1, which is more severe in nature; all eight parental transmissions demonstrating anticipation were through the female lineage (de Die-Smulders C.E. et al. 1994).

While genetic anticipation arises mainly through maternal transmissions, the opposite scenario involving loss of DM1 genotype and phenotype can also arise and are mainly attributed to the paternal lineage. One mode of mutation loss is a result of infertility: paternal infertility due to testicular atrophy; infertility due to impaired cognitive development which contributes to a lack of social skills, inability to find a partner, and ultimately the lack of

procreation; and infertility due to early death. A second mode of intergenerational disease regression is contraction of the CTG repeats resulting in lower severity disease phenotypes, primarily observed through paternal transmission. While contractions are rare, one study looking at DNA from peripheral blood leukocytes of 1489 DM1 patients reported there to be intergenerational repeat contractions in 10% of paternal transmissions and in only 3% of maternal transmissions (Ashizawa et al. 1994); 7.4% of transmissions resulted in repeat contraction in the French-Canadian population, all in the cases of paternal transmission (Bianco et al. 2009). An earlier case-study similarly reported three cases of reduced repeat size in the progeny; one of these cases showed a complete loss of the DM1 genotype in which the progeny of a DM1 father had no repeat expansion despite inheriting the mutant DMPK allele (Hoy et al. 1993).

1.2 SUB-CELLULAR PATHOMECHANISMS OF DM1

1.2.1 The role of DMPK in disease manifestation: DMPK haploinsufficiency does not contribute significantly to the DM1 phenotype.

Following the discovery of DMPK-associated CTG expansion as the causative genotype in DM1 (Brook et al. 1992; Jansen et al. 1992), several groups set out to dissect the downstream effects of this mutation, many focusing on DMPK gene products. Fu *et al.* compared DMPK mRNA and protein levels in 20 patients with adult DM1 to that of 7 unaffected patients, reporting a reduced level of both DMPK mRNA and protein in DM1 patient samples and alluding

to DMPK haploinsufficiency (protein level reduced to half) as a cause of disease (Fu et al. 1993); reduced endogenous DMPK protein was also reported by other patient-centred studies looking at samples from both adult and congenital DM1, compared to that of non-DM1 samples (Koga et al. 1994; Salvatori et al. 2005). However, contradictory findings were reported by a study assessing DMPK mRNA in congenital DM1 patient tissues, summarizing that CTG expansions do not impair transcription of the mutant allele and, in fact, steady state levels of mutant mRNA are increased (Sabourin et al. 1993); no protein data was available. Analysis of DMPK mRNA localization in control versus DM1 patient fibroblasts found DMPK transcripts to accumulate in the nucleus of only patient cells (Davis et al. 1997). Taken together, it was concluded that mutant DMPK mRNA is transcribed normally but retained in the nucleus and, as such, is not able to be translated to protein, resulting in an observable reduction in DMPK protein in DM1 patients.

Following the initial discovery of DMPK-CTG repeat expansions, two different animal (mouse) models of DMPK knockout attempted to clarify the role of DMPK haploinsufficiency in DM1. One study reported that the homozygous loss of DMPK protein is not sufficient to recapitulate the vast majority of the full DM1 disease phenotype (Jansen et al. 1996). In these mice, only mild myopathic features relating to muscle degeneration – some central nucleation and muscle fibre hypotrophy – were observed, and only in adult mice at that. Neither the homozygous nor the heterozygous DMPK knockout mice presented with any observable survival issues, developmental abnormalities, other histological aberrations, or any other DM1-related signs and symptoms relating to myotonia, infertility, cataracts, etc., thus effectively

countering the model of DMPK haploinsufficiency as a major mechanism for disease phenotype. Another study also developed a mouse model with both heterozygous and homozygous knockout of the DMPK gene (Reddy et al. 1996). No defects in reproductive capacity was apparent. In newborn pups, these mice showed no outward signs of physical abnormalities, respiratory distress or muscle hypotonia, suggesting DMPK loss does not cause congenital DM1. In older mice, some progressive myopathy was observed, such as increased muscle fibre degeneration and muscle weakness; myotonia was absent in all assessed cases, as were other non-muscle DM1 features. This suggests that while reduced DMPK may contribute to some muscle-related features of DM1, it is not sufficient to elicit disease phenotype on a broader scale. A more recent study reassessed the impact of DMPK gene deletion in mice – one experiment assessed heterozygous knockout mice ($DMPK^{+/-}$) with 50% reduction in DMPK and a follow-up approach assessed the same heterozygous $DMPK^{+/-}$ mice further depleted of DMPK (up to 90% reduction) using antisense oligonucleotides (ASO). These studies found there to be no major impact on cardiac or skeletal muscle upon DMPK knockdown (Carrell et al. 2016). The minimal impact resulting from the loss of DMPK protein may lie either in the non-critical functionality of the DMPK protein or the presence of other kinases which recapitulate DMPK protein function.

As a serine/threonine (ser/thr) protein kinase, DMPK functions by phosphorylating proteins at serine or threonine residues to regulate their function (Timchenko et al. 1995). There are seven reported isoforms of the DMPK protein arising from distinct alternatively spliced DMPK mRNA, which are differentially expressed in the various tissues. In general, DMPK

is highly expressed in skeletal muscle, cardiac muscle and smooth muscle, and can also be found in the brain, bone, lung, liver, eyes, skin and testis (Jansen et al. 1992; Magana et al. 2012; Ophuis et al. 2009). These expression patterns are similar to those observed in mouse tissues – mouse DMPK is found in mouse skeletal, cardiac and smooth muscles, as well as in bone, testis, pituitary, brain, eye, skin, thymus and lung; no DMPK mRNA was found in mouse ovary, pancreas or kidney (Sarkar et al., 2004). It is likely that the ubiquitous expression profile of DMPK plays a role in the multisystemic nature of the disease. The seven isoforms are conserved at the N-terminus containing a Leucine-rich N-terminus, protein kinase, and coiled-coil domains, and vary at the C-terminus due to alternative splicing primarily within the last 8 exonic regions, mapping towards the 3' end of the mRNA (Magana et al. 2012). The DMPK mRNA consists of up to 15 exons in both human and mouse. The initial study by Groenen *et al* compiled cDNA libraries of the DMPK gene in both models, identifying six distinct endogenous isoforms (DMPK A – F) (Groenen et al. 2000). Much like the similarity in tissue expression profile of DMPK observed between the two species (Jansen et al. 1992; Ophuis et al. 2009; Sarkar, Han, and Reddy 2004), the respective isoforms also have similar sub-cellular localization and expression profiles. Inclusion of exons 13 and 14 gives rise to a more hydrophobic C-terminus in full-length DMPK isoforms A – D, anchoring them to membranes of the endoplasmic reticulum (isoforms A and B) and mitochondria (C – D); these isoforms are predominantly found in heart, diaphragm and skeletal muscle (Ophuis et al. 2009). DMPK isoforms E and F, however, lack exons 13 and 14, and are localized to the cytosol; these short-form proteins are found primarily in the bladder and stomach. Both short and long isoforms are found in the brain. While much is known about the structure and expression of this protein, there is very little

clarity with regards to the specific sub-cellular role of DMPK - the functional targets of the DMPK protein can be highly variable and dependent on tissue type, just as the isoform type, expression, and localization varies from tissue-to-tissue. As a serine/threonine kinase, DMPK has high sequence homology to other kinases of the same family, alluding to a redundancy in function amongst similar kinases.

1.2.2 The role of CTG repeats in disease manifestation: RNA gain of function is the primary disease mechanism for DM1

To date, the most widely supported mechanism of DM1 pathogenesis is a toxic RNA gain-of-function model. Initial studies tracking DMPK transcripts in patient fibroblasts by fluorescent *in situ* hybridization (FISH) with a short repeat $(CAG)_{30}$ probe identified aggregates of mutant DMPK mRNA in intranuclear foci (Davis et al. 1997). The CUG repeat region of the mRNA forms a secondary hairpin structure through C-G base pairing (Michalowski et al. 1999; Napierała and Krzyzosiak 1997), which results in a pathogenic sequestration of RNA binding proteins (RBPs) to the double-stranded RNA (dsRNA) region of the hairpin; chief among these RBPs is muscleblind-like 1 (MBNL1) (Mankodi et al. 2003; Miller et al. 2000).

Muscleblind (*mbl*) was first characterised in *Drosophila melanogaster* to regulate muscle development (Artero et al. 1998) and photoreceptor differentiation in the eyes of this organism (Begemann et al. 1997). In a human context, MBNL1 regulates alternative splicing of numerous gene transcripts to produce mature mRNA used for coding functional proteins. In unaffected, non-DM1 cells MBNL is localized primarily in the nucleoplasm as well as the cytoplasm, where it

regulates alternative splicing. MBNL1 typically binds to its target transcripts by docking to the CHHG or CHG nucleotide sequence, where H is A, U or C, and thus has a direct affinity for the CUG repeats in the DMPK foci (CUGCUG) (Kino et al. 2004). Due to its sequestration to CUG foci in DM1 cells, bioavailable MBNL1 is depleted from the nucleoplasm where it may normally function and is concentrated in the nuclear CUG-RNA foci (Miller et al. 2000). In fact, MBNL1 has been shown to be essential for maintaining foci integrity as knocking down this CUG binding protein using siRNA resulted in reduced number of observable RNA foci (Dansithong et al. 2005). Taken together, the experimental findings outlined above suggest a critical role for MBNL1 in DM1 molecular pathogenesis.

Furthermore, a study involving MBNL1 knockout mice lacking exon 3 in the MBNL1 gene ($MBNL1^{\Delta E3/\Delta E3}$) mimicked various signs and molecular traits characteristic of DM1 (Kanadia et al. 2003).The MBNL1 knockout mice experienced myotonia, observed both symptomatically as well as by electromyographic (EMG) recordings, which showed “myotonic discharge” in the form of a prolonged electrical signaling in skeletal muscle. Other evidence of DM1-like muscle pathology in these knockout animals included reduced staining for chloride channel protein in $MBNL1^{\Delta E3/\Delta E3}$ mice and abnormal muscle histology compared to that of wildtype mice ($MBNL1^{+/+}$). The knockout mice also developed cataracts like those seen in DM1. This evidence further supports that MBNL1 plays a key role in DM1 pathogenesis.

Sequestration of MBNL1 to nuclear foci and the resulting reduction in free MBNL1 has been implicated in aberrant splicing (spliceopathy) of various transcripts in DM1. Alternative

splicing defects in DM1 give rise to fetal forms of certain processed mRNA which are not appropriate for post-natal development. A number of gene transcripts that are mis-spliced in DM1 correlate with disease phenotypes. For example, exon 11 exclusion in the insulin receptor (IR) mRNA results in an abnormally higher level of IR-A transcripts encoding an insulin receptor with reduced insulin affinity compared to full length IR-B leading to insulin resistance in DM1 patients (Savkur et al. 2001). Similarly, exon 5 inclusion in human cardiac troponin T (cTNT) mRNA is thought to contribute to DM1 cardiomyopathy (Philips, Timchenko, and Cooper 1998) while exon 22 exclusion in sarcoplasmic/endoplasmic reticulum Ca^{2+} ATPase 1 (SERCA1) gives rise to higher SERCA1-B transcripts over SERCA1-A, leading to aberrant calcium conduction and muscle wasting (Hino et al. 2007). Intron 2 and exon 6b7a inclusions in chloride channel (CLCN1) mRNA leads to an early stop codon, arising in reduced expression of the transcript, and thus protein, leading to myotonia (Charlet-B et al. 2002).

A secondary splicing factor that is also mis-regulated in DM1 is the CUG binding protein (CUGBP1). It was initially named as so because of its suspected affinity to CUG trinucleotide sequences, particularly, UG-rich sequences (Roberts et al. 1997; Timchenko et al. 1995). However, it was later demonstrated that while the CUGBP1 protein is involved in DM1, it neither directly binds to the CUG dsRNA of the mutant DMPK hairpin structure nor co-localizes to the nuclear foci; rather, it follows the same localization patterns observed in control cells (Fardaei et al. 2001; Michalowski et al. 1999). It has been renamed as CUG binding protein elav-like family 1 (CELF1) (Kino et al. 2004). Expression of the mutant DMPK mRNA activates protein kinase C (PKC), resulting in the hyper-phosphorylation and stabilization of CELF in DM1

cells (Kuyumcu-Martinez, Wang, and Cooper 2007). CELF1 can bind intronic elements of various pre-mRNA transcripts and has also been linked to aberrant splicing in CLCN1 (Charlet-B et al. 2002), IR (Savkur et al. 2001), and cTNT (Philips et al. 1998). CELF1 overexpression in a mouse model resulted in a significant reduction in muscle weight and function as well as an abnormal muscle histology, similar to that observed in DM1, implying that CELF1 may also play a role in DM1 pathogenesis (Ward et al. 2010).

Interestingly, MBNL and CELF proteins have overlapping mRNA targets with antagonistic alternative splicing outcomes. An RNAseq comparison of CELF1 and MBNL1-bound mRNA identified 206 unique exons which are antagonistically regulated by both proteins (Wang et al. 2015). CELF1 is typically involved in pre-natal alternative splicing and is significantly reduced during post-natal development (Kalsotra et al. 2008). Conversely, post-natal expression of MBNL1 is increased and, as such, MBNL1 becomes the predominant alternative splicing regulator during development. In DM1, there is a reduced level of free MBNL1 as most of it is bound to the CUG repeat region and an increase in CELF1 levels, both of which are reverse of that required for normal cellular functioning. Therefore, it may be speculated that both proteins contribute to DM1 pathogenesis.

1.2.3 Secondary molecular mechanisms in DM1 play a minor role is disease manifestation

Epigenetic modification of neighbouring genes. Following the discovery of CTG repeat expansion in the 3'UTR of the DMPK gene, it was found that CTG expansions disrupts the promoter region of *SIX5* and suppresses SIX5 gene expression, also known as DM locus-

associated homeodomain protein (DMAHP), which is the immediate 3' neighbour of DMPK (Boucher et al. 1995; Klesert et al. 1997). SIX5 downregulation, however, was shown to be variable and tissue-specific (Korade-Mirnics et al. 1999). It has since been established that partial or complete loss of SIX5 contributes to the development of cataracts, but does not account for much else in DM1 disease progression (Klesert et al. 2000; Matynia et al. 2010; Sarkar et al. 2000; Winchester et al. 1999). It is important to note MBNL1 knockout mice also developed cataracts, implying an additional role for MBNL1, perhaps a mis-spliced gene, as well as SIX5 in the development of this feature (Kanadia et al. 2003).

RAN translation. While the CTG repeats in DM1 are located in the 3' UTR, which is typically not translated during AUG-driven protein synthesis, repeat expansions can trigger a process called repeat-associated non-AUG (RAN) translation (Cleary, Pattamatta, and Ranum 2018; Cleary and Ranum 2013). This in turn can produce poly-peptide chains from three different reading frames on both the sense (CTG) and antisense (CAG) mRNA strands – poly-leucine from CUG, poly-cysteine from UGC, poly-alanine from GCU, poly-glutamine from CAG, and poly-serine from AGC. In patient cells, only poly-glutamines have been detected in heart and skeletal muscle. The role of these RAN proteins in DM1 pathogenesis has not been further clarified.

Antiviral-like immune response. Expanded CUGs in the DMPK mRNA form hairpins through G-C base-pairing, which mimics double-stranded RNA structures characteristic of viral infections. As such, the antiviral, dsRNA-dependent protein kinase, PKR (protein kinase RNA-

activated) is found to be activated in DM1 (Huichalaf et al. 2010; Tian et al. 2000). Activation of this protein typically results in translational shutdown, activation of the innate immune system and apoptosis. More recently, transcriptomic analysis of the global mRNA profile of lens cells from DM1 cataracts identified several genes which are dysregulated in DM1, a majority of them being interferon-regulated genes involved in innate immune response (Rhodes et al. 2012). This suggests a further role for immune involvement in the development of cataracts in DM1.

1.3 *IN VIVO* DISEASE MODELS OF DM1

1.3.1 HSA^{LR} mice

The HSA^{LR} mouse model was genetically engineered to overexpress 250 CTG repeats (long repeat, LR) in the 3' UTR of the human skeletal actin (HSA) (Mankodi et al. 2000). This mouse model recapitulates only skeletal muscle-specific phenotypes, from myonuclear accumulation of CUG-foci, MBNL1 sequestration and DM1-related spliceopathy to functional manifestation of myotonia and muscle weakness. Additionally, it shows evidence of myopathic histopathology, as demonstrated by central nucleation, a marker of muscle regeneration, and increased variability in fibre size.

1.3.2 DM300 and DMSXL mice

A second set of mouse models of DM1 preserved the genetic context of the disease by overexpressing a 45kb human genomic region which included the *DMPK* gene carrying 55 CTG

repeats (DM55) or 300 CTG repeats (DM300), obtained from a father with mild DM1 and his daughter with classical DM1 (Gourdon et al. 1997; Seznec et al. 2000). The DM300 mice were reported to have both muscular and neuronal involvements (Seznec et al. 2001). Skeletal muscle defects specifically include fibre size variability and increased central nucleation, as well as myotonia. Brain abnormalities include accumulation of micro-tubule binding tau proteins, similar to that observed in human DM1 patients. In addition, these mice also exhibit molecular pathomechanisms such as the accumulation of nuclear CUG foci (Seznec et al. 2001).

Through intergenerational repeat instability, the DM300 repeat mice underwent repeat expansion giving rise to progeny containing greater than 1000 CTG repeats (DMSXL mice), reminiscent of the genetic anticipation observed in human patients (Huguet et al. 2012; Seznec et al. 2000). RNA analysis of the DMSXL mice showed the transgene to be systematically overexpressed at varying levels in heart, skeletal muscles, diaphragm, brain, and kidney (Huguet et al. 2012). mRNA encoded by the large-repeat transgene forms CUG nuclear foci and sequester muscleblind proteins, especially in skeletal muscle and the brain. While these mice display some alternative splicing defects, the spliceopathy outcome is quite mild. On a functional level, no myotonia has been reported in the DMSXL mice, but these mice do exhibit other compromised muscular functions such as reduced muscle force. Neuronal studies of the DMSXL mice reported behavioral abnormalities which include, but are not limited to, increased anxiety as measured by novelty-induced inhibition, impaired spatial memory as measured by reduced entry into the target quadrant of the Morris water maze, and anhedonic-like behaviour

(inability to experience pleasure) as measured by lowered interest in accessing a saccharine solution.

1.4 THERAPEUTIC STRATEGIES FOR DM1

1.4.1 Targeted symptom management does not treat the disease as a whole

Myotonia – In DM1, myotonia, the hallmark trait of sustained muscle contraction, is associated with depleted chloride channel protein due to CLCN1 missplicing (Charlet-B et al. 2002). When at rest, the resting membrane potential of the muscle fibres of -70 to -90V is normally maintained primarily by chloride (Cl^-) anions and also balanced by potassium (K^+) and sodium (Na^+) cations (Hopkins 2006). Preceding muscle contraction, electrical action potential signal increases the membrane potential to a threshold of -55mV, opening voltage-gated sodium channels in the cell membrane (sarcolemma). The resulting flow of Na^+ cations into the cell triggers a cascade resulting in the release of Ca^{2+} ions which drives the contractile machinery. At the end of a contraction, the critical restoration of negative membrane potential occurs by intracellular flow of Cl^- anions through the chloride channel. With depleted chloride channels in the sarcolemma, as in the case of CLCN1 spliceopathy in DM1, muscle contraction is prolonged, and relaxation is delayed. One strategy to alleviate this myotonic outcome was to block the influx of Na^+ ions by using a sodium channel blocker, Mexiletine. Mexiletine directly binds to the sarcolemma-bound sodium channels, arresting them in the inactive state and thus, blocking the entry of Na^+ ions (Courtney 1981; Jarvis and Coukell 1998; Nakagawa, Munakata,

and Sunami 2019). A clinical study looking at placebo versus mexiletine treatment of 20 DM1 patients proved sodium channel blocking to be effective in the relief of myotonia, as measured by the grip relaxation time (Logigian et al. 2010). However, this class of drugs also reduces muscle power which can exacerbate DM1-related muscle weakness.

Muscle weakness – Myotonia often gives way to muscle weakness in cases of DM1 with worsening phenotypes. One natural method of intervention has been to prescribe exercise for delaying progressive muscle weakness and even improving the condition. A controlled clinical study comparing DM1 patients subscribing to daily exercise to a cohort of sedentary counterparts reported marked improvements in handgrip strength and knee extension torque (Brady, MacNeil, and Tarnopolsky 2014). Similar outcome was reported more recently *in vivo* in DM1 mice, attributing the increased muscle strength and endurance, as well as amelioration of myotonia, to exercise-induced correction in myopathies and correction in related splicing defects such as CLCN1 (Manta et al. 2019). Interestingly, chronic exercise in this mouse study also led to improvements in RNA toxicity related to CUG foci and MBNL1 sequestration, making it a promising avenue as a generalizable therapy to treat DM1 as a whole; however, clinical assessment of other non-myogenic features remains to be evaluated.

Cataracts and Ptosis (ocular involvement) – Cataracts, the opacification of the lens of the eye resulting in reduced vision, is another common feature of adult onset DM1 (Liu et al. 2017) and is treated by surgical replacement of the occluded lens with an artificial intraocular lens (Gagnon et al. 2007). Eyelid ptosis resulting from weak ocular muscles is another ocular

sign in DM1 patients that, when sufficiently severe, can be corrected by blepharoplasty (Burnstine and Putterman 2002), silicone sling placement, or levator (muscle in the eyelid) resection and advancement (Wong et al. 2002).

Bacterial overgrowth – DM1 patients also present with various gastrointestinal signs and symptoms, those which are attributed to bacterial overgrowth. Small intestinal bacterial overgrowth in DM1 patients, presenting with diarrhea as a primary symptom, has been treated by an oral dose of ciprofloxacin; patients also had a mild response to the antibiotic tetracycline (Tarnopolsky et al. 2010).

Diabetes – As a result of aberrant IR splicing, DM1 patients are susceptible to developing insulin resistance and diabetes. Metformin is used to manage cases of Type 2 diabetes as is done for non-DM1 related diabetes (Takeshima et al. 2018)

Excessive daytime sleepiness – EDS is a commonly reported symptom by DM1 patients (Caso et al. 2014; Heatwole et al. 2012), which, in severe debilitating cases, are treated by modafinil, a psychostimulant drug used typically for anti-narcoleptic intervention (Hilton-Jones et al. 2012; Laberge, Gagnon, and Dauvilliers 2013).

As summarized above, most approved DM1 therapies to date are directed towards management of specific signs and/or symptoms such as myotonia, cataracts, gastrointestinal symptoms, diabetes and EDS. Unfortunately, sodium channel blockers, surgery, antibiotics,

anti-diabetes drugs, and anti-narcoleptic drugs do not confer any generalizable impact to the plethora of other issues confronting an individual with DM1. Moreover, the simultaneous use of some or all of these approaches may not always be compatible in terms of deleterious drug interaction or exacerbation of other phenotypes as in the case of mexiletine worsening muscle weakness. The need for an overarching therapeutic approach addressing the root cause of DM1, and thus with the potential to ameliorate the many findings which afflict patients, is required.

1.4.2 Regulation of splicing factors MBNL1 and CELF1

In the realm of gene therapy, exogenous overexpression of MBNL1 has been hugely beneficial in treating DM1 mice, reversing spliceopathies and alleviating myotonia, along with various other DM1 molecular defects (Chamberlain and Ranum 2012; Kanadia et al. 2006). Additionally, this approach is well-tolerated and efficacious in various target tissues, providing a multifaceted solution to a multisystemic disorder. On the other hand, knockout of the aberrantly activated CELF1 protein does not elicit the same benefits as MBNL1 overexpression; while CELF1 knockout rescues some myopathies, DM1 spliceopathy, myotonia and muscle weakness remain unaffected (Kim et al. 2014). The biggest limitation of this gene therapy approach is that it has only been proven effective in mouse models; to date, no human trials have been reported.

1.4.3 Oligonucleotides target RBP sequestration and CTG expansions at its root

Initial application of oligonucleotides used CAG morpholinos to competitively disrupt the interaction between MBNL1 and the CUG repeat region of the DMPK mRNA, which has shown pre-clinical promise in significantly reversing fetal splicing patterns to a post-natal splicing pattern (Wheeler et al. 2009). Currently, the most promising nucleotide therapy is the use of gapmer antisense oligonucleotides (gapmer ASOs) targeting nuclear (CUG)n RNA for RNase H-mediated degradation (Wheeler et al. 2012). ASO-mediated degradation of expanded CUG RNA leads to foci disassembly, spliceopathy correction, and reduced myotonia in DM1 mice containing human skeletal actin with long CUG repeats and has advanced to clinical trials. However, clinical efficacy was limited, and further drug development is required.

1.5 Rationale and Research Objectives

Given the substantial literature supporting the central role of foci in DM1 pathogenesis and the fact that the dissolution of foci, for example by ASO treatment, has proven to reverse DM1 symptoms in mouse models (Wheeler et al. 2012), we aim to target intranuclear CUG RNA foci integrity for therapeutic consideration. The main objectives were to establish a good cellular model of DM1 and execute a series of high-throughput screens for rapid and unbiased/hypothesis-free discovery of novel therapeutic interventions in DM1. Results are hereafter summarized from screens using a:

1. Kinome siRNA library to interrogate the highly druggable kinase population and assess candidates which reduce intranuclear CUG foci.

2. Blood-brain barrier penetrant drug library to analyse transcriptomic drug-gene interactions and identify small molecule regulators of DMPK and associated MBNL proteins.
3. FDA-approved drug library to identify compounds which reduce intranuclear CUG foci and reposition/repurpose clinically approved compounds for DM1 therapy.
4. Chemogenomic library to identify compounds which reduce intranuclear CUG foci; these compounds are said to be specific to key cellular pathways and can aid in discovery of novel pathways involved in DM1 pathogenesis as well as compounds that can be used in drug development.

CHAPTER 2: GENERAL MATERIALS AND METHODS

2.1 CELL CULTURE

All patient and control cells, regardless of tissue origin, were maintained as an adherent monolayer, grown on tissue culture plates (Corning) in humidified incubators at 37˚C and 5% CO_2. Specific conditions are listed in the respective chapters.

Adherent cells were passaged by trypsinization for which old media was aspirated, and cells were washed with 1X PBS (Fisher Scientific) to remove residual serum from the FCS; the PBS (Fisher Scientific) was then aspirated, cells were incubated in 1X (0.25%) trypsin (Gibco; reconstituted in 15mM NaCl (Fisher Scientific), 0.5mM EDTA (Sigma), and 1X PBS (Fisher Scientific)) for 3-7min at 37°C to lift them from the plate, and then trypsin was inhibited using complete growth media containing fetal calf serum (FCS). For general passaging and maintenance, a fraction of the cell suspension was plated to new tissue culture plates and incubated as described above.

Additional cell stocks for long term storage were trypsinized, washed, centrifuged at 300xg for 5min, and the cell pellet was resuspended and frozen in freezing media by slow-cooling to -80°C in a Mr. Frosty Freezing Container (Thermo Fisher Scientific); cells were thereafter stored in liquid nitrogen vapour (CryoExtra 20, Thermo Scientific). To recover the cells, the vials were rapidly thawed in a 37°C water-bath, the cell suspension was immediately diluted in complete growth media, and centrifuged at 300xg for 5min; the cell pellet was

resuspended in fresh complete growth media, plated in tissue culture plates, and incubated as previously described.

2.2 HIGH-THROUGHPUT SCREENS ANALYZING $(CUG)_{EXP}$ FOCI IN DM1 PATIENT CELLS

2.2.1 Cell growth, treatment, and staining

Cells were grown and treated in 384-well, clear-bottom plates at 37°C and 5% CO_2. For each screen, one well corresponded to one treatment condition with technical replicates repeated across triplicate plates (n=3). Post-treatment, the cells were fixed in 4% formaldehyde at room temperature for 10 – 20min, washed to remove the fixative, permeabilized in 70% ethanol (EtOH) at 4°C and incubated 3 x 5-10min with 1X Phosphate Buffered Saline (PBS, Fisher Scientific) at room temperature to rehydrate the cells. The cells were then hybridized with 0.3ng/µL of Alexa555-$(CAG)_{10}$ probe (custom oligos from Invitrogen) diluted in hybridization buffer at 37°C overnight for the purpose of fluorescence *in situ* hybridization (FISH) analysis. The wells were then washed to remove residual hybridization buffer and probe. The nuclei were stained with 5ug/mL of Hoechst 33342 DNA stain (Sigma) diluted in 1X PBS (Fisher Scientific) at room temperature for 10-20min followed by 3x5min washes in 1X PBS (Fisher Scientific) at room temperature. The fixed, probed and stained samples were stored in 50-75µL of 1X PBS (Fisher Scientific) at 4°C before and after imaging. Additional methodologic details are outlined in the respective screening chapter.

The Alexa555-$(CAG)_{10}$ probe (custom oligos from Invitrogen) was resuspended from a lyophilized pellet in nuclease-free Tris-EDTA (TE) buffer, pH 8.0 (Ambion). The resuspended probe was further aliquoted into light-protective, dark tubes and stored long-term at -80°C. Hoechst 33342 (Sigma) was aliquoted into light-protective dark tubes and stored at 4°C.

2.2.2 Image acquisition and analysis

The plates were scanned using the Opera high-content screening system (Perkin Elmer) and 16-20 fields were captured per well to acquire a representative sample of images – Nuclei (Hoechst: excitation at 346nm, emission at 460nm; Sigma) and CUG foci (Alexa555-$(CAG)_{10}$: excitation at 555nm, emission at 565nm; custom oligos from Invitrogen). Columbus software (Perkin Elmer) was used to analyze foci content. Treatment data points were normalized to negative control samples within each assay plate; the normalized technical replicates from triplicate plates were then averaged.

2.3 PROTEIN EXTRACTION AND WESTERN BLOT

2.3.1 Protein extraction and quantification

After treatment, media was aspirated, the cells were washed with 1X PBS (Fisher Scientific) to remove residual serum, the PBS was aspirated, and cells were harvested by either trypsinization or by scraping. To harvest by trypsinization, cells were lifted from the plate by incubating at 37°C with 1X (0.25%) trypsin (Gibco; reconstituted in 15mM NaCl (Fisher

Scientific), 0.5mM EDTA (Sigma), and 1X PBS (Fisher Scientific)) for 3-7min, the trypsin was then inhibited using media containing 10-30% FBS, and the cell suspension was transferred to tubes and centrifuged at 300xg for 5-10min. The supernatant was then removed, the cell pellet washed gently in 1X PBS (Fisher Scientific) to remove residual serum, centrifuged further at 300xg for5-10min, and the final wash supernatant then removed, leaving the cell pellet. The cell pellet was then resuspended in lysis buffer and incubated for 20-30 min at 4°C to extract the protein. Cells were then lysed directly on-plate following the PBS wash for 20-30 min at 4°C using lysis buffer; the lysed samples were then collected by scraping and transferred to tubes. Unless otherwise specified, the cells were lysed in RIPA buffer (Radioimmunoprecipitation assay buffer) containing a cocktail of protease and phosphatase inhibitors, diluted as per manufacturer's instructions (Halt protease and phosphatase inhibitor cocktail, Thermo Scientific). The lysed cell suspensions were further subjected to sonication (8 x 15sec on, 60sec off) in a Bioruptor water bath sonicator (Diagenode), and centrifuged at 13,000xg for 30min at 4°C; the supernatant containing the protein was recovered and retained. Protein concentrations were determined by Bradford protein assay using a Bio-Rad protein assay kit (Bio-Rad) or DC protein assay kit (Bio-Rad), and BSA (Sigma) standards ranging from 0.125–2μg/μL.

2.3.2 Western Blot

Loading samples were prepared in Laemmli buffer (Bio-Rad) containing 1% β-mercaptoethanol (β-Me, Sigma) and heated for 5min at 95°C. The samples were separated by SDS-PAGE and transferred to a porous membrane. The membranes were blocked at room

temperature for 30-60min in 5% milk in 1X PBS or tris-buffered saline (TBS) containing 0.1% Tween-20, under agitation on a table-top rocker at low speed. Primary antibodies were diluted in 1% milk in 1X PBS or TBS containing 10% sodium azide (NaAz); membranes were incubated overnight at 4°C, on a table-top rocker at low speed. HRP-linked secondary antibodies were diluted in 5% milk and used for 1hr at room temperature. HRP-tagged antibody complexes were activated by incubation with enhanced luminol-based chemiluminescent (ECL) substrate. The signal was visualized by autoradiography using X-Ray film (Kodak) or using a camera-based system (ChemiDoc Imaging System, Bio-rad). Quantification was performed by scanning the autoradiographs and densitometric signal intensities determined using Image J software. Alternatively, if the images were acquired by the ChemiDoc system, they were also subjected to densitometric analysis, but using the ImageLab software (Bio-rad).

2.4 RNA EXTRACTION AND POLYMERASE CHAIN REACTION (PCR)

2.4.1 RNA Extraction and cDNA synthesis

Cell culture. After treatment, media was aspirated, the cells were washed with 1X PBS (Fisher Scientific) to remove residual serum and harvested as a cell pellet or directly on plate. To harvest as a cell pellet by trypsinization, cells were lifted from the plate by incubating at 37°C with 1X (0.25%) trypsin (Gibco; reconstituted in 15mM NaCl (Fisher Scientific), 0.5mM EDTA (Sigma), and 1X PBS (Fisher Scientific)) for 3-7min, the trypsin was then inhibited using media containing 10-30% FBS, and the cell suspension were transferred to tubes and centrifuged at

300xg for 5-10min. The supernatant was then removed, the cell pellet was washed gently in 1X PBS (Fisher Scientific) to remove residual serum, centrifuged further at 300xg for5-10min, and the final wash supernatant was removed, leaving the cell pellet. The cell pellet was then resuspended in lysis buffer and incubated for 5-10 min at room temperature to extract the RNA. To harvest on-plate, lysis buffer was added directly to the cells on-plate following the PBS wash and incubated at room temperature for 5-10min. RNA extractions were done using the RNeasy micro kit with on-column DNAse treatment, as per the manufacturer's protocol (Qiagen) with the following modifications: at each wash step with RW1 buffer, RPE buffer and 80% EtOH, column-tubes were inverted 5-10 times to resuspend all contaminants; and for the last step of RNA elution, the columns were incubated with 20-22µL of RNase-free H_2O for at least 5min at room temperature. All RNA was quantified using a nanodrop1000 spectrophotometer (Thermo Scientific).

Mouse Tissue. Upon dissection, the tissues were immediately flash-frozen in liquid nitrogen. The frozen tissues were either homogenized or crushed. For the homogenization, 1mL of Qiazol (Qiagen) was added to each sample of frozen tissue and homogenized using a PRO 200 tissue homogenizer (Diamed) at room temperature. Alternatively, the frozen tissues were crushed into a fine powder using a tissue pulveriser on dry ice, about 50-100ug of the crushed tissue per sample, to which 1mL of TRIzol (Thermo Fisher Scientific) was added, and the lysing tissue samples were further frozen at -80°C to allow for optimal lysis. The remaining extraction was done on-column using the RNeasy mini kit (Qiagen) or Purelink RNA mini kit/Trizol Plus RNA Purification Kit (Thermo Fisher Scientific), with on-column DNAse treatment,

as per the manufacturer's instruction. All RNA was quantified using a nanodrop1000 spectrophotometer (Thermo Scientific).

All cDNA was synthesized from RNA using reverse transcription (RT) at a 1:1 ratio using the iScript Advanced cDNA synthesis kit (Bio-Rad), as per manufacturer's protocol; each 20uL RT reaction was thereafter diluted at least 10-fold in nuclease-free H_2O before use in PCR reactions.

2.4.2 Radioactive PCR for alternative splicing

The forward (FWD) primers were radioactively labelled with γ-^{32}P-adenoside triphosphate (γ-^{32}P-ATP; BLU002A250UC, Perkin Elmer) at the 5' end using T4 polynucleotide kinase (T4 PNK; Fermentas) for 30min at 37°C (Ladd, Charlet-B., and Cooper 2001); each 10uL reaction contained 22.5ηM FWD primer (IDT); 22.5ηM γ-^{32}P-ATP (BLU002A250UC, Perkin Elmer); 1X Buffer A and 0.5U/uL T4 PNK (Fermentas). The radio-labelled FWD primers were used for PCR amplification of splice products in a reaction comprised of 1X GoTaq Green Mastermix (Promega), 4.5ηM γ-^{32}P-FWD primer (10uL of the 22.5ηM reaction), 0.62µM reverse (REV) primer, and up to 50ηg of cDNA. The amplification protocol for IR was 95.0°C for 2min, 25 x (95.0°C for 30sec, 55.0°C for 30sec, 72.0°C for 30sec), 72.0°C for 2min. The IR primer sequences were (5' → 3') FWD CCAAAGACAGACTCTCAGAT and REV AACATCGCCAAGGGACCTGC; these primers generate 167bp (IR-B, +exon 11) or 131bp (IR-A, –exon 11) product fragments (Savkur et al. 2001). Following amplification, the samples were loaded on to a 5% non-denaturing polyacrylamide gel in 1X TBE for DNA gel electrophoresis and

resolved at 200V. The gel was then transferred to a Whatman paper (details, company) and dried for 2hrs at 85°C (Slab Dryer Model 483, Bio-Rad; GelMaster gel dryer vacuum system Model 1426, Welch). The radioactive signal from the dried gel was visualized by autoradiography using X-Ray film (Kodak). Quantification was performed by scanning the autoradiographs and densitometric signal intensities determined using Image J software.

2.4.3 Non-radioactive PCR for alternative splicing

PCR reactions were done using 1X GoTaq Green Mastermix (Promega), 0.2µM FWD primer, 0.2µM REV primer, and up to 50ηg of cDNA. The amplification protocol for was 95.0°C for 2min, 25 x (95.0°C for 30sec, 55.0°C for 30sec, 72.0°C for 30sec), 72.0°C for 2min. The primer sequences are summarized below (Ravel-Chapuis et al. 2018). Following amplification, the samples were loaded on to a 5% non-denaturing polyacrylamide gel in 1X TBE for DNA gel electrophoresis and resolved at 200V. The gel was then stained with 1/10,000 GelRed nucleic acid gel stain (VWR) diluted in 1X TBE. The gels were imaged using the ChemiDoc imaging system (Bio-Rad) and quantified by densitometric analysis using ImageLab (Bio-Rad).

The primer sequences for mouse PCR were (5' → 3'):

SERCA1	FWD ATCTTCAAGCTCCGGGCCCT;	REV CAGCTTTGGCTGAAGATGCA
RYR1	FWD GACAATAAGAGCAAAATGGC;	REV CTTGGTGCGTTCCTGATCTG
CLCN1	FWD GGAATACCTCACACTCAAGGCC;	REV CACGGAACACAAAGGCACTGAATGT

2.4.4 Quantitative, Real-time PCR (qPCR) for steady-state mRNA levels and alternative splicing

PCR reactions were set up as duplicates for each cDNA sample in hard-shell 96-well PCR plates (Bio-Rad); each plate was sealed with Microseal 'B' PCR Plate Sealing Film (Bio-Rad). For splicing assays, each 20µL PCR reaction consisted of 1X iQ SYBR Green qPCR Supermix (Bio-Rad), 0.5µM FWD primer, 0.5µM REV primer, and up to 50ηg of cDNA. For quantification of total transcribed mRNA for each gene, each 20µL PCR reaction consisted of 1X iQ SYBR Green qPCR Supermix (Bio-Rad), 0.25µM FWD primer, 0.25µM REV primer, and up to 50ηg of cDNA. The CFX96 Touch Real-Time PCR Detection System (Bio-Rad) was used for qPCR reactions as well as SYBR green signal measurement; the general amplification protocol was 95.0°C for 3min, 40 x (95.0°C for 10sec, 60.0°C for 30sec, 72.0°C for 30sec), 95.0°C for 10sec. Following the amplification, a melt curve assay was also performed in order to assess purity and homogeneity of the amplified products: 65.0°C to 95.0°C, increment 0.5°C for 5sec with readout of SYBR green signal. The raw data was further processed using the CFX Manager Software (Bio-Rad) and converted to relative expression levels using the ΔΔCq formula (Bustin et al. 2009).

All primers were optimized for use at 60°C annealing temperature and the SybrGreen signal was acquired after extension at 72°C.

The primer sequences for human qPCR were (5' → 3'):

DMPK	FWD GGCTCACTGCCATGGTGA;	REV GCTGTTTCATCCTGTGGGGA
PACT	FWD GCCATGCACATCAGAGAAAG;	REV AGGGCCTGTTAGTGCTGTCC

MBNL1	FWD TGATTGTCGGTTTGCTCATC;	REV TTGATCTTGGCTTGCAAATG
GAPDH	FWD TGCACCACCAACTGCTTAGC;	REV GGCATGGACTGTGGTCATGAG
HPRT	FWD TGACACTGGCAAAACAATGCA;	REV GGTCCTTTTCACCAGCAAGCT
SERCA1-A	FWD CCCTCCTCCATCTCTGAGC;	REV AGCTCTGCCTGAAGATGTGTC
SERCA1-AB	FWD CTCCATCTGCCTCTCCATGT;	REV CTTGAGGACCATGAGCCACT
IR-B	FWD AAAACCTCTTCAGGCACTGG;	REV CGACTCCTTGTTCACCACCT
IR-AB	FWD GGCAACATCACCCACTACCT;	REV ACTCGAATGGTGGAGACCAG.

The primer sequences for mouse qPCR were (5’ → 3’):

MBNL1	FWD GACCCGGCCAGTTCCCTTT;	REV ACGGGAAAGGCACTTCTTA
MBNL2	FWD CGGCTCGCAGAGTACAATAAAC;	REV TTTGAGCAGGATGGCGCTTT
GAPDH	FWD CGTCCCGTAGACAAAATGGT;	REV CTCCTGGAAGATGGTGATGG
HPRT	FWD GCAAACTTTGCTTTCCCTGGTT;	REV CAAGGGCATATCCAACAACA

CHAPTER 3: INTEROGATING THE KINOME BY siRNA SCREENING TO IDENTIFY NOVEL GENE TARGETS FOR DM1 THERAPY

3.1 BACKGROUND AND RATIONALE FOR INTEROGATING THE HUMAN KINOME

The human genome encodes over 500 protein and lipid kinases; collectively, this accounts for about 2% of the approximately 19,000 genes which comprise the human genome, a relatively large fraction. Kinases are proteins which regulate cellular pathways through phosphorylation of target proteins and lipids, thereby affecting their function (Heath, Stahl, and Barbieri 2003; Manning et al. 2002). Altogether, the catalytic and regulatory subunits of each kinase complex totals to approximately 692 proteins (Qiagen library). Kinases play roles in diverse pathways such as cytoskeletal organization, metabolic signalling, cell death, cell cycle regulation, and more. Over 900 mutations in the human kinome have been found to cause human diseases such as cancer, inflammation, neurological and developmental disorders, and more (Cohen 2002, 2009; Lahiry et al. 2010); almost half (244 kinases) are in known disease-causing loci (Manning et al. 2002).

Over the decades, the kinome has emerged as one of the most druggable subset of the human proteome (Hopkins and Groom 2002). As of 2015, there were approximately 250 kinase inhibitors in clinical trials and 28 which were FDA approved (Wu, Nielsen, and Clausen 2015); since then, an additional 20 kinase inhibitors have been approved by the US FDA, increasing the total to 48 compounds (Roskoski 2019). *In silico* chemogenomic mapping of known small molecules to kinase targets identified thousands of potential inhibitors estimated to target over

half of the kinome (Hu, Kunimoto, and Bajorath 2016). Thus, the regulatory role of kinases combined with the druggable nature of the kinome makes it an attractive target for therapeutic initiatives in DM1. Additionally, compared to the genome, screening the kinome is more feasible in terms of availability, cost, time and technical labour.

3.2 MATERIALS AND METHODS

3.2.1 Fibroblast Cell Culture

All DM1 patient human fibroblasts (HF) and Control HF 4 were obtained from Coriell Biorepository (Control HF4, GM04603; $DM1_{66CTG}$, GM06076; $DM1_{500CTG}$, GM03987; $DM1_{1000CTG}$, GM04033; $DM1_{1600CTG}$, GM04602; $DM1_{2000CTG}$ 1, GM03132; $DM1_{2000CTG}$ 2, GM03989; $DM1_{2000CTG}$ 3, GM03759) and the remaining Control HF cell lines were obtained from the CHEO Care for Rare repository (Control HF 1, CH3014F; Control HF 2, CH3009; Control HF 3, CH3013). All cells were maintained in complete fibroblast growth media made up of High Glucose Dulbecco's Modified Eagle Media (DMEM; Gibco), supplemented with 0.292mg/mL L-glutamine in 0.0085% NaCl (HyClone), 10% fetal calf serum (FCS; HyClone) and 100units/mL penicillin/ 100µg/mL streptomycin (HyClone). Cells were passaged when they reached 70-90% confluence and was split at a ratio of one-third to one-fourth to achieve 20-30% seeding density. For cryo-preserved cells stocks, the freezing media was DMEM, 20% FCS and 10% dimethyl sulfoxide (DMSO, Sigma).

3.2.2 Reverse Transfection of siRNA

Fibroblasts were reverse transfected with siRNA using Lipofectamine RNAi MAX (Invitrogen). The siRNAs were generally used at a final concentration of 5-20nM, relative to the final transfection volume (diluted siRNA, lipofectamine, cell suspension); and the lipofectamine was used at a ratio of 2µL per 1mL final transfection volume. The siRNA and lipofectamine were first separately diluted in optiMEM reduced serum medium (Gibco) and incubated at room temperature for 5min – each siRNA/optiMEM and lipofectamine/optiMEM dilution represented one-eighth of the final transfection volume. The diluted siRNA and lipofectamine were then combined and incubated at room temperature for approximately 20 min to allow the siRNA-lipid complex to form – this complex represented one-fourth of the final transfection volume. During this time, the cell suspension was prepared: media was aspirated, cells were washed with 1X PBS (Fisher Scientific), incubated with 1X (0.25%) trypsin (Gibco; reconstituted in 15mM NaCl (Fisher Scientific), 0.5mM EDTA (Sigma), and 1X PBS (Fisher Scientific)) at 37°C for 5-7min, and the trypsin was inhibited by adding complete DMEM growth media containing 10% FCS; cells were manually counted using a Bright-Line hemocytometer (Sigma) under an EVOS AMG bright-field microscope at 10x magnification (Thermo Scientific). The siRNA-lipid complex was then mixed with the trypsinized cell suspension and plated in a tissue culture dish. The treatments were performed at 37°C in the presence of 5% CO_2 for 24-96hrs. Each sample set contained at least a negative control non-targeting siRNA (Qiagen). The non-targeting siRNA and gene-specific targeted siRNA (Qiagen) for PACT, HIPK4 and PKA2β were all resuspended in RNAse-free H_2O from lyophilized pellets to make 10 or 20µM stocks; each stock was further aliquoted and stored at -20°C.

3.2.3 Kinome siRNA screen and RNA FISH analysis

For the kinome screen reverse transfections, the siRNA-lipid complex was formed in 384-well Falcon culture plates (VWR) and cell suspension was added to the wells thereafter; to avoid edge-effect, the outer wells of the Falcon 384-well plates were not used. In addition to negative controls, transfection efficiency was assessed by reverse transfecting cells with the cytotoxic ALL-STAR Death Control siRNA (Invitrogen); the degree of cell death corresponded to transfection efficiency.

RNA FISH was performed as described in Chapter 2.2. The hybridization buffer used was DIG Easy Hyb (Sigma); following hybridization, the wells were washed 3 x 5-10min with 1X PBS (Fisher Scientific). After FISH and Hoechst staining, the plates were imaged as previously described in Chapter 2.2.2. Cells were scored based on the number of foci detected per nucleus and on the total surface area of foci as determined by the number of pixels in each focus. A minimum signal intensity threshold was included as the lower end of detection to ensure that background signal was not included in quantification. The Z-score was then used to rank samples based on the number of standard deviations each data point was from the sample mean. Negative Z-score values represent a decrease in the parameter (foci size or number) and a positive value indicates an increase. Samples which had a mean z-score less than -2.00 in either foci number per nuclei or mean foci area from three repeats were considered hits for further validation.

3.2.4 Western Blot

Protein samples were prepared as described in the 'General Material and Methods' chapter. The samples were separated by 11% SDS-PAGE gel and transferred to 0.45µm nitrocellulose membrane. The membranes were blocked in blocking solution: 5% milk, 1X PBS or TBS, 0.1% Tween-20. Primary antibodies were purchased from Abcam and used at the following concentrations: MBNL1-mouse IgG (1:5000), PACT-rabbit IgG (1:2000). HSP90 primary antibody was purchased from Cell Signalling and used at a dilution of 1:2000. HRP-linked secondary antibodies were diluted in 5% milk and used for 1hr at room temperature: anti-mouse (1:5000) and anti-rabbit (1:2000) (Cell Signalling). Antibody complexes were visualized by autoradiography using ECL western blotting system (GE Healthcare) and X-Ray film (Kodak). Quantification was performed by scanning the autoradiographs and densitometric signal intensities determined using Image J software.

3.2.5 PKR inhibition

The PKR inhibitor C16 (PKRi; Sigma and Merck) was dissolved in DMSO (Sigma). Cells were grown in 384-well falcon plates (VWR). The cells were treated with DMSO (Sigma) or C16 PKRi every 48hrs for up to 7days. The treatments were performed at 37°C in the presence of 5% CO_2. Following treatment, cells were fixed, stained by RNA FISH and analysed for foci content as previously described.

3.3 RESULTS

3.3.1 Nuclear CUG foci are unique biomarkers in DM1 human fibroblasts

A robust quantification of nuclear RNA foci in DM1 cell lines was initially established (Figure 3.1). Hybridization with Alexa555-$(CAG)_{10}$ fluorescent probe identified nuclear CUG foci in the DM1 primary skin fibroblast cell lines (DM1 HF), but not in unaffected control human fibroblast cell lines (Control HF), consistent with a high signal to noise ratio. Six DM1 cell lines, containing 500 CTG repeats or more, were found to have, on average, two foci per nucleus, regardless of CTG repeat size. In the DM1 cell line containing 66 CTG repeats ($DM1_{66CTG\ HF}$), the foci signal was comparable to that observed in Control HFs, suggesting a threshold repeat-size for either nuclear foci formation or signal detection. DM1 HF containing 500 CTG repeats ($DM1_{500\ CTG\ HF}$) were selected for the kinome-wide siRNA screen based on its ready availability, efficient growth, and transfection capacity.

3.3.2 PACT siRNA reduced CUG foci in DM1 human fibroblasts

A partial, primary kinome screen done by Sean O'Reilly, a previous M.Sc. candidate, identified PACT (protein kinase R activator), also known as PRKRA (protein kinase, interferon inducible double stranded RNA dependent activator), as one of the top targets for foci reduction (Figure 3.2A; Supplementary Table 3.1, PRKRA Z-score: foci count -1.97, foci area -1.95). In the screen, each well contained a pool of four different siRNA targeted towards the same gene. The pool of PACT siRNA's were deconvoluted in order to confirm that PACT was an

(A)

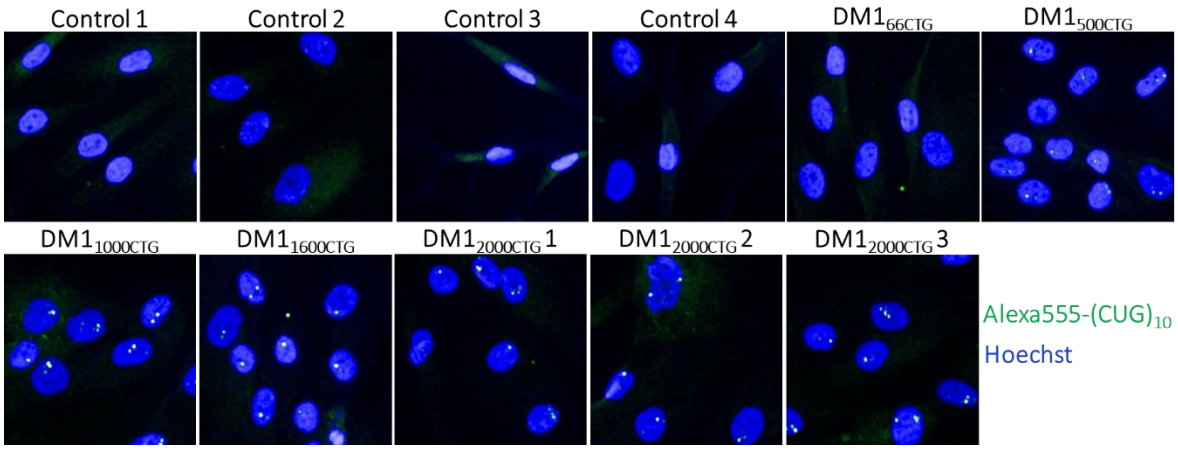

(B)

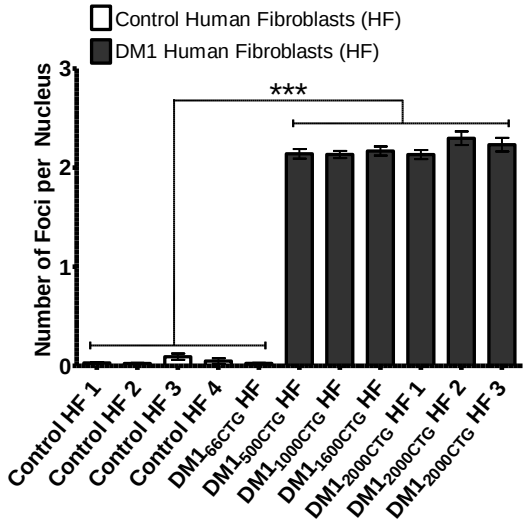

(C)

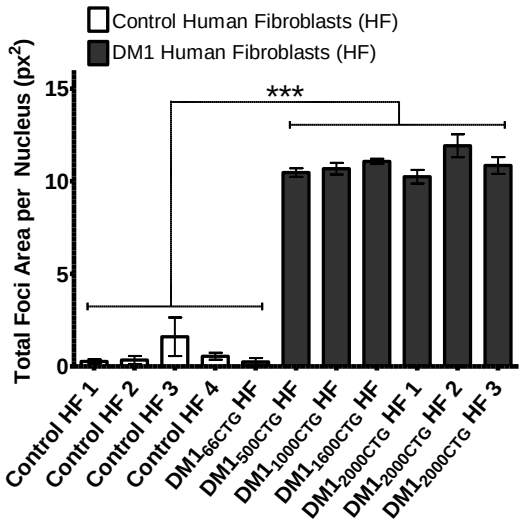

Figure 3.1. CUG-RNA foci are unique biomarkers in DM1 patient fibroblasts and are absent in unaffected control fibroblasts. (A) Representative images of nuclear foci after RNA-FISH detection of CUG foci in control and patient skin fibroblasts. Quantification of (B) number of foci per nucleus and (C) total foci area per nucleus using averages from five replicate wells (n=5; two-way ANOVA; error bars represent SD).

(A)

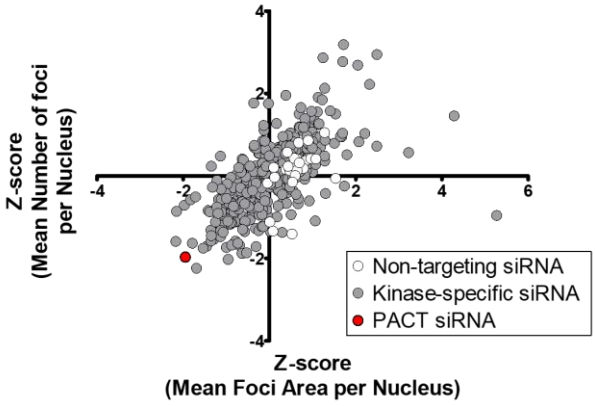

(B)

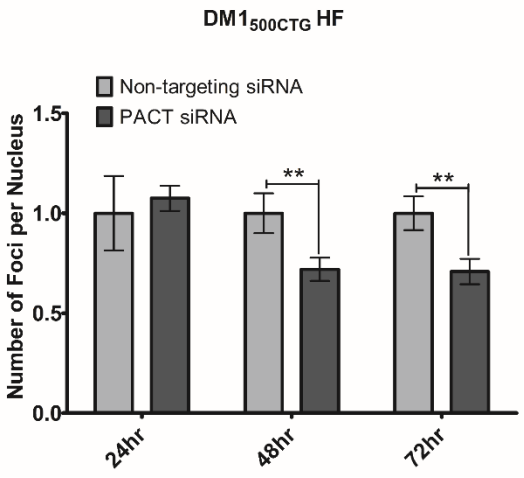

(C)

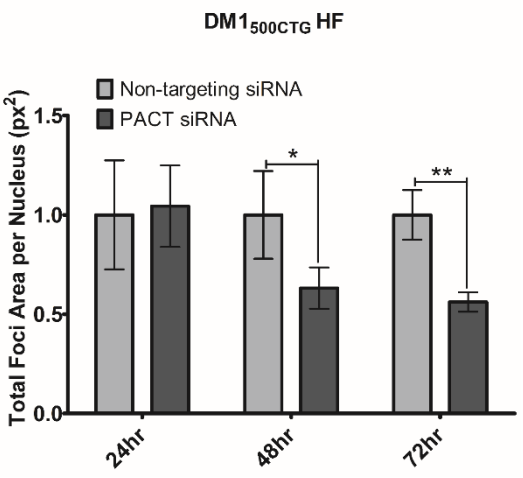

(Figure 3.2 continued on next page)

(D)

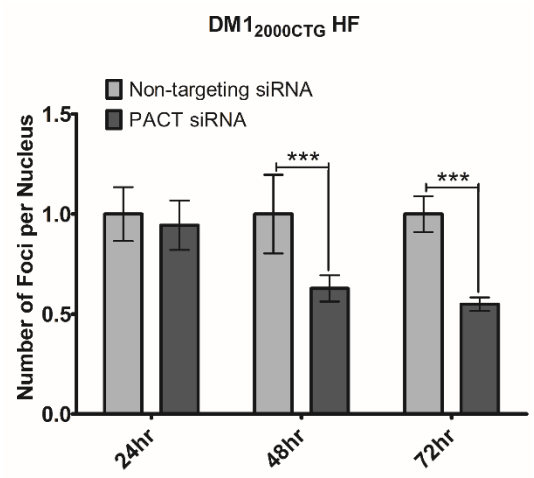

(E)

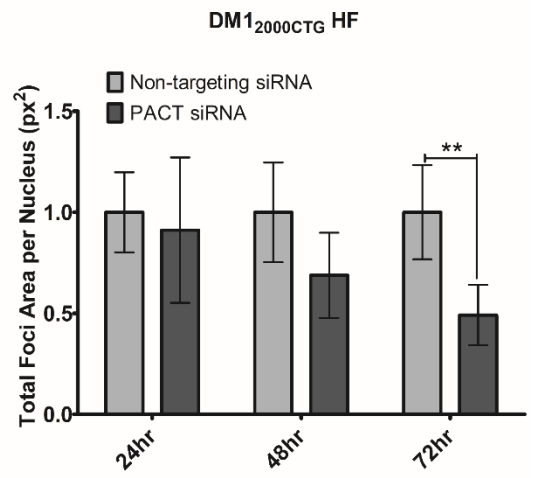

Figure 3.2. A partial kinome RNAi screen in a DM1$_{500\ CTG}$ patient fibroblast line identified PACT as a down-regulator of CUG-foci. (A) The screen was done in triplicate using 10nM of pooled siRNA with an end-point readout conducted at 96 hrs; due to technical errors, this original screen included only a portion of the entire kinome RNAi library. Cells were probed with Alexa-555 (CAG)$_{10}$ probes to detect foci and was imaged by the Opera high-content screening system. Quantification of number of foci per nucleus and total foci area per nucleus was done using the Columbus software. The data was normalized to the sample mean per plate and is represented as average Z-score values. (B-C and D-E) Effect of PACT knockdown on foci validated in DM1$_{500\ CTG}$ HF and DM1$_{2000\ CTG}$ HF, respectively. Cells were probed with Alexa-555 (CAG)$_{10}$ probes to detect foci and was imaged by the Opera high-content screening system. Quantification of (B and D) number of foci per nucleus and (C and E) total foci area per nucleus was done using the Columbus software (n=4; two-way ANOVA; error bars represent SD). For statistical analysis, each trial consisted of mean data from 3-9 replicate wells per sample with corresponding SD. The data was converted to fold change relative to non-targeting siRNA to accommodate plate-to-plate variability and the SD was adjusted to the same ratio. The fold change and SD data were averaged across all trials. *P < 0.05, **P < 0.01, ***P< 0.001

on-target hit – the impact of the four PACT siRNAs, individually and pooled, was assessed for PACT protein level and nuclear foci number and size in $DM1_{500\ CTG}$ patient cells (Supplementary Figure 3.1). All siRNAs knocked down the PACT protein to varying degrees (Supplementary Figure 3.1 A-B). Similarly, all four siRNAs reduced foci to some extent, ranging from 10-45% reduction, depending on time-point and siRNA (Supplementary Figure 3.1 C-D). These findings suggested that the foci modulation was due to PACT knockdown and not an off-target effect of the siRNA. The PACT siRNA having the most robust effect on PACT protein knockdown and foci reduction (PACT siRNA 1, referred to as PACT siRNA from this point onwards) was used for further analysis.

PACT was further validated to reduce foci in not only $DM1_{500\ CTG\ HF}$ (Figure 3.2B-C), but also $DM1_{2000\ CTG\ HF}$ (Figure 3.2D-E), supporting a biological reproducibility in human fibroblasts. PACT knockdown was confirmed at both the protein (Figure 3.3 A-B) and mRNA level (Figure 3.3 C-D) in both DM1 fibroblast cell lines. Since CUG-foci are a representation of mutant DMPK mRNA, DMPK mRNA was quantified by qPCR analysis, in order to determine whether a reduction in foci was a direct result of reduction in the DMPK mRNA. Although PACT knockdown significantly reduced CUG-foci, there was no reduction in total DMPK mRNA, wild-type or mutant, in either cell line (Figure 3.4). This suggests that PACT knockdown does not reduce CUG-foci by reducing the steady state levels of DMPK mRNA.

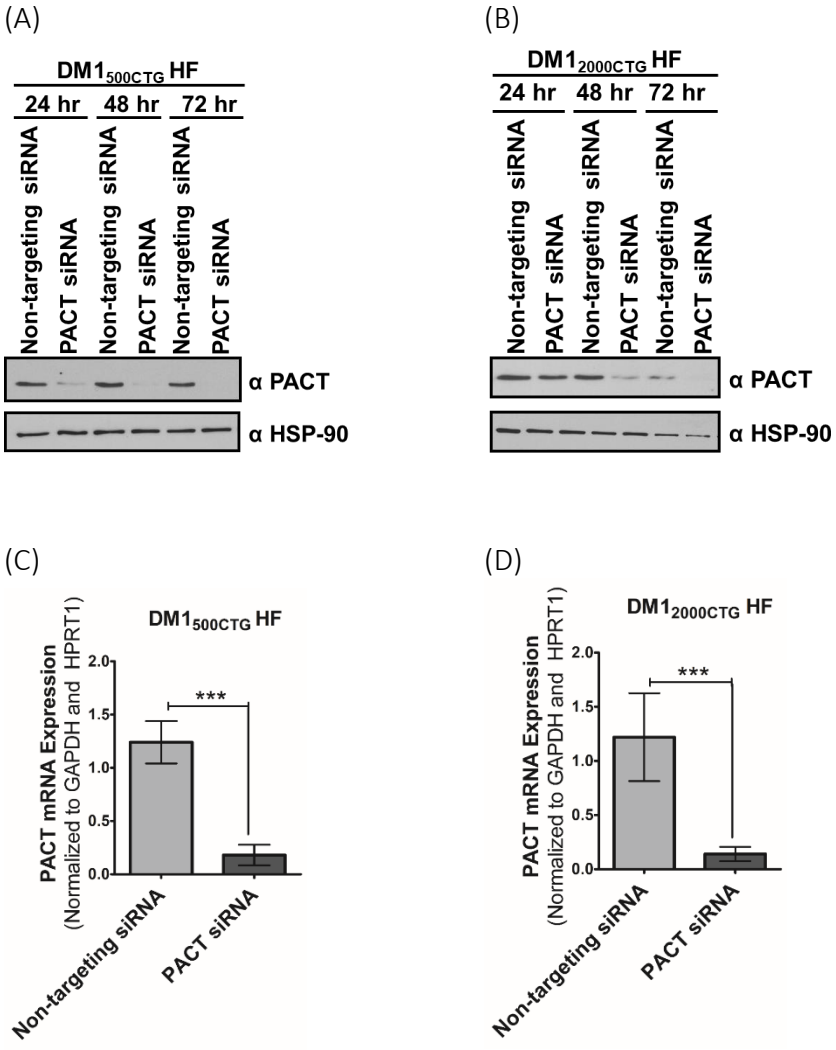

Figure 3.3. PACT protein and mRNA levels were reduced in both $DM1_{500\ CTG}$ and $DM1_{2000\ CTG}$ fibroblasts with PACT siRNA treatment over a 72hr time-course. (A-B) Western blot analysis of PACT protein levels upon knockdown using PACT siRNA in (A) $DM1_{500\ CTG}$ and (B) $DM1_{2000\ CTG}$ patient fibroblasts in a 24hr, 48hr and 72hr time-course. (C-D) RT-qPCR analysis of PACT transcript levels in (C) $DM1_{500CTG}$ and (D) $DM1_{2000CTG}$ HF, after a 72hr treatment with PACT siRNA; target genes were normalized to GAPDH and HPRT1 as reference genes. Samples were run in duplicates for each gene, in each replicate (unpaired t-test, n=5, error bars represent SD). *P < 0.05, **P < 0.01, ***P< 0.001

(A) (B)

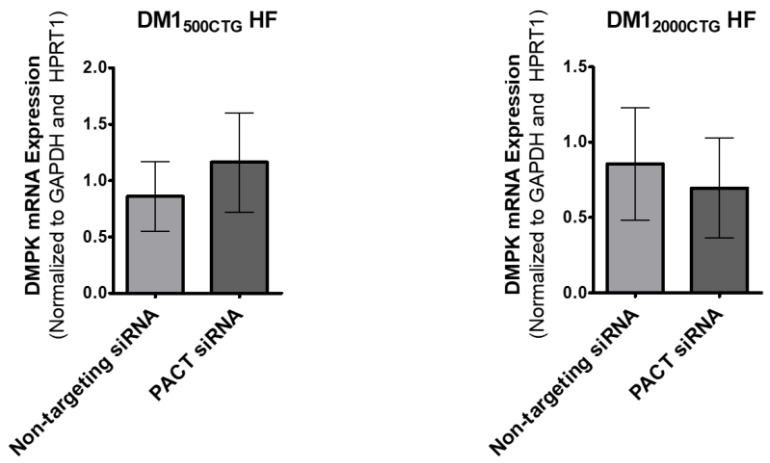

Figure 3.4. DMPK transcript levels were unchanged with PACT knockdown. RT-qPCR analysis of DMPK mRNA levels in (A) $DM1_{500CTG}$ and (B) $DM1_{2000CTG}$ HF after a 72hr treatment with PACT siRNA. DMPK expression was normalized to GAPDH and HPRT as reference genes. Samples were run in duplicates for each gene, in each replicate (unpaired t-test, n=5, error bars represent SD). *P < 0.05, **P < 0.01, ***P< 0.001

3.3.3 PACT knockdown increased MBNL1 in both DM1 and control fibroblasts

Given the misregulation of MBNL1 in DM1, the impact of PACT knockdown on MBNL1 protein levels in DM1 cells was assessed. Western blot analysis showed that PACT knockdown induced an approximate two to three-fold induction of MBNL1 protein in both $DM1_{500\ CTG}$ and $DM1_{2000\ CTG}$ patient fibroblasts (Figure 3.5A-D). However, MBNL1 transcript levels were not significantly changed by PACT siRNA treatment (Figure 3.5E-F), suggesting a post-transcriptional mechanism for MBNL1 protein induction. The effects of PACT knockdown on MBNL1 expression was also assessed in Control HF cells (Control HF 2 in the full panel of cells). Similar to that observed in DM1 cells, a statistically significant increase in MBNL1 protein, but not mRNA, was observed in the NHF (Figure 3.6), suggesting that PACT-mediated increase in MBNL1 protein is independent of the DM1 genotype.

3.3.4 PACT knockdown in DM1 fibroblasts did not change DM1-related spliceopathy

To investigate whether the increase in MBNL1 protein level and/or reduction in foci number/size upon PACT knockdown in DM1 HF resulted in the normalization of dysregulated splicing in DM1, transcript ratios for genes encoding IR was quantified using radioactive PCR (Figure 3.7A-B), as previously published (Savkur et al. 2001), and using a newly developed qPCR assay (Figure 3.7C-E); transcript ratios for SERCA1 were quantified using a qPCR assay (Figure 3.5F-H). Quantification by radioactive PCR of the IR splice products showed that, upon treatment with PACT siRNA, there was no significant splicing rescue for IR. In order to reinforce this finding, SERCA1 splicing was also assessed; however, radioactive PCR was not sensitive

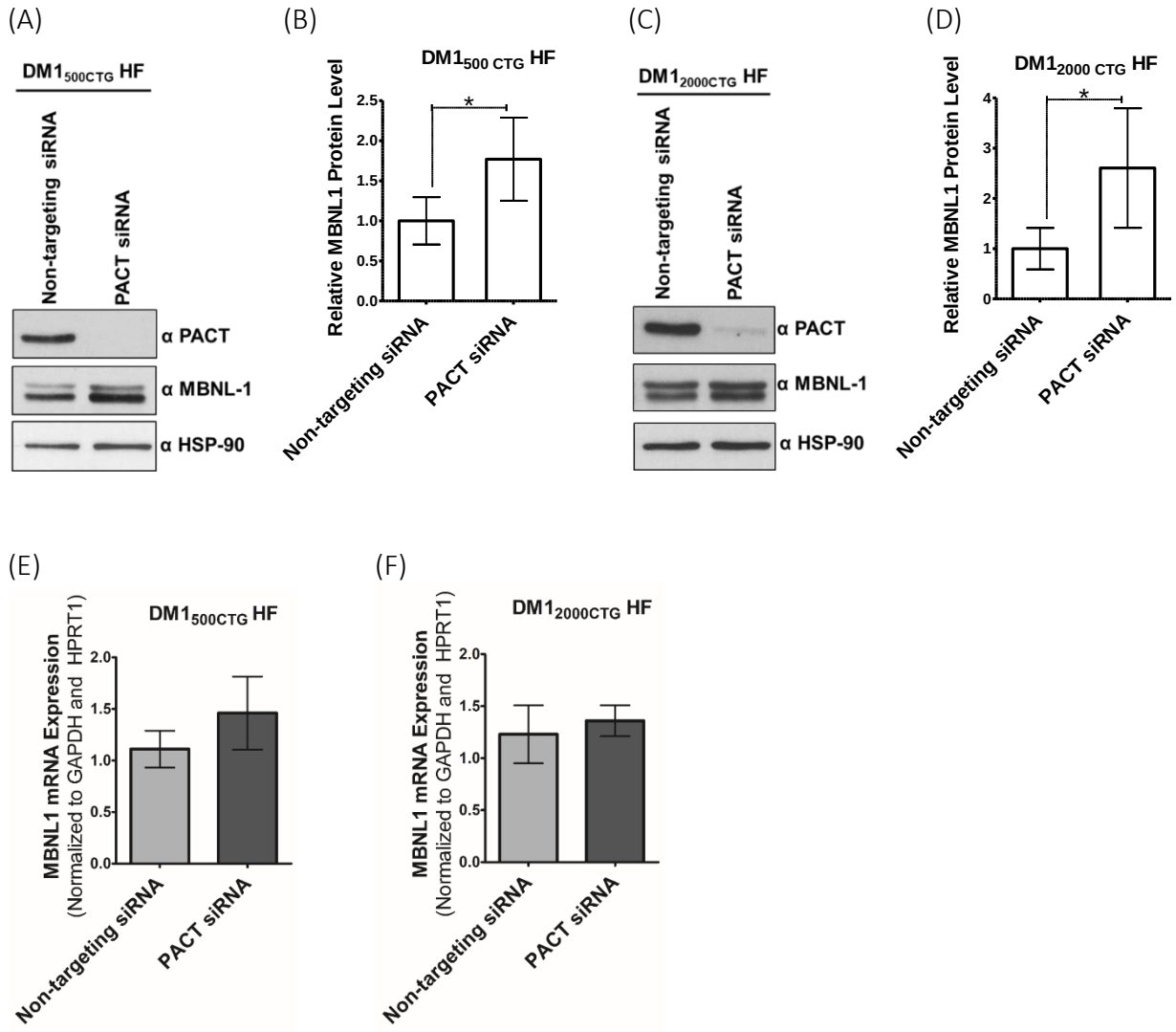

Figure 3.5. PACT knockdown induced MBNL1 protein expression but not MBNL1 mRNA. (A-D) Western blot analysis of MBNL1 protein levels upon PACT knockdown in (A) $DM1_{500\ CTG}$ and (C) $DM1_{2000\ CTG}$ HF. Corresponding quantification of MBNL1 protein in (B) $DM1_{500\ CTG}$ and (D) $DM1_{2000\ CTG}$ HF was done using Image J. MBNL1 protein level was normalized to HSP90 loading control, averaged across trials and presented as relative fold-change to non-targeting siRNA (n=4, unpaired t-test, error bars represent SD). (E-F) RT-qPCR analysis of MBNL1 transcript levels in (E) $DM1_{500CTG}$ and (F) $DM1_{2000CTG}$ HF, after a 72hr treatment with PACT siRNA, normalized to GAPDH and HPRT1 as reference genes. The non-targeting siRNA-treated sample in one trial was set as the "control" sample and all other samples – meaning non-targeting siRNA and PACT siRNA treated samples from all other trials – were quantified relative to this "control" (unpaired t-test, n=5, error bars represent SD). *$P < 0.05$, **$P < 0.01$, ***$P < 0.001$

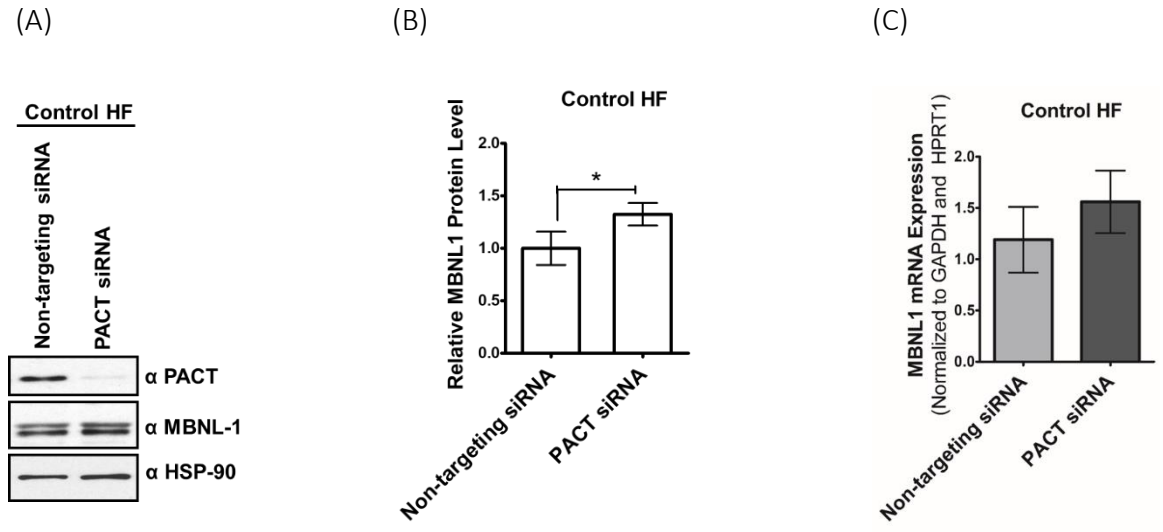

Figure 3.6. MBNL1 was increased with PACT knockdown in Control HF. (A) Western blot analysis of MBNL1 protein levels upon PACT knockdown and (B) the corresponding quantification using Image J software (n=3; unpaired t-test; error bars represent SD). MBNL1 protein level was normalized to HSP90 loading control and the normalized values were averaged across trials. (C) MBNL1 mRNA expression with reference to GAPDH and HPRT upon PACT knockdown. The non-targeting siRNA-treated sample in one trial was set as the "control" sample and all other samples – meaning non-targeting siRNA and PACT siRNA treated samples from all other trials – were quantified relative to this "control" (n=5; unpaired t-test; error bars represent SD). *$P < 0.05$, **$P < 0.01$, ***$P< 0.001$

(A)

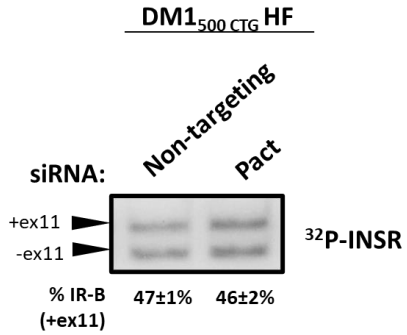

(B)

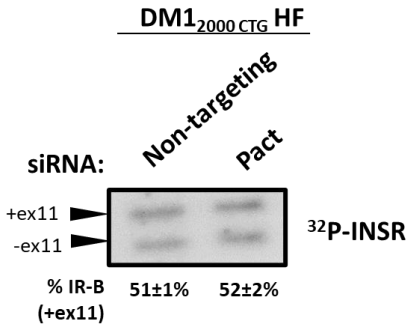

(C)

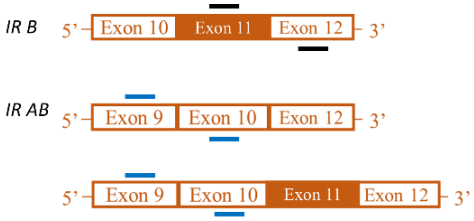

(D)

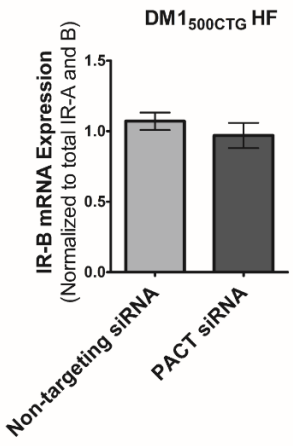

(E)

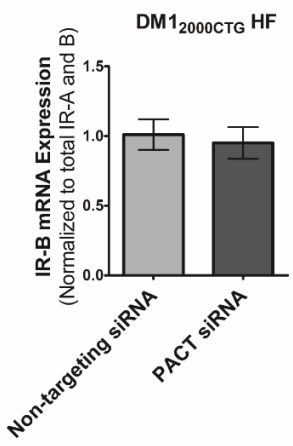

(Figure 3.7 continued on next page)

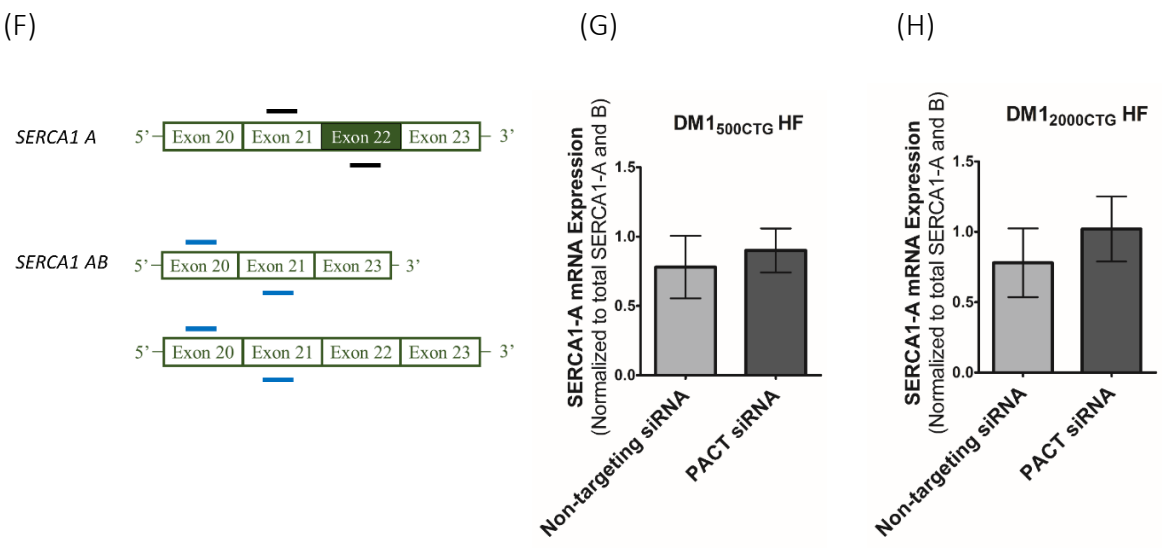

Figure 3.7. PACT knockdown did not correct IR or SERCA1 alternative splicing in DM1 cells. (A-B) Radioactive RT-sqPCR analysis of IR splicing patterns in (A) $DM1_{500\ CTG}$ and (B) $DM1_{2000\ CTG}$ fibroblasts treated with PACT siRNA (20nM, 72hr) (n=3; unpaired t-test; error represents SEM). (C-H) RT-qPCR analysis of (C-E) IR and (F-H) SERCA1 alternative splicing upon PACT knockdown in $DM1_{500\ CTG}$ and $DM1_{2000\ CTG}$ fibroblasts. The non-targeting siRNA-treated sample in one trial was set as the "control" sample and all other samples – meaning all non-targeting siRNA and PACT siRNA treated samples from all other trials – were quantified relative to this "control" (n=5; unpaired t-test; error bars represent SD). *$P < 0.05$, **$P < 0.01$, ***$P < 0.001$

enough to accurately and quantitatively visualize the SERCA1 transcripts in fibroblasts. Thus, a more sensitive qPCR approach was established (Supplementary Figure 3.2).

We next studied SERCA1 mRNA splicing for which the predominant isoform in unaffected cells is normally a full-length isoform containing exon 22 (SERCA1-A). Uniquely in DM1 patients, an isoform missing exon 22 (SERCA1-B) is more readily observed with a corresponding reduction in the level of full-length SERCA1-A. In order to assess SERCA1 splicing patterns, a transcript-specific RT-qPCR assay was designed in which SERCA1-A (using primer sets with one primer within exon 22) was measured relative to total SERCA1-A and B (using primers amplifying exons common to both SERCA1-A and SERCA1-B) as the reference gene (Figure 3.7F). In the case of the IR gene, there is normally an IR-B isoform, which encodes an insulin-sensitive receptor, and IR-A isoform, which lacks exon 11 and encodes a less-sensitive insulin receptor. In unaffected individuals, the IR exists predominantly as IR-B whereas in DM1 patients, the relative level of IR-B is reduced. Similar to the design of SERCA1 splicing assay, IR-B (using primer sets with one primer within exon 11) was measured relative to total IR-A and B (using primers amplifying exons common to both SERCA1-A and SERCA1-B) as the reference gene (Figure 3.7C). RT-qPCR quantification revealed a decreased level of SERCA1-A in DM1 HF cells compared to control HF cells (Supplementary Figure 3.2A). The significant variability observed in control HF cell IR-B transcript levels (Supplementary Figure 3.2B) precluded a rigorous assessment of PACT knockdown on IR spliceopathy by qPCR assay.

As a positive control to ensure that these qPCR assays can detect changes in transcript ratios in response to exogenous treatments, a subset of control and DM1 HF cells were treated with non-targeting or MBNL1 siRNA. MBNL1 is a master splicing regulator of both SERCA1 and IR, and, as such, knocking down this splicing factor should alter the splicing ratios to mimic that in DM1 as a result of MBNL1 sequestration. MBNL1 siRNA effectively reduced MBNL1 mRNA (Supplementary Figure 3.2C) and reduced the relative levels of both SERCA1-A and IR-B in both control and DM1 HF (Supplementary Figure 3.2D and E, respectively).

PACT siRNA treatment conferred no significant splicing rescue for IR (Figure 3.7D-E) or SERCA1 (Figure 3.7G-H). This suggests that neither the observed reduction in foci, nor the increase in MBNL1 from PACT knockdown was sufficient to moderate the spliceopathy believed to underpin DM1 pathogenesis, at least in the fibroblast lineage.

3.3.5 C16 inhibitors of PKR, a substrate of PACT, reduced nuclear foci, but was toxic

While PACT knockdown reduced foci, it was not one of the many druggable candidates of the kinome as there exists no small molecule PACT inhibitors. As such, in order to further investigate how PACT knockdown conferred foci reduction in $DM1_{500CTG\ HF}$ and $DM1_{2000CTG\ HF}$ and identify a druggable candidate, the PKR (protein kinase RNA-activated) signalling pathway, which maps downstream to PACT and has small molecule inhibitors (Patel and Sen 1998), was assessed . DM1 fibroblasts were treated with PKR inhibitor imidazole oxindole C16 (C16 PKRi), a compound previously reported to reduce DM1 foci at 1µM (Wojciechowska et al., 2014). $DM1_{500CTG}$ HF and $DM1_{2000CTG}$ HF were treated with C16 PKRi obtained from two sources (Sigma

(A)

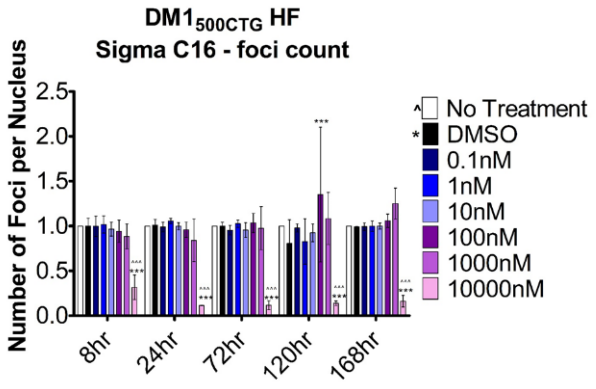

(B)

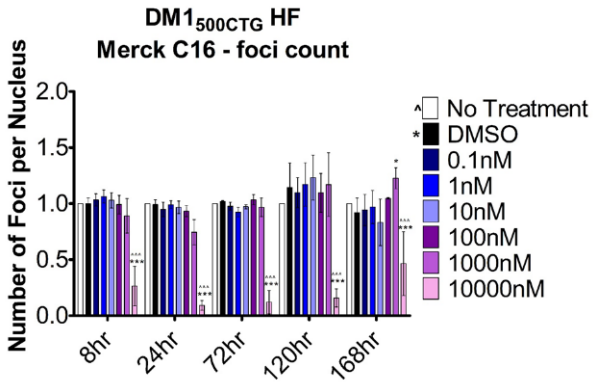

(C)

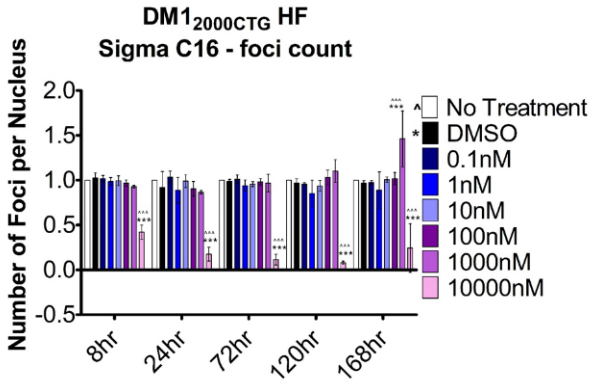

(D)

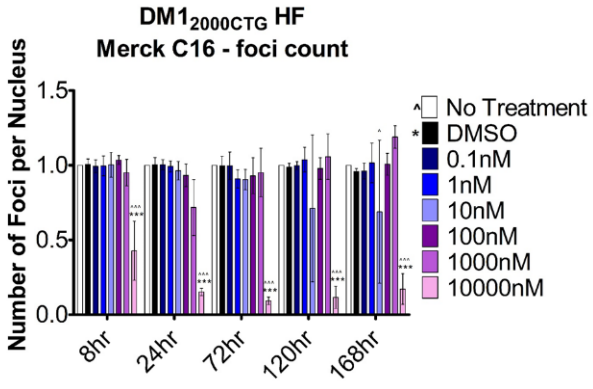

(E)

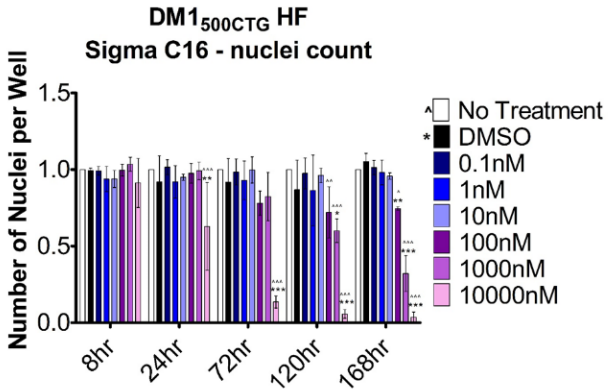

(F)

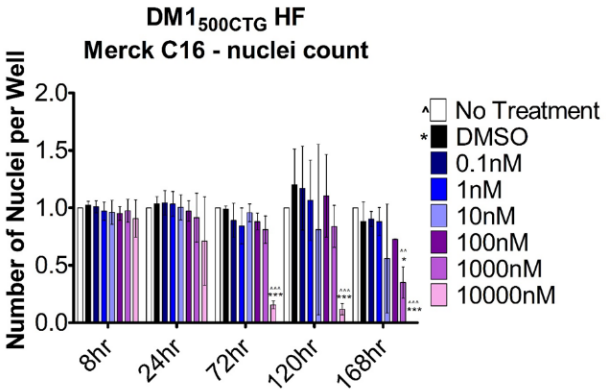

(Figure 3.8 continued on next page)

(G)

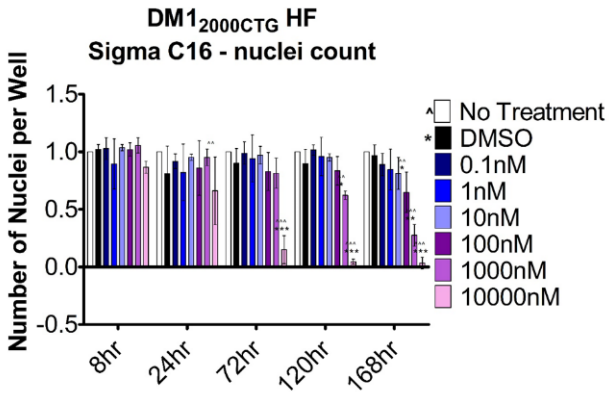

(H)

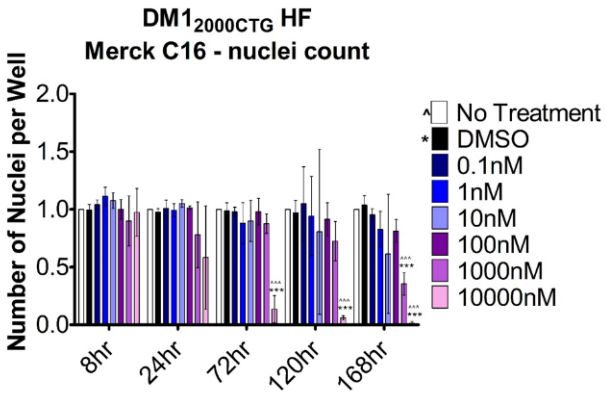

Figure 3.8. PKR inhibition reduced foci but caused cellular toxicity. Small molecule PKR inhibitor C16 from two different manufacturers, Sigma and Merck, was used to treat $DM1_{500CTG\ HF}$ or $DM1_{2000CTG\ HF}$ at doses ranging from 0.1nM-10,000nM for 8hrs up to 168hrs (7 days) following which (A-D) (CUG)n foci were detected by RNA FISH and foci number and area quantified, and (E-H) nuclei were detected by Hoechst staining and used as a measure of cellular toxicity (n=3; two-way ANOVA; error bars represent SD).

and Merck) at concentrations ranging from 0.1nM to 10μM at 8hrs, 24hrs, 72hrs, 120hrs and 168hrs; foci number was reduced with the highest C16 PKRi concentration (10μM), starting as early as 8hrs (Figure 3.8). However, at this level there was also substantial cytotoxicity, as measured by reduced nuclear count, starting at 24hrs post-treatment and increasing over time.

To assess whether reduction in foci is a consequence of cell toxicity, we explored the impact of another known cytotoxic agent on foci number. DM1 cells were treated with All-star death siRNA (Qiagen), a proprietary cocktail of siRNA sequences designed to induce cell death. There was a time-dependent increase in cell death with All-star death siRNA treatment in both $DM1_{500CTG}$ HF and $DM1_{2000CTG}$ HF (Supplementary Figure 3.3); the reduction in foci number in both $DM1_{500CTG}$ and $DM1_{2000CTG}$ HF was only observed later, at 72hrs. These data suggest that the reduction in foci due to cytotoxicity follows the cell death time-point. In contrast, C16 PKRi mediated foci reduction preceded the observable cell death (Figure 3.8). Taken together, we concluded the reduction in foci mediated by C16 PKRi was likely not related to cytotoxicity, although the 10μM dose, which was the only foci disrupting concentration, is ultimately cytotoxic. We also confirmed that PACT knockdown did not reduce cell viability (Supplementary Figure 3.4) and, thus, PACT siRNA-mediated reduction in foci was not due to cytotoxic effects (Figure 3.2).

3.3.6 PKA2β and HIPK4 siRNA reduced CUG foci in DM1 human fibroblasts

A second kinome screen was performed to survey the full kinome library for additional candidates. Applying the Z-scores for PACT knock down in this second assessment as a

threshold cut-off for foci reduction (-1.48 for foci area, -1.58 for foci count) identified cAMP-dependent protein kinase type II beta regulatory chain (PRKAR2β aka PKA2β; Z-score -1.59 for foci area, -2.09 for foci count, Supplementary Table 3.2) and homeodomain interacting kinase 4 (HIPK4; Z-score: -foci count 2.54, foci area 2.20, Supplementary Table 3.2) as new hits (Figure 3.9). PKA2β (Figure 3.10) and HIPK4 (Figure 3.11) were both validated to reduce foci in $DM1_{500\ CTG}$ HF and confirmed to be knocked down by the respective siRNA's, either at the protein or mRNA level based on availability of primers and functional antibodies. However, reminiscent of the PACT story, neither had an impact on IR splicing, as assessed by radioactive PCR.

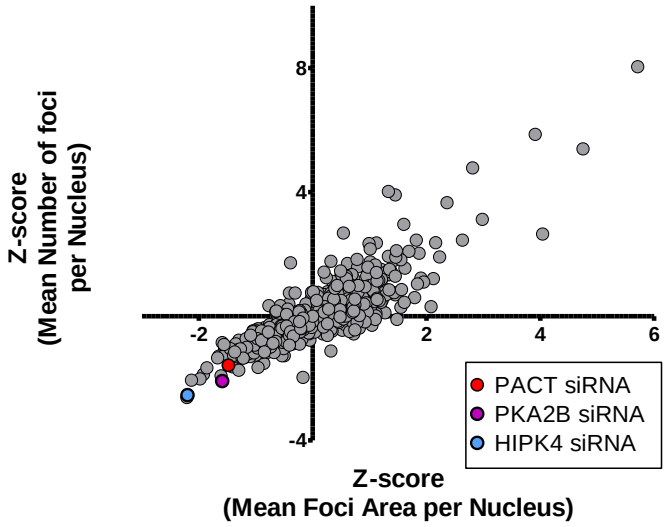

Figure 3.9. A complete kinome RNAi screen in a $DM1_{500\ CTG}$ patient fibroblast line identified HIPK4 and PKA2β as down-regulators of CUG-foci. The screen was done in triplicate using 10nM of pooled siRNA with an end-point readout conducted at 72hrs. Cells were probed with Alexa-555 $(CAG)_{10}$ probes to detect foci and was imaged by the Opera high-content screening system. Quantification of number of foci per nucleus and total foci area per nucleus was done using the Columbus software. The data was normalized to the sample mean per plate and is represented as average Z-score values.

(A)

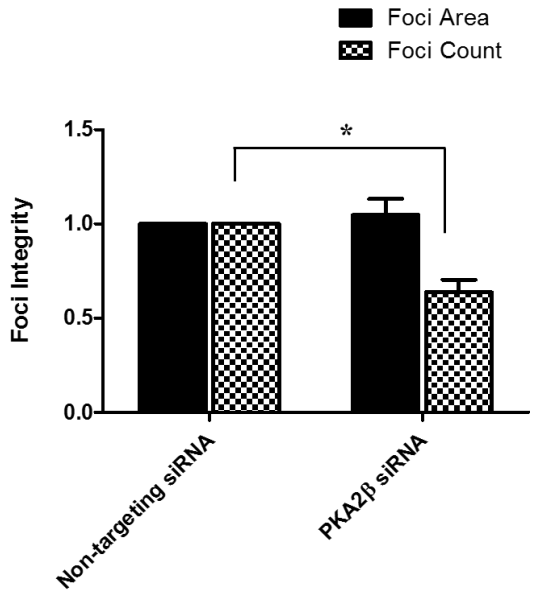

(B)

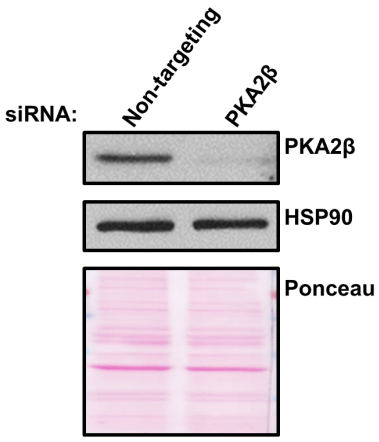

(C)

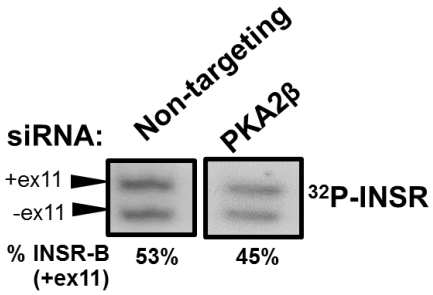

Figure 3.10. PKA2β was validated to reduce foci number in DM1$_{500\ CTG}$ HF but did not correct IR spliceopathy. (A) Normalized individual foci area and number of foci per nucleus were determined from RNA-FISH using Columbus (unpaired t-test, n=3, errors bars represent SD). (B) Western blot of PKA2β protein after 72hr siRNA-mediated knockdown. (C) IR transcripts were amplified through radioactive RT-PCR and resolved on a 7% polyacrylamide gel. The blots were quantified using Image J (n=2).

(A)

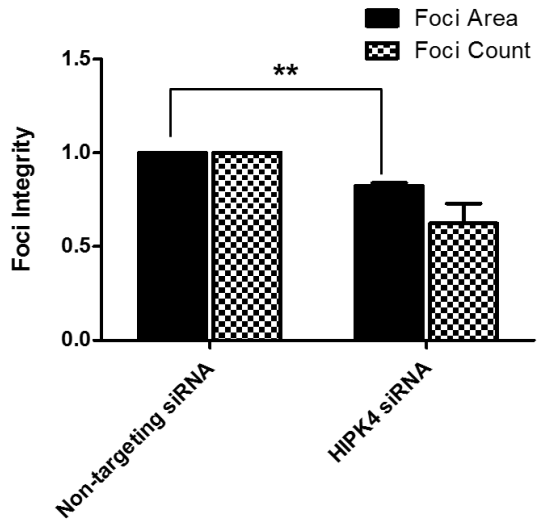

(B)

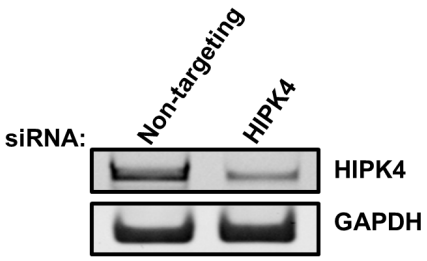

(C)

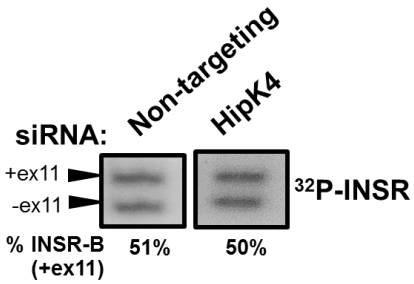

Figure 3.11. HIPK4 was validated to reduce foci number in $DM1_{500\ CTG}$ HF but did not correct IR spliceopathy. (A) Normalized individual foci area and number of foci per nucleus were determined from RNA-FISH using Columbus (unpaired t-test, n=3, error bars represent SD). (B) RT-PCR analysis of HIPK4 mRNA levels after 72hr HIPK knockdown by siRNA. (C) IR transcripts were amplified through radioactive RT-PCR and resolved on a 7% polyacrylamide gel. The blots were quantified using Image J (n=2).

3.4 DISCUSSION

This chapter highlights a high-throughput genetic screen for kinases involved in DM1-associated nuclear CUG_n foci integrity using siRNA-mediated gene knockdown. The nuclear CUG foci were used as the screen readout as they are both a clear biomarker and pathogenic driver of this trinucleotide repeat disorder (Figure 3.1). PACT was identified by the primary screen as a hit for foci reduction and was validated to reduce foci in two DM1 fibroblast cell lines in a time-dependent manner (Figure 3.2). However, PACT knockdown failed to correct IR and SERCA1 spliceopathy (Figure 3.7). This is despite a two-fold increase in MBNL1 protein in the DM1 fibroblasts (Figure 3.5). While RNA FISH analysis of CUG foci is a direct representation of the expanded repeats, which are central to the molecular etiology of the disease, it is not the direct cause of observable signs and symptoms. Rather, the repeats trigger a cascade of subcellular dysregulation including MBNL sequestration, CELF activation and more, which collectively result in the aberrant alternative splicing directly associated with disease manifestation. As such, while the CUG foci make a logical disease target, it is important to conduct downstream analysis of DM1-related spliceopathy to validate the therapeutic efficacy of any hits. In this regard, PACT is not an appropriate target for DM1 because, despite reduction in foci and increase in MBNL1, it does not mediate splicing rescue.

While MBNL1 overexpression has proven to be therapeutically beneficial in pre-clinical studies (Chamberlain and Ranum 2012; Kanadia et al. 2006), it is possible that an approximately two-fold induction in MBNL1 protein by PACT knockdown is insufficient for splicing rescue,

especially given that in animal models over-expressing MBNL1, there was a robust 8-16 fold induction of the protein (Chamberlain and Ranum 2012). Further investigation is required to delineate the minimum and maximum thresholds of MBNL1 overexpression *in vitro* and *in vivo* required to elicit MBNL1-mediated correction of DM1 pathology without reaching toxicity. Similarly, there may be a minimum threshold of foci reduction required for resulting correction of aberrant splicing in DM1.

Using a system very similar to the one described in our paper, Ketley *et al.* screened several libraries of small molecule compounds, including phosphatase and kinase inhibitors for modulators of nuclear foci in DM1 fibroblasts and converted myoblasts (Ketley et al. 2014). The PKC inhibitor Ro 31-8220 was found to reduce RNA foci, redistribute MBNL1 protein to the cytoplasm and normalize alternative splicing of IR and ATP2B1 (or SERCA1). Although Ro 31-8220 was originally developed as an inhibitor of protein kinase C (PKC), the authors demonstrated that the impact of this compound on DM1 pathomechanism was independent of PKC, suggesting involvement of other kinases or even a non-kinase role. Ro 31-8220 reduced foci to the point of complete disappearance compared to PACT knockdown, which reduced foci up to only 50% (Figure 3.2); no kinase knocked down in our screen approximated this effect of Ro 31-8220. This discrepancy might be explained by more than one kinase being targeted by RO31-8220 in contrast to our screen which targets only single kinases.

In this regard, one major limitation of a kinome siRNA screen is that the outcome is dependent on single-kinase regulators of foci. The data from the kinome siRNA screens suggest

that, at least within the human kinome, there exists no single master regulator of foci capable of correcting the disease-associated spliceopathies. This single-gene interrogation approach does not address the possibility of combination knockdown of multiple kinases for therapeutic efficacy in DM1; this is especially important to consider given the evidence for redundancy in the kinome with overlapping or compensatory roles within a group of kinases. For example, redundancy in the receptor tyrosine kinases has been implicated in chemotherapeutic drug resistance (Sun and Bernards 2014).

Another limitation to consider are false-negatives – while using a pool of four unique siRNA's would increase the possibility of targeted knockdown, we cannot be certain that each kinase was knocked down sufficiently at a given dose and time-point. A lack of sufficient knockdown may in part explain why PKR siRNA was not a hit from our kinase screens; however, this remains to be confirmed.

Interestingly, DMPK, which itself is a kinase and is therefore included in the siRNA library, did not make the hit-list (z-score: foci count 0.31, foci area 0.39; Supplementary Table 3.2). ASO data has demonstrated that downregulation of the DMPK mRNA is sufficient for foci ablation, resulting in splicing correction, both *in vitro* and *in vivo*, and attenuation of myotonia in mice (Wheeler et al. 2012). Given this, one would expect DMPK siRNA to be an effective hit for foci reduction in our kinome screens. It may be that DMPK knockdown by the screened siRNA was insufficient either because siRNA was unable to access the CTG expanded-DMPK

mRNA which is sequestered to the nucleus as reported in human DM1 fetal myoblasts (Langlois et al. 2005) or for other reasons associated with siRNA sequence or chemistry.

While it is shown here that PACT does not reduce foci by a direct reduction in DMPK mRNA (Figure 3.4), the mechanism by which PACT does modulate foci integrity remains unclear. Interestingly, the PACT pathway has a pre-existing link to DM1 pathogenesis through association with PKR. PACT was shown to interact with and thereby activate PKR in the context of a subcellular stress response, resulting in downstream inhibition of protein synthesis and activation of apoptosis (Patel and Sen 1998; Singh and Patel 2012). PKR, a signalling partner of PACT, has been found to be over-expressed in DM1 cells and has been suggested to bind the double stranded DMPK CUG RNA (Huichalaf et al. 2010; Tian et al. 2000). In fact, when foci-forming CUG repeats are overexpressed, PKR is activated, similar to a viral response pathway which is activated by the presence of double-stranded viral RNA (Tian et al. 2000). Given this connection to DM1 dysregulation and PACT, PKR was of interest for further evaluation in our DM1 fibroblast model.

Foci reduction following C16 PKRi treatment was only observable at the high, toxic dose of 10µM (Figure 3.8), which is 10-fold higher than the effective dose of 1µM previously reported (Wojciechowska et al. 2014), a dose at which we found CUG foci remained unaltered in $DM1_{500\ CTG}$ HF and $DM1_{2000\ CTG}$ HF. In addition, the reported IC50 of C16 for PKR, the concentration at which 50% PKR inhibition is attained, ranges from 141nM (Lo et al. 2019) to 210nM (Jammi, Whitby, and Beal 2003); at 10µM (about 50-fold greater than the IC50), there is

almost certainly off-target activity which can account for the foci reduction. An example of such off-target activity is the inhibition of cyclin dependent kinases in neurons treated with 10μM PKRi (Chen, Wang, and D'Mello 2008). Even at the previously reported dose of 1μM (approximately five-fold above the IC50), off-target effects have been reported – *in silico* predictions and *in vitro* kinase assays showed 93% inhibition of FGFR2 with 1μM C16 PKRi (FGFR2 IC50 = 31.8nM), which is higher than the reported 88% inhibition of the intended target, PKR (IC50 141nM); C16 PKRi also has inhibitory capacity against Aurora A (IC50 = 114nM), FGFR3 (IC50 = 478nM) and RET (33.8nM) (Lo et al. 2019). In line with the notion that any foci disrupting effect seen by C16 treatment is owed to off-target regulation, in addition to or in spite of PKR inhibition, single-gene knockdown of PKR did not emerge as a hit in the kinome screen (Supplementary Table 3.1 and Supplementary Table 3.2: PRKR).

Based on the PKR activation observed in DM1, PKR knockout (PKR KO) mice were crossed with a DM1 mouse model to assess whether PKR knockdown had any impact on disease pathology. However, the resulting PKR KO/DM1 offspring displayed no changes in disease development, calling into question the significance of the interaction between DMPK mRNA and PKR in DM1 disease (Mankodi et al. 2003). With evidence from our studies and literature summaries, we can conclude that while PKR and PACT may play some role in DM1 pathogenesis, the centrality of such a role is not sufficient to make them therapeutic targets.

The second kinome screen revealed additional hits, HIPK4 and PKA2β (Figure 3.9). As was observed with the PACT inhibition, the inhibition of both genes reduced foci but neither

gene knockdowns resulted in splicing correction (Figure 3.10-3.11). This again speaks to the assertion that single-gene knockdowns are not sufficient to modulate a complex, multi-systemic disease like DM1.

CHAPTER 4: SMALL MOLECULE SCREENING TO IDENTIFY DRUG CANDIDATES FOR DM1 THERAPY

4.1 BACKGROUND AND RATIONALE

At the forefront of promising pre-clinical DM1 therapy are oligonucleotide interventions, including ASO-mediated degradation of the DMPK mRNA and morpholino-mediated competitive disaggregation of RNA-protein foci (Langlois et al. 2003; Wheeler et al. 2009, 2012). However, setbacks associated with oligonucleotide and other gene therapy approaches, such as cost, bioavailability and efficacy, have raised questions about their long-term suitability as DM1 therapies. DMPK ASO (IONIS-DMPK-2.5Rx) developed by Ionis pharmaceuticals, in collaboration which Dr. Charles Thornton's research team, reached Phase II of clinical trials, at which stage the drug failed efficacy testing as a result of insufficient tissue levels in patient skeletal muscles. While DM1 remains without an approved therapy, there are other examples of clinically approved oligonucleotides (Bennett 2019; Muth 2018; Verma 2018).

Clinical interventions using oligonucleotide-based gene therapy can be costly, as exemplified by the nusinersen (Spinraza) ASO therapy for spinal muscular atrophy (SMA). Nusinersen is one of the first ASOs to have received FDA approval for the treatment of a genetic neuromuscular disease. However, the required dosage per patient costs $750,000 for the first year and $350,000 per subsequent year as needed, totalling over one million dollars per patient (Friedmann 2017). In addition, due to the progressive nature of this disease, early intervention is critical to attain therapeutic efficacy. Etiplersen is another example of an FDA-

approved ASO used for Duchenne's Muscular Dystrophy (DMD), which costs approximately $300,000 per year for the duration of the patient's life (Aartsma-Rus and Krieg 2017). These high costs for oligonucleotide interventions are unfortunately in keeping with costly orphan disease therapies, making them virtually inaccessible to many financially-burdened patient communities and healthcare systems.

An alternative to molecular therapies such as ASO's is chemical therapies, such as the use of small molecule compounds, to regulate key disease pathways – this was the second approach used for our high-throughput DM1 screening and the focus of this chapter. This approach can potentially offer a low-cost alternative to ASO therapy with equally or more efficacious drug delivery methods and outcome.

4.2 MATERIALS AND METHODS

4.2.1 Cell Culture

Fibroblasts and Converted Myoblasts. Fibroblasts were maintained as described in Chapters 2 and 3. Fibroblasts converted to myoblasts were continually maintained in complete fibroblast growth media, as outlined for fibroblasts.

Immortalized primary myoblasts. All immortalized human DM1 and control myoblasts were obtained as a gift from Dr. Elena Pegoraro's group (Pantic et al. 2016). All cells were

grown on ECM gel-coated tissue culture plates and maintained in complete myoblast growth media made up of Ham's F14 Media (VWR), supplemented with 30% FCS (HyClone), 10 µg/ml insulin (Sigma), 25ηg/ml bFGF (basic fibroblast growth factor; Life Technologies), 10ηg/mL EGF (epidermal growth factor; LifeTechnologies), 100units/mL penicillin/ 100µg/mL streptomycin (HyClone) and 2µg/ml Amphotericin B (Gibco). Cells were passaged before they reached 50% confluence and split at a ratio of one-fifth to achieve 10% seeding density, on ECM gel-coated plates. For cryo-preserved cell stocks, a freezing media of Ham's F14, 20% FCS and 10% dimethyl sulfoxide (DMSO, Sigma) was used and the thawed cells were, again, grown on ECM gel-coated plates.

To coat plates with the ECM Gel from Engelbreth-Holm-Swarm murine sarcoma (Sigma), the concentrate was first diluted one-tenth in the base Ham's F14 media. Cold, diluted ECM Gel was used to cover the bottom of the plate and excess ECM gel was recovered for reuse. The ECM gel-coated plate was then incubated at 37°C for at least 15min in order to allow the ECM to polymerise on the plate surface.

To differentiate proliferative myoblasts to myotubes, cells were grown to 70-90% confluence. The complete myoblast growth media was aspirated, the cells were washed with 1X PBS (Fisher Scientific) to remove residual FCS and growth factors, and then incubated with differentiation media (Ham's F14 media, 1-2% horse serum (HS), 100units/mL penicillin/ 100µg/mL streptomycin (HyClone) and 2µg/ml Amphotericin B (Gibco)). *In vitro* differentiation

was induced at 37°C and 5% CO_2 for a variable period (from 4-9days), depending on the cell line and treatment.

4.2.2 Conversion of fibroblasts to myoblasts

Human fibroblasts were converted to myoblasts by lentiviral mediated overexpression of MyoD protein (Larsen et al. 2011). The second-generation lentiviral packaging system plasmids were a generous gift from Dr. Bernard Jasmin's lab (University of Ottawa). For virus production, the plasmids were diluted together in optiMEM (6µg pCDH-MyoD, 4µg psPAX2, and 2µg pMD2.G) and Lipofectamine 2000 (Invitrogen) was diluted separately in optiMEM at 3µL per µg of plasmid DNA; the dilutions were separately incubated at room temperature for 5min – each plasmid/optiMEM and lipofectamine/optiMEM dilution represented one-sixth of the final transfection volume. Diluted plasmid and lipid were mixed and incubated at room temperature for 20min. The lipid-plasmid complex was added to Hek293T cells in growth media (same as fibroblast growth media) and incubated overnight at 37°C, 5% CO_2; after overnight incubation (approximately 16hr post-transfection), transfection media was removed and fresh growth media was added. Media containing viral particles was collected 48hr post-transfection and cleared through a 0.45µm syringe-filter system; fresh media was added to virus-producing Hek293T cells. First infection of fibroblasts was done using filtered virus collected 48hr post-transfection: virus was diluted to 25-50% in fibroblast growth media, combined with 6µg/mL polybrene, and incubated with fibroblasts at 37°C, 5% CO_2. Approximately 16hr post-infection of fibroblasts, media was removed and a second infection of fibroblasts was done using filtered virus from Hek293T collected 64hr post-transfection, as described above for the first infection.

Total 24hr post-infection (8hr after second infection) of fibroblasts, cells were replaced with fresh media and allowed to grow for at least 48hrs before experimental implementation.

4.2.3 Southern Blot

Southern blot analysis of DM1 myoblasts was performed by the CHEO genetics clinic. Genomic DNA was extracted using DNA mini kit (Qiagen), digested with CutSmart EcoRI-HF (NEB) for 5hr to overnight, and resolved on 0.6% agarose gel. Gel was stained with 0.6µg/mL ethidium bromide in 0.5X TBE for 30min at room temperature and imaged. Subsequently, the gel was denatured in a solution of 0.4M NaOH and 1.5M NaCl for 2x10min under agitation and transferred overnight at room temperature to Biodyne B nylon membrane (Thermo Scientific) in 20X SSC buffer. Post-transfer, the membrane was neutralized in 0.2M Tris pH 7.5 and 2X SSC buffer for 15min at room temperature, baked between Whatman 3M paper for 2hours at 80°C, and pre-hybridized in a PEG hybridization solution of 10% PEG Glycol 8000, 1.5X SSPE, and 7% SDS for 1hr at 65°C under rotation. Hybridization probes were radioactively labelled with ^{32}P using Prime-It II Random Primer Labeling Kit (Agilent), purified using Sephadex G-50 Nick column (GE Lifesciences), and verified to have radioactivity of 0.3x10mR/hr or more per membrane. The radioactive probe was then mixed with 2mg/mL salmon sperm DNA, denatured at 100°C for 5min, diluted approximately 1/10 in PEG hybridization buffer, and used to hybridize the membrane at 65°C for 3hrs to overnight under rotation. Following hybridization, the membrane was washed in a solution of 0.1X SSC and 0.1% SDS for 2x15min at room temperature under agitation. Hybridized membranes were imaged using X-ray film.

4.2.4 Forward transfection of ASO's and siRNA

Differentiated myoblasts were forward transfected with siRNA or ASO using Lipofectamine RNAi MAX (Invitrogen). The siRNAs were generally used at a final concentration of 5-20nM and ASOs were used at around 1µM, relative to the final transfection volume (diluted siRNA and lipofectamine, and differentiation media); and the lipofectamine was used at a ratio of 2µL per 1mL final transfection volume. The siRNA/ASO and lipofectamine were first separately diluted in optiMEM reduced serum medium (Gibco) and incubated at room temperature for 5min – each siRNA or ASO/optiMEM and lipofectamine/optiMEM dilution represented one-eighth of the final transfection volume. The diluted siRNA and lipofectamine were then combined and incubated at room temperature for approximately 20min to allow the siRNA-lipid complex to form – this complex represented one-fourth of the final transfection volume. The nucleotide-lipid complex was then mixed with differentiation media and added to differentiated myoblasts. The treatments were performed at 37°C in the presence of 5% CO_2 for 24-72hrs. Each sample set contained at least a negative control, either non-targeting siRNA (Qiagen) or control ASO (Isis No. 549148, Ionis Pharmaceutical). The non-targeting siRNA and gene-specific targeted siRNA (Qiagen) for HDACs were all resuspended in RNAse-free H_2O from lyophilized pellets to make 10µM stocks; each stock was further aliquoted and stored at -20°C. The control (Isis No. 549148) and DMPK (Isis No. 486178) ASOs (Ionis Pharmaceutical) were diluted in nuclear-free H_2O from lyophilized pellets to make 1mM stocks; each stock was further aliquoted and stored at -80°C.

4.2.5 High-throughput screen set-up

Neuronal transcriptome screen employing blood-brain-barrier (BBB) penetrant drugs. This screen, unlike the phenotype-based foci screening platform, was done using RNAseq technology to analyse global transcriptomic changes in response to approximately 200 BBB-penetrant clinically approved drugs. The primary screen was done by Jeremiah Hadwen, an MD/PhD student, as previously described (Hadwen et al., 2018).

Myoblast FDA-approved compound screen and Chemogenomic screen. For the small molecule screens in myoblasts, proliferative cells were plated in 384-well collagen I-coated CellCarrier-384 Ultra microplates (Perkin Elmer); all wells, including peripheral columns and rows, were used. Collagen I-coating works similar to ECM gel for improving cell adherence and were used given that ECM gel-coated 384-well plates are not commercially available. For follow-up validation assessing CUG foci, cells were grown on 384-well falcon plates which were hand coated with ECM gel, as described above. Once 70-90% confluence was attained, cells were differentiated for six days. Stock compounds which were constituted in DMSO (Sigma) were diluted in differentiation media and added to the differentiated cells. DMSO vehicle was used as a negative control. DMPK ASO (Isis No. 486178, IONIS Pharmaceuticals) were forward transfected as positive controls for foci reduction (Wheeler et al. 2012).

RNA FISH was performed as described in the 'General Material and Methods' chapter (Chapter 2.2.1), with the following modifications: immediately prior to the overnight hybridization step, the samples were pre-hybridized with 40% formamide (Sigma) and 2X saline

sodium citrate buffer (SSC; Sigma) for 10min at room temperature; the hybridization buffer constituted of 40% formamide (Sigma), 2X SSC, 0.2% bovine serum albumin (BSA; Sigma), 1mg/mL tRNA (Roche), 1mg/mL single-stranded DNA from salmon testes (Sigma), 2mM vanadyl ribonucleoside complex (VRC; Sigma), and 10% dextran sulfate (Sigma); following hybridization, the wells were first washed 3 x 20min in 40% formamide/2X SSC at 37°C, then washed 3 x 5-10min with 1X PBS (Fisher Scientific) to remove the formamide and SSC prior to Hoechst staining. After FISH and Hoechst staining, the plates were imaged as described in Chapter 2.2.2. Cells were scored based on the total foci signal (number of pixels) to nuclear signal (number of pixels). A minimum signal intensity threshold was included as the lower end of detection to ensure that background signal was not included in quantification. For each plate, the foci signal and nuclear signal in each well was normalized to that of DMSO negative control and represented as a fold-change; normalized foci area per nuclear and nuclei for each treatment, relative to DMSO negative control, were averaged across the respective triplicate plates.

4.2.6 Western Blot

Protein samples were prepared as described in the 'General Material and Methods' chapter. The samples were separated by a 10% SDS-PAGE gel prepared using the TGX stain-free FastCast acrylamide kit (Bio-Rad), run at 200V. The resolved protein gels were activated under UV in the ChemiDoc imaging system (Bio-Rad) in order to cross-link the stain-free molecule to the protein. The protein was then transferred to low-fluorescence (LF) PVDF membrane using the Trans-Blot Turbo RTA LF PVDF transfer kit and the Trans-Blot Turbo Transfer System, as per manufacturer's instructions (Bio-Rad). The membranes were imaged for stain-free signal in the

ChemiDoc (Bio-Rad) and blocked in blocking solution: 5% milk, 1X PBS or TBS, 0.1% Tween-20. Primary antibodies purchased from Abcam were used at the following concentrations: MBNL1-mouse IgG (1:5000). HRP-linked secondary antibodies were diluted in 5% milk and used for 1hr at room temperature: anti-mouse (1:5000) and anti-rabbit (1:5000) (Bio-Rad). Chemiluminescence signal from antibody complexes was visualized by a camera-based system (ChemiDoc, Bio-rad). Quantification was performed by densitometric analysis using the ImageLab software (Bio-Rad).

4.2.7 *In vivo* small molecule trials in mice

In vivo *validation for neuronal screen hit, nilotinib*. Animals were housed and treated as previously described (Hadwen et al. 2018). C57BL6 mice at 8 weeks were treated daily with 10mg/kg aminophylline by intraperitoneal (i.p.) injection or 25mg/kg nilotinib by oral gavage for 8 days; control mice were treated with vehicle by i.p. injection or oral gavage, respectively. Skeletal muscle was dissected and flash-frozen in liquid nitrogen for molecular analysis – RNA extraction and qPCR are described in chapter 2, sections 2.4.1 and 2.4.4, respectively.

In vivo *validation for FDA-approved drug screen hit, vorinostat (SAHA).* All *in vivo* experiments were approved by the Animal Care and Veterinary Service (University of Ottawa) in compliance with the guidelines of the Canadian Council on Animal Care and the Animals for Research Act. Wild-type FVB/N, control HSA^{SR} (short CTG repeat) and DM1 HSA^{LR} (long CTG repeat) mice (Mankodi et al. 2000) were used in collaboration with Dr. Bernard Jasmin's lab (University of Ottawa). DM1 HSA^{LR} mice were treated daily with 50mg/kg vorinostat (Cayman

Chemical) or vehicle by i.p. injections For *in vivo* studies, vorinostat stock was reconstituted at 7.5mg/mL in 5% DMSO (Sigma), 300mg/mL HPBCD (Cedarlane), and 0.9% NaCl (Fisher Scientific); vehicle stock solutions were comprised of 5% DMSO (Sigma), 300mg/mL HPBCD (Cedarlane), and 0.9% NaCl (Fisher Scientific). Mice were weighed weekly. 24hr after the final injection, mice were euthanized by 120mg/kg euthanyl and cervical dislocation. Skeletal muscles were dissected (i) for cryostat sectioning by embedding in Tissue-Tek OCT compound (VWR) and flash-freezing in isopentane cooled with liquid nitrogen and (ii) for molecular analysis by flash-freezing directly in liquid nitrogen for cryostat sectioning. Tissue staining and image analysis is described below (section 4.2.8). RNA extraction and qPCR are described in chapter 2, sections 2.4.1 and 2.4.3, respectively. All treatments, sample processing and data analysis were completed in a double-blind context.

4.2.8 Tissue sectioning, staining and image analysis

Mouse tissues from the vorinostat (SAHA) *in vivo* trials were processed for microscopy as previously described (Ravel-Chapuis et al. 2018). Tissues were sectioned using Microm HM 500 M cryostat into 10µm thick sections and collected on microscope glass slides (Fisher Scientific). For central nucleation analysis, tissue slides were stained by hematoxylin and eosin staining, mounted using Permount mounting media (Fisher Scientific), and covered with microscope cover glass no. 1.5 (Fisher Scientific). Stained tissues were visualized at 20x magnification using the EVOS FL Auto 2 microscope (Thermo Scientific) and manually counted using Image J counter.

4.3 RESULTS

4.3.1 RNAseq-based transcriptome screen employing blood-brain barrier (BBB) penetrant drugs in mouse cortical neurons identified compounds which upregulated MBNL.

A mouse neuronal drug screen looking at gene expression by RNAseq to identify potentially therapeutic drug-gene interactions for rare diseases was previously done as part of the Care4Rare initiative (Hadwen et al. 2018). Given the neurological manifestations of DM1 including hypocognition and fatigue, it would be beneficial to identify drugs which can penetrate the blood-brain barrier in order to treat symptoms stemming from the brain. To identify therapeutically relevant molecules, specific transcriptomic changes relevant to the DM1 context was assessed: DMPK downregulation, MBNL upregulation. No drugs were found to reduce DMPK mRNA. Several compounds were found to increase MBNL1 and MBNL2 levels after 8hrs (Table 4.1). While MBNL1 is the key regulator of splicing in muscle over MBNL2, MBNL2 has a greater role in neuronal alternative splicing and has also been implicated in DM1 pathogenesis (Charizanis et al. 2012); as such, drugs modulating MBNL2 were also assessed.

cDNA samples from the original neuron screen were re-tested with in-house qPCR primers to verify MBNL upregulation as seen by RNAseq analysis. Of the drugs tested in this preliminary follow-up, Aminophylline (2-fold) and Nilotinib (6-fold) had the greatest impact on MBNL1 upregulation in mouse neurons (Figure 4.1A-B) along with Dexamethasone (3-fold) and

Table 4.1. RNAseq data of FDA-approved compounds which upregulate MBNL1 and MBNL2 in mouse primary neurons after 8hr treatments. Mouse neurons were harvested at embryonic age day 16 (E16) and plated in 6-well dishes for treatment. After 8hrs of treatment, RNA was extracted, and a cDNA library was created using adapter sequences for RNAseq.

Drug Name	Drug #	Z-score	Final Dose (µM)
MBNL1 (upregulation)			
Aminophylline	8	4	90.00
Nilotinib	133	2.18	10.00
MBNL2 (upregulation)			
Dexamethasone	25	5.26	0.50
Betamethasone	51	3.18	0.40
Aprepitant	88	3.81	2.00
Cyproheptadine	89	3.72	0.10
Sulfamethoxazole	185	3.27	200.00
Theophylline	186	3.34	80.00
Ciprofibrate	251	3.02	50.00

(A)

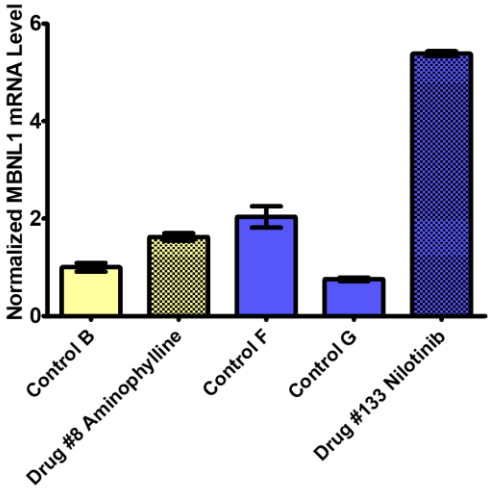

(B)

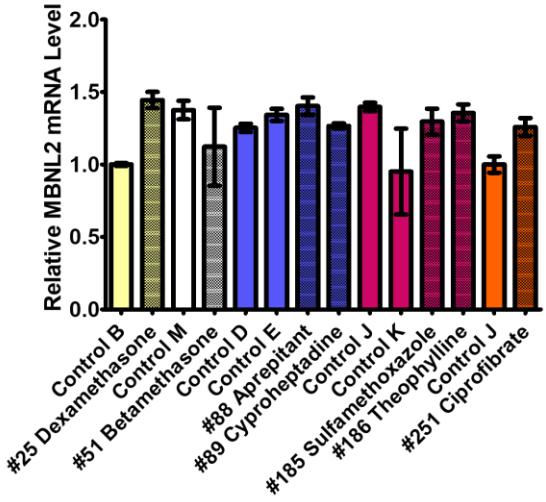

(C)

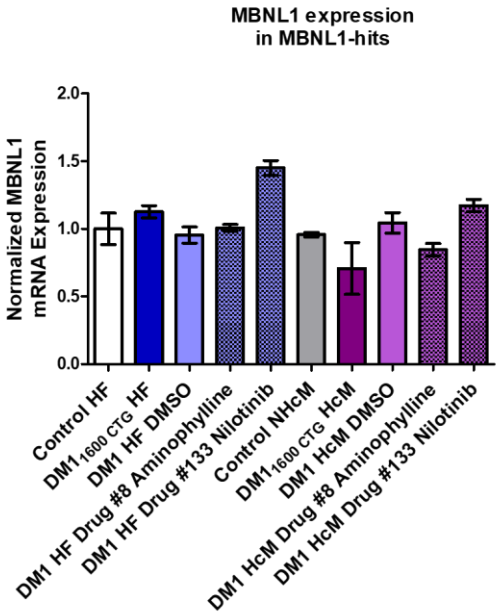

(Figure 4.1 continued on next page)

(D)

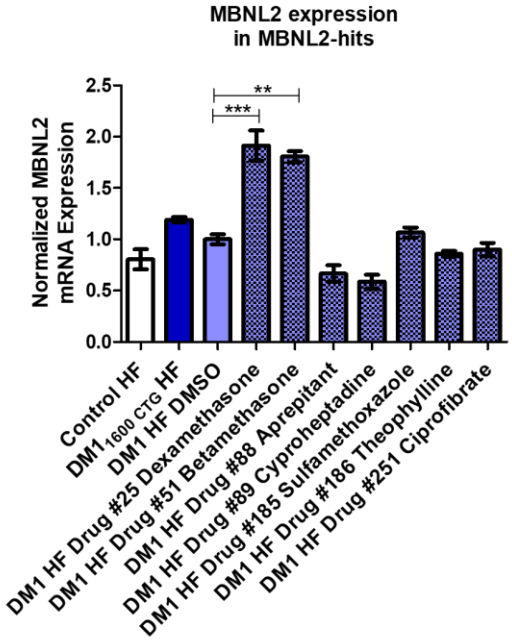

(E)

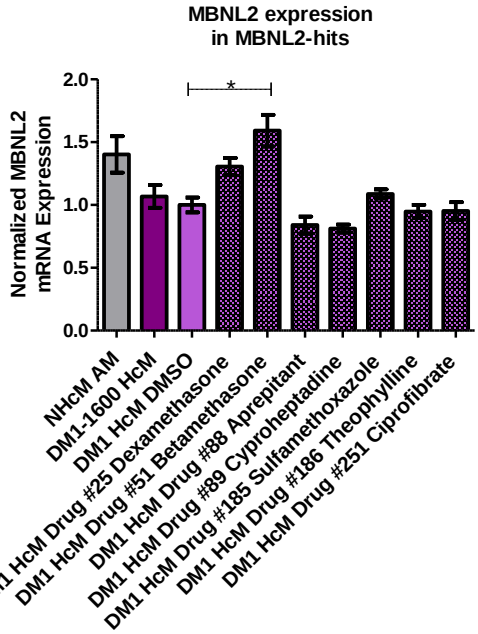

(F)

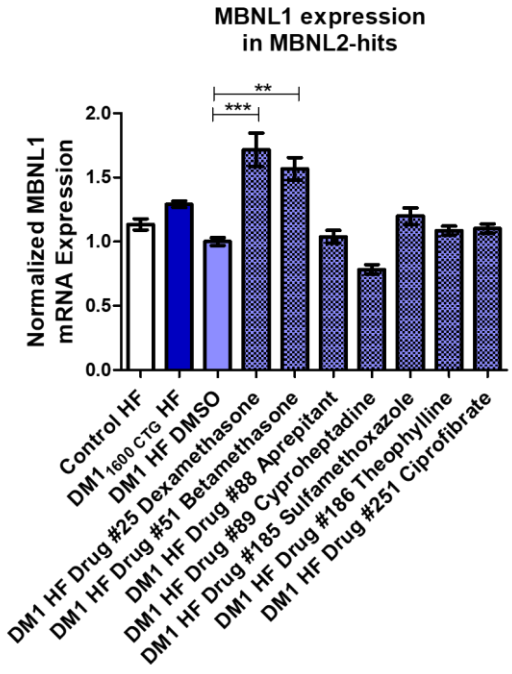

(G)

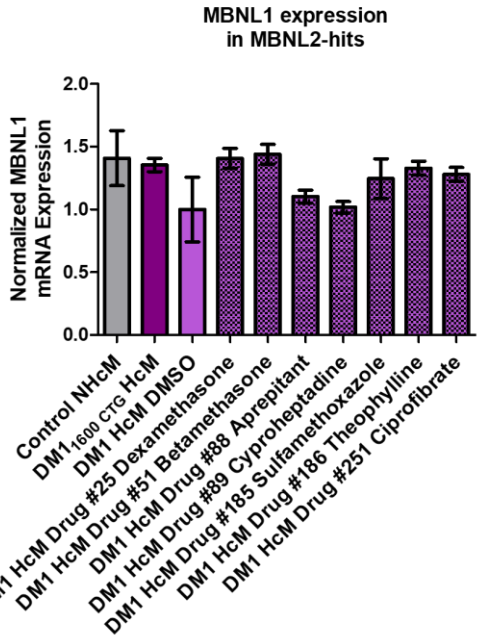

Figure 4.1. Validation of MBNL1 and MBNL2 mRNA upregulation in mouse neurons and DM1 patient cells containing 1600 CUG repeats, referred to as $DM1_{1600CTG}$. (A-B) Mouse neurons were harvested at embryonic age day 16 (E16) and plated in 6-well dishes for treatment. After 8hrs of treatment, RNA was extracted, and converted to cDNA by reverse transcription. MBNL1 and MBNL2 levels were checked in samples identified as upregulators of the respective proteins

as outlined in Table 4.1. (C-G) DM1 patient fibroblasts were plated in duplicate sets in 6-well cell culture dishes. One set was converted to a myoblast-like lineage by MyoD overexpression using lentiviral transduction. The converted cells were then selected for using puromycin for 5-7 days. Both the human fibroblast (blue; HF) and human converted myoblast (purple; HcM) cell lines were treated for 8hrs. Treatment sets were grouped by drugs that induced MBNL1 or MBNL2 expression according to Table 1 and each group had its own set of controls (unaffected control cells with no treatment, Control HF or Control HcM; patient cells with no treatment, $DM1_{1600\ CTG}$ HF or $DM1_{1600\ CTG}$ HcM; and patient cells treated with DMSO vehicle, DM1 HF DMSO or DM1 HcM DMSO). RNA was extracted and converted to cDNA for mRNA expression analysis by qPCR. Treatment samples were checked for over-expression of the (C-E) respective MBNL genes from Table 1 RNAseq hits and (F-G) cross-checked for over-expression of MBNL1 in MBNL2 hits; MBNL2 overexpression in MBNL1 hits were not tested. (n=2, one-way ANOVA; error bars represent SEM). *$P < 0.05$, **$P < 0.01$, ***$P< 0.001$

Ciprofibrate (3-fold) (Figure 4.1F-G). Compared to these effects on MBNL1 upregulation, none of the compounds were able to induce MBNL2 beyond the 30% induction from ciprofibrate treatment.

These compounds were further tested in DM1 human fibroblasts and converted myoblasts, which are more disease and species-relevant models. A maximum 50% induction of MBNL1 mRNA in samples treated with Nilotinib (Figure 4.1C), Betamethasone and Dexamethasone (Figure 4.1F) was observed exclusively in fibroblasts. There was up to 2-fold induction of MBNL2 mRNA in samples treated with betamethasone and dexamethasone (Figure 4.1D) in fibroblasts and, to a lesser extent, in converted myoblasts (Figure 4.1E). Nilotinib was the only compound to partially correct SERCA1 splicing in both fibroblasts and converted myoblasts and to only a modest, statistically non-significant level (Figure 4.2). Subsequent testing *in vivo* for mice treated orally with aminophylline or nilotinib revealed no increase in MBNL1 or MBNL2 in skeletal muscle (Figure 4.3). In fact, aminophylline appeared to reduce MBNL1 mRNA *in vivo.* Due to variability in efficacy in non-neuronal models and a lack of access to a neuronal model of DM1, further testing was discontinued.

(A)

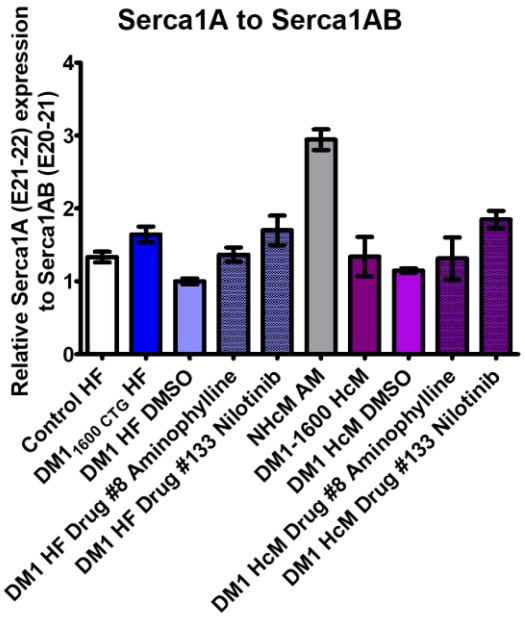

(B)

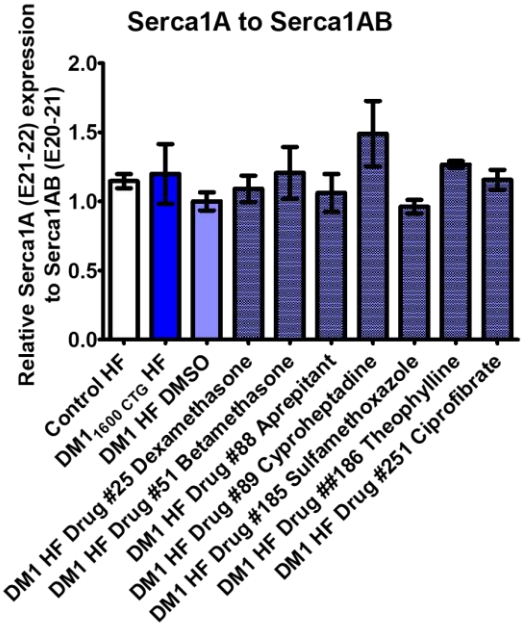

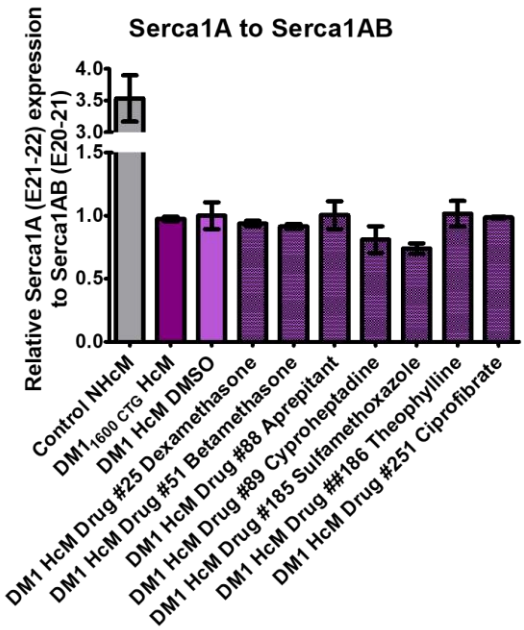

(Figure 4.2 continued on next page)

Figure 4.2. Nilotinib increased relative SERCA1-A transcript in both patient fibroblasts and converted myoblasts. DM1 patient fibroblasts were plated in duplicate sets in 6-well cell culture dishes. One set was converted to a myoblast-like lineage by MyoD overexpression using lentiviral transduction. The converted cells were then selected for using puromycin for 5-7 days. Both the human fibroblast (blue; HF) and human converted myoblast (purple; HcM) cell lines were treated for 8hrs. Treatment sets were grouped by drugs that induce MBNL1 or MBNL2 expression according to Table 1 – (A) MBNL1 inducers and (B) MBNL2 inducers – and each group had its own set of controls (unaffected control cells with no treatment, Control HF or Control HcM; patient cells with no treatment, $DM1_{1600\ CTG}$ HF or $DM1_{1600\ CTG}$ HcM; and patient cells treated with DMSO vehicle, DM1 HF DMSO or DM1 HcM DMSO). RNA was extracted and converted to cDNA for mRNA expression analysis by qPCR. (n=2, one-way ANOVA; error bars represent SEM). *$P < 0.05$, **$P < 0.01$, ***$P< 0.001$

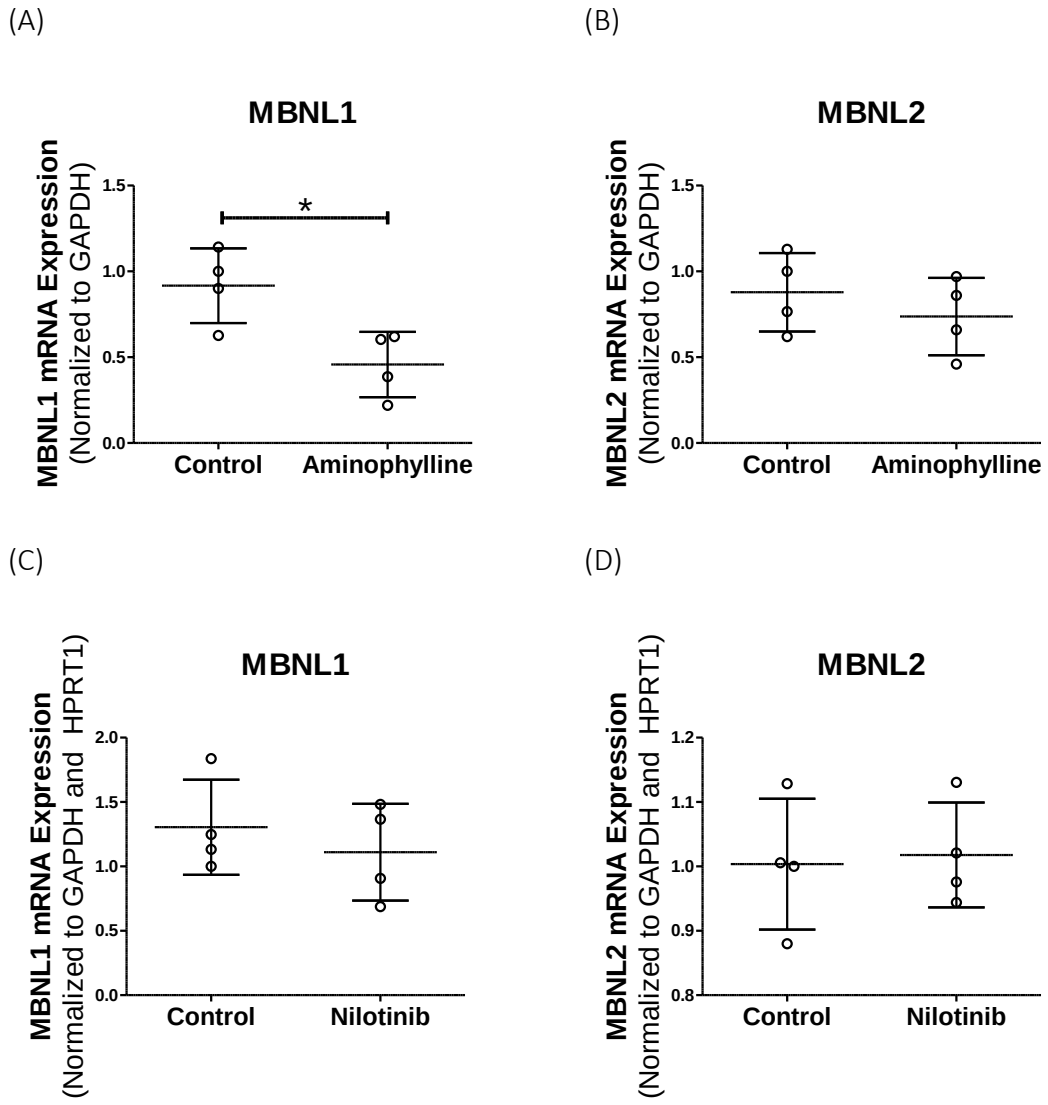

Figure 4.3. Aminophylnine and Nilotinib did not increase MBNL mRNA levels *in vivo.* Mice were treated (A-B) by i.p. injections of vehicle or 10mg/kg aminophylline, or (C-D) by oral gavage of vehicle or 25mg/kg nilotinib for 8 days. Skeletal muscle was homogenized in Qiazol using a tissue homogenizer and RNA was extracted using the RNeasy mini kit (Qiagen). RNA was converted to cDNA (Biorad, iScript Advanced cDNA synthesis kit) and (A, C) MBNL1 and (B, D) MBNL2 were quantified using RT-qPCR, normalized to GAPDH and HPRT1. (n=4, unpaired t-test; error bars represent SD). *$P < 0.05$, **$P < 0.01$, ***$P< 0.001$

4.3.2 Immortalized DM1 patient myoblasts contained distinct nuclear CUG foci and hallmark aberrant splicing traits.

Following the low yield of effective compounds from patient fibroblast-based screens and neuronal screens of cells from non-DM1 and non-human lineages, it was important to establish a more disease-relevant model of DM1 for further screening. As such, patient myoblasts were investigated. Pantic *et al* immortalized two patient DM1 myoblast cell lines, which were made available through the Euro Biobank. Although originally reported to have greater than 500 CTG repeats (Pantic et al. 2016), our southern blotting analysis established that these cells contained approximately 3600 ($DM1_{3600CTG}$) and 3300 ($DM1_{3300CTG}$) CTG repeats (Figure 4.4A). RNA FISH showed DM1 patient myoblasts, and not unaffected control myoblasts, uniquely had detectable nuclear CUG-foci (Figure 4.5B-C); in addition, differentiated DM1 cells (Figure 4.4C) had approximately 3 times more foci than proliferative DM1 myoblasts (Figure 4.4B). This was in line with greater expression of DMPK mRNA in differentiated versus proliferative myoblasts (Supplementary Figure 4.1). Proliferative DM1 myoblasts had mild dysregulation of SERCA1 splicing, a classic feature of DM1; this spliceopathy was more pronounced in differentiated myoblasts (Figure 4.4D).

4.3.3 FDA-approved drug screen in DM1 myoblasts identified bortezomib, vorinostat, and gemcitabine as potential therapeutic candidates.

Differentiated myoblasts had more foci than proliferative myoblasts, allowing for more sensitive detection in changes and thus were used for the screen. In addition, differentiated

(A)

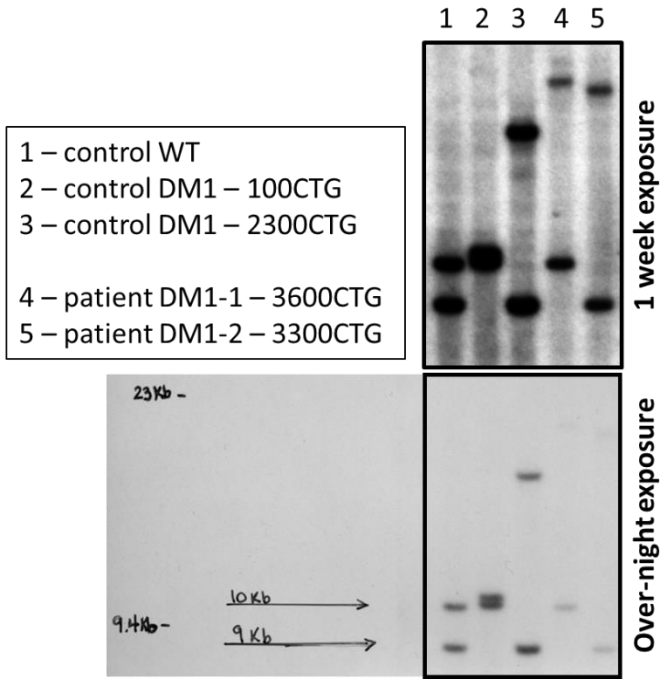

(B)

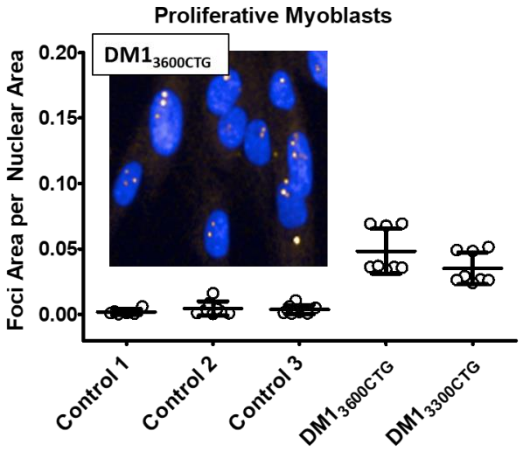

(C)

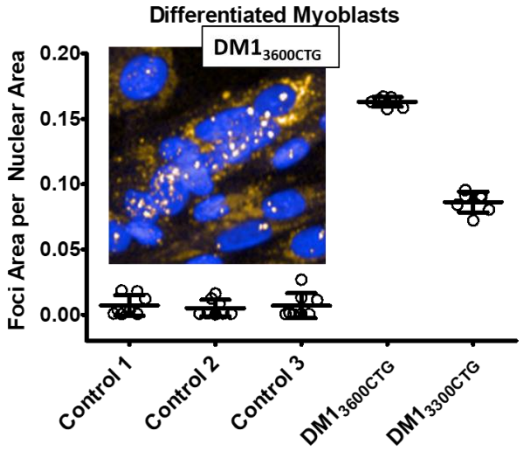

(Figure 4.4 continued on next page)

(D)

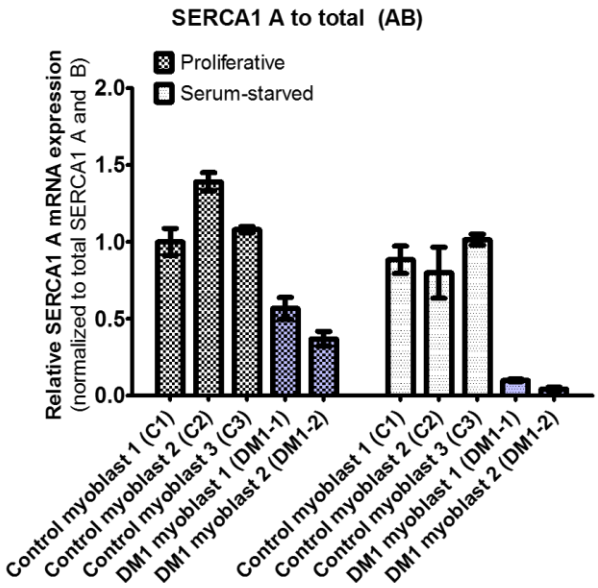

Figure 4.4. DM1 myoblasts contained 3000+ CTG repeats, had intranuclear CUG-foci and had SERCA1 spliceopathy. (A) Southern blot analysis of genomic DNA extracted from two immortalized DM1 myoblasts. (B) RNA FISH for the analysis of intranuclear CUG-foci. Cells were grown and/or differentiated for 7 days in a 384-well plate (n=7) and fixed with 4% PFA. DNA was stained with Hoechst and CUG RNA foci were probed by Alexa555-$(CAG)_{10}$ oligonucleotide probe. Average foci area per nuclear area is presented from (B) proliferative myoblasts growing in Ham's F14 complete growth media containing 30% FBS or (C) differentiated myoblasts serum-starved in Ham's F14 growth media supplemented with 1% horse-serum. (D) RT-qPCR analysis of SERCA1 spliceopathy in proliferative and differentiated myoblasts. DM1-1 cells are $DM1_{3600\ CTG}$ and DM1-2 cells are $DM1_{3300\ CTG}$.

$DM1_{3600CTG}$ myoblasts, which had more foci and greater spliceopathy than $DM1_{3300CTG}$ myoblasts, were chosen as the screening model. DMPK ASO (ISIS486178, Ionis Pharmaceuticals) was used as a positive control for foci reduction; there was a 30% reduction in CUG-foci with 20nM DMPK ASO compared to control ASO and no change in nuclei count (Supplementary Figure 4.2). The Z-prime factor, reflecting the degree of separation between positive and negative controls, can be used to validate a screening assay (Zhang, Chung, and Oldenburg 1999). Typically, Z'-factor between 0-0.5 is acceptable, between 0.5-1 is excellent, and 1 is ideal. In this regard, the Z'-factor for foci area per nuclear area was 0.84 when comparing the DMPK ASO and vehicle treated cells, indicating an "excellent" assay.

All the compounds in the FDA-approved small-molecule screen were assayed at a final concentration of 2µM. $DM1_{3600CTG}$ myoblasts were differentiated for 7days, treated for 24hrs in triplicate plates and fixed in 4% PFA. DNA was stained with Hoechst and CUG_n RNA foci were detected with Alexa555-$(CAG)_{10}$ oligonucleotide probe; cells were imaged using the Opera high content screening system and analysed by Columbus software. Due to clustering of nuclear foci and thus difficulties discerning individual foci within a nucleus, the aggregate area subtended by all foci per nuclear area was measured instead. Each assay plate was internally normalized to DMSO control data and the relative fold change to DMSO was averaged. Any treatment which reduced foci content by 30% or greater were "hits" to be further studied in secondary validation; a 30% threshold was set based on the effects of the DMPK ASO. To avoid toxic compounds, any treatment that resulted in 50% or greater reduction in nuclei were omitted from the hit list. Using these metrics, Vorinostat, an HDAC-inhibitor; gemcitabine, a

deoxycytidine nucleoside; and bortezomib, a proteasome inhibitor, were identified as potential foci-shrinkers (Figure 4.5).

The top three hits, bortezomib, vorinostat and gemcitabine, were next tested in both DM1 myoblast cell lines at a range of drug concentrations. Bortezomib had small reductive impact on foci in only one cell line and also proved to be cytotoxic at higher doses (Figure 4.6A-B). Treatment with vorinostat showed a dose-dependent decrease in foci area per nuclear area in both $DM1_{3600CTG}$ and $DM1_{3300CTG}$ differentiated myoblasts, starting at 0.5uM (Figure 4.6C). This reduction increased up to 10uM at which point toxicity, as indicated by the lower nuclei count, supervened (Figure 4.6D). Similar to vorinostat, gemcitabine also reduced foci in a dose-dependent manner (Figure 4.6E) and was relatively non-toxic (Figure 4.6F).

4.3.4 Vorinostat (SAHA), but not gemcitabine, rescued SERCA1 spliceopathy.

Vorinostat was found to reduce DMPK mRNA levels, as measured by RT-qPCR (Figure 4.7A). This effect was not seen with a low dose of 0.1uM, which also did not reduce foci (Figure 4.6C); the reduction in DMPK mRNA was observed at both a non-toxic concentration of 1uM and a high/toxic concentration of 10uM. This data suggests that vorinostat might reduce foci by reducing DMPK mRNA. SERCA1 splicing was also assayed by RT-qPCR by measuring the relative SERCA1-A levels compared to total SERCA1-A and B. There was a partial, dose-dependent rescue of SERCA1-A (Figure 4.7B). Gemcitabine, in contrast, did not reduce DMPK mRNA (Figure 4.7C) and did not change SERCA1 splicing (Figure 4.7D); as such, gemcitabine was not pursued further.

(A)

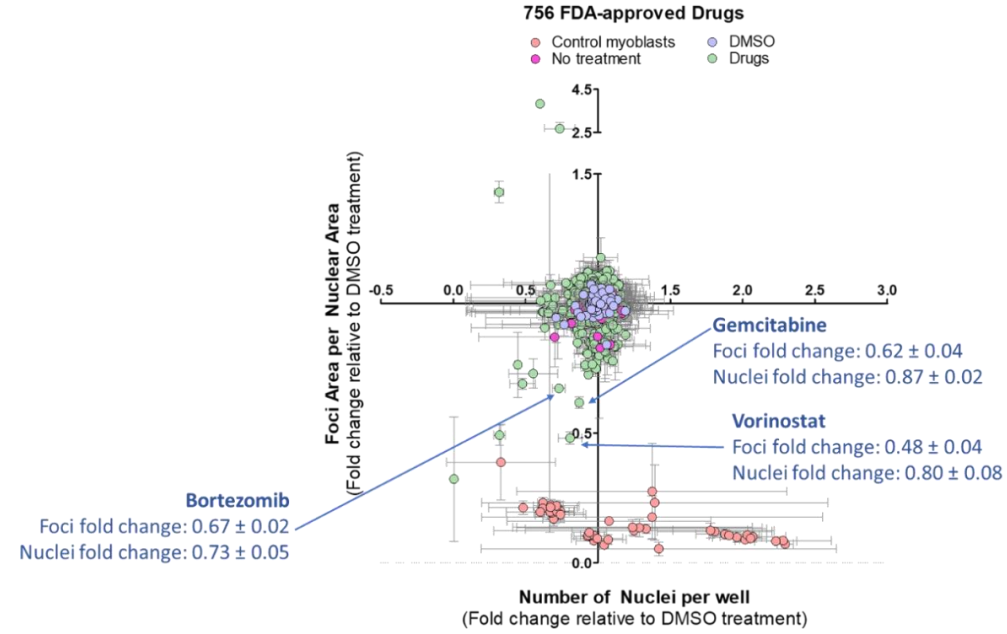

(B)

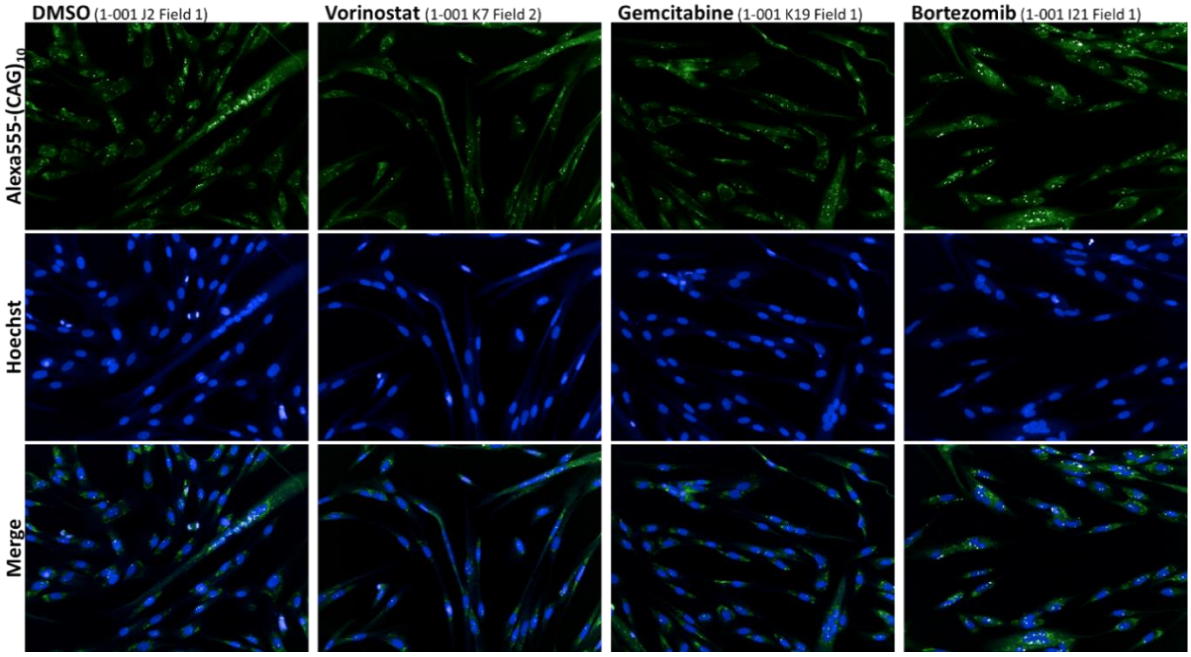

Figure 4.5. FDA small-molecule screen identified vorinostat, gemcitabine and bortezomib as potential down-regulators of CUG foci. $DM1_{3600CTG}$ myoblasts were serum-starved in 384-well plates for 7 days and treated with 2uM of drugs for 24hrs. Post-treatment, cells were stained with Hoechst for DNA and $Alexa555\text{-}(CAG)_{10}$ for CUG RNA foci. Foci area per nuclear area and number of nuclei per well were quantified using Columbus and normalized to DMSO control data per plate. (A) Data is presented as the average fold-change relative to DMSO treatment (n=3, error bars represent SD). (B) Representative images of top hits for small molecules which reduce foci. Full data set is summarized in Supplementary Table 4.1.

(A)

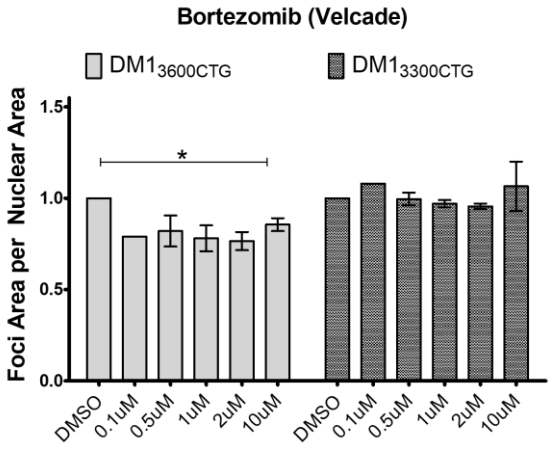

(B)

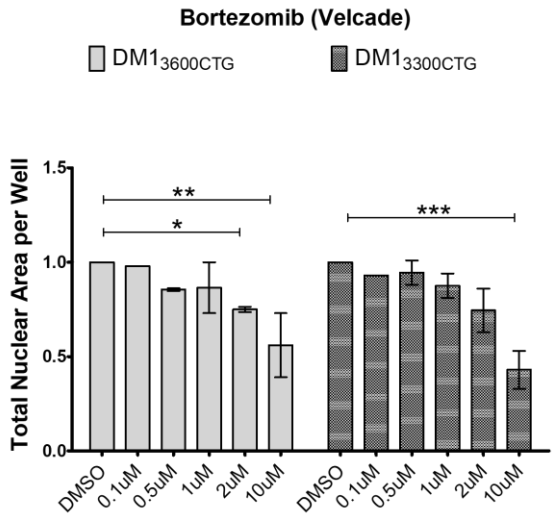

(C)

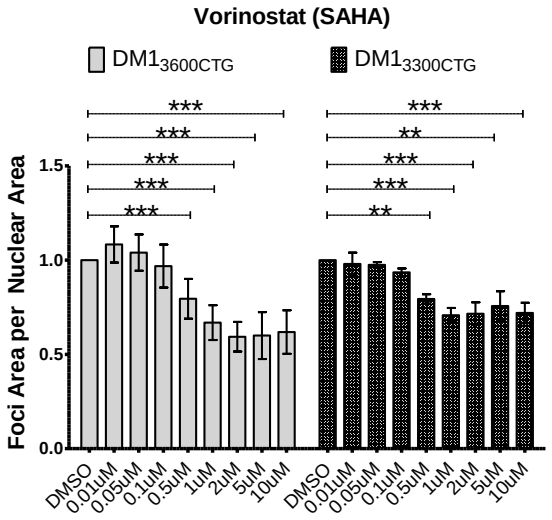

(D)

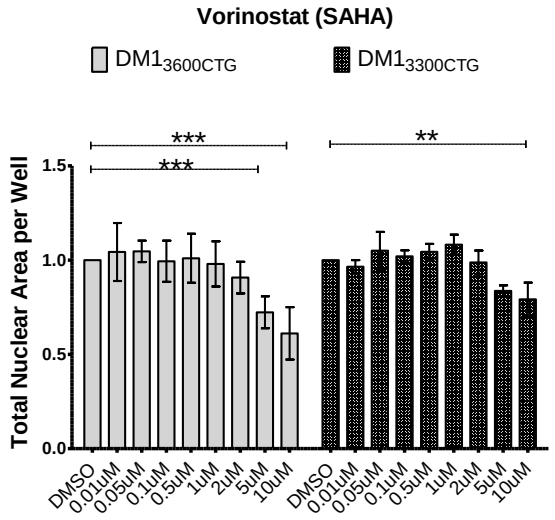

(Figure 4.6 continued on next page)

(E)

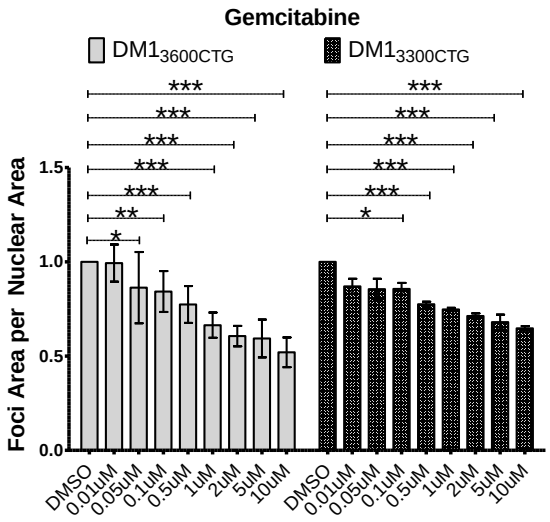

(F)

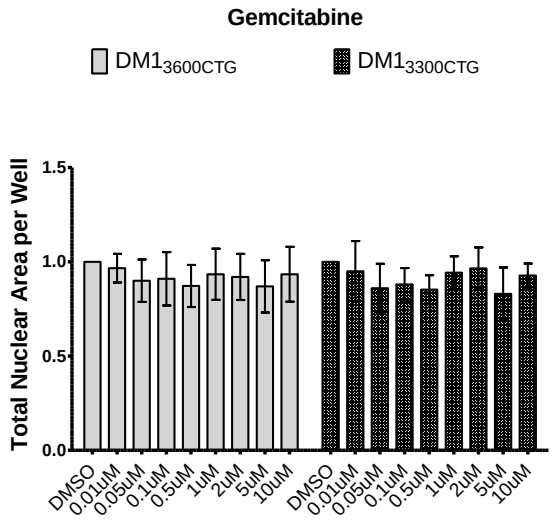

Figure 4.6. Bortezomib minimally reduced foci; vorinostat (SAHA) and gemcitabine reduced foci in both $DM1_{3600CTG}$ and $DM1_{3300CTG}$ differentiated myoblasts. $DM1_{3600CTG}$ and $DM1_{3300CTG}$ myoblasts were serum-starved in 384-well plates for 7 days and treated with 0.1-10uM of (A-B) bortezomib, (C-D vorinostat (SAHA), and (E-F) gemcitabine. Post-treatment, cells were fixed with 4% PFA, DNA was stained with Hoechst and CUG RNA foci were probed by Alexa555-$(CAG)_{10}$ fluorescent oligo. (A, C, E) Foci area per nuclear area and (B, D, F) total nuclear area per well (to assess treatment-associated toxicity) were quantified using Columbus and normalized to DMSO control; data is presented as fold-change relative to DMSO treatment (n ranges from 1 (for Bortezomib 0.1µM) to 8, two-way ANOVA ; error bars represent SD). *$P < 0.05$, **$P < 0.01$, ***$P< 0.001$

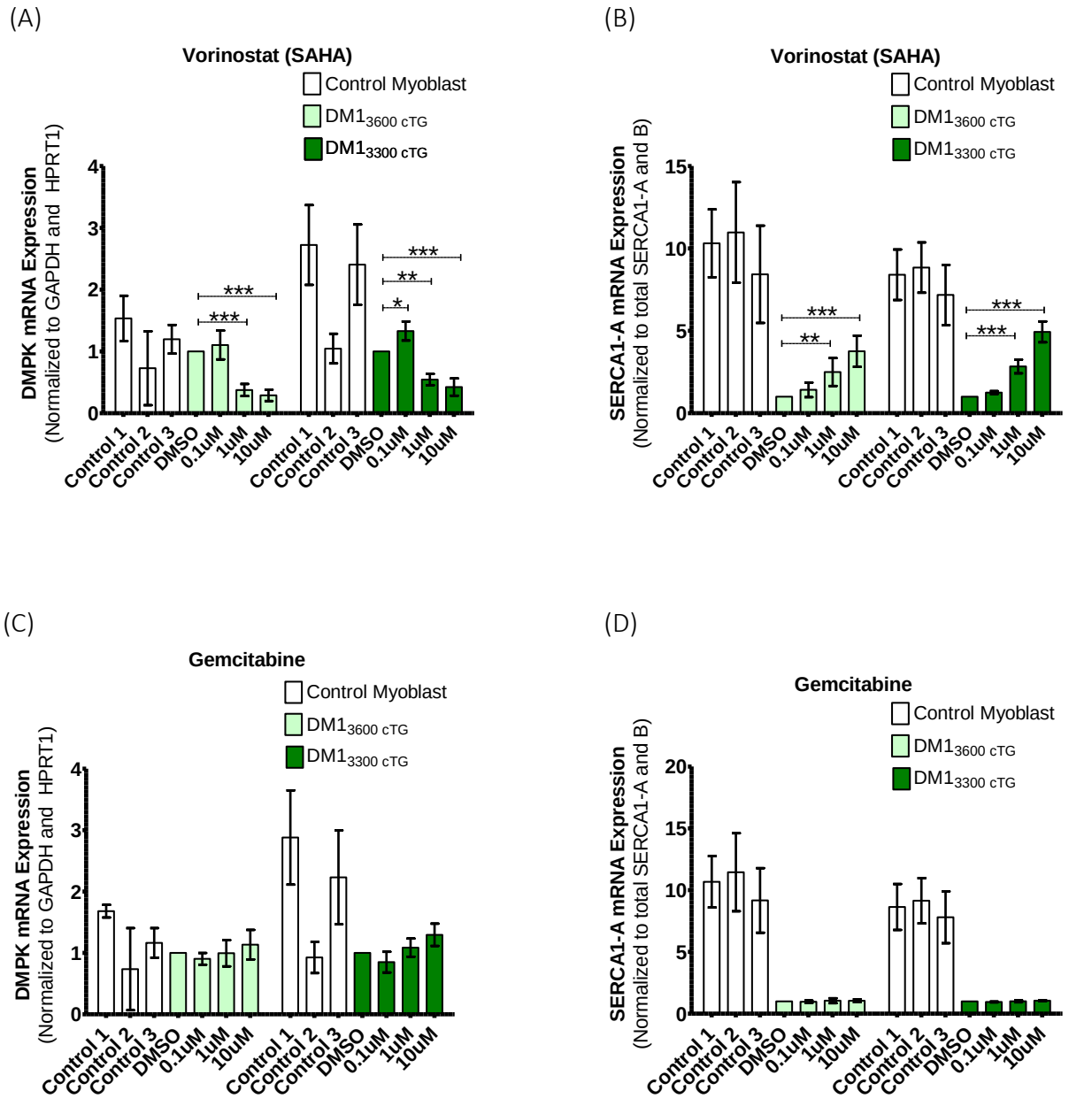

Figure 4.7. Vorinostat (SAHA), but not gemcitabine, reduced DMPK mRNA levels and rescued SERCA1-A splice product in both $DM1_{3600CTG}$ and $DM1_{3300CTG}$ differentiated myoblasts. Control, $DM1_{3600CTG}$ and $DM1_{3300CTG}$ myoblasts were serum-starved in 6-well plates for 7 days. DM1 cells were treated with DMSO alone or 0.1, 1 or10uM of (A-B) vorinostat (SAHA) or (C-D) gemcitabine; control myoblasts were treated with DMSO and used for baseline quantification in unaffected cells. RNA was extracted (RNeasy micro kit, Qiagen) and reverse-transcribed to cDNA (iScript Advanced RT kit, Biorad). RT-qPCR was performed (iQ Sybr green supermix, Biorad) to assess mRNA levels (n=6, two-way ANOVA; error bars represent SD). *P < 0.05, **P < 0.01, ***P< 0.001

Pfizer has also independently documented that vorinostat mediated upregulation of MBNL1 protein in a flow-cytometry-based screen assessing GFP-tagged MBNL1 expression in artificial HeLa cell models of expanded-CTG-repeats and DM1 fibroblasts (Zhang et al., 2017). As such, we assessed the MBNL1 protein content in differentiated DM1 myoblasts (Figure 4.8). Vorinostat increased MBNL1 protein in $DM1_{3600CTG}$ myoblasts by up to 2.5-fold but only minimally affected MBNL1 in $DM1_{3300CTG}$ myoblasts. In $DM1_{3600CTG}$ myoblasts, there was no change in MBNL1 protein with a 0.1uM dose, a 1.5-fold increase with a 1uM dose and a 2.5-fold increase with a 10uM dose. It is possible that the induction in MBNL1 protein plays a role in the observed normalization of SERCA1 spliceopathy. Interestingly, and in contrast to the protein, vorinostat reduced MBNL1 transcript level (Figure 4.8C).

4.3.5 Pan-HDAC inhibition is involved in modulating DM1 pathogenic features.

In order to assess whether the vorinostat-mediated normalization of DM1 cellular phenotypes is a result of panHDAC inhibition or an off-target effect, we assessed two other pan-HDAC inhibitors which function similarly to vorinostat; belinostat and trichostatin A (TSA) were used to treat both proliferative and differentiated DM1 myoblasts. As seen in Figure 4.9, belinostat (Figure 4.9A-B) decreased foci in both cell lines in a dose-dependent manner similar to vorinostat; TSA reduced foci but with a higher-degree of variability and had the highest cellular toxicity at lower doses. Together, this suggests a role for panHDAC inhibition in foci reduction. These additional HDAC inhibitors also reduced DMPK mRNA and corrected SERCA1 splicing (Figure 4.10). DMPK mRNA was also reduced in control myoblasts by all three inhibitors, suggesting a DM1-independent mechanism (Supplementary Figure 4.3).

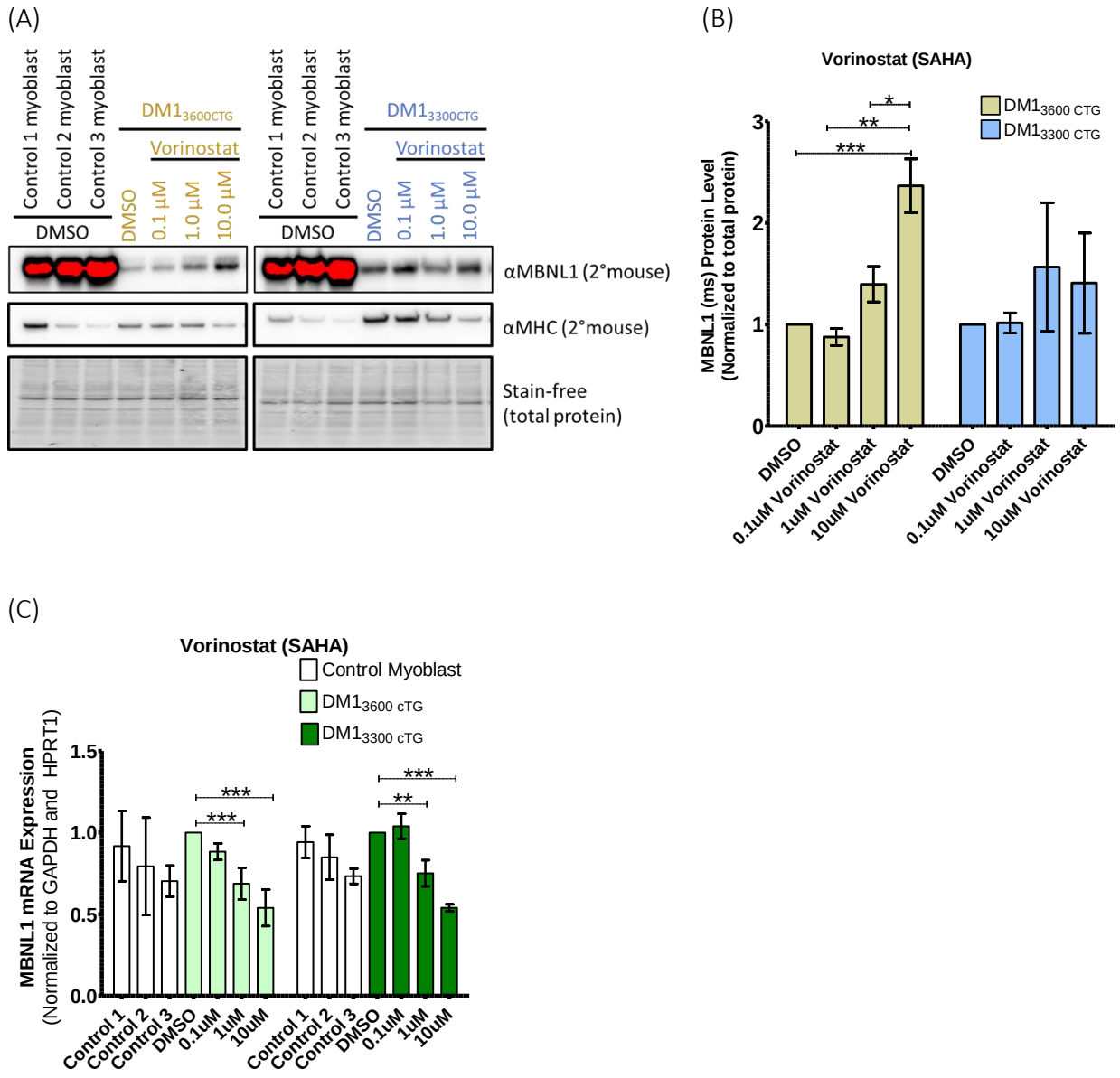

Figure 4.8. Vorinostat increased MBNL1 protein in $DM1_{3600CTG}$ differentiated myoblasts but decreased MBNL1 mRNA. (A-B) $DM1_{3600CTG}$ and $DM1_{3300CTG}$ myoblasts were serum-starved in 6cm plates for 7 days and treated with DMSO alone or 0.1, 1 and 10uM of vorinostat (SAHA). 24hr post-treatment, cells were trypsinized and extracted for protein using RIPA lysis buffer for western blot analysis. (A) Western blot images; (B) quantification of MBNL1 protein normalized to total protein and presented as fold-change relative to DMSO control (n=2; two-way ANOVA). (C) $DM1_{3600CTG}$ and $DM1_{3300CTG}$ myoblasts were serum-starved in 6-well plates or 6cm plates and treated with DMSO alone or 0.1, 1 and 10uM of vorinostat (SAHA). 24hr post-treatment, cells were lysed directly on plate (6-well plate) or trypsinized and the pellet lysed (6cm plate). RNA was extracted (RNeasy micro kit, Qiagen) and reverse-transcribed to cDNA (iScript Advanced RT kit, Biorad). RT-qPCR was performed (iQ Sybr green supermix, Biorad) to assess mRNA levels (n=6, two-way ANOVA; error bars represent SD). *P < 0.05, **P < 0.01, ***P< 0.001

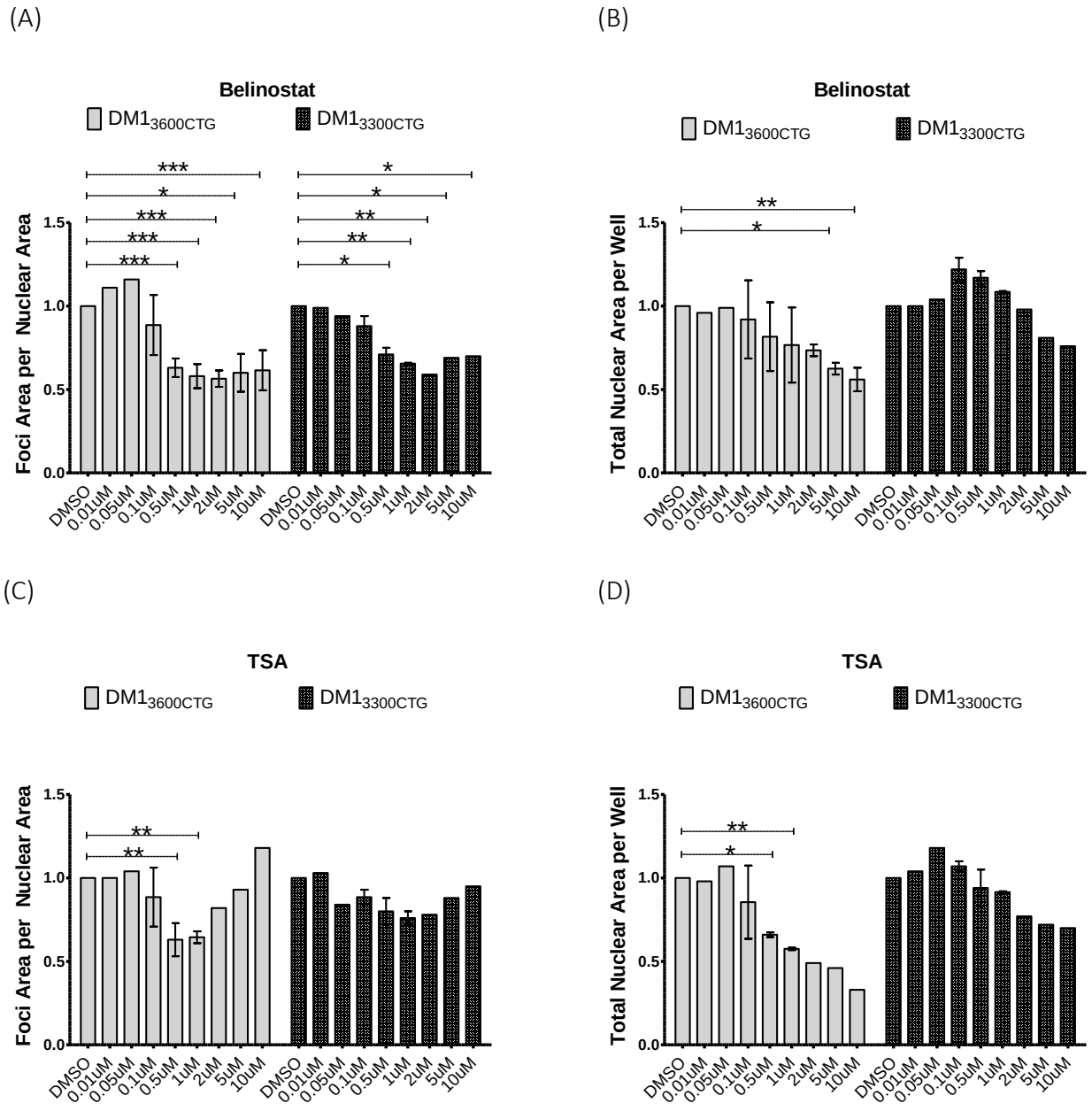

Figure 4.9. Two pan-HDAC inhibitors, belinostat and trichostatin A (TSA), were validated to reduce foci in differentiated DM1 myoblasts. $DM1_{3600CTG}$ and $DM1_{3300CTG}$ myoblasts were grown and/or serum-starved in 384-well plates for 7 days and treated with DMSO alone or 0.01, 0.05, 0.1, 0.5, 1, 2, 5 and 10uM of HDAC inhibitor. 24hr post-treatment, cells were fixed with 4% PFA, DNA was stained with Hoechst and CUG RNA foci were probed by Alexa555-$(CAG)_{10}$ fluorescent oligo. Foci area per nuclear area and total nuclear area per well (to assess treatment-associated toxicity) were quantified using Columbus and normalized to DMSO control; data is presented as fold-change relative to DMSO treatment (n ranges from 1 to 3, two-way ANOVA ; error bars represent SD). *P < 0.05, **P < 0.01, ***P< 0.001

(A) (B)

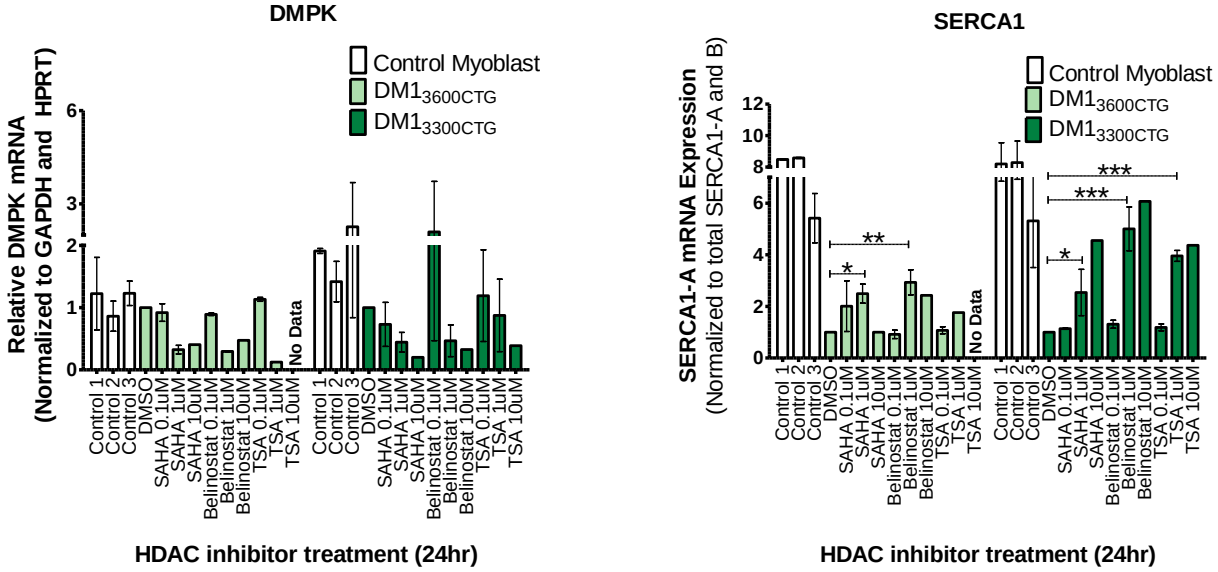

Figure 4.10. Pan-HDAC inhibitors, vorinostat (SAHA), belinostat and TSA, all reduced DMPK mRNA levels and rescued SERCA1-A splice product in both $DM1_{3600CTG}$ and $DM1_{3300CTG}$ differentiated myoblasts. $DM1_{3600CTG}$ and $DM1_{3300CTG}$ myoblasts were serum-starved in 6-well plates for 7 days. DM1 cellls were treated with DMSO alone or 0.1, 1 or10uM of vorinostat (SAHA), belinostat and TSA. RNA was extracted (RNeasy micro kit, Qiagen) and reverse-transcribed to cDNA (iScript Advanced RT kit, Biorad). RT-qPCR was performed (iQ Sybr green supermix, Biorad) to assess mRNA levels of (A) DMPK and (B) SERCA1 splicing. (n ranges from 1 to 2, two-way ANOVA; error bars represent SD). *$P < 0.05$, **$P < 0.01$, ***$P< 0.001$

In an effort to identify which HDAC or HDACs is/are involved in improving the DM1 phenotype, the four HDACs which are primary targets of vorinostat, belinostat and trichostatin A – HDACs 1, 2, 3, and 6 – were targeted for knock-down by siRNA-mediated mRNA degradation. Four siRNAs, alone and pooled, were used to target each HDAC. However, no reduction of a single HDAC or combination of up to all four HDACs resulted in foci reduction (Figure 4.11). siRNAs against HDACs 1, 2 and 6 were shown to knock down their respective proteins to varying degrees (Supplementary Figure 4.4); HDAC 3 siRNAs failed to have any knock-down effect at the protein level. This suggests either a central role for HDAC3, which remains to be effectively tested, involvement of other untested HDACs, or a more complex mechanism underpinning HDAC-mediated correction, possibly including non-HDAC mediators, whether directly or indirectly regulated by vorinostat, belinostat, or TSA. Regardless of the mechanism, the relative safety of vorinostat along with downregulation of foci and DMPK mRNA combined with MBNL1 upregulation and splicing normalization made it an ideal candidate for pre-clinical *in vivo* testing.

4.3.6 Vorinostat (SAHA) showed promising therapeutic effect in DM1 HSA^{LR} mouse model

A DM1 mouse model overexpressing 250 CTG repeats, driven by the human skeletal actin promoter (HSA^{LR}) was used; HSA^{LR} mice were given daily injections of vehicle or 50mg/kg vorinostat (SAHA) for 4 weeks. The mice were then sacrificed by lethal injection and cervical dislocation – skeletal muscle tissue from one hind leg was frozen in OCT for sectioning and

(A)

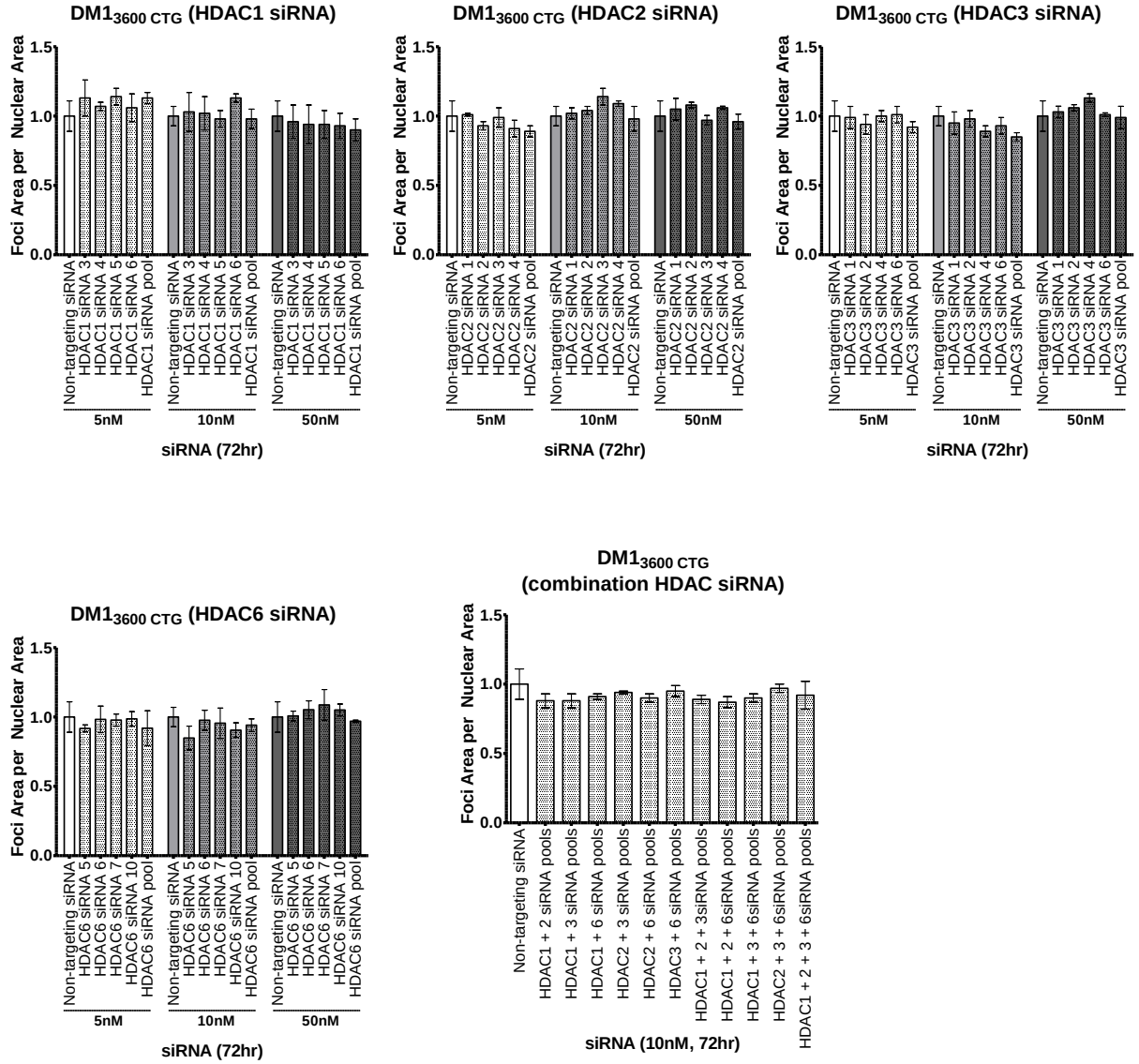

(Figure 4.11 continued on next page)

(B)

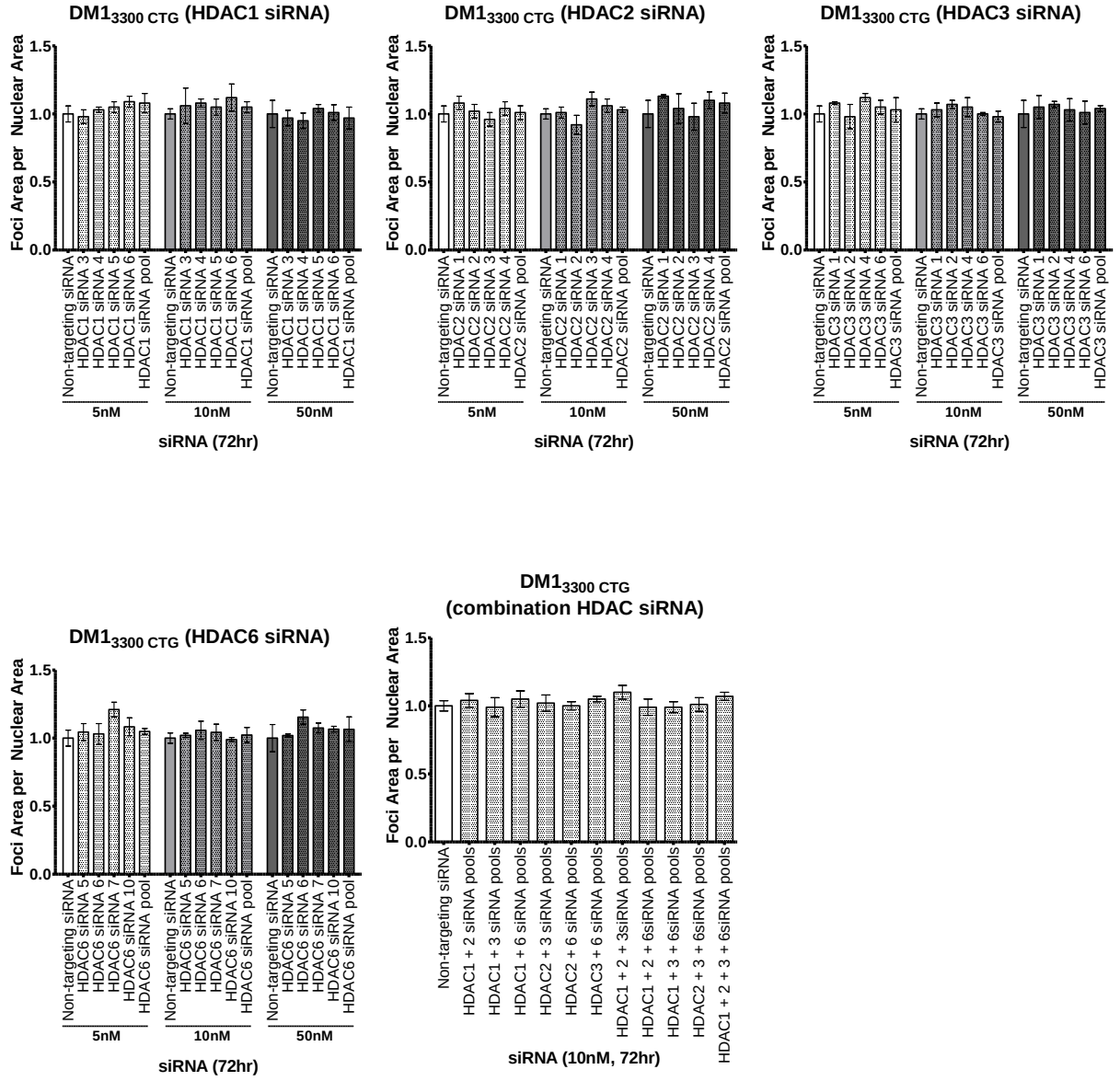

Figure 4.11. Deconvolution of pan-HDAC inhibitor targets (specific or combination HDAC siRNA treatments) did not recapitulate the robust effects on CUG-foci conferred by small-molecule pan-HDAC inhibitors. (A) $DM1_{3600CTG}$ and (B) $DM1_{3300CTG}$ myoblasts were serum-starved in 6-well plates for 7 days and non-targeting or HDAC siRNA were forward transfected using lipofectamine RNAi MAX. 72hr post-treatment, cells were fixed with 4% PFA, DNA was stained with Hoechst and CUG RNA foci were probed by Alexa555-$(CAG)_{10}$ fluorescent oligo. Foci area per nuclear area was quantified using Columbus and normalized to non-targeting siRNA control of the respective siRNA concentration; data is presented as fold-change relative to Non-targeting siRNA (n=1, average of triplicate wells, error bars represent SD between triplicate wells).

imaging while tissue from the other hind leg was flash frozen in liquid nitrogen for RNA workup. All experiments and workup were done by individuals blinded to the treatment regimen in keeping with *in vivo* study recommendations (Landis et al. 2012). The drug was well tolerated with no overt weight loss or other observable toxic effects (Supplementary Figure 4.5). Vorinostat treatment resulted in significant rescue of both dysregulated RYR1 splicing, which has been linked to muscle weakness (Kimura et al. 2005) as well as SERCA1 spliceopathy in TA muscle. Analysis of a third gene known to be misspliced, CLCN1, revealed no dysregulation in TA between wild-type and vehicle-treated DM1 mice (Figure 4.12A-B). While there was splicing correction in the EDL as well, the effects were more modest for RYR1 and SERCA1; however, CLCN1 spliceopathy was both present in vehicle-treated DM1 mice and corrected with vorinostat treatment in the EDL (Figure 4.12C-D). Histological analysis looking at central nucleation, a marker of muscle regeneration and an indicator of muscle damage, showed reduced central nucleation in TA muscle with vorinostat (SAHA) treatment but not in EDL (Figure 4.12E-F). Collectively, these data showed great promise towards a therapeutic outcome using vorinostat.

4.3.7 Chemogenomic screen using the CG3000 library in DM1 myoblasts further identified HDAC inhibitors as potential therapeutic candidates

Given the success of the FDA approved drug library screen, a second small-molecule library of chemogenomic compounds was screened for foci down-regulators in immortalized DM1 myoblasts. The chemogenomic library is designed to target roughly one thousand key pathways

with high specificity, acting in a way as a genetic screen as well as a small molecule screen (Jones and Bunnage 2017)

(A)

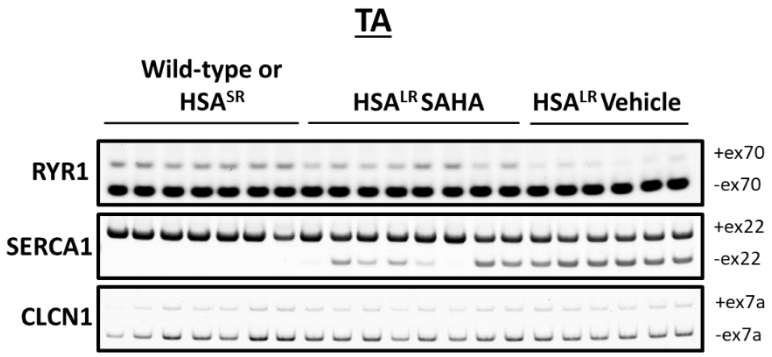

(B)

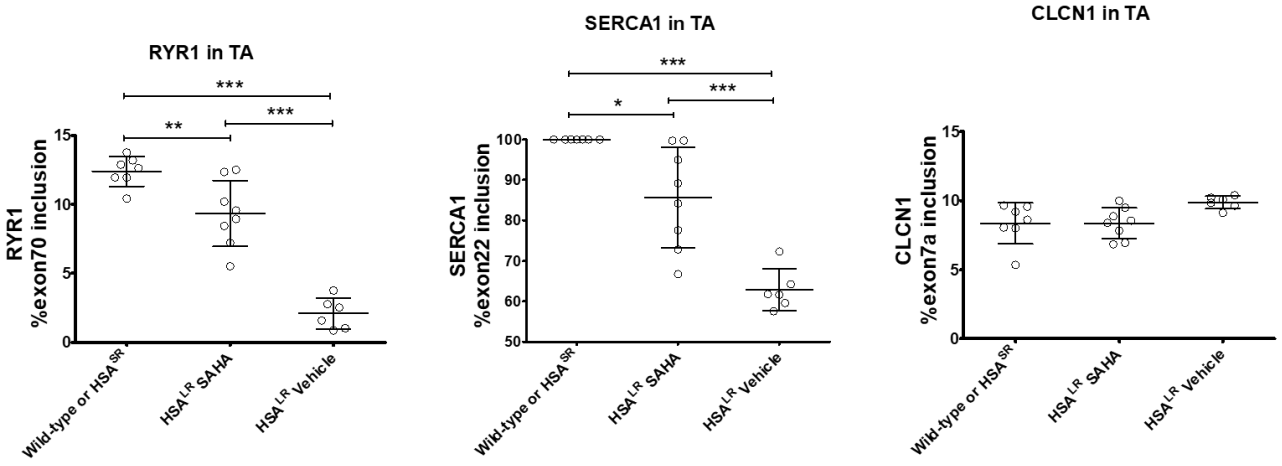

(C)

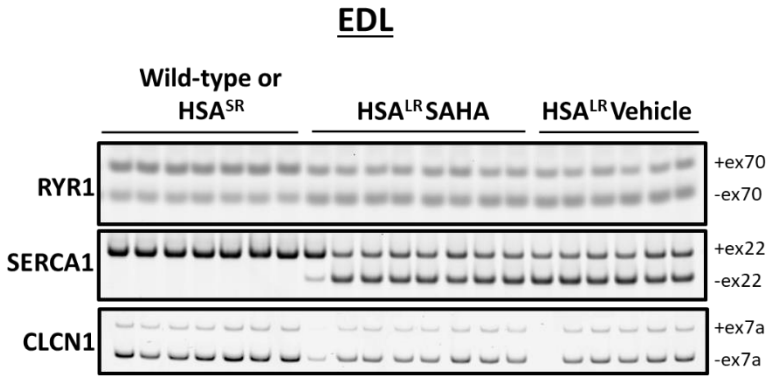

(Figure 4.12 continued on next page)

(D)

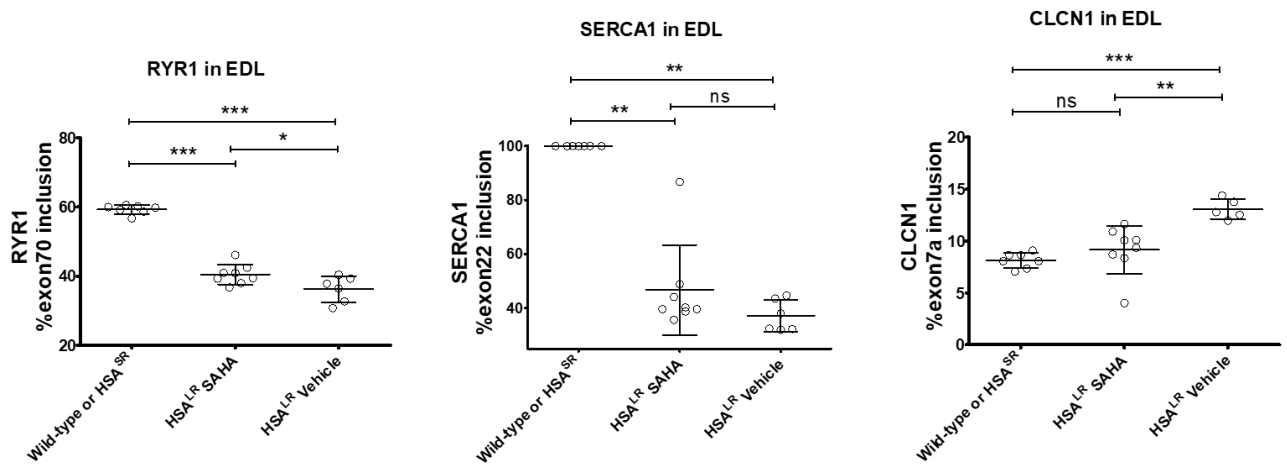

(E)

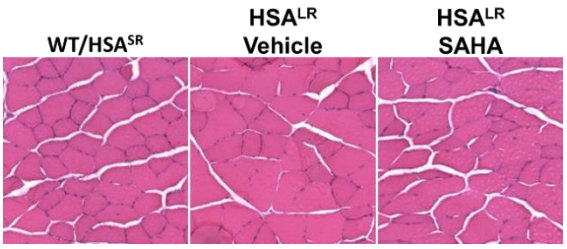

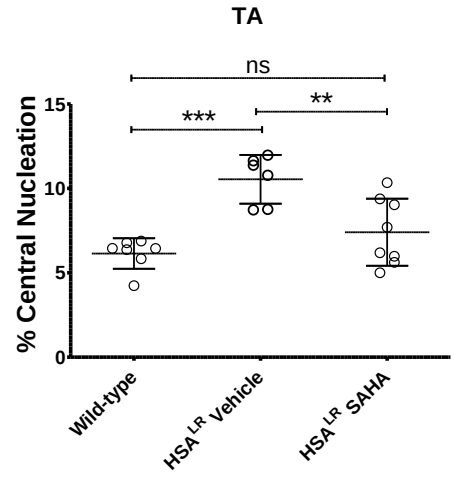

(F)

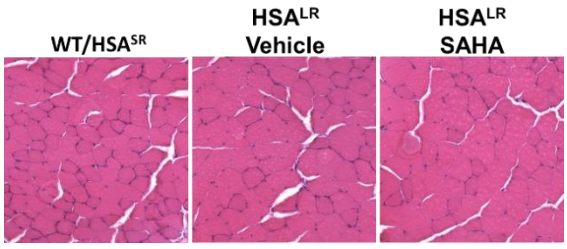

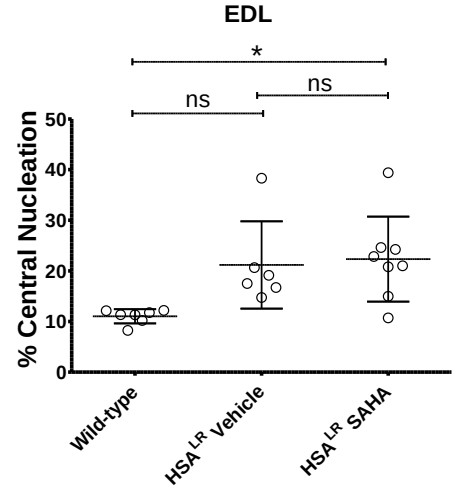

(Figure 4.12 continued on next page)

Figure 4.12. Vorinostat (SAHA) showed promising therapeutic effects in DM1 HSA^{LR} mouse model, with greater impact in TA than EDL. Mice at approximately 4 weeks of age were injected (IP) daily with vehicle or 50mg/kg vorinostat (SAHA) for 4 weeks. The mice were sacrifice by lethal injection and cervical dislocation. Skeletal muscle tissue from one hind leg was frozen in OCT for sectioning and imaging, and skeletal muscle tissue from the other hind leg was flash frozen in liquid nitrogen for RNA workup. (A-D) Analysis of DM1 related spliceopathy. Flash frozen tissue was ground to a powder and a portion used for Trizol RNA extraction using the Purelink RNA mini kit (Invitrogen) and reverse transcribed to cDNA (iScript Advanced RT kit, Biorad). RT-sqPCR products using cDNA from (A-B) TA and (C-D) EDL were resolved on 7% acrylamide gel, stained with Gel Red and imaged using the ChemiDoc (Biorad). Quantification of transcript ratios was done using ImageLab (Biorad). (E-F) Analysis of central nucleation in (E) TA and (F) EDL. Tissues flash frozen in OCT were sectioned at 10um thickness and subjected to H&E staining. Brightfield images were taken at 20x using EVOS cell imaging system and whole sections were manually counted for central nucleation. (n ranges from 6 to 8, two-way ANOVA; error bars represent SD). *$P < 0.05$, **$P < 0.01$, ***$P< 0.001$

The primary screen assessed de-identified drugs at 3uM. 91 leads were selected for a secondary screen at a 10-point dose curve – these candidates were selected based on at least a 30% or greater reduction in foci in the primary screen or a need for reassessment at a lower dose due to a high level of toxicity at the 3uM dose used in the primary screen (Figure 4.13A). At this stage, the targets of the compounds were unblinded, but the chemical names remained blinded (the numbers are drug batch #s and are used to identify the compounds). 28 compounds were ranked in the secondary screen for further validation, most of which showed efficacy for foci downregulation at high, off-target doses (Figure 4.13B). Of the 28 ranked compounds, 11 compounds were provided by Pfizer for other secondary validation studies. These 11 compounds were tested again for foci downregulation (Figure 4.14) and SERCA1 splicing rescue (Figure 4.15). Only three of the 11 compounds showed any change in SERCA1 splicing - compounds 24754357, 25778359, and 25778329 – which were de-blinded and found to be vorinostat (SAHA), Quisinostat, and Trichostatin A (TSA), all HDAC inhibitors, two of which we had already validated and are not just HDAC6-specific inhibitors as was categorized by Pfizer.

Quisinostat, a novel candidate resulting from the CG3000 screen, was ordered from a third party and tested for DMPK mRNA and SERCA1 splicing. Preliminary results show that, as with the other HDAC inhibitors, Quisinostat reduces DMPK mRNA and increases relative SERCA1-A. While this compound was in fact designed for HDAC1 inhibition, the IC 50 is only 0.11nM; it is more likely that quisinostat functions through pan-HDAC inhibition like SAHA, and not just HDAC1, especially given the high effective dose of 0.01uM (Figure 4.15). However,

given the low effective dose (0.0316uM) compared to the other panHDAC inhibitors, a dose at which the drug is not toxic (Figure 4.14A, drug 25778359), quisinostat may be as promising as vorinostat for *in vivo* therapeutic efficacy. Further validation steps are required to fully characterize this novel compound for potential DM1 therapeutics.

(A)

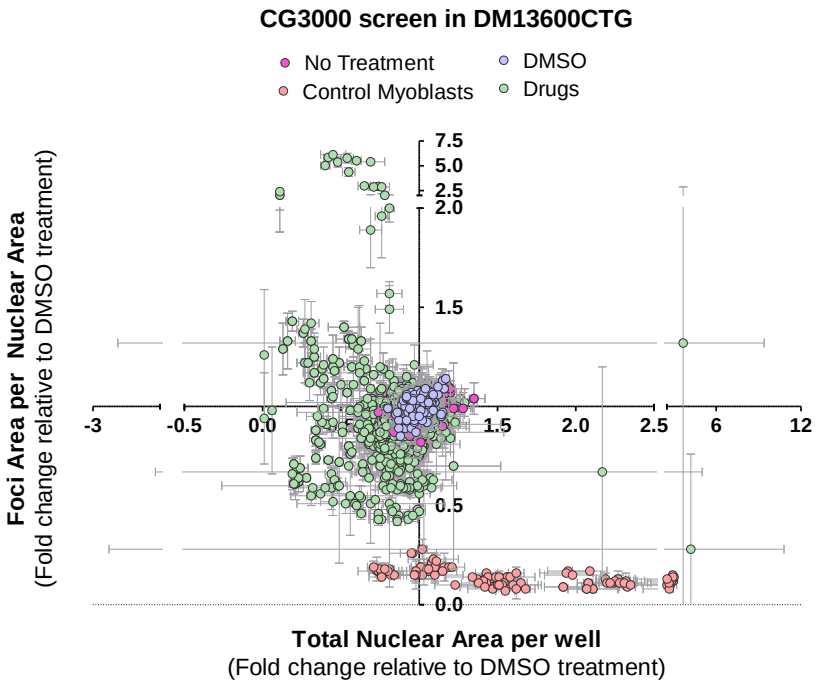

(B)

Priority Primary Targets (11)	
3703879	cyclin-dependent kinase 4 (CDK4)
6590247	cyclin-dependent kinase 7 (CDK7)
8519662	ATP-binding cassette, sub family G (WHITE), member 2 (ABCG2)
8633402	protein kinase N2 (PKN2)
8906013	IL2-inducible T-cell kinase (ITK)
20184860	nuclear factor, erythroid 2-like 2 (NFE2L2)
25284441	protein kinase C, epsilon (PRKCE)
25467904	rat bromodomain containing 4 (Brd4)
25778329	HISTONE DEACETYLASE 6
19379177	sirtuin 1 (SIRT1)
25778359	HISTONE DEACETYLASE 1

Potential Secondary Targets (9)	
2728378	cyclin D1 (CCND1)
2767650	cyclin-dependent kinase 2 (CDK2)
4324505	prostaglandin E receptor 1 (subtype EP1), 42kDa (PTGER1)
5968532	ATP-binding cassette, sub-family A (ABC1), member 1 (ABCA1)
18508130	protein kinase, AMP-activated, alpha 2 catalytic subunit (PRKAA2)
25082316	potassium intermediate/small conductance calcium-activated channel, subfamily N, member 2 (KCNN2)
25258500	prostaglandin E receptor 3 (subtype EP3) (PTGER3)
25360348	rat bromodomain containing 4 (Brd4)
20715417	histone deacetylase 2 (HDAC2)

Potential Tertiary Targets (8)	
14975536	mitogen-activated protein kinase kinase 6 (MAP2K6)
24103641	dopamine receptor D5 (DRD5)
121634	Methionine aminopeptidase non-specific
13922055	mitogen-activated protein kinase kinase kinase 8 (MAP3K8)
2727298	cyclin D1 (CCND1)
6096737	transferrin (TF)/PCSK9 secretion; ribosome binding scaffold
25778343	HISTONE DEACETYLASE 3
18913521	cyclin-dependent kinase 7 (CDK7)

(Figure 4.13 continued on next page)

Figure 4.13. CG3000 chemogenomic screen in differentiated $DM1_{3600CTG}$ myoblasts identified several new small-molecule regulators of CUG foci. $DM1_{3600CTG}$ myoblasts were serum-starved in 384-well plates and treated with of drugs (n=3) for 24hrs. Post-treatment, cells were fixed with 4% PFA, DNA was stained with Hoechst and CUG RNA foci were probed by Alexa555-$(CAG)_{10}$ fluorescent oligo. Foci area per nuclear area and total nuclear area per well (to assess treatment-associated toxicity) were quantified using Columbus and normalized to DMSO control data per plate. Data is presented as the average fold-change relative to DMSO treatment. (A) The primary screen was done using 3uM of drug, blinded. (B) List of drug "hits" after a secondary screen. 91 candidates selected for a secondary screen at a 10-point dose curve – these candidates were selected based on at least a 30% or greater reduction in foci in the primary screen or a need for reassessment at a lower dose due to a high level of toxicity at the 3uM dose used in the primary screen. At this stage, the targets of the compounds were unblinded, but the chemical names remained blinded (the numbers are drug batch #s and are used to identify the compounds). Of the 28 compounds ranked in the secondary screen, 11 compounds were provided by Pfizer for other secondary validation studies.

(A)

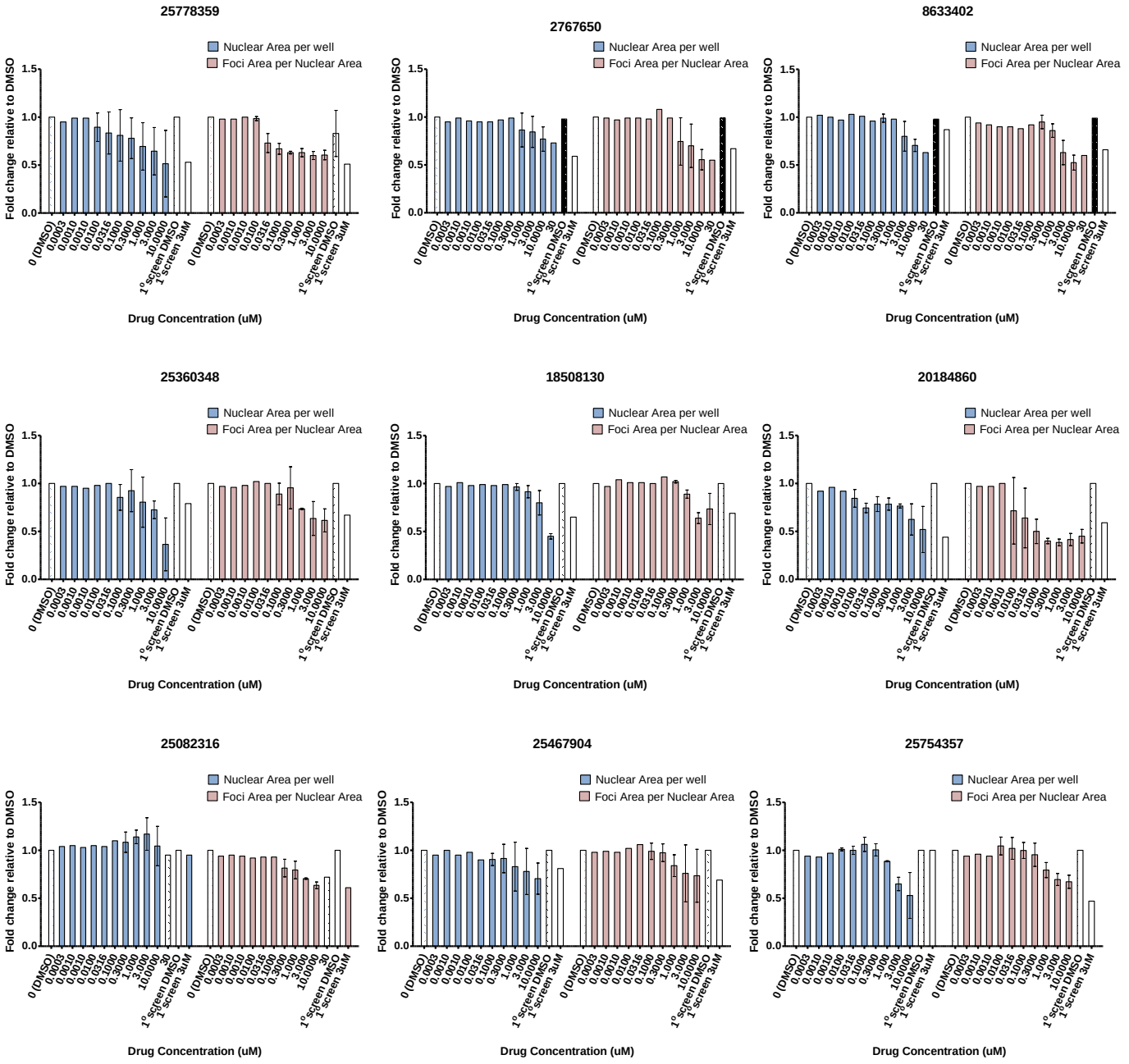

(Figure 4.14 continued on next page)

(A)

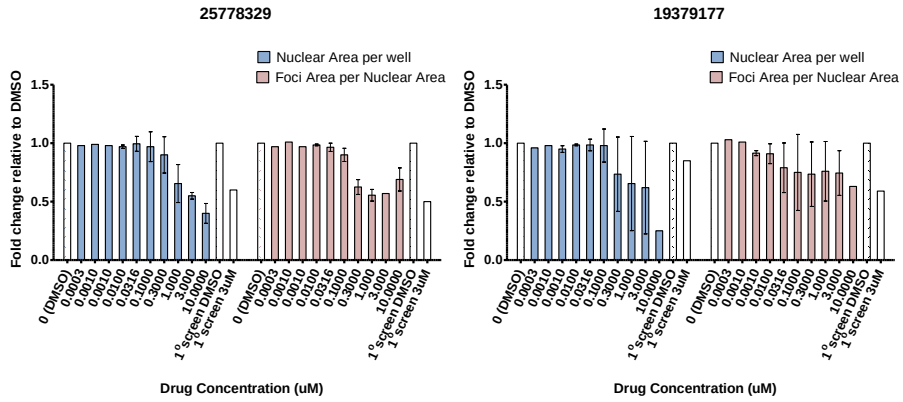

(B)

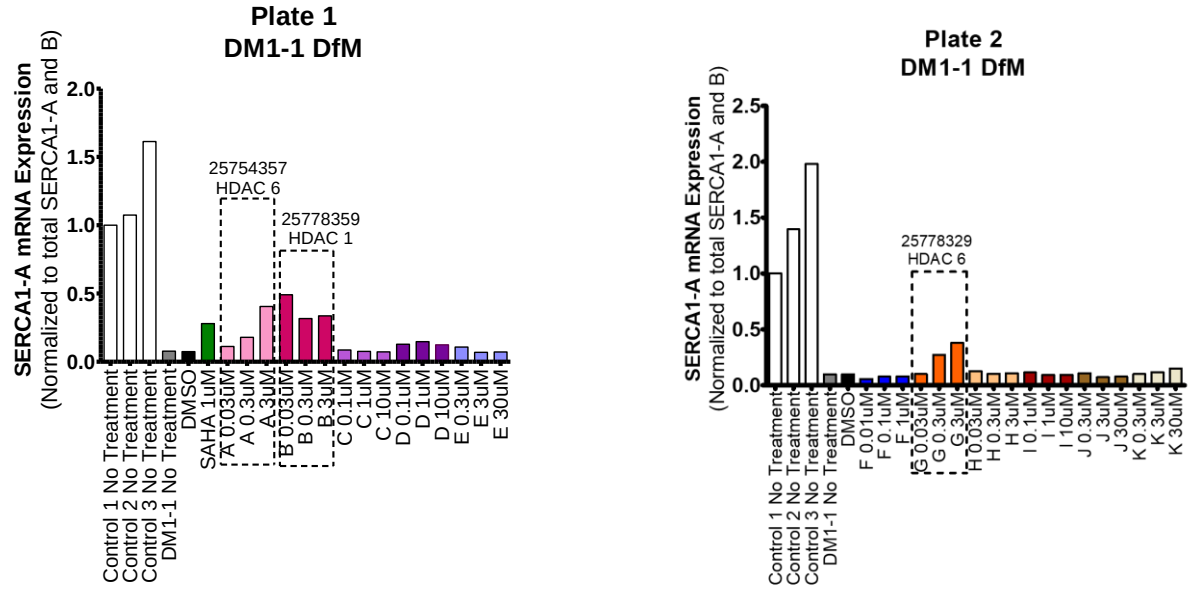

(Figure 4.14 continued on next page)

Figure 4.14. Of the eleven compounds from the secondary screen that were tested foci reduction and toxicity, only three compounds were found to correct SERCA1 splicing, all targeting HDACs. (A) $DM1_{3600CTG}$ myoblasts were serum-starved in 384-well plates and treated with of drugs for 24hrs. Post-treatment, cells were fixed with 4% PFA, DNA was stained with Hoechst and CUG RNA foci were probed by Alexa555-$(CAG)_{10}$ fluorescent oligo. Foci area per nuclear area and total nuclear area per well (to assess treatment-associated toxicity) were quantified using Columbus and normalized to DMSO control data per plate. Data was combined with dose-curve data from the secondary screen and is presented as the average fold-change relative to DMSO treatment (n=2, SD). (B) Control and $DM1_{3600CTG}$ (DM1-1) myoblasts were serum-starved (DfM) in 6-well plates and DM1 cells were treated with DMSO alone or drugs at a 3-point dose-curve for 24hr. Vorinostat (SAHA) was used as a positive control. RNA was extracted (RNeasy micro kit, Qiagen) and reverse-transcribed to cDNA (iScript Advanced RT kit, Biorad). RT-qPCR was performed (iQ SYBR green supermix, Biorad) to assess SERCA1 splicing patterns (n=1). Compounds 25754357, 25778359, and 25778329 were de-blinded and revealed to be vorinostat (SAHA), quisinostat, and trichostatin A (TSA).

(A)

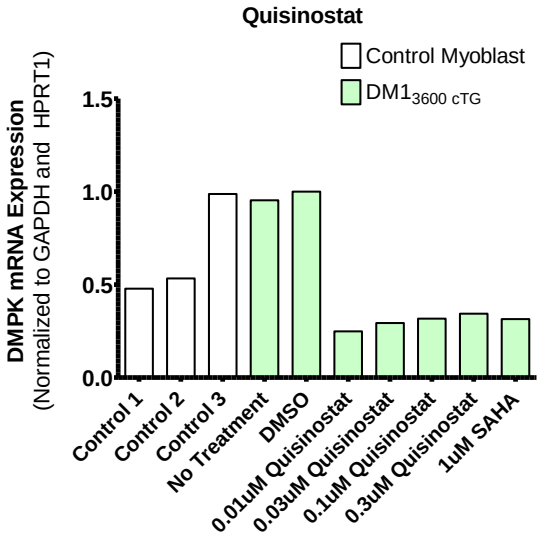

(B)

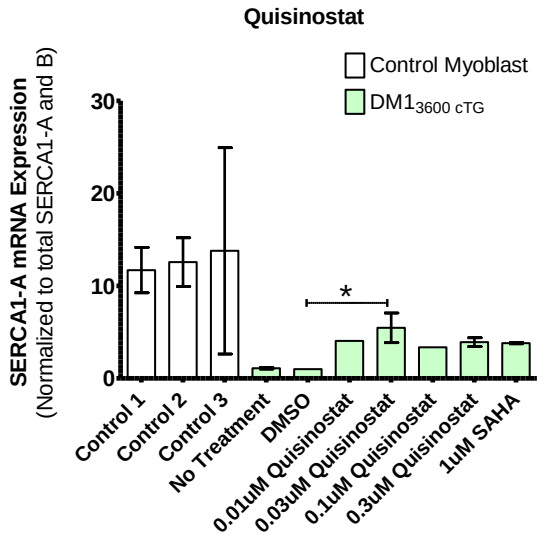

Figure 4.15. Quisinostat had similar effects on DM1 cells as SAHA – it reduced DMPK mRNA levels and increased relative SERCA1-A levels. Control and $DM1_{3600CTG}$ (DM1-1) myoblasts were serum-starved (DfM) in 6-well plates and DM1 cellls were treated with DMSO alone or drugs at a 4-point dose-curve for 24hr; vorinostat (SAHA) was used as a positive control. RNA was extracted (RNeasy micro kit, Qiagen) and reverse-transcribed to cDNA (iScript Advanced RT kit, Biorad). RT-qPCR was performed (iQ Sybr green supermix, Biorad) to assess (A) DMPK mRNA expression normalized to GAPDH and HPRT1 (n=1), and (B) SERCA1-A splicing ratio normalized to total SERCA1 A and B (n ranges from 1 to 2, one-way ANOVA; error bars represent SD). *P < 0.05, **P < 0.01, ***P < 0.001

4.4 DISCUSSION

4.4.1 RNAseq-based mouse neuronal screen of BBB-penetrant drugs

RNAseq data from the neuronal screen of 218 BBB-penetrant drugs was used to identify transcriptomic changes in genes relevant to DM1 pathogenesis, either downregulating DMPK or upregulating muscleblind proteins. All drugs from this screen were either FDA approved or shelved phase II compounds from Pfizer, making it an attractive subset for rapid drug-development (Hadwen et al. 2018). This screen was additionally interesting as it could identify small molecules with BBB-penetrant capabilities to potentially treat the neurological symptoms associated with DM1. While several compounds were identified to upregulate both MBNL1 and MBNL2 (Table 4.1), none were found to decrease DMPK mRNA levels. The top hits for MBNL1 and MBNL2 induction were tested in *in vitro* DM1 models, specifically human fibroblasts and fibroblasts converted to myoblasts by overexpression of *MyoD*. Of the compounds validated to induce MBNL1 and/or MBN2, only nilotinib induced a modest splicing correction of SERCA1 in both DM1 fibroblasts and converted myoblasts (Figure 4.2). Further *in vivo* assessment of nilotinib failed to reproduce MBNL1 or MBNL2 induction in mouse skeletal muscle (Figure 4.3). It is possible that while nilotinib is classified as a BBB-penetrant drug, sufficient concentrations of the drug administered by oral gavage did not accumulate in the mouse skeletal mouse; alternatively, it is also possible the drug does not function in muscle as it does in brain, owing perhaps to the transcriptional differences between the two tissue types. It would be of interest to test these compounds in both a *in vitro* human neuronal model of DM1 and in an *in vivo*

animal model of DM1, particularly one which models the neurological manifestations of the disease.

One obvious limitation of this screen platform is the use of mouse neuronal cultures to elucidate chemical modifiers of human disease. While there are specific cell types that are conserved between mice and human brains, RNAseq analysis reported significant differences in proportion of cell types and gene expression between the two species, making clinical translation based on murine pre-clinical outcomes difficult (Hodge et al. 2019). In this case, screening on a converted human neuronal model of DM1 would be beneficial, possibly derived from induced pluripotent stem-cells (Xia et al. 2013).

4.4.2 CUG foci screen of small molecules in patient myoblasts

Small molecule screening for foci reducers in DM1 patient myoblasts proved to be a productive avenue, identifying vorinostat as an effective splicing modulator agent both *in vitro* and *in vivo*. Vorinostat, also known as SAHA or commercially known as Zolinza, is a pan-HDAC inhibitor, targeting several the histone deacytalases (HDAC). Its use, which increases acetylated histones and altered gene expression, can result in the downstream induction of apoptosis and cell growth arrest (Richon 2006). It was originally developed as an anti-cancer agent and has since been clinically approved to treat cutaneous T-cell lymphoma (Mann et al. 2007). More recently, vorinostat has also been shown to reduce tumor growth and formation in several murine models of cancer, such as metastatic bone cancer, uterine sarcoma, and estrogen receptor-negative mammary tumors (Hrzenjak et al. 2010; Pratap et al. 2010; Tran et al. 2013).

Additionally, this FDA-approved agent is currently in several clinical trials for re-purposing to other chronic disorders, unrelated to cancer. One trial is exploring the tolerability of oral vorinostat (200 and 400 mg) 3 days on/4 days off for the neurodegenerative lysosomal storage disorder Niemann-Pick disease type C (NCT02124083); a second is determining the maximal tolerable oral daily dose (100 to 400 mg) of vorinostat in Alzheimer disease patients (NCT03056495). Importantly, the doses in both trials are associated with peak serum values of 5μM, whereas reduction in foci (Figure 4.6C-D) and DMPK mRNA as well as correction for splicing in DM1 begins to be observed as low as 1μM (Figure 4.7A-B). Similar splicing corrections were also observed *in vivo* in HSA^{LR} mice, demonstrating *in vivo* efficacy (Figure 4.11). Reduction in DMPK mRNA from vorinostat treatment was also observed in control myoblast cultures (Supplementary Figure 4.3); this indicates that vorinostat reduces DMPK through a mechanism that is either altogether independent of CTG repeats or associated with even short, non-pathogenic repeat sizes. Together, this data suggests vorinostat reduces foci by reducing DMPK mRNA, independent of expanded CUG repeats, and results in splicing correction in DM1. It remains to be elucidated whether vorinostat reduces DMPK mRNA by affecting transcript expression, stability or both. Ultimately, functional testing, such as measurement of myotona grade, should be conducted to verify if the *in vivo* splicing corrections result in alleviation of disease. Myotonia grade is measured by EMG and classified as grade 0 (no myotonia), 1 (myotonic discharge in less than 50% of needle insertions), 2 (myotonic discharge in greater than 50% of needle insertions), or 3 (myotonic discharge in almost 100% of needle insertions) (Kanadia et al. 2006).

To test the involvement of HDAC inhibition, two additional pan-HDAC inhibitors, belinostat and TSA, were tested *in vitro*. Both small molecules demonstrated a similar effect on foci reduction (Figure 4.9) and splicing correction (Figure 4.10) as vorinostat, which suggests an underlying class effect involving of HDAC's. However, targeted inhibition of a number of primary HDAC targets common to all three compounds (HDAC's 1, 2, 3, and 6) using siRNA knockdown failed to recapitulate the same impact on DM1-associated dysregulated splicing as the pan-HDAC inhibitors (Figure 4.9 and Figure 4.10); although, HDAC3 siRNA failed to knockdown its target (Supplementary Figure 4.4). It may be that single HDACs are not solely responsible for splicing modulation, but rather a combination of many must be inhibited/knocked down at specific proportions, or that, despite a similar outcome using three pan-HDAC inhibitors, there exist off-target non-HDAC pathways which underly the *in vitro* therapeutic potential. Given the relatively high effective concentration for each compound, especially compared to their respective binding affinity to target HDACs, both theories are possible. The inhibitory constant (Ki) is a measure of affinity for a drug to its target and correlates with the concentration at which 50% of targets are bound, the IC50. Reportedly, at 1μM, vorinostat (SAHA) can also target HDAC 8, belinostat can also target HDACs 4, 5, 7, 8 and 9, and TSA can also target HDACs 5, 7, 8 and 9 (Wagner et al. 2013). Targeted inhibition of these additional HDACs to determine their individual impact on DM1 associated missplicing is also required, especially for HDAC 8, which is common to all three pan-HDAC inhibitors but was not listed as a primary target due to a lower affinity by each drug compared to HDACs 1, 2, 3 and 6.

Vorinostat and TSA also emerged as hits from a larger, blinded screen of approximately 3000 chemogenomic compounds (Figure 4.13-4.15; compounds 25754357 and 25778329, respectively). From this screen, yet another HDAC inhibitor, quisinostat, was identified to both reduce foci and rescue SERCA1 splicing *in vitro* (Figure 4.14-4.16). While library annotation identified quisinostat as an HDAC 1-specific inhibitor (IC50 = 0.11nM), it can exhibit properties of pan-HDAC inhibition at higher doses (Wagner et al. 2013). In the context of DM1, at the lowest tested effective dose of 0.03µM for foci reduction (Figure 4.14) as well as DMPK reduction and splicing correction (Figure 4.15), quisinostat can also inhibit HDAC 2, 4, 10 and 11, but not HDACs 3, 5, 6, 7, 8 and 9.

Interestingly, there already exists a connection between HDAC's to repeat expansion and contraction (Debacker et al. 2012). Specifically, HDAC3 was found to promote CTG·CAG expansions in human astrocytes; siRNA mediated knockdown or chemical inhibition of HDAC3 reduced the frequency of expansion events. Whether this was through direct interaction with the repeat region or by an indirect mechanism was not reported. It should be noted that while HDAC3 inhibition and knockdown reduced frequency of expansion, there was no report of any impact on foci nor a repeat contraction. Such a contraction at the DNA level could be associated with the reduction in CUG foci and correction of downstream splicing (but not the observed reduction in DMPK mRNA) by vorinostat and similar pan-HDAC inhibitors. As such, a link between the effects of HDACs on somatic repeat expansion at the DNA level and reduction in overall DMPK mRNA shown in this study remains unclear.

In addition to vorinostat, gemcitabine, which is another chemotherapeutic agent and is commercially known as Gemzar, was the second drug from the FDA-approved drug screen validated to reduce CUG foci in both DM1 myoblast cell lines (Figure 4.6). However, unlike vorinostat, gemcitabine had no impact on DMPK mRNA levels or SERCA1 spliceopathy (Figure 4.7). It appears that the compound causes foci disaggregation without affecting transcript expression or stability. This begs the question why no splicing correction was observed since it has been previously shown that morpholino-mediated competitive displacement of bound proteins such as MBNL1 from CUG foci led to dispersal of the foci, rescuing DM1 spliceopathy, and even alleviating myotonia is HSA^{LR} mice (Wheeler et al. 2009). It is also important to consider the cell-cycle arrest function of gemcitabine in the mechanism for foci reduction - gemcitabine is a cytidine analog which integrates into the replicating DNA and terminates replication, resulting in a halt in the cell cycle and leading to cell death (De Sousa Cavalcante and Monteiro 2014). Relating to the cell cycle, it has been demonstrated that in DM1 neural stem cells, foci are most prominent prior to mitosis, during interphase, and disappear during the cell division process through mitosis (Xia and Ashizawa 2015). Given this observation, cell-cycle arrest by gemcitabine should in fact increase accumulation of foci, not a reduction. However, it should also be noted that the data presented here is primarily modeled in serum-starved, non-proliferative, differentiated myoblasts – a culture population which is considered to be already in cell-cycle arrest prior to treatments. Taken together, the cell cycle arrest function of gemcitabine is likely ineffective/irrelevant in foci reduction. There may also be a more technical explanation for observing foci reduction but not splicing correction: as

mentioned before, gemcitabine is a cytidine analog (De Sousa Cavalcante and Monteiro 2014), meaning it mimics the structure of the nucleotide base cytosine, and may bind to the G-rich foci, thereby blocking the binding of the Alexa555-(CAG)10 probe. In this case, the foci would still be present but undetected and disease pathology would remain unaffected.

CHAPTER 5: GENERAL DISCUSSION AND CONCLUDING REMARKS

5.1 Successes and lessons learned from DM1 high-throughput screening

The overall goal of this thesis project was to identify key pathways and/or agents for the development of novel DM1 therapeutics. To this end, several high-throughput screening approaches were used, all assessing the microscopic integrity of pathogenic CUG foci, which are unique DM1 biomarkers in patient cells. These screens were founded on two key evidence-based concepts for DM1 pathology: 1) the expanded repeats lead to an RNA gain-of-function which leads to the formation of intranuclear DMPK-expanded CUG foci associated downstream pathogenesis such as wide-spread spliceopathy (Davis et al. 1997; Lin et al. 2006; Michalowski et al. 1999; Napierała and Krzyzosiak 1997); and 2) targeting these foci for disaggregation or degradation effectively alleviates the disease phenotype (Langlois et al. 2003; Wheeler et al. 2009, 2012). The results from the primary screens were validated with variable success, with only one agent, vorinostat (SAHA), reaching pre-clinical *in vivo* testing (Figure 4.12).

One major lesson from our studies was that selection of a specific cell types can underly the success and failure of a screening platform. For example, fibroblasts are dividing cells, whereas many of the prominently affected cell populations in DM1 (skeletal muscle, cardiac muscle, neurons, etc.) are generally non-dividing. It has been previously highlighted that CUG foci are most prominent in cells arrested from the cell cycle or in interphase, disappearing completely in mitotic cells (Xia and Ashizawa 2015). It is possible that foci reductions observed

in fibroblasts, as with the kinome screens summarized in Chapter 3, was a result of cell cycle regulation, rather than some other foci-specific mechanism, giving rise to false positive candidates which in fact may not impact foci in post-mitotic cells. For example, while PACT knockdown reduced observable foci (Figure 3.2), it had no impact on DMPK mRNA (Figure 3.4) and did not rescue aberrant splicing (Figure 3.7); however, PACT knockdown did increase the cell population, as indicated by the small but significant increase in nuclei count (Supplementary Figure 4), which could be indicative of upregulated cell cycling and could account for PACT-mediated foci reduction.

Another note of interest is that no single treatment in our studies elicited complete disappearance of the foci or complete downstream rescue of molecular dysregulation, whether by siRNA knockdown of genes or small molecule-mediated molecular regulation. While a single agent was not successful in fully alleviating molecular signatures of the disease, they can be good candidates for combination therapies with additive or synergistic effects. Combination drug therapy has been proven effective for treating, for example, asthma pain, diabetes, and more (Tangalos and Zarowitz 2005). In these cases, increased efficacy and reduced adverse effects are key benefits, especially for such chronic conditions.

Conversely, the highlight of these studies was the identification of vorinostat, which has already been FDA-approved for cancer therapy and is currently in several clinical trials for the treatment of other, non-tumorigenic contexts, as mentioned in Chapter 4. The concept of repurposing or repositioning FDA approved compounds has emerged in the last decade as an

avenue for rapid and cost-effective drug development; in fact, this method could and should be extended to compounds which have failed clinical trials or shelved by pharmaceutical industries. While *de novo* production of new compounds reportedly takes up to 16 years and $2 billion in investments to go from benchtop to bedside, repositioned candidates, whether effective from on- or off-target engagement, are estimated to take only 6 years of development and cost only about $300 million (Nosengo 2016). This is largely a reflection of existing synthesis and manufacturing protocols, and de-risked clinical status, obviating Phase I clinical trials. Over the last four decades, repositioned drugs have been shown to be effective in combatting drug-resistant bacteria, various cancers, HIV, psychological disorders, and even genetic disorders (Pushpakom et al. 2018).

5.2 Extended applications of DM1 screen results to other repeat disorders

To date, approximately 40 repeat-expansion disorders have been reported (Paulson and Arbor 2006; Zhang and Ashizawa 2017). While the threshold for disease-causing repeat length varies between diseases, virtually all, including DM1, show an inverse correlation between repeat length and age of onset, as well as a direct repeat length-to-severity correlation; additionally, intergenerational anticipation can be seen. As with DM1, several of these repeat-expansion genetic diseases are caused by pathogenic RNA gain of function. Intranuclear foci accumulation with RBP sequestration has been reported in myotonic dystrophy Type 2 (DM2), arising from a tetranucleotide expansion of CCTG repeats in intron 1 of *ZNF9* (aka *CNBP*) gene;

Fuchs endothelial corneal dystrophy (FECD) caused by a trinucleotide expansion of CTG repeats in intron 3 of *TCF4*; huntington's disease (HD), which stems from CAG expansion in the coding region *HTT* (De Mezer et al. 2011); huntington disease-like 2 (HDL2) originating from CTG trinucleotide repeat expansion in 3' UTR of *JPH3*; C9orf72-amyotrophic lateral sclerosis/frontotemporal dementia (C9orf72-ALS/FTD), stemming from an intronic hexanucleotide expansion of GGGCCC in *C9orf72*; fragile X-associated tremor/ataxia syndrome (FXTAS), arising from CGG expansion in *FMR1*; and several types of spinocerebellar ataxia (SCA) arising from tri-, penta-, and hexanucleotide expansions in various genes: SCA3 caused by CTG expansion in exon 8 of *ATXN3*, SCA8 caused by CTG expansion in the 3' UTR of *ATXN8OS*, SCA10 caused by ATTCT pentanucleotide expansion in intron 9 of *ATXN10*, SCA31 caused by TGGAA expansion in inter-gene intronic region of *BEAN* and *TK2*, and SCA36 caused by GGCCTG hexanucleotide expansion in intron 1 of *NOP56*. Some of these diseases share repeat sequences while others share sequestered RBP's, and some share both. For example, sequestration of muscleblind proteins, which largely accounts for a vast number of DM1 spliceopathies, is also observed in DM2 (CCUG repeats), FECD (CUG repeats), HD (CAG repeats), HDL2 (CUG repeats), SCA3 (CUG repeats) and SCA8 (CUG repeats), all of which form double-stranded RNA hairpins displaying MBNL1 binding motifs CHHG or CHG, where H is A, U or C (Kino et al. 2004). These shared properties may help inform generalizable repurposing therapeutic strategies for a number of different repeat disorders further expediting drug development and reducing costs associated with a collective increase in patient pool.

With regards to vorinostat, the exact mechanism by which it reduces CUG foci in DM1 (Figure 4.6), leading to splicing correction both *in vitro* (Figure 4.7) and *in vivo* (Figure 4.12), remains unclear. While a reduction in DMPK mRNA (Figure 4.7) has been associated to the observed reduction in CUG foci, it has not been established whether this is driving the foci reduction or whether vorinostat reduces DMPK mRNA level through direct interaction with the gene itself or some unknown effect on the CUG repeats. Since vorinostat reduces DMPK mRNA in control myoblasts (Supplementary Figure 4.3), it is likely the mechanism is not dependent on expanded repeats. However, the repeat length in our control myoblasts is unknown and so a minimum repeat threshold cannot be determined, leaving open the possible involvement of short, non-pathogenic CUG tracks, especially given that vorinostat shows therapeutic promise in HSA^{LR} mice which models a non-DMPK, CTG repeat genetic context. All that to say, if vorinostat acts through a CTG or CUG repeat-dependent mechanism, this drug may also prove effective in other CTG repeat disorders like FECD, HDL2, SCA3 and SCA8. Although, one must proceed with caution since although downregulation of DMPK, the gene context for CTG repeats in DM1, is relatively non-consequential (Seznec et al. 2001), downregulation of genes in other repeat expansion disorders may only exacerbate the disease, depending on the functional role of the affected gene. Vorinostat also upregulates MBNL1 protein (Zhang et al. 2017), which may also contribute to the splicing rescue. In this case, MBNL1 upregulation may also benefit other repeat disorders which exhibit sequestration of this particular RBP to nuclear foci. In the context of DM1, MBNL1 upregulation has proven effective and may be beneficial for these related RNA gain-of-function repeat disorders.

5.3 Conclusion

High-throughput screening of CUG foci in DM1 left us with many lessons and some successes. Our findings imply the success of positive hits may be contingent on choice of disease model – for example, CTG expansion in myoblasts and myotubes from a muscle origin, and therefore more disease-relevant, may be more suitable for drug screening in DM1 than fibroblasts cell lines which are minimally affected in disease context. Overall, this thesis also highlights the risk of false-positives and the importance of secondary validations of downstream mechanisms, such as splicing, to identify candidates with true therapeutic benefit. Through this process, we have identified vorinostat (SAHA) as the most promising drug, which has shown some efficacy in early pre-clinical trials.

APPENDIX

Supplementary Table 3.1. Z-score data for nuclei count, foci count and foci area from a partial kinome RNAi screen in a $DM1_{500\ CTG}$ patient fibroblast line. The screen was done in triplicate using 10nM of pooled siRNA with an end-point readout conducted at 96 hrs; due to technical errors, this original screen included only a portion of the entire kinome RNAi library. The data was normalized to the sample mean per plate and is represented as average Z-score values.

siRNA	Plate	Well Name	Row	Column	Z-score (nuclei count)	Z-score (foci count)	Z-score (foci area)
PRKAA1	hKQsi002	B3	2	3	0.05	1.51	1.53
PRKCA	hKQsi002	B4	2	4	0.58	0.19	0.47
PRKG2	hKQsi002	B5	2	5	-0.03	0.29	0.45
MAP2K5	hKQsi002	B6	2	6	0.40	0.51	0.38
RAGE	hKQsi002	B7	2	7	0.24	-0.72	-0.24
SGK	hKQsi002	B8	2	8	-1.41	-0.31	-0.44
AURKA	hKQsi002	B10	2	10	0.36	-0.39	-0.72
TK2	hKQsi002	B11	2	11	-0.46	0.10	0.18
MAP3K12	hKQsi002	B12	2	12	-0.42	0.25	0.03
IKBKG	hKQsi002	B13	2	13	-0.44	-0.98	-0.62
CDC2L5	hKQsi002	B14	2	14	0.12	-0.73	-0.71
CDK5R2	hKQsi002	B15	2	15	-0.57	-0.11	-1.22
DGKI	hKQsi002	B17	2	17	-1.32	-1.38	-0.70
AKAP6	hKQsi002	B18	2	18	0.01	0.26	-0.11
ARK5	hKQsi002	B19	2	19	1.48	0.14	-0.26
PAK4	hKQsi002	B20	2	20	-0.03	-1.07	-0.46
NEK6	hKQsi002	B21	2	21	-0.46	-0.33	-0.36
AKAP11	hKQsi002	B22	2	22	0.89	-1.36	-1.08
PRKAA2	hKQsi002	C3	3	3	0.39	0.74	0.35
PRKCB1	hKQsi002	C4	3	4	0.51	0.54	0.28
MAPK1	hKQsi002	C5	3	5	-1.13	0.42	0.23
MAP2K6	hKQsi002	C6	3	6	-0.02	-0.51	-0.40
RAF1	hKQsi002	C7	3	7	0.44	0.30	0.25
SKP1A	hKQsi002	C8	3	8	-0.06	-0.23	-0.04
CDKL5	hKQsi002	C10	3	10	0.94	-1.17	-0.91
TRIO	hKQsi002	C11	3	11	0.14	-0.35	-0.32

MAPKAPK3	hKQsi002	C12	3	12	-0.68	1.58	1.41
IKBKAP	hKQsi002	C13	3	13	-0.44	-0.62	-0.93
MAP2K1IP1	hKQsi002	C14	3	14	-0.94	-1.28	-0.32
RPS6KA4	hKQsi002	C15	3	15	-0.41	0.85	-0.16
MAP3K13	hKQsi002	C17	3	17	-0.77	-1.11	-0.54
ROCK2	hKQsi002	C18	3	18	-0.62	-0.58	-0.35
XYLB	hKQsi002	C19	3	19	0.26	-0.64	-0.52
TESK2	hKQsi002	C20	3	20	1.65	-1.32	-1.13
FASTK	hKQsi002	C21	3	21	0.06	-0.11	0.03
AKAP10	hKQsi002	C22	3	22	4.73	-0.17	-0.46
PRKAB1	hKQsi002	D3	4	3	1.19	-0.45	-0.66
PRKCD	hKQsi002	D4	4	4	-0.24	-0.88	-1.26
MAPK3	hKQsi002	D5	4	5	3.08	0.79	0.36
MAP2K7	hKQsi002	D6	4	6	-0.77	-0.48	-0.31
RET	hKQsi002	D7	4	7	-0.34	-0.04	-0.02
SKP2	hKQsi002	D8	4	8	-1.46	0.25	0.81
STK10	hKQsi002	D10	4	10	-0.11	0.46	0.34
TTK	hKQsi002	D11	4	11	-2.37	0.94	1.10
AKAP1	hKQsi002	D12	4	12	-1.32	-0.02	-0.42
DGKZ	hKQsi002	D13	4	13	0.44	-1.32	-1.36
TNK1	hKQsi002	D14	4	14	0.77	0.34	0.10
CDKL2	hKQsi002	D15	4	15	0.35	-0.35	-0.90
DCAMKL1	hKQsi002	D17	4	17	0.60	0.58	0.46
MAPK8IP1	hKQsi002	D18	4	18	-0.11	-1.11	-0.80
OSR1	hKQsi002	D19	4	19	1.38	-0.57	-1.18
MAP3K7IP1	hKQsi002	D20	4	20	-0.80	-0.08	0.82
ASK	hKQsi002	D21	4	21	-0.36	0.08	0.27
PACSIN2	hKQsi002	D22	4	22	-0.25	0.09	1.00
PRKAB2	hKQsi002	E3	5	3	2.10	1.18	0.98
PRKCE	hKQsi002	E4	5	4	-0.46	-0.76	-0.80
MAPK4	hKQsi002	E5	5	5	1.21	1.50	0.69
PRKR	hKQsi002	E6	5	6	-0.90	-0.60	-0.20
GRK1	hKQsi002	E7	5	7	1.26	-0.96	-0.75
SRC	hKQsi002	E8	5	8	0.25	-0.15	0.37
STK11	hKQsi002	E10	5	10	-0.32	0.48	0.47
TXK	hKQsi002	E11	5	11	-0.55	-0.69	-0.46
NME5	hKQsi002	E12	5	12	-1.03	0.54	0.11
DGKE	hKQsi002	E13	5	13	0.42	0.33	0.30
RIPK1	hKQsi002	E14	5	14	-0.64	-0.36	0.20
MAP3K14	hKQsi002	E15	5	15	-0.99	-0.61	-0.55

AURKB	hKQsi002	E17	5	17	-1.03	0.71	0.99
AKAP5	hKQsi002	E18	5	18	0.06	-0.27	-0.45
AKT3	hKQsi002	E19	5	19	1.13	0.63	0.60
MERTK	hKQsi002	E20	5	20	-1.20	-1.12	-1.25
TLK2	hKQsi002	E21	5	21	0.12	-2.24	-1.69
STK38	hKQsi002	E22	5	22	1.72	0.51	-0.09
PRKACA	hKQsi002	F3	6	3	1.55	0.19	-0.24
PRKCG	hKQsi002	F4	6	4	0.00	0.13	0.13
MAPK6	hKQsi002	F5	6	5	0.40	0.48	0.44
PRKRIR	hKQsi002	F6	6	6	-1.10	0.47	0.40
ROCK1	hKQsi002	F7	6	7	0.52	-1.17	-0.96
SRMS	hKQsi002	F8	6	8	0.67	0.83	0.55
AURKC	hKQsi002	F10	6	10	-0.06	-0.83	-0.85
TYK2	hKQsi002	F11	6	11	-0.27	0.42	0.25
PIP5K1A	hKQsi002	F12	6	12	0.58	-0.15	-0.34
DGKD	hKQsi002	F13	6	13	0.60	0.49	0.31
RIPK2	hKQsi002	F14	6	14	-0.38	1.24	0.83
STK29	hKQsi002	F15	6	15	-1.42	-1.00	-0.47
RPS6KA5	hKQsi002	F17	6	17	-0.63	-1.21	-1.12
CDC42BPB	hKQsi002	F18	6	18	-0.63	0.24	0.32
GNE	hKQsi002	F19	6	19	-0.54	0.51	0.58
STK25	hKQsi002	F20	6	20	0.50	-1.14	-0.88
RIPK3	hKQsi002	F21	6	21	2.23	-1.14	-0.91
PTK9L	hKQsi002	F22	6	22	-0.96	-0.68	-0.54
PRKACB	hKQsi002	G3	7	3	-1.23	-0.02	0.70
PRKCH	hKQsi002	G4	7	4	1.21	-0.28	-0.66
MAPK7	hKQsi002	G5	7	5	0.23	1.04	0.49
PRKX	hKQsi002	G6	7	6	0.28	-1.69	-0.69
ROS1	hKQsi002	G7	7	7	-0.89	0.97	0.87
SRPK1	hKQsi002	G8	7	8	-1.47	-0.12	-0.15
SYK	hKQsi002	G10	7	10	-0.78	-0.96	-0.79
TYRO3	hKQsi002	G11	7	11	0.37	0.36	-0.01
PIP5K1B	hKQsi002	G12	7	12	0.72	-0.71	-0.69
CAMK1	hKQsi002	G13	7	13	-0.60	0.66	0.85
RIOK3	hKQsi002	G14	7	14	-0.35	0.31	-0.04
MAP3K6	hKQsi002	G15	7	15	2.31	-0.92	-0.91
MAPKAPK2	hKQsi002	G17	7	17	-0.28	-0.13	-0.68
AKAP12	hKQsi002	G18	7	18	-0.37	-0.78	-0.43
SGK2	hKQsi002	G19	7	19	0.59	1.77	-0.37
CIB2	hKQsi002	G20	7	20	-1.64	0.03	-0.14

PIM2	hKQsi002	G21	7	21	-0.28	-0.66	-0.94
AAK1	hKQsi002	G22	7	22	-0.45	-0.14	0.04
PRKACG	hKQsi002	H3	8	3	-0.85	-0.17	-0.35
PRKCI	hKQsi002	H4	8	4	-0.43	3.19	1.72
MAPK8	hKQsi002	H5	8	5	-0.74	-0.15	0.42
PRKY	hKQsi002	H6	8	6	-0.92	0.19	0.48
RPS6KA1	hKQsi002	H7	8	7	-0.02	2.77	1.70
SRPK2	hKQsi002	H8	8	8	-0.08	-0.89	-0.25
MAP3K7	hKQsi002	H10	8	10	0.68	0.47	-0.08
TYROBP	hKQsi002	H11	8	11	-0.22	0.90	0.39
PIP5K2B	hKQsi002	H12	8	12	-0.03	-1.11	-1.18
MAPKAPK5	hKQsi002	H13	8	13	-0.27	0.70	0.27
DYRK4	hKQsi002	H14	8	14	-1.46	-0.05	0.25
PKMYT1	hKQsi002	H15	8	15	0.62	-0.21	0.38
STK17B	hKQsi002	H17	8	17	0.51	-0.65	-0.61
AATK	hKQsi002	H18	8	18	-1.57	-0.43	1.30
HIPK3	hKQsi002	H19	8	19	-0.42	0.69	-0.36
AKAP3	hKQsi002	H20	8	20	0.00	-0.44	-0.16
CIT	hKQsi002	H21	8	21	-0.38	0.68	0.72
LMTK2	hKQsi002	H22	8	22	1.03	-0.87	-0.82
PKIA	hKQsi002	I3	9	3	0.54	0.16	-0.07
PRKCL1	hKQsi002	I4	9	4	-0.02	0.09	-0.03
MAPK11	hKQsi002	I5	9	5	2.04	1.10	0.77
PRSS7	hKQsi002	I6	9	6	0.12	0.70	0.23
RPS6KA2	hKQsi002	I7	9	7	0.51	-0.39	-0.21
NEK4	hKQsi002	I8	9	8	-0.66	0.55	-0.25
TEC	hKQsi002	I10	9	10	0.39	1.56	1.11
UGP2	hKQsi002	I11	9	11	-0.27	0.42	1.14
ULK1	hKQsi002	I12	9	12	0.43	-0.16	-0.33
CDK10	hKQsi002	I13	9	13	0.28	-1.27	-1.13
CDKL1	hKQsi002	I14	9	14	-0.21	0.71	0.02
LATS1	hKQsi002	I15	9	15	1.19	0.02	-0.17
STK17A	hKQsi002	I17	9	17	0.35	-1.54	-1.29
IKBKE	hKQsi002	I18	9	18	0.73	-0.03	-0.42
AKAP9	hKQsi002	I19	9	19	0.58	0.25	-0.65
ERN2	hKQsi002	I20	9	20	-0.86	0.65	1.06
KALRN	hKQsi002	I21	9	21	0.38	0.57	3.23
ICK	hKQsi002	I22	9	22	-0.21	0.68	0.28
PKIB	hKQsi002	J3	10	3	0.03	-0.07	-0.57
PRKCL2	hKQsi002	J4	10	4	-0.32	-1.34	-1.08

MAPK9	hKQsi002	J5	10	5	-0.87	0.51	1.80
PSKH1	hKQsi002	J6	10	6	0.41	-0.72	-0.46
RPS6KA3	hKQsi002	J7	10	7	-0.15	-0.22	-0.46
STK3	hKQsi002	J8	10	8	-0.95	-0.84	-0.78
TEK	hKQsi002	J10	10	10	0.36	-0.44	-0.19
UMPK	hKQsi002	J11	10	11	-0.46	-0.79	-0.74
STK24	hKQsi002	J12	10	12	1.52	-0.22	0.04
PDXK	hKQsi002	J13	10	13	-0.34	-0.46	-1.08
KSR	hKQsi002	J14	10	14	-0.21	0.95	1.24
HGS	hKQsi002	J15	10	15	-1.52	0.55	-0.24
TAO1	hKQsi002	J17	10	17	0.73	1.19	0.69
ULK2	hKQsi002	J18	10	18	-1.42	0.39	0.75
TNK2	hKQsi002	J19	10	19	-0.54	-0.82	-1.11
PDLIM5	hKQsi002	J20	10	20	0.23	-0.54	-0.44
PKIG	hKQsi002	J21	10	21	-0.37	-1.71	-1.46
SORCS3	hKQsi002	J22	10	22	-0.52	-0.41	-0.41
PRKAG1	hKQsi002	K3	11	3	1.76	1.91	1.13
PRKCM	hKQsi002	K4	11	4	0.62	-0.56	-0.72
MAPK10	hKQsi002	K5	11	5	0.69	1.85	1.22
PTK2	hKQsi002	K6	11	6	0.03	0.94	0.58
RPS6KB1	hKQsi002	K7	11	7	1.09	-0.91	-0.99
STK4	hKQsi002	K8	11	8	0.33	-0.41	0.41
TESK1	hKQsi002	K10	11	10	0.06	0.80	1.50
VRK1	hKQsi002	K11	11	11	-1.01	0.40	-0.11
DYRK3	hKQsi002	K12	11	12	2.46	-0.20	-0.06
MADD	hKQsi002	K13	11	13	0.33	0.36	-0.01
CDK5R1	hKQsi002	K14	11	14	-0.77	0.34	0.42
DYRK1B	hKQsi002	K15	11	15	-0.06	-0.90	-0.39
TAO1	hKQsi002	K17	11	17	0.39	0.66	1.09
SLK	hKQsi002	K18	11	18	-0.15	-0.03	-0.06
NME6	hKQsi002	K19	11	19	0.75	0.41	-0.63
CAMKK2	hKQsi002	K20	11	20	0.07	0.34	0.57
MAP4K5	hKQsi002	K21	11	21	0.36	-1.05	-0.96
MAPKBP1	hKQsi002	K22	11	22	0.89	-0.44	-0.51
PRKAR1A	hKQsi002	L3	12	3	-1.78	-0.58	-1.00
PRKCQ	hKQsi002	L4	12	4	0.46	0.23	-0.26
MAPK13	hKQsi002	L5	12	5	-0.46	0.44	0.79
PTK6	hKQsi002	L6	12	6	-0.57	0.48	0.28
RPS6KB2	hKQsi002	L7	12	7	0.24	-0.47	-0.73
TGFBR1	hKQsi002	L10	12	10	1.38	0.53	0.17

VRK2	hKQsi002	L11	12	11	-0.48	1.43	0.95
DYRK2	hKQsi002	L12	12	12	0.35	0.27	0.48
MKNK1	hKQsi002	L13	12	13	-2.00	-0.82	-0.07
AKAP4	hKQsi002	L14	12	14	-0.76	0.63	-0.09
MAP4K4	hKQsi002	L17	12	17	0.66	-0.25	1.74
IHPK1	hKQsi002	L18	12	18	0.48	2.87	1.24
CNKSR1	hKQsi002	L19	12	19	0.32	0.05	-0.13
PMVK	hKQsi002	L20	12	20	0.44	-1.10	-0.57
MAP4K1	hKQsi002	L21	12	21	0.57	2.69	2.05
PRKAR1B	hKQsi002	M3	13	3	0.93	0.66	0.71
PRKCZ	hKQsi002	M4	13	4	1.10	1.38	1.02
MAP2K1	hKQsi002	M5	13	5	-0.11	0.57	0.68
PTK7	hKQsi002	M6	13	6	-1.13	0.62	0.41
RYK	hKQsi002	M7	13	7	-0.30	-1.74	-1.00
TGFBR2	hKQsi002	M10	13	10	-0.13	-1.11	-0.77
WEE1	hKQsi002	M11	13	11	-2.47	-0.25	-0.12
CDC42BPA	hKQsi002	M12	13	12	0.35	2.13	1.28
CASK	hKQsi002	M13	13	13	0.33	1.27	1.15
STK19	hKQsi002	M14	13	14	0.34	0.17	-0.15
EIF2AK3	hKQsi002	M17	13	17	1.05	1.46	4.28
GIT2	hKQsi002	M18	13	18	-0.49	-0.35	0.53
AKAP8	hKQsi002	M19	13	19	-0.74	-0.67	0.66
PLK4	hKQsi002	M20	13	20	0.30	-0.16	0.09
CHEK2	hKQsi002	M21	13	21	0.81	-1.58	-1.36
PRKAR2A	hKQsi002	N3	14	3	1.35	-0.07	-0.68
PRKDC	hKQsi002	N4	14	4	0.68	0.53	-0.08
MAP2K2	hKQsi002	N5	14	5	-0.31	0.21	0.48
PTK9	hKQsi002	N6	14	6	-0.53	1.06	0.99
MAPK12	hKQsi002	N7	14	7	-0.76	-0.38	-0.20
TIE	hKQsi002	N10	14	10	-0.08	-0.42	-0.57
YES1	hKQsi002	N11	14	11	-0.93	0.45	-0.05
MAP4K3	hKQsi002	N12	14	12	1.24	1.66	0.73
PRKRA	hKQsi002	N13	14	13	1.49	-1.97	-1.95
SPHK1	hKQsi002	N14	14	14	-0.29	0.06	0.16
PRKCABP	hKQsi002	N17	14	17	-1.14	-0.27	0.01
MELK	hKQsi002	N18	14	18	-1.51	-0.91	-0.83
SPEG	hKQsi002	N19	14	19	-2.03	0.72	2.49
MAP3K2	hKQsi002	N20	14	20	-0.37	-0.67	0.29
IRAK3	hKQsi002	N21	14	21	0.98	0.13	0.48
PRKAR2B	hKQsi002	O3	15	3	-0.28	-0.31	-0.44

PRKG1	hKQsi002	O4	15	4	0.61	-1.15	-0.91
MAP2K3	hKQsi002	O5	15	5	1.32	2.95	2.49
MAP4K2	hKQsi002	O6	15	6	-1.81	1.25	1.14
MAP2K4	hKQsi002	O7	15	7	-1.10	-0.70	-0.40
TK1	hKQsi002	O10	15	10	-2.52	0.16	-0.43
ZAP70	hKQsi002	O11	15	11	-0.29	-0.49	-0.37
PIK3R3	hKQsi002	O12	15	12	-0.72	-0.29	-0.44
STK16	hKQsi002	O13	15	13	-0.68	-0.65	-0.89
PRPF4B	hKQsi002	O14	15	14	1.46	0.23	0.29
AKAP7	hKQsi002	O17	15	17	-0.16	-1.47	-1.14
TLK1	hKQsi002	O18	15	18	-0.60	-1.62	-0.78
BCKDK	hKQsi002	O19	15	19	0.14	-0.53	-0.11
PLK2	hKQsi002	O20	15	20	0.51	-0.13	-0.37
AKAP13	hKQsi002	O21	15	21	-0.36	-1.75	-1.54
STK38L	hKQsi003	B3	2	3	0.91	-0.19	-0.53
MAPK8IP2	hKQsi003	B4	2	4	-0.04	0.95	1.17
LATS2	hKQsi003	B5	2	5	0.35	-1.58	-0.79
EEF2K	hKQsi003	B6	2	6	0.85	0.07	-0.14
JIK	hKQsi003	B7	2	7	-1.12	0.01	0.52
SNRK	hKQsi003	B8	2	8	0.88	-0.58	-0.62
RFK	hKQsi003	B10	2	10	-0.16	0.01	0.82
SPHK2	hKQsi003	B11	2	11	0.08	0.48	1.28
FN3K	hKQsi003	B12	2	12	-0.35	0.24	-0.32
FN3KRP	hKQsi003	B13	2	13	-0.67	-0.45	0.29
UCK1	hKQsi003	B14	2	14	-1.60	0.43	0.88
PSKH2	hKQsi003	B15	2	15	-0.93	-0.04	-0.90
GRK7	hKQsi003	B17	2	17	0.87	-0.70	-1.79
TTBK2	hKQsi003	B18	2	18	0.38	0.48	-1.14
NRK	hKQsi003	B19	2	19	0.92	-0.99	0.18
MAST4	hKQsi003	B20	2	20	0.46	0.68	0.99
MAST3	hKQsi003	C3	3	3	3.86	-0.63	-0.22
CCRK	hKQsi003	C4	3	4	-1.45	0.52	0.30
STK23	hKQsi003	C5	3	5	-0.36	-1.34	0.02
NME7	hKQsi003	C6	3	6	0.54	0.87	1.29
PRKAG2	hKQsi003	C7	3	7	-0.64	0.57	0.25
EPS8L1	hKQsi003	C8	3	8	0.29	-1.22	-0.18
STK32B	hKQsi003	C10	3	10	-0.84	-0.07	0.38
PAK6	hKQsi003	C11	3	11	-0.02	-0.21	-0.23
NJMU-R1	hKQsi003	C12	3	12	0.99	0.67	-0.30
LRRK1	hKQsi003	C13	3	13	-0.65	-0.49	-0.10

RPS6KL1	hKQsi003	C14	3	14	0.13	0.08	-0.02
NYD-SP25	hKQsi003	C15	3	15	0.37	1.27	0.16
STK11IP	hKQsi003	C17	3	17	0.64	-0.87	-1.38
HIPK4	hKQsi003	C18	3	18	1.36	-0.71	-1.97
HIPK1	hKQsi003	C19	3	19	-0.43	-0.61	0.92
SBK1	hKQsi003	C20	3	20	0.66	1.18	0.79
TNIK	hKQsi003	D3	4	3	-0.32	-0.24	-0.17
DAPK2	hKQsi003	D4	4	4	-0.60	0.81	0.98
RPS6KC1	hKQsi003	D5	4	5	0.57	0.41	0.59
PKN3	hKQsi003	D6	4	6	0.26	0.31	0.31
IHPK2	hKQsi003	D7	4	7	-0.44	0.98	0.42
PXK	hKQsi003	D8	4	8	0.15	-1.02	0.03
STYK1	hKQsi003	D10	4	10	-0.53	-0.44	-0.22
SPEC2	hKQsi003	D11	4	11	-1.07	-0.27	0.47
NUCKS	hKQsi003	D12	4	12	-1.27	0.39	0.60
PIP5K2C	hKQsi003	D13	4	13	-1.23	-0.45	-0.64
RIOK1	hKQsi003	D14	4	14	-1.33	-0.62	-0.63
NYD-SP25	hKQsi003	D15	4	15	1.00	-0.20	-0.98
HAK	hKQsi003	D17	4	17	0.94	-1.59	-2.17
PDIK1L	hKQsi003	D18	4	18	-1.08	0.39	-0.61
PRPS1L1	hKQsi003	D19	4	19	-1.41	-0.29	-0.19
discontinued	hKQsi003	D20	4	20	-0.67	-0.17	-0.31
SMG1	hKQsi003	E3	5	3	-0.23	0.79	0.34
PRKCBP1	hKQsi003	E4	5	4	-0.80	0.60	0.61
AKAP8L	hKQsi003	E5	5	5	0.76	0.28	-0.21
NRBP	hKQsi003	E6	5	6	0.73	0.25	-0.04
NIPA	hKQsi003	E7	5	7	-0.64	0.50	0.18
URKL1	hKQsi003	E8	5	8	1.22	-1.68	-0.88
PI4KII	hKQsi003	E10	5	10	-1.01	0.38	0.57
CAMK1D	hKQsi003	E11	5	11	-0.45	-1.88	-0.64
CERK	hKQsi003	E12	5	12	0.62	-0.20	-0.37
NEK11	hKQsi003	E13	5	13	0.21	-0.46	-0.55
MGC4796	hKQsi003	E14	5	14	-2.56	0.02	-0.41
ADCK2	hKQsi003	E15	5	15	0.21	0.11	-0.38
IHPK3	hKQsi003	E17	5	17	-1.59	-0.73	-0.84
SNF1LK	hKQsi003	E18	5	18	-0.42	-0.27	-1.33
ERK8	hKQsi003	E19	5	19	-0.45	0.11	-0.16
discontinued	hKQsi003	E20	5	20	-0.15	0.23	-0.08
ARHGAP26	hKQsi003	F3	6	3	1.77	-0.53	-0.18
STK22B	hKQsi003	F4	6	4	-0.63	-0.34	-0.48

TPK1	hKQsi003	F5	6	5	-0.50	-0.62	-0.05
PACSIN1	hKQsi003	F6	6	6	1.07	0.00	-0.04
CINP	hKQsi003	F7	6	7	-0.72	-0.08	-0.76
ULK4	hKQsi003	F8	6	8	-0.61	-0.32	-0.36
ALS2CR2	hKQsi003	F10	6	10	0.35	0.63	0.21
ADCK1	hKQsi003	F11	6	11	-0.01	0.37	0.53
PINK1	hKQsi003	F12	6	12	1.83	-0.74	-0.79
ADCK4	hKQsi003	F13	6	13	0.18	-0.94	-0.17
STK22D	hKQsi003	F14	6	14	0.40	-0.16	0.18
NEK9	hKQsi003	F15	6	15	-1.83	-0.57	-1.12
CIB3	hKQsi003	F17	6	17	-0.77	-0.76	-1.22
WDSUB1	hKQsi003	F18	6	18	-0.77	-0.86	-2.15
ANKK1	hKQsi003	F19	6	19	-0.55	-0.91	-1.19
discontinued	hKQsi003	F20	6	20	0.35	0.54	0.37
CDK11	hKQsi003	G3	7	3	1.46	-0.55	0.67
SGKL	hKQsi003	G4	7	4	-0.90	0.42	0.13
HRI	hKQsi003	G5	7	5	1.24	-0.02	-0.41
SH3KBP1	hKQsi003	G6	7	6	0.45	0.04	0.02
NLK	hKQsi003	G7	7	7	-0.83	-0.10	-0.36
AKIP	hKQsi003	G8	7	8	-0.47	0.44	0.99
CAMKIINALPHA	hKQsi003	G10	7	10	-0.13	0.64	-0.11
PAK7	hKQsi003	G11	7	11	0.35	-0.94	0.50
ALS2CR7	hKQsi003	G12	7	12	-0.03	-0.21	0.08
PANK2	hKQsi003	G13	7	13	0.33	-1.10	-0.97
SSTK	hKQsi003	G14	7	14	0.43	-1.71	-0.31
MLCK	hKQsi003	G15	7	15	-1.16	-0.87	-1.12
PIK3AP1	hKQsi003	G17	7	17	0.44	-0.41	-0.53
CNKSR3	hKQsi003	G18	7	18	-1.76	0.24	-0.45
MGC40579	hKQsi003	G19	7	19	0.04	0.54	0.48
discontinued	hKQsi003	G20	7	20	0.32	0.23	0.58
MAP3K7IP2	hKQsi003	H3	8	3	0.16	-1.33	-0.25
PRKCN	hKQsi003	H4	8	4	-0.32	-0.93	-1.11
EIF2AK4	hKQsi003	H5	8	5	0.45	-0.44	0.62
HUNK	hKQsi003	H6	8	6	0.30	0.24	-0.02
UMP-CMPK	hKQsi003	H7	8	7	-0.33	-0.33	-0.62
FLJ10761	hKQsi003	H8	8	8	0.10	-0.37	-0.63
ETNK1	hKQsi003	H10	8	10	-0.82	0.13	-0.42
CAMK1G	hKQsi003	H11	8	11	-0.88	0.29	0.90
PRKWNK1	hKQsi003	H12	8	12	-1.05	0.15	0.51
LAK	hKQsi003	H13	8	13	0.40	0.64	-0.09

CAMKK1	hKQsi003	H14	8	14	-0.90	-1.16	-0.09
LYK5	hKQsi003	H15	8	15	-0.65	-0.60	-0.11
LRRK2	hKQsi003	H17	8	17	0.49	-1.45	-1.35
AKAP28	hKQsi003	H18	8	18	-1.02	-0.58	-1.83
MAGI-3	hKQsi003	H19	8	19	1.00	0.74	-0.35
LOC392265	hKQsi003	H20	8	20	-1.37	-1.63	-0.74
MAST2	hKQsi003	I3	9	3	0.97	-0.67	0.40
CARKL	hKQsi003	I4	9	4	0.02	0.66	0.88
STK36	hKQsi003	I5	9	5	-0.98	-0.47	-1.05
PIK3R4	hKQsi003	I6	9	6	-1.89	-1.37	0.30
CRK7	hKQsi003	I7	9	7	1.17	-0.14	-0.15
PANK4	hKQsi003	I8	9	8	0.07	-0.78	-0.72
HSMDPKIN	hKQsi003	I10	9	10	0.99	0.05	-0.75
CLK4	hKQsi003	I11	9	11	0.60	0.07	-0.16
FLJ13052	hKQsi003	I12	9	12	1.73	0.28	1.07
ITPKC	hKQsi003	I13	9	13	-0.07	0.31	-0.16
KIAA1811	hKQsi003	I14	9	14	-0.60	-1.09	1.06
PRKCDBP	hKQsi003	I15	9	15	1.87	-0.29	-0.67
CSNK1A1L	hKQsi003	I17	9	17	0.12	-1.63	-1.79
DGKH	hKQsi003	I18	9	18	-1.48	0.24	-1.35
STK32C	hKQsi003	I19	9	19	0.50	1.96	0.38
discontinued	hKQsi003	I20	9	20	-0.35	-0.68	-0.57
MAPK8IP3	hKQsi003	J3	10	3	0.12	0.65	0.66
DUSTYPK	hKQsi003	J4	10	4	1.06	-0.03	0.63
RPS6KA6	hKQsi003	J5	10	5	-0.56	0.33	0.28
MINK	hKQsi003	J6	10	6	1.30	-0.81	-0.16
RP6-213H19.1	hKQsi003	J7	10	7	-0.72	-0.01	-0.19
FLJ10986	hKQsi003	J8	10	8	1.26	-0.51	-0.13
NAGK	hKQsi003	J10	10	10	0.57	0.03	-0.15
KIDINS220	hKQsi003	J11	10	11	0.40	-0.17	-0.06
WNK4	hKQsi003	J12	10	12	-0.69	0.26	0.05
SKIP	hKQsi003	J13	10	13	-0.32	-0.66	-0.68
KIAA1804	hKQsi003	J14	10	14	0.42	0.06	-0.10
TP53RK	hKQsi003	J15	10	15	-0.11	-0.02	-0.55
AK7	hKQsi003	J17	10	17	-0.38	-1.30	-0.62
CSNK1A1P	hKQsi003	J18	10	18	-1.65	-0.51	-1.71
LOC283155	hKQsi003	J19	10	19	-0.15	0.20	-0.71
LOC407835	hKQsi003	J20	10	20	-0.28	-0.36	-0.39
PASK	hKQsi003	K3	11	3	0.47	0.38	0.19
PRKD2	hKQsi003	K4	11	4	-0.23	0.02	-0.63

STK39	hKQsi003	K5	11	5	-0.79	1.18	0.71
AK3L1	hKQsi003	K6	11	6	0.77	-1.35	-0.58
ZAK	hKQsi003	K7	11	7	-0.11	0.43	0.08
PI4K2B	hKQsi003	K8	11	8	-1.09	-0.81	-0.72
BMP2K	hKQsi003	K10	11	10	-0.52	0.73	0.40
KIAA1361	hKQsi003	K11	11	11	0.19	0.01	0.12
PRKWNK3	hKQsi003	K12	11	12	-0.10	0.11	-0.26
GKAP1	hKQsi003	K13	11	13	0.51	-0.28	-0.83
TTBK1	hKQsi003	K14	11	14	1.35	0.11	0.70
LMTK3	hKQsi003	K15	11	15	-0.24	-0.84	-1.42
UHMK1	hKQsi003	K17	11	17	-0.23	0.09	-0.66
MGC45428	hKQsi003	K18	11	18	-2.95	0.58	0.16
KSR2	hKQsi003	K19	11	19	0.72	1.23	-0.14
MAST4	hKQsi003	L3	12	3	-0.22	0.36	1.28
DKFZP434C131	hKQsi003	L4	12	4	-0.98	-0.81	-0.27
GIT1	hKQsi003	L5	12	5	-0.23	0.48	0.14
TNNI3K	hKQsi003	L6	12	6	0.78	0.28	-0.01
PANK1	hKQsi003	L7	12	7	-0.58	0.95	1.67
RIOK2	hKQsi003	L10	12	10	1.13	-0.15	0.15
KIAA1446	hKQsi003	L11	12	11	0.70	-0.33	0.20
PRKWNK2	hKQsi003	L12	12	12	0.39	-0.04	0.04
TRAF3IP3	hKQsi003	L13	12	13	-0.09	-0.33	-0.66
FLJ14800	hKQsi003	L14	12	14	0.56	-0.20	0.02
IRAK1BP1	hKQsi003	L17	12	17	-0.45	-0.41	-1.02
FUK	hKQsi003	L18	12	18	-3.06	-0.96	5.27
NEK8	hKQsi003	L19	12	19	-1.46	0.85	-0.11
SIK2	hKQsi003	M3	13	3	0.03	0.56	0.92
IBTK	hKQsi003	M4	13	4	-1.78	1.39	0.82
HIPK2	hKQsi003	M5	13	5	-1.49	0.14	0.86
IRAK4	hKQsi003	M6	13	6	0.92	0.58	1.09
PRKAG3	hKQsi003	M7	13	7	-1.48	0.48	0.49
TOPK	hKQsi003	M10	13	10	-0.79	-0.07	0.43
MARK4	hKQsi003	M11	13	11	-0.20	-0.72	0.20
STK33	hKQsi003	M12	13	12	-0.84	-1.86	-0.53
STK22C	hKQsi003	M13	13	13	-0.45	0.73	0.48
MASTL	hKQsi003	M14	13	14	-0.83	0.42	0.68
PNCK	hKQsi003	M17	13	17	0.18	-0.55	-1.00
PIP5K3	hKQsi003	M18	13	18	-2.41	-0.04	0.54
discontinued	hKQsi003	M19	13	19	-0.79	2.22	2.32
PIP5K1C	hKQsi003	N3	14	3	-0.58	1.03	2.21

AK5	hKQsi003	N4	14	4	-1.00	0.42	0.32
TBK1	hKQsi003	N5	14	5	0.69	0.37	0.36
VRK3	hKQsi003	N6	14	6	0.19	0.67	0.55
CSNK1G1	hKQsi003	N7	14	7	-0.79	0.17	-0.02
LOC55971	hKQsi003	N10	14	10	-0.25	0.76	0.92
TSKS	hKQsi003	N11	14	11	0.34	0.78	0.91
MAPKAP1	hKQsi003	N12	14	12	0.00	-0.74	-0.48
SNARK	hKQsi003	N13	14	13	-0.72	-0.37	-0.67
PDXK	hKQsi003	N14	14	14	0.35	1.11	-0.13
NEK7	hKQsi003	N17	14	17	-0.85	-0.32	-1.13
STK32A	hKQsi003	N18	14	18	-0.10	0.21	-0.10
NEK5	hKQsi003	N19	14	19	-0.03	0.47	0.42
P101-PI3K	hKQsi003	O3	15	3	0.62	1.57	0.98
HSPB8	hKQsi003	O4	15	4	0.70	-2.02	-0.96
PACSIN3	hKQsi003	O5	15	5	0.43	0.83	1.00
CDKL3	hKQsi003	O6	15	6	-0.98	0.16	-0.14
ANKRD3	hKQsi003	O7	15	7	-0.04	-0.08	0.35
STK31	hKQsi003	O10	15	10	-0.78	0.96	1.65
RBKS	hKQsi003	O11	15	11	1.24	0.96	0.31
PANK3	hKQsi003	O12	15	12	-0.37	-0.95	-0.23
SHARPIN	hKQsi003	O13	15	13	0.57	-0.75	-0.25
MYLK2	hKQsi003	O14	15	14	-0.43	0.83	2.07
STK35	hKQsi003	O17	15	17	0.04	1.75	-0.02
ADCK5	hKQsi003	O18	15	18	-2.50	-1.23	-0.15
CDKL4	hKQsi003	O19	15	19	-0.48	1.04	1.70

Supplementary Table 3.2. Z-score data for nuclei count, foci count and foci area from a complete kinome RNAi screen in a $DM1_{500\ CTG}$ patient fibroblast line. The screen was done in triplicate using 10nM of pooled siRNA with an end-point readout conducted at 72hrs. The data was normalized to the sample mean per plate and is represented as average Z-score values.

siRNA	Plate	Well Name	Row	Column	Z-score (nuclei count)	Z-score (foci count)	Z-score (foci area)
ABL1	hKQsi001	B3	2	3	-0.16	-0.18	-0.36
AKT2	hKQsi001	B4	2	4	0.87	-0.79	-1.07
BUB1	hKQsi001	B5	2	5	0.53	-0.52	-0.63
CDK3	hKQsi001	B6	2	6	0.39	0.02	0.52
CHEK1	hKQsi001	B7	2	7	-0.84	-0.36	-0.04
MAP3K8	hKQsi001	B8	2	8	-0.64	0.62	0.27
CSNK2B	hKQsi001	B10	2	10	-0.18	0.79	0.26
EPHA2	hKQsi001	B11	2	11	-0.62	-0.10	-0.20
ERBB3	hKQsi001	B12	2	12	-0.77	0.39	0.32
FLT4	hKQsi001	B13	2	13	-0.03	-0.18	0.24
GSK3B	hKQsi001	B14	2	14	1.17	1.30	0.95
JAK1	hKQsi001	B15	2	15	-0.70	4.78	2.81
LYN	hKQsi001	B17	2	17	-0.93	3.12	2.98
MOS	hKQsi001	B18	2	18	0.82	-0.44	-0.64
NTRK2	hKQsi001	B19	2	19	-0.30	-0.75	-0.09
PDK1	hKQsi001	B20	2	20	1.53	-0.56	-0.78
PGK2	hKQsi001	B21	2	21	-0.50	-0.50	-0.71
PIK3CG	hKQsi001	B22	2	22	0.83	-1.14	-0.68
ABL2	hKQsi001	C3	3	3	-0.47	-0.43	-0.83
ALK	hKQsi001	C4	3	4	-0.20	0.69	1.45
BUB1B	hKQsi001	C5	3	5	-0.86	-0.20	-0.07
CDK4	hKQsi001	C6	3	6	-0.63	0.08	0.32
CHKA	hKQsi001	C7	3	7	0.41	-0.64	-0.30
MAPK14	hKQsi001	C8	3	8	-0.52	0.28	1.19
DGKA	hKQsi001	C10	3	10	-0.07	-0.42	-0.23
MARK2	hKQsi001	C11	3	11	-0.12	0.34	0.65
ERBB4	hKQsi001	C12	3	12	-1.20	0.00	-0.40
FRK	hKQsi001	C13	3	13	-0.82	1.01	1.18

GUK1	hKQsi001	C14	3	14	0.34	-0.52	-0.65
JAK2	hKQsi001	C15	3	15	-0.23	0.29	0.81
MARCKS	hKQsi001	C17	3	17	-0.39	-0.17	-0.17
MST1R	hKQsi001	C18	3	18	-0.11	-0.05	0.11
NTRK3	hKQsi001	C19	3	19	0.14	-0.21	-0.13
PDK2	hKQsi001	C20	3	20	-0.61	-0.01	-0.36
PHKA1	hKQsi001	C21	3	21	-1.63	-0.29	-0.48
PIK3R1	hKQsi001	C22	3	22	1.47	-0.74	-0.76
ACVR1	hKQsi001	D3	4	3	0.51	0.19	-0.07
ARAF1	hKQsi001	D4	4	4	0.42	-0.57	-0.74
DDR1	hKQsi001	D5	4	5	0.53	0.02	0.22
CDK5	hKQsi001	D6	4	6	-1.45	0.21	-0.43
CHKB	hKQsi001	D7	4	7	-1.10	0.49	0.50
CSK	hKQsi001	D8	4	8	-0.43	1.75	1.01
DGKB	hKQsi001	D10	4	10	-1.01	-1.17	-1.55
EPHA1	hKQsi001	D11	4	11	1.79	-0.52	-0.40
ERN1	hKQsi001	D12	4	12	0.69	-0.34	0.02
FYN	hKQsi001	D13	4	13	-1.15	0.43	0.54
HCK	hKQsi001	D14	4	14	-0.78	0.28	0.33
JAK3	hKQsi001	D15	4	15	0.31	-0.39	-0.47
MAK	hKQsi001	D17	4	17	-0.24	-0.12	-0.10
MUSK	hKQsi001	D18	4	18	-0.14	-0.39	-0.57
ROR1	hKQsi001	D19	4	19	0.07	1.79	1.42
PDK3	hKQsi001	D20	4	20	1.07	1.04	0.53
PHKA2	hKQsi001	D21	4	21	-1.19	-0.85	-1.15
PIK3R2	hKQsi001	D22	4	22	-0.12	-0.65	-0.75
ACVR1B	hKQsi001	E3	5	3	0.76	-0.58	-0.38
ATM	hKQsi001	E4	5	4	-0.65	-0.13	-0.05
CALM1	hKQsi001	E5	5	5	-0.22	0.01	0.00
CDK6	hKQsi001	E6	5	6	-0.71	-0.52	-0.43
CHUK	hKQsi001	E7	5	7	-1.17	-0.58	-0.54
CSNK1A1	hKQsi001	E8	5	8	-0.29	0.03	0.13
DGKG	hKQsi001	E10	5	10	-0.57	8.04	5.71
EPHA3	hKQsi001	E11	5	11	-0.30	1.07	1.18
PTK2B	hKQsi001	E12	5	12	1.88	-0.35	-0.54
GAK	hKQsi001	E13	5	13	-0.24	-0.11	-0.01
HK1	hKQsi001	E14	5	14	0.97	-0.86	-0.72
KDR	hKQsi001	E15	5	15	-0.52	0.23	0.14
MARK1	hKQsi001	E17	5	17	0.98	-0.22	-0.48
MVK	hKQsi001	E18	5	18	0.71	-0.76	-0.95

ROR2	hKQsi001	E19	5	19	0.25	-0.78	-1.07
PDK4	hKQsi001	E20	5	20	0.69	0.39	0.56
PHKB	hKQsi001	E21	5	21	0.09	0.66	0.62
PIK4CA	hKQsi001	E22	5	22	1.16	-0.80	-1.14
ACVR2	hKQsi001	F3	6	3	0.01	0.52	0.12
ATR	hKQsi001	F4	6	4	-0.07	0.12	-0.23
CALM2	hKQsi001	F5	6	5	0.94	-0.41	-0.38
CDK7	hKQsi001	F6	6	6	0.06	0.28	0.10
CKB	hKQsi001	F7	6	7	-0.11	0.18	0.14
CSNK1D	hKQsi001	F8	6	8	-1.06	0.02	-0.12
DGKQ	hKQsi001	F10	6	10	-0.71	0.43	0.44
EPHA4	hKQsi001	F11	6	11	-0.20	0.04	-0.21
FER	hKQsi001	F12	6	12	-0.01	-0.73	-1.04
GALK1	hKQsi001	F13	6	13	-0.69	0.10	0.09
HK2	hKQsi001	F14	6	14	-1.18	0.55	1.01
KHK	hKQsi001	F15	6	15	0.91	-0.39	-0.01
MARK3	hKQsi001	F17	6	17	-0.03	0.12	-0.37
MYLK	hKQsi001	F18	6	18	2.01	-0.49	-0.50
DDR2	hKQsi001	F19	6	19	-0.29	0.20	0.60
PDPK1	hKQsi001	F20	6	20	-0.16	-0.52	-0.62
PHKG1	hKQsi001	F21	6	21	0.91	0.16	0.09
PIK4CB	hKQsi001	F22	6	22	-0.82	-0.75	-0.84
ACVR2B	hKQsi001	G3	7	3	-0.26	1.70	0.61
AXL	hKQsi001	G4	7	4	0.07	-0.41	-0.09
CALM3	hKQsi001	G5	7	5	-0.05	-0.07	0.19
CDK8	hKQsi001	G6	7	6	-0.45	0.60	1.00
CKM	hKQsi001	G7	7	7	-0.08	-0.19	-0.21
CSNK1E	hKQsi001	G8	7	8	-0.37	-0.46	-0.41
DAPK1	hKQsi001	G10	7	10	0.02	0.50	0.27
EPHA5	hKQsi001	G11	7	11	-1.39	0.51	1.22
FES	hKQsi001	G12	7	12	0.27	-0.05	0.20
GALK2	hKQsi001	G13	7	13	1.58	-0.21	-0.23
HK3	hKQsi001	G14	7	14	0.96	-0.02	-0.32
KIT	hKQsi001	G15	7	15	0.74	-0.55	-0.42
MATK	hKQsi001	G17	7	17	0.57	-1.03	-1.17
NEK1	hKQsi001	G18	7	18	-0.74	0.54	0.78
PAK1	hKQsi001	G19	7	19	1.05	-0.35	-0.56
PFKFB1	hKQsi001	G20	7	20	-1.20	0.11	1.27
PHKG2	hKQsi001	G21	7	21	-0.35	0.56	0.58
PIP5K2A	hKQsi001	G22	7	22	0.45	-0.95	-0.95

ACVRL1	hKQsi001	H3	8	3	-0.08	-0.55	-0.55
BCR	hKQsi001	H4	8	4	-0.64	0.70	0.53
CAMK4	hKQsi001	H5	8	5	-0.99	1.34	1.34
CDK9	hKQsi001	H6	8	6	0.70	0.02	0.00
CKMT1B	hKQsi001	H7	8	7	1.29	0.01	-0.43
CSNK1G2	hKQsi001	H8	8	8	1.55	-0.52	-0.32
DAPK3	hKQsi001	H10	8	10	-0.79	-0.45	-0.64
EPHA7	hKQsi001	H11	8	11	-1.05	0.63	0.79
FGFR1	hKQsi001	H12	8	12	-0.06	0.11	-0.10
GCK	hKQsi001	H13	8	13	-1.04	-0.40	-0.22
IKBKB	hKQsi001	H14	8	14	1.22	-0.64	-0.36
LCK	hKQsi001	H15	8	15	-0.68	0.81	0.54
MAP3K1	hKQsi001	H17	8	17	-0.62	-0.18	-0.24
NEK2	hKQsi001	H18	8	18	-0.27	-0.59	-0.68
PAK2	hKQsi001	H19	8	19	-0.99	-0.29	0.15
PFKFB2	hKQsi001	H20	8	20	-0.89	-0.01	0.08
PIK3C2A	hKQsi001	H21	8	21	-0.31	-0.57	0.18
PKLR	hKQsi001	H22	8	22	0.56	-0.45	0.52
ADK	hKQsi001	I3	9	3	-0.46	2.45	2.63
BLK	hKQsi001	I4	9	4	0.27	-0.11	-0.06
CAMK2A	hKQsi001	I5	9	5	-0.06	-0.35	0.28
CDKN1A	hKQsi001	I6	9	6	5.02	-1.20	-1.21
CKMT2	hKQsi001	I7	9	7	0.16	0.15	0.34
CSNK1G3	hKQsi001	I8	9	8	-0.42	-0.14	-0.22
DCK	hKQsi001	I10	9	10	-0.22	0.24	0.62
EPHA8	hKQsi001	I11	9	11	2.07	-0.52	-0.44
FGFR3	hKQsi001	I12	9	12	0.58	0.30	0.07
GK	hKQsi001	I13	9	13	-0.79	0.10	1.11
ILK	hKQsi001	I14	9	14	1.72	-0.11	-0.40
LIMK1	hKQsi001	I15	9	15	-0.52	-0.18	0.16
MAP3K3	hKQsi001	I17	9	17	-0.40	5.39	4.75
NEK3	hKQsi001	I18	9	18	-0.95	0.29	0.11
PAK3	hKQsi001	I19	9	19	-0.83	-0.08	0.06
PFKFB3	hKQsi001	I20	9	20	-0.75	1.33	0.50
PIK3C2B	hKQsi001	I21	9	21	0.43	-0.54	-0.78
PKM2	hKQsi001	I22	9	22	-0.52	-0.72	-0.41
ADRBK1	hKQsi001	J3	10	3	-0.67	-0.08	0.00
BMPR1A	hKQsi001	J4	10	4	-0.38	0.42	0.16
CAMK2B	hKQsi001	J5	10	5	-0.35	-0.98	-1.52
CDKN1B	hKQsi001	J6	10	6	0.78	-0.38	-0.45

CKS1B	hKQsi001	J7	10	7	-0.66	0.91	0.85
CSNK2A1	hKQsi001	J8	10	8	-0.28	0.12	0.56
DGUOK	hKQsi001	J10	10	10	-0.75	-0.37	-0.85
EPHB1	hKQsi001	J11	10	11	1.97	-0.47	-0.63
FGFR2	hKQsi001	J12	10	12	0.24	0.14	-0.18
GK2	hKQsi001	J13	10	13	-0.02	0.40	-0.42
IRAK1	hKQsi001	J14	10	14	1.44	-0.72	-0.64
LIMK2	hKQsi001	J15	10	15	-0.42	-0.48	0.34
MAP3K4	hKQsi001	J17	10	17	-0.98	1.44	1.38
NME1	hKQsi001	J18	10	18	0.22	-0.27	-0.76
PCK1	hKQsi001	J19	10	19	-0.46	0.28	0.27
PFKFB4	hKQsi001	J20	10	20	0.78	-1.18	-1.25
PIK3C2G	hKQsi001	J21	10	21	-1.37	0.18	1.02
PLAU	hKQsi001	J22	10	22	-0.74	-1.09	-1.55
ADRBK2	hKQsi001	K3	11	3	0.11	-0.07	-0.28
BMPR1B	hKQsi001	K4	11	4	-1.10	-0.07	0.05
CAMK2D	hKQsi001	K5	11	5	-0.27	-0.87	-0.59
CDKN1C	hKQsi001	K6	11	6	-0.25	-0.01	-0.09
CKS2	hKQsi001	K7	11	7	0.27	-0.84	-0.74
CSNK2A2	hKQsi001	K8	11	8	-0.46	-0.06	-0.05
DMPK	hKQsi001	K10	11	10	-0.28	0.31	0.39
EPHB2	hKQsi001	K11	11	11	-0.83	-0.40	-0.96
FGFR4	hKQsi001	K12	11	12	-0.44	0.19	0.34
GRK4	hKQsi001	K13	11	13	-0.82	0.92	1.24
IRAK2	hKQsi001	K14	11	14	-0.40	0.16	0.22
LTK	hKQsi001	K15	11	15	0.13	0.70	0.20
MAP3K5	hKQsi001	K17	11	17	-0.87	-0.06	0.31
NME2	hKQsi001	K18	11	18	1.22	-0.45	-0.22
PCTK1	hKQsi001	K19	11	19	0.00	-0.33	-0.35
PFKL	hKQsi001	K20	11	20	-1.04	0.25	0.35
PIK3C3	hKQsi001	K21	11	21	1.33	0.13	-0.51
PLK1	hKQsi001	K22	11	22	-1.97	-1.87	-1.92
AK1	hKQsi001	L3	12	3	-0.33	0.60	-0.02
BMPR2	hKQsi001	L4	12	4	-0.64	0.01	0.78
CAMK2G	hKQsi001	L5	12	5	1.46	-0.40	-0.66
CDKN2A	hKQsi001	L6	12	6	1.16	0.57	0.86
CLK1	hKQsi001	L7	12	7	-0.46	0.03	0.00
DOK1	hKQsi001	L10	12	10	-0.26	-0.09	0.05
EPHB3	hKQsi001	L11	12	11	0.84	-0.03	0.14
FGR	hKQsi001	L12	12	12	0.53	-0.04	-0.05

GRK5	hKQsi001	L13	12	13	-0.06	-0.03	-0.34
ITK	hKQsi001	L14	12	14	-0.11	0.58	0.10
MET	hKQsi001	L17	12	17	2.08	-0.75	-1.05
NME3	hKQsi001	L18	12	18	-0.28	0.09	0.36
PCTK2	hKQsi001	L19	12	19	0.79	-0.23	-0.06
PFKM	hKQsi001	L20	12	20	-0.31	1.21	0.72
PIK3CA	hKQsi001	L21	12	21	-0.08	-0.49	-0.34
AK2	hKQsi001	M3	13	3	1.22	-1.11	-1.16
BMX	hKQsi001	M4	13	4	-1.20	0.90	0.76
CDC2	hKQsi001	M5	13	5	-1.31	0.52	1.04
CDKN2B	hKQsi001	M6	13	6	-0.58	-0.03	0.02
CLK2	hKQsi001	M7	13	7	-0.58	0.19	0.70
DTYMK	hKQsi001	M10	13	10	1.00	-0.54	-0.15
EPHB4	hKQsi001	M11	13	11	1.11	0.11	0.43
FLT1	hKQsi001	M12	13	12	-0.05	0.45	1.20
GRK6	hKQsi001	M13	13	13	1.97	-0.13	-0.30
ITPK1	hKQsi001	M14	13	14	0.07	0.07	0.72
MAP3K9	hKQsi001	M17	13	17	2.50	-0.86	-0.85
NME4	hKQsi001	M18	13	18	-0.40	-0.48	-0.74
PCTK3	hKQsi001	M19	13	19	0.49	-0.08	0.14
PFKP	hKQsi001	M20	13	20	0.76	-0.46	-0.48
PIK3CB	hKQsi001	M21	13	21	-0.80	-0.14	-0.20
AK3	hKQsi001	N3	14	3	-0.53	-0.10	-0.14
BRAF	hKQsi001	N4	14	4	-1.13	-0.29	1.04
CDC2L1	hKQsi001	N5	14	5	-0.90	-0.68	-0.16
CDKN2C	hKQsi001	N6	14	6	1.12	-0.46	-0.50
CLK3	hKQsi001	N7	14	7	0.36	0.19	0.61
DYRK1A	hKQsi001	N10	14	10	1.44	-0.76	-0.34
EPHB6	hKQsi001	N11	14	11	-0.03	-0.01	-0.21
FLT3	hKQsi001	N12	14	12	0.45	-0.20	-0.34
MKNK2	hKQsi001	N13	14	13	-0.32	0.33	0.52
ITPKA	hKQsi001	N14	14	14	0.01	0.27	0.23
MAP3K10	hKQsi001	N17	14	17	0.20	-0.16	0.06
NRGN	hKQsi001	N18	14	18	0.14	-0.26	-0.35
PDGFRA	hKQsi001	N19	14	19	-0.22	-0.47	-0.36
PFTK1	hKQsi001	N20	14	20	-0.66	-0.27	0.57
PIM1	hKQsi001	N21	14	21	0.53	-1.27	-1.33
AKT1	hKQsi001	O3	15	3	-0.08	-0.43	0.32
BTK	hKQsi001	O4	15	4	-1.03	-0.80	-1.03
CDK2	hKQsi001	O5	15	5	-1.06	-1.17	-1.54

CDKN2D	hKQsi001	O6	15	6	0.19	-1.31	-1.39
PLK3	hKQsi001	O7	15	7	-0.18	-0.30	-0.47
EGFR	hKQsi001	O10	15	10	-0.11	-0.65	-0.68
ERBB2	hKQsi001	O11	15	11	3.54	-0.50	-0.86
FLT3LG	hKQsi001	O12	15	12	-0.09	-0.62	-0.77
GSK3A	hKQsi001	O13	15	13	-0.60	0.98	0.98
ITPKB	hKQsi001	O14	15	14	1.01	-0.51	-0.82
MAP3K11	hKQsi001	O17	15	17	-0.17	-0.82	-0.59
NTRK1	hKQsi001	O18	15	18	0.79	1.59	0.79
PDGFRB	hKQsi001	O19	15	19	-0.33	-0.54	-0.74
PGK1	hKQsi001	O20	15	20	-0.13	-0.85	-0.81
PIK3CD	hKQsi001	O21	15	21	-0.62	-0.89	-0.35
PRKAA1	hKQsi002	B3	2	3	-0.82	0.39	0.76
PRKCA	hKQsi002	B4	2	4	-0.70	-1.04	-0.97
PRKG2	hKQsi002	B5	2	5	-0.56	1.28	1.15
MAP2K5	hKQsi002	B6	2	6	1.91	-0.30	-0.26
RAGE	hKQsi002	B7	2	7	0.87	-0.83	-0.38
SGK	hKQsi002	B8	2	8	-0.79	0.45	0.15
AURKA	hKQsi002	B10	2	10	-0.95	2.03	1.87
TK2	hKQsi002	B11	2	11	-0.94	1.24	1.22
MAP3K12	hKQsi002	B12	2	12	-0.54	0.94	0.72
IKBKG	hKQsi002	B13	2	13	-0.58	-0.40	0.01
CDC2L5	hKQsi002	B14	2	14	0.50	-0.77	-1.30
CDK5R2	hKQsi002	B15	2	15	0.11	0.75	-0.41
DGKI	hKQsi002	B17	2	17	-0.33	0.68	0.42
AKAP6	hKQsi002	B18	2	18	0.02	1.12	0.35
ARK5	hKQsi002	B19	2	19	2.10	-0.10	-0.55
PAK4	hKQsi002	B20	2	20	-0.23	0.04	-0.38
NEK6	hKQsi002	B21	2	21	-0.66	0.76	1.38
AKAP11	hKQsi002	B22	2	22	0.53	-0.64	-0.79
PRKAA2	hKQsi002	C3	3	3	0.16	0.03	0.22
PRKCB1	hKQsi002	C4	3	4	0.08	-0.55	-0.33
MAPK1	hKQsi002	C5	3	5	-1.00	0.82	1.15
MAP2K6	hKQsi002	C6	3	6	0.04	-0.35	-0.47
RAF1	hKQsi002	C7	3	7	0.34	0.21	0.19
SKP1A	hKQsi002	C8	3	8	-0.47	0.48	0.41
CDKL5	hKQsi002	C10	3	10	1.07	0.02	-0.01
TRIO	hKQsi002	C11	3	11	0.90	-0.26	-0.20
MAPKAPK3	hKQsi002	C12	3	12	-0.42	1.08	1.13
IKBKAP	hKQsi002	C13	3	13	-0.33	0.03	0.21

MAP2K1IP1	hKQsi002	C14	3	14	0.15	-0.24	-0.42
RPS6KA4	hKQsi002	C15	3	15	0.53	0.53	0.36
MAP3K13	hKQsi002	C17	3	17	-0.31	-0.62	-0.48
ROCK2	hKQsi002	C18	3	18	-1.05	0.05	-0.15
XYLB	hKQsi002	C19	3	19	0.42	-0.06	0.02
TESK2	hKQsi002	C20	3	20	2.12	-1.01	-1.02
FASTK	hKQsi002	C21	3	21	0.16	0.15	0.13
AKAP10	hKQsi002	C22	3	22	3.24	-0.55	-0.81
PRKAB1	hKQsi002	D3	4	3	1.77	-0.83	-0.55
PRKCD	hKQsi002	D4	4	4	-0.43	-0.02	-0.47
MAPK3	hKQsi002	D5	4	5	1.10	1.51	1.20
MAP2K7	hKQsi002	D6	4	6	-0.43	-0.20	0.46
RET	hKQsi002	D7	4	7	-0.47	0.25	0.58
SKP2	hKQsi002	D8	4	8	-1.11	1.34	1.34
STK10	hKQsi002	D10	4	10	-1.01	1.23	1.90
TTK	hKQsi002	D11	4	11	-0.48	-0.10	1.48
AKAP1	hKQsi002	D12	4	12	-0.38	0.77	0.09
DGKZ	hKQsi002	D13	4	13	0.73	-1.10	-0.95
TNK1	hKQsi002	D14	4	14	-0.46	0.10	0.28
CDKL2	hKQsi002	D15	4	15	0.34	-0.37	-0.65
DCAMKL1	hKQsi002	D17	4	17	0.89	0.86	0.37
MAPK8IP1	hKQsi002	D18	4	18	-0.58	-0.15	-0.15
OSR1	hKQsi002	D19	4	19	2.42	0.75	-0.31
MAP3K7IP1	hKQsi002	D20	4	20	-1.17	0.80	1.08
ASK	hKQsi002	D21	4	21	-0.73	-0.29	-0.38
PACSIN2	hKQsi002	D22	4	22	-0.65	-0.79	-0.80
PRKAB2	hKQsi002	E3	5	3	2.94	-1.52	-0.86
PRKCE	hKQsi002	E4	5	4	-0.94	-0.92	-0.91
MAPK4	hKQsi002	E5	5	5	0.54	0.61	1.00
PRKR	hKQsi002	E6	5	6	-0.20	-0.14	-0.37
GRK1	hKQsi002	E7	5	7	1.29	-1.17	-0.90
SRC	hKQsi002	E8	5	8	0.68	0.36	0.39
STK11	hKQsi002	E10	5	10	-0.02	-0.58	-0.48
TXK	hKQsi002	E11	5	11	-0.66	0.40	0.66
NME5	hKQsi002	E12	5	12	-0.47	0.28	0.01
DGKE	hKQsi002	E13	5	13	-0.67	0.11	0.16
RIPK1	hKQsi002	E14	5	14	-0.10	0.53	0.51
MAP3K14	hKQsi002	E15	5	15	1.75	-0.79	-0.87
AURKB	hKQsi002	E17	5	17	-0.99	2.65	4.04
AKAP5	hKQsi002	E18	5	18	0.79	-0.56	-0.51

AKT3	hKQsi002	E19	5	19	2.38	-0.84	-0.77
MERTK	hKQsi002	E20	5	20	-0.82	-0.30	-0.02
TLK2	hKQsi002	E21	5	21	-0.64	-0.13	-0.46
STK38	hKQsi002	E22	5	22	1.83	0.17	-0.24
PRKACA	hKQsi002	F3	6	3	1.35	-0.77	-0.74
PRKCG	hKQsi002	F4	6	4	0.05	-0.12	-0.33
MAPK6	hKQsi002	F5	6	5	0.17	-0.44	-0.23
PRKRIR	hKQsi002	F6	6	6	-0.99	0.75	0.32
ROCK1	hKQsi002	F7	6	7	-0.11	-1.16	-0.79
SRMS	hKQsi002	F8	6	8	0.84	0.15	0.11
AURKC	hKQsi002	F10	6	10	-0.26	-0.36	0.00
TYK2	hKQsi002	F11	6	11	-0.36	0.01	1.11
PIP5K1A	hKQsi002	F12	6	12	0.07	-0.54	-0.29
DGKD	hKQsi002	F13	6	13	0.12	0.56	0.75
RIPK2	hKQsi002	F14	6	14	0.81	0.93	0.88
STK29	hKQsi002	F15	6	15	-1.13	-0.47	-0.47
RPS6KA5	hKQsi002	F17	6	17	-0.34	-0.37	-0.16
CDC42BPB	hKQsi002	F18	6	18	-0.47	0.23	0.55
GNE	hKQsi002	F19	6	19	-0.28	-0.53	-0.48
STK25	hKQsi002	F20	6	20	0.60	-0.36	-0.34
RIPK3	hKQsi002	F21	6	21	1.81	-1.04	-1.04
PTK9L	hKQsi002	F22	6	22	-0.42	-1.07	-1.35
PRKACB	hKQsi002	G3	7	3	-0.75	-0.63	-0.08
PRKCH	hKQsi002	G4	7	4	1.65	-0.77	-0.05
MAPK7	hKQsi002	G5	7	5	0.55	-0.06	0.04
PRKX	hKQsi002	G6	7	6	0.57	-0.99	-0.49
ROS1	hKQsi002	G7	7	7	-0.80	-0.06	0.43
SRPK1	hKQsi002	G8	7	8	-0.89	-0.30	-0.20
SYK	hKQsi002	G10	7	10	-0.65	-0.56	-0.06
TYRO3	hKQsi002	G11	7	11	0.79	-0.15	0.05
PIP5K1B	hKQsi002	G12	7	12	-0.02	-0.60	-0.46
CAMK1	hKQsi002	G13	7	13	-0.93	0.29	1.55
RIOK3	hKQsi002	G14	7	14	0.28	-0.50	-0.36
MAP3K6	hKQsi002	G15	7	15	3.82	-1.92	-1.61
MAPKAPK2	hKQsi002	G17	7	17	0.19	-0.27	-0.64
AKAP12	hKQsi002	G18	7	18	-0.37	-0.41	-0.06
SGK2	hKQsi002	G19	7	19	-0.30	3.91	1.45
CIB2	hKQsi002	G20	7	20	-1.22	1.34	0.69
PIM2	hKQsi002	G21	7	21	0.01	-1.29	-1.65
AAK1	hKQsi002	G22	7	22	0.32	-1.20	-1.20

PRKACG	hKQsi002	H3	8	3	-1.34	-0.65	-0.60
PRKCI	hKQsi002	H4	8	4	-0.64	1.03	0.65
MAPK8	hKQsi002	H5	8	5	-0.62	-0.57	0.72
PRKY	hKQsi002	H6	8	6	-1.03	0.20	0.11
RPS6KA1	hKQsi002	H7	8	7	-1.11	1.42	1.29
SRPK2	hKQsi002	H8	8	8	-0.68	-0.49	0.65
MAP3K7	hKQsi002	H10	8	10	-1.28	-0.36	-0.06
TYROBP	hKQsi002	H11	8	11	-0.09	0.02	0.25
PIP5K2B	hKQsi002	H12	8	12	-0.04	-0.89	-1.35
MAPKAPK5	hKQsi002	H13	8	13	-0.82	0.60	0.96
DYRK4	hKQsi002	H14	8	14	-0.72	-0.35	-0.26
PKMYT1	hKQsi002	H15	8	15	-0.52	0.39	0.88
STK17B	hKQsi002	H17	8	17	0.58	-0.44	-0.26
AATK	hKQsi002	H18	8	18	-0.94	-0.67	-0.32
HIPK3	hKQsi002	H19	8	19	-0.97	2.68	0.54
AKAP3	hKQsi002	H20	8	20	-0.52	-0.23	0.07
CIT	hKQsi002	H21	8	21	0.12	0.05	0.02
LMTK2	hKQsi002	H22	8	22	0.74	-0.75	-0.66
PKIA	hKQsi002	I3	9	3	1.74	-1.33	-1.20
PRKCL1	hKQsi002	I4	9	4	-0.69	-1.27	-0.50
MAPK11	hKQsi002	I5	9	5	1.19	0.34	0.40
PRSS7	hKQsi002	I6	9	6	-0.03	0.69	0.72
RPS6KA2	hKQsi002	I7	9	7	-0.82	0.16	0.45
NEK4	hKQsi002	I8	9	8	-1.01	1.65	1.10
TEC	hKQsi002	I10	9	10	0.04	-1.42	-1.34
UGP2	hKQsi002	I11	9	11	0.45	0.02	0.00
ULK1	hKQsi002	I12	9	12	0.54	-0.55	-0.12
CDK10	hKQsi002	I13	9	13	0.04	-0.90	-0.82
CDKL1	hKQsi002	I14	9	14	-0.34	0.77	-0.02
LATS1	hKQsi002	I15	9	15	2.13	-0.54	-0.24
STK17A	hKQsi002	I17	9	17	0.70	-0.90	-0.86
IKBKE	hKQsi002	I18	9	18	0.05	0.58	0.33
AKAP9	hKQsi002	I19	9	19	0.08	1.29	0.59
ERN2	hKQsi002	I20	9	20	-0.31	0.27	0.33
KALRN	hKQsi002	I21	9	21	-0.16	0.22	0.09
ICK	hKQsi002	I22	9	22	0.22	-0.48	-0.26
PKIB	hKQsi002	J3	10	3	-0.41	0.04	-0.62
PRKCL2	hKQsi002	J4	10	4	-0.40	-0.97	-0.93
MAPK9	hKQsi002	J5	10	5	-0.46	-0.43	-0.12
PSKH1	hKQsi002	J6	10	6	-0.16	-0.86	-0.57

RPS6KA3	hKQsi002	J7	10	7	-0.01	-0.49	-0.14
STK3	hKQsi002	J8	10	8	-1.03	-0.66	-0.75
TEK	hKQsi002	J10	10	10	-0.51	0.39	0.52
UMPK	hKQsi002	J11	10	11	-0.52	-0.95	-0.81
STK24	hKQsi002	J12	10	12	0.25	-0.86	-0.70
PDXK	hKQsi002	J13	10	13	-0.33	0.11	-0.12
KSR	hKQsi002	J14	10	14	-0.35	0.15	0.42
HGS	hKQsi002	J15	10	15	-0.83	-0.66	-1.00
TAO1	hKQsi002	J17	10	17	1.15	0.28	0.22
ULK2	hKQsi002	J18	10	18	-0.83	0.65	0.32
TNK2	hKQsi002	J19	10	19	-0.47	1.24	0.24
PDLIM5	hKQsi002	J20	10	20	-0.32	-0.10	-0.30
PKIG	hKQsi002	J21	10	21	-0.04	-1.30	-1.58
SORCS3	hKQsi002	J22	10	22	-0.17	-1.27	-0.54
PRKAG1	hKQsi002	K3	11	3	1.40	0.22	0.57
PRKCM	hKQsi002	K4	11	4	0.41	-0.80	-0.63
MAPK10	hKQsi002	K5	11	5	0.23	0.63	0.87
PTK2	hKQsi002	K6	11	6	-0.30	0.19	0.07
RPS6KB1	hKQsi002	K7	11	7	1.31	-1.04	-0.51
STK4	hKQsi002	K8	11	8	0.68	-0.85	-0.74
TESK1	hKQsi002	K10	11	10	0.17	1.19	1.21
VRK1	hKQsi002	K11	11	11	-0.78	2.36	1.12
DYRK3	hKQsi002	K12	11	12	1.96	-0.69	-0.73
MADD	hKQsi002	K13	11	13	0.47	-0.45	-0.50
CDK5R1	hKQsi002	K14	11	14	-0.37	-0.21	-0.03
DYRK1B	hKQsi002	K15	11	15	-0.97	-1.25	-1.00
TAO1	hKQsi002	K17	11	17	1.06	-0.78	-0.38
SLK	hKQsi002	K18	11	18	0.15	-0.87	-0.39
NME6	hKQsi002	K19	11	19	1.11	0.34	-0.57
CAMKK2	hKQsi002	K20	11	20	0.52	0.01	-0.08
MAP4K5	hKQsi002	K21	11	21	-0.91	-0.51	0.04
MAPKBP1	hKQsi002	K22	11	22	1.72	-1.63	-1.41
PRKAR1A	hKQsi002	L3	12	3	-1.04	-0.52	-0.36
PRKCQ	hKQsi002	L4	12	4	0.14	-0.08	-0.11
MAPK13	hKQsi002	L5	12	5	-0.61	0.56	0.61
PTK6	hKQsi002	L6	12	6	-0.76	0.50	0.36
RPS6KB2	hKQsi002	L7	12	7	-0.19	-0.61	-0.76
TGFBR1	hKQsi002	L10	12	10	0.10	-0.17	-0.14
VRK2	hKQsi002	L11	12	11	-0.43	2.45	1.82
DYRK2	hKQsi002	L12	12	12	-0.31	0.14	0.41

MKNK1	hKQsi002	L13	12	13	-1.08	0.45	0.96
AKAP4	hKQsi002	L14	12	14	-0.27	0.65	0.09
MAP4K4	hKQsi002	L17	12	17	-0.23	0.69	1.29
IHPK1	hKQsi002	L18	12	18	-0.26	5.86	3.91
CNKSR1	hKQsi002	L19	12	19	0.39	0.40	-0.12
PMVK	hKQsi002	L20	12	20	0.87	-0.07	-0.21
MAP4K1	hKQsi002	L21	12	21	-0.23	1.15	1.16
PRKAR1B	hKQsi002	M3	13	3	1.25	-0.38	-0.29
PRKCZ	hKQsi002	M4	13	4	0.28	-0.38	-0.66
MAP2K1	hKQsi002	M5	13	5	-0.12	-0.74	-0.19
PTK7	hKQsi002	M6	13	6	-0.77	0.00	0.21
RYK	hKQsi002	M7	13	7	-0.11	-1.12	0.32
TGFBR2	hKQsi002	M10	13	10	-0.69	-0.25	-0.01
WEE1	hKQsi002	M11	13	11	-1.25	-0.33	-0.61
CDC42BPA	hKQsi002	M12	13	12	0.25	1.93	1.33
CASK	hKQsi002	M13	13	13	-0.93	1.03	0.57
STK19	hKQsi002	M14	13	14	0.89	-0.39	-0.56
EIF2AK3	hKQsi002	M17	13	17	-0.44	0.52	0.67
GIT2	hKQsi002	M18	13	18	-0.77	0.29	0.15
AKAP8	hKQsi002	M19	13	19	0.29	-0.74	-0.78
PLK4	hKQsi002	M20	13	20	-0.48	-0.43	-0.71
CHEK2	hKQsi002	M21	13	21	1.73	-1.08	-1.32
PRKAR2A	hKQsi002	N3	14	3	1.56	-0.66	-0.63
PRKDC	hKQsi002	N4	14	4	0.11	-0.43	-0.16
MAP2K2	hKQsi002	N5	14	5	-0.57	-0.04	0.98
PTK9	hKQsi002	N6	14	6	-0.49	-0.18	0.70
MAPK12	hKQsi002	N7	14	7	-1.05	0.29	0.33
TIE	hKQsi002	N10	14	10	-0.37	-0.80	-0.95
YES1	hKQsi002	N11	14	11	-0.57	0.19	0.55
MAP4K3	hKQsi002	N12	14	12	0.63	1.58	0.97
PRKRA	hKQsi002	N13	14	13	1.77	-1.58	-1.48
SPHK1	hKQsi002	N14	14	14	-0.63	0.61	0.88
PRKCABP	hKQsi002	N17	14	17	-0.66	0.08	0.87
MELK	hKQsi002	N18	14	18	-0.37	-0.64	-0.64
SPEG	hKQsi002	N19	14	19	-0.67	-0.30	-0.20
MAP3K2	hKQsi002	N20	14	20	0.42	-1.15	-1.11
IRAK3	hKQsi002	N21	14	21	1.33	-0.82	-0.40
PRKAR2B	hKQsi002	O3	15	3	0.96	-2.09	-1.59
PRKG1	hKQsi002	O4	15	4	0.91	-1.97	-0.17
MAP2K3	hKQsi002	O5	15	5	0.40	0.76	1.43

MAP4K2	hKQsi002	O6	15	6	-1.14	1.01	1.05
MAP2K4	hKQsi002	O7	15	7	0.00	-0.52	-0.41
TK1	hKQsi002	O10	15	10	0.04	0.79	0.01
ZAP70	hKQsi002	O11	15	11	1.09	-0.09	-0.01
PIK3R3	hKQsi002	O12	15	12	0.45	-0.42	-0.36
STK16	hKQsi002	O13	15	13	-0.57	0.73	0.44
PRPF4B	hKQsi002	O14	15	14	3.04	-0.45	-0.11
AKAP7	hKQsi002	O17	15	17	1.25	-1.17	-0.68
TLK1	hKQsi002	O18	15	18	1.06	-1.74	-1.30
BCKDK	hKQsi002	O19	15	19	1.82	-1.65	-0.96
PLK2	hKQsi002	O20	15	20	0.59	-0.36	-0.41
AKAP13	hKQsi002	O21	15	21	2.28	-1.30	-1.10
STK38L	hKQsi003	B3	2	3	-0.38	-2.62	-2.21
MAPK8IP2	hKQsi003	B4	2	4	-0.37	0.28	0.13
LATS2	hKQsi003	B5	2	5	-0.31	-0.72	-1.17
EEF2K	hKQsi003	B6	2	6	2.98	-1.31	-1.31
JIK	hKQsi003	B7	2	7	-1.35	0.78	0.80
SNRK	hKQsi003	B8	2	8	-0.03	0.00	-0.22
RFK	hKQsi003	B10	2	10	-0.73	0.60	1.79
SPHK2	hKQsi003	B11	2	11	-1.08	0.82	1.06
FN3K	hKQsi003	B12	2	12	0.43	-0.67	-0.84
FN3KRP	hKQsi003	B13	2	13	-0.45	-0.07	0.43
UCK1	hKQsi003	B14	2	14	-1.50	0.45	1.61
PSKH2	hKQsi003	B15	2	15	-0.42	-0.14	0.13
STK11IP	hKQsi003	B17	2	17	1.45	-0.24	-0.05
TTBK2	hKQsi003	B18	2	18	-0.10	-0.90	-0.23
NRK	hKQsi003	B19	2	19	0.15	-0.68	-0.71
MAST4	hKQsi003	B20	2	20	-0.69	0.58	1.13
MAST3	hKQsi003	C3	3	3	4.01	-2.02	-1.98
CCRK	hKQsi003	C4	3	4	-0.59	-0.08	0.27
STK23	hKQsi003	C5	3	5	-0.31	-0.26	-0.63
NME7	hKQsi003	C6	3	6	0.62	0.15	0.17
PRKAG2	hKQsi003	C7	3	7	-0.86	0.36	0.18
EPS8L1	hKQsi003	C8	3	8	0.06	1.32	0.51
STK32B	hKQsi003	C10	3	10	-0.59	0.03	0.10
PAK6	hKQsi003	C11	3	11	-0.59	-0.07	0.04
NJMU-R1	hKQsi003	C12	3	12	0.77	0.23	-0.44
LRRK1	hKQsi003	C13	3	13	-0.67	-0.06	0.19
RPS6KL1	hKQsi003	C14	3	14	-0.24	0.47	1.10
NYD-SP25	hKQsi003	C15	3	15	-0.31	2.34	0.99

HAK	hKQsi003	C17	3	17	0.16	-0.62	0.26
HIPK4	hKQsi003	C18	3	18	1.50	-2.54	-2.20
HIPK1	hKQsi003	C19	3	19	-0.69	1.14	1.13
SBK1	hKQsi003	C20	3	20	1.10	2.09	1.69
TNIK	hKQsi003	D3	4	3	-0.90	0.28	0.16
DAPK2	hKQsi003	D4	4	4	-1.17	1.55	1.62
RPS6KC1	hKQsi003	D5	4	5	1.11	-0.52	-0.55
PKN3	hKQsi003	D6	4	6	-0.53	-0.08	0.17
IHPK2	hKQsi003	D7	4	7	0.16	0.10	-0.59
PXK	hKQsi003	D8	4	8	-0.52	0.15	0.58
STYK1	hKQsi003	D10	4	10	-0.79	0.34	-0.77
SPEC2	hKQsi003	D11	4	11	-0.88	-0.16	0.44
NUCKS	hKQsi003	D12	4	12	-0.75	0.58	0.28
PIP5K2C	hKQsi003	D13	4	13	-1.04	-0.19	0.09
RIOK1	hKQsi003	D14	4	14	-0.71	-0.35	-0.54
NYD-SP25	hKQsi003	D15	4	15	1.21	-0.85	-1.59
IHPK3	hKQsi003	D17	4	17	0.40	-1.66	-1.86
PDIK1L	hKQsi003	D18	4	18	-0.41	1.51	1.35
PRPS1L1	hKQsi003	D19	4	19	-1.02	-0.45	-1.01
discontinued	hKQsi003	D20	4	20	-1.20	1.21	2.12
SMG1	hKQsi003	E3	5	3	0.62	-0.47	-1.05
PRKCBP1	hKQsi003	E4	5	4	-0.74	-0.10	1.10
AKAP8L	hKQsi003	E5	5	5	0.31	-0.04	0.11
NRBP	hKQsi003	E6	5	6	0.31	-0.09	0.54
NIPA	hKQsi003	E7	5	7	-1.10	-0.31	-0.56
URKL1	hKQsi003	E8	5	8	1.07	-0.50	-1.05
PI4KII	hKQsi003	E10	5	10	-0.34	3.66	2.36
CAMK1D	hKQsi003	E11	5	11	-0.48	-0.54	-0.07
CERK	hKQsi003	E12	5	12	1.45	0.41	0.08
NEK11	hKQsi003	E13	5	13	-0.15	-0.45	-0.35
MGC4796	hKQsi003	E14	5	14	-1.34	-0.22	-0.17
ADCK2	hKQsi003	E15	5	15	-0.81	1.04	0.62
CIB3	hKQsi003	E17	5	17	-1.30	0.31	0.21
SNF1LK	hKQsi003	E18	5	18	-0.81	0.20	0.16
ERK8	hKQsi003	E19	5	19	-0.60	0.43	0.94
discontinued	hKQsi003	E20	5	20	-0.01	-0.43	-0.16
ARHGAP26	hKQsi003	F3	6	3	1.57	-1.04	-1.45
STK22B	hKQsi003	F4	6	4	-0.78	-0.64	-0.59
TPK1	hKQsi003	F5	6	5	-0.30	-1.21	-1.13
PACSIN1	hKQsi003	F6	6	6	0.19	0.01	0.54

CINP	hKQsi003	F7	6	7	0.16	-1.18	-1.03
ULK4	hKQsi003	F8	6	8	-0.53	-0.87	-0.83
ALS2CR2	hKQsi003	F10	6	10	-0.88	1.09	0.58
ADCK1	hKQsi003	F11	6	11	0.20	0.15	0.96
PINK1	hKQsi003	F12	6	12	2.70	-0.82	-0.72
ADCK4	hKQsi003	F13	6	13	0.15	-1.03	-0.79
STK22D	hKQsi003	F14	6	14	-0.56	0.39	0.90
NEK9	hKQsi003	F15	6	15	-1.08	-0.46	-0.63
PIK3AP1	hKQsi003	F17	6	17	-1.00	-0.11	-0.37
WDSUB1	hKQsi003	F18	6	18	-0.45	-1.34	-1.67
ANKK1	hKQsi003	F19	6	19	1.66	-0.99	-0.74
discontinued	hKQsi003	F20	6	20	-0.69	0.95	0.92
CDK11	hKQsi003	G3	7	3	1.16	1.42	0.20
SGKL	hKQsi003	G4	7	4	-0.84	-0.06	-0.07
HRI	hKQsi003	G5	7	5	0.68	0.02	-0.06
SH3KBP1	hKQsi003	G6	7	6	1.08	-0.71	-0.68
NLK	hKQsi003	G7	7	7	-0.87	-0.98	-0.99
AKIP	hKQsi003	G8	7	8	-1.10	1.29	1.45
CAMKIINALPHA	hKQsi003	G10	7	10	-0.53	0.20	-0.14
PAK7	hKQsi003	G11	7	11	-0.33	0.01	0.59
ALS2CR7	hKQsi003	G12	7	12	-0.87	1.91	2.23
PANK2	hKQsi003	G13	7	13	-0.19	0.85	1.34
SSTK	hKQsi003	G14	7	14	0.57	-0.84	-0.53
MLCK	hKQsi003	G15	7	15	0.49	-1.26	-1.39
LRRK2	hKQsi003	G17	7	17	0.34	-0.50	-0.22
CNKSR3	hKQsi003	G18	7	18	-0.93	0.18	0.40
MGC40579	hKQsi003	G19	7	19	-0.66	1.10	1.95
discontinued	hKQsi003	G20	7	20	0.70	0.18	0.11
MAP3K7IP2	hKQsi003	H3	8	3	-0.52	-0.40	-0.20
PRKCN	hKQsi003	H4	8	4	-0.68	1.77	0.32
EIF2AK4	hKQsi003	H5	8	5	0.29	0.00	0.11
HUNK	hKQsi003	H6	8	6	-0.45	0.15	-0.65
UMP-CMPK	hKQsi003	H7	8	7	-1.14	-0.36	-0.76
FLJ10761	hKQsi003	H8	8	8	1.36	-0.35	-0.32
ETNK1	hKQsi003	H10	8	10	-1.13	-0.04	0.00
CAMK1G	hKQsi003	H11	8	11	-1.11	1.82	1.55
PRKWNK1	hKQsi003	H12	8	12	0.06	0.99	0.80
LAK	hKQsi003	H13	8	13	0.31	-0.38	0.82
CAMKK1	hKQsi003	H14	8	14	-0.26	-0.16	-0.41
LYK5	hKQsi003	H15	8	15	-0.35	-0.97	-0.82

CSNK1A1L	hKQsi003	H17	8	17	1.25	-0.70	-0.57
AKAP28	hKQsi003	H18	8	18	0.18	-0.52	-0.50
MAGI-3	hKQsi003	H19	8	19	1.58	-0.84	-0.86
LOC392265	hKQsi003	H20	8	20	-1.57	0.17	-0.64
MAST2	hKQsi003	I3	9	3	1.22	0.06	-0.46
CARKL	hKQsi003	I4	9	4	2.32	-0.74	-0.39
STK36	hKQsi003	I5	9	5	-1.02	-0.31	-0.46
PIK3R4	hKQsi003	I6	9	6	-1.56	-0.18	0.92
CRK7	hKQsi003	I7	9	7	1.92	0.09	-0.20
PANK4	hKQsi003	I8	9	8	0.30	-0.88	-0.94
HSMDPKIN	hKQsi003	I10	9	10	1.08	-0.52	-0.80
CLK4	hKQsi003	I11	9	11	1.35	-0.76	-0.48
FLJ13052	hKQsi003	I12	9	12	1.38	0.05	0.28
ITPKC	hKQsi003	I13	9	13	0.03	-0.07	0.16
KIAA1811	hKQsi003	I14	9	14	0.23	-0.20	0.78
PRKCDBP	hKQsi003	I15	9	15	1.24	-0.42	-0.27
AK7	hKQsi003	I17	9	17	-0.33	-0.47	-0.90
DGKH	hKQsi003	I18	9	18	-0.54	0.51	0.07
STK32C	hKQsi003	I19	9	19	0.11	1.90	1.46
discontinued	hKQsi003	I20	9	20	0.84	-0.91	-1.56
MAPK8IP3	hKQsi003	J3	10	3	0.03	-0.14	0.19
DUSTYPK	hKQsi003	J4	10	4	1.12	-1.02	-0.97
RPS6KA6	hKQsi003	J5	10	5	-0.86	0.25	0.49
MINK	hKQsi003	J6	10	6	0.11	0.18	-0.23
RP6-213H19.1	hKQsi003	J7	10	7	-1.23	0.51	0.50
FLJ10986	hKQsi003	J8	10	8	2.04	-0.27	-0.22
NAGK	hKQsi003	J10	10	10	0.64	-0.10	-0.16
KIDINS220	hKQsi003	J11	10	11	0.30	0.13	0.20
WNK4	hKQsi003	J12	10	12	-0.95	0.49	0.38
SKIP	hKQsi003	J13	10	13	-0.29	-0.93	-1.02
KIAA1804	hKQsi003	J14	10	14	0.39	-0.41	-0.47
TP53RK	hKQsi003	J15	10	15	-0.55	-0.20	-0.06
UHMK1	hKQsi003	J17	10	17	-0.19	-0.43	-0.57
CSNK1A1P	hKQsi003	J18	10	18	0.60	0.21	0.48
LOC283155	hKQsi003	J19	10	19	-0.73	-1.00	-1.16
LOC407835	hKQsi003	J20	10	20	0.45	-0.16	-0.20
PASK	hKQsi003	K3	11	3	0.80	-0.35	-0.51
PRKD2	hKQsi003	K4	11	4	-0.78	1.72	-0.39
STK39	hKQsi003	K5	11	5	-1.99	-0.35	0.19
AK3L1	hKQsi003	K6	11	6	1.05	-0.57	-0.42

ZAK	hKQsi003	K7	11	7	-0.34	0.56	0.37
PI4K2B	hKQsi003	K8	11	8	-0.98	-0.28	-0.17
BMP2K	hKQsi003	K10	11	10	-0.14	0.02	0.82
KIAA1361	hKQsi003	K11	11	11	1.44	-1.34	-1.24
PRKWNK3	hKQsi003	K12	11	12	0.73	-0.25	-0.09
GKAP1	hKQsi003	K13	11	13	-0.26	0.14	-0.24
TTBK1	hKQsi003	K14	11	14	2.45	1.83	0.78
LMTK3	hKQsi003	K15	11	15	-0.49	-0.64	-0.66
GRK7	hKQsi003	K17	11	17	0.24	1.41	1.12
MGC45428	hKQsi003	K18	11	18	-1.19	2.96	1.60
KSR2	hKQsi003	K19	11	19	-0.40	1.21	0.59
MAST4	hKQsi003	L3	12	3	-0.14	0.37	0.74
DKFZP434C131	hKQsi003	L4	12	4	-0.22	-1.05	-1.27
GIT1	hKQsi003	L5	12	5	-0.78	0.90	0.39
TNNI3K	hKQsi003	L6	12	6	0.06	-0.18	-0.32
PANK1	hKQsi003	L7	12	7	-0.60	1.04	1.84
RIOK2	hKQsi003	L10	12	10	-0.19	0.31	2.08
KIAA1446	hKQsi003	L11	12	11	1.07	-0.15	-0.04
PRKWNK2	hKQsi003	L12	12	12	-0.16	-0.18	-0.16
TRAF3IP3	hKQsi003	L13	12	13	-0.89	0.96	0.64
FLJ14800	hKQsi003	L14	12	14	1.29	-0.82	-0.47
IRAK1BP1	hKQsi003	L17	12	17	-0.38	-0.32	-0.54
FUK	hKQsi003	L18	12	18	0.31	-0.72	-0.97
NEK8	hKQsi003	L19	12	19	-0.70	0.99	0.43
SIK2	hKQsi003	M3	13	3	0.49	0.23	0.28
IBTK	hKQsi003	M4	13	4	-0.99	2.17	1.01
HIPK2	hKQsi003	M5	13	5	-0.16	-0.24	0.26
IRAK4	hKQsi003	M6	13	6	-0.05	-0.36	-0.02
PRKAG3	hKQsi003	M7	13	7	-0.76	-0.17	0.00
TOPK	hKQsi003	M10	13	10	1.07	-1.35	-1.22
MARK4	hKQsi003	M11	13	11	-0.84	-0.29	-0.06
STK33	hKQsi003	M12	13	12	-0.50	-0.39	-0.54
STK22C	hKQsi003	M13	13	13	-0.11	0.13	0.70
MASTL	hKQsi003	M14	13	14	-0.16	0.50	1.17
PNCK	hKQsi003	M17	13	17	1.28	-0.92	-0.84
PIP5K3	hKQsi003	M18	13	18	0.47	-0.78	-0.90
discontinued	hKQsi003	M19	13	19	-0.59	2.37	2.16
PIP5K1C	hKQsi003	N3	14	3	0.07	0.54	1.13
AK5	hKQsi003	N4	14	4	-0.52	-0.32	-0.46
TBK1	hKQsi003	N5	14	5	1.35	-0.62	-0.41

VRK3	hKQsi003	N6	14	6	-0.13	0.86	1.56
CSNK1G1	hKQsi003	N7	14	7	-0.57	-0.50	-0.39
LOC55971	hKQsi003	N10	14	10	-0.62	-0.64	-0.34
TSKS	hKQsi003	N11	14	11	0.30	0.30	0.71
MAPKAP1	hKQsi003	N12	14	12	0.04	-0.39	-0.21
SNARK	hKQsi003	N13	14	13	0.31	-0.81	-0.65
PDXK	hKQsi003	N14	14	14	1.74	0.00	0.00
NEK7	hKQsi003	N17	14	17	0.23	-0.51	-0.78
STK32A	hKQsi003	N18	14	18	-0.03	-0.06	-0.17
NEK5	hKQsi003	N19	14	19	-0.37	1.46	0.49
P101-PI3K	hKQsi003	O3	15	3	0.41	-0.17	-0.23
HSPB8	hKQsi003	O4	15	4	2.46	-2.06	-2.13
PACSIN3	hKQsi003	O5	15	5	0.09	-0.44	0.74
CDKL3	hKQsi003	O6	15	6	-0.96	-0.61	-1.09
ANKRD3	hKQsi003	O7	15	7	0.86	-0.93	-0.41
STK31	hKQsi003	O10	15	10	-0.89	-0.02	0.48
RBKS	hKQsi003	O11	15	11	1.36	-0.87	-0.70
PANK3	hKQsi003	O12	15	12	-0.94	4.02	1.33
SHARPIN	hKQsi003	O13	15	13	1.90	-1.15	-0.85
MYLK2	hKQsi003	O14	15	14	-0.46	2.11	1.47
STK35	hKQsi003	O17	15	17	0.33	0.17	0.72
ADCK5	hKQsi003	O18	15	18	-0.54	-1.15	-1.37
CDKL4	hKQsi003	O19	15	19	0.29	0.55	0.74

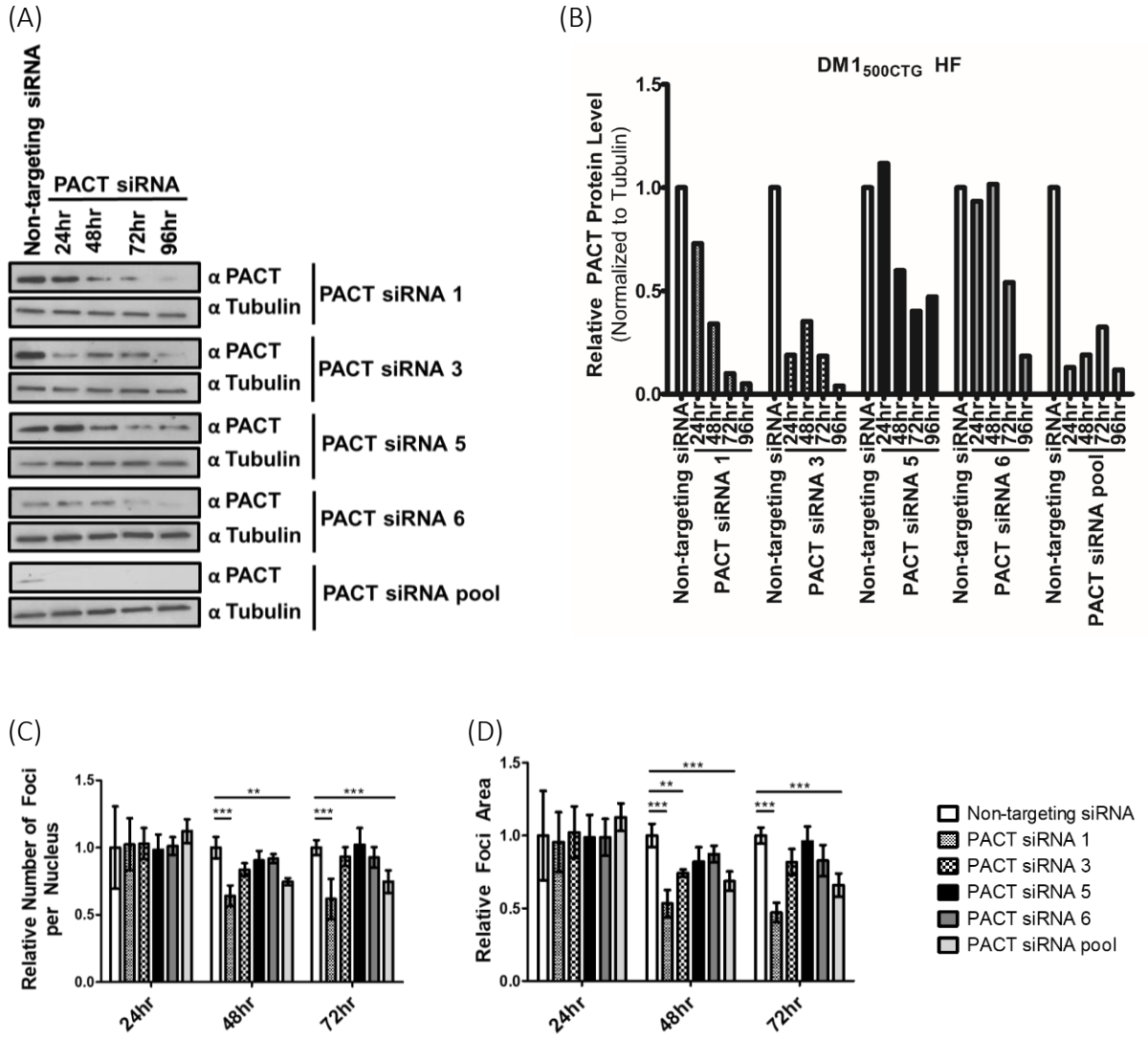

Supplementary Figure 3.1. Validation of PACT knockdown as a novel modulator of DM1 foci in $DM1_{500CTG\ HF}$. (A) Western blot analysis of PACT knockdown using individual and pooled PACT siRNA. (B) Quantification of PACT knockdown in (A) was done by densitometric analysis using Image J. (C-D) Foci integrity upon PACT knockdown. Cells were probed with Alexa-555 (CAG)10 probes to detect and image foci. Quantification of (C) number of foci per nucleus and (D) total foci area per nucleus was done using the Columbus software and mean data from five replicate wells is shown (n=5; two-way ANOVA; error bars represent SD).

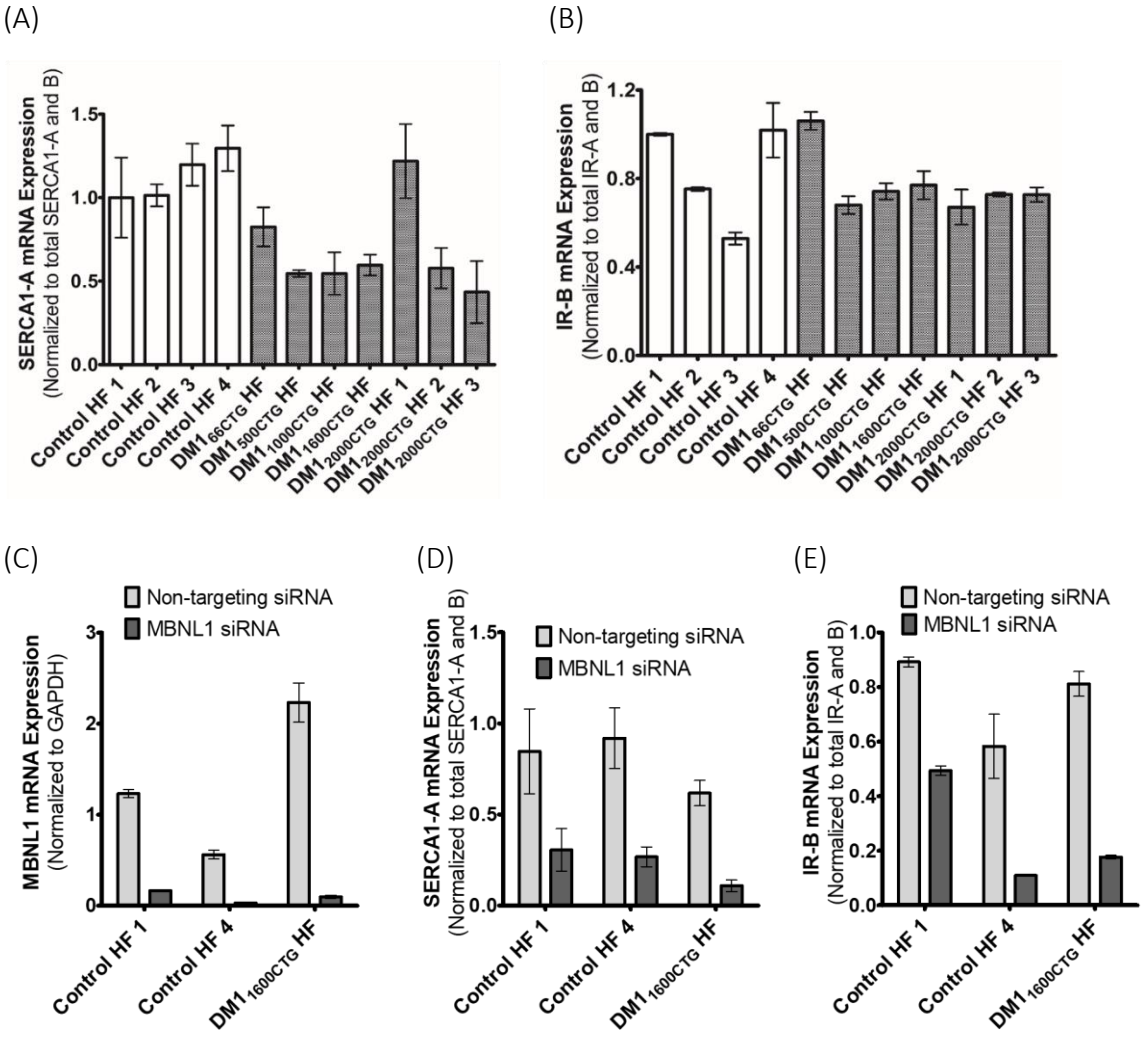

Supplementary Figure 3.2. Assessment of DM1 spliceopathy by RT-qPCR compared to Control HF. (A) SERCA1 and (B) IR splicing patterns in Control HF versus DM1 HF using RT-qPCR. Error bars are representative of duplicate qPCR runs, SEM. (A) SERCA1-A levels were measured using an exon 22-specific primer and quantified against total SERCA1-A and B as the reference gene. (B) IR-B mRNA levels were measured using an exon 11-specific primer and quantified against total IR-A and B as the reference gene. MBNL1 knockdown was used to validate sensitivity of the assay in detecting changes in splicing upon treatment. (C) MBNL1 with reference to GAPDH confirmed MBNL1 knockdown.

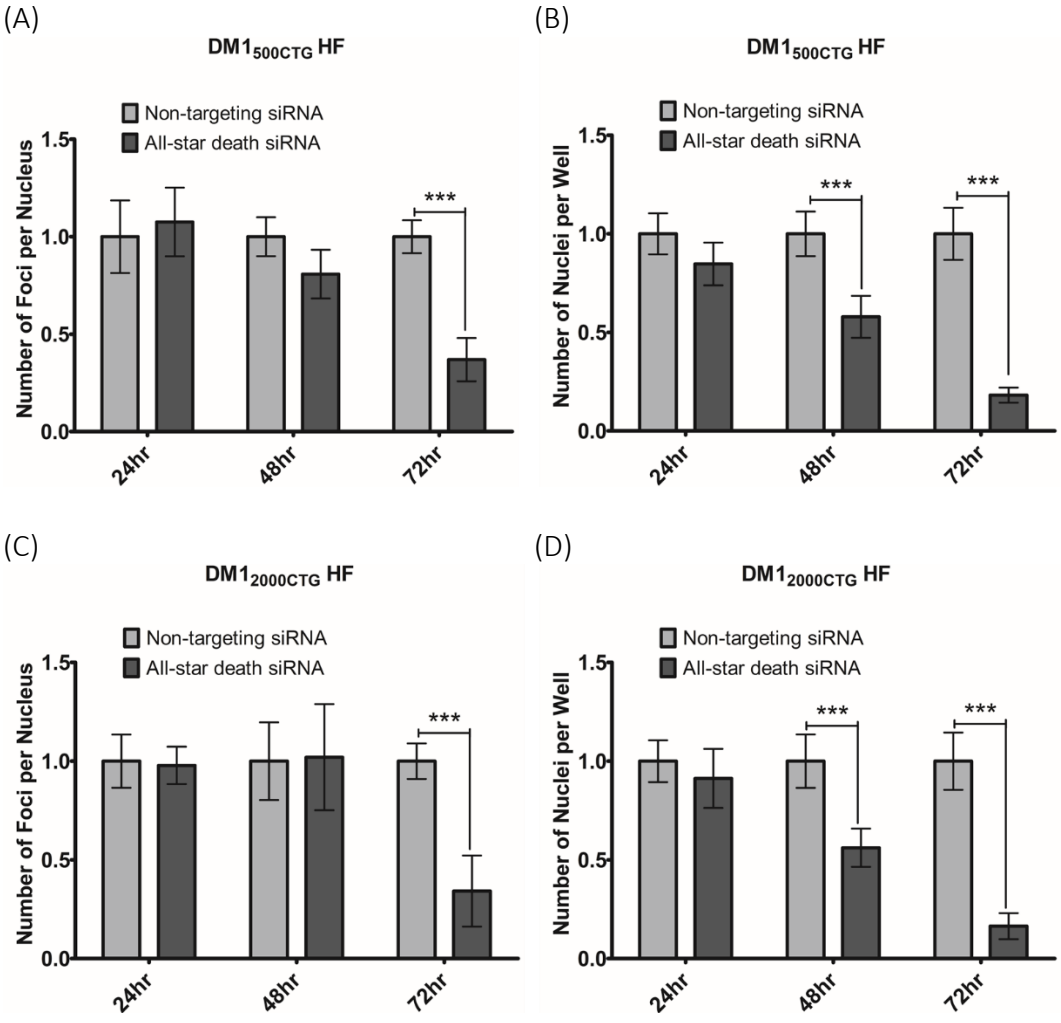

Supplementary Figure 3.3. All-star death siRNA kills cells in a time-dependent manner and likely reduces nuclear foci as a result. Effect of All-star death siRNA on number of cells and number of foci per nucleus in (A-B) DM1500 CTG and (C-D) DM12000 CTG. Cells were stained with Hoechst to visualize nuclei and with Alexa-555 $(CAG)_{10}$ probe to detect foci. Quantification was done using the Columbus software (n=4; two-way ANOVA; error bars represent SD). For statistical analysis, each trial consisted of mean data from 3-9 replicate wells per sample with corresponding SD. The data was converted to fold change relative to non-targeting siRNA and the SD was adjusted to the same ratio. The fold change and SD data were averaged across all trials.

(A)

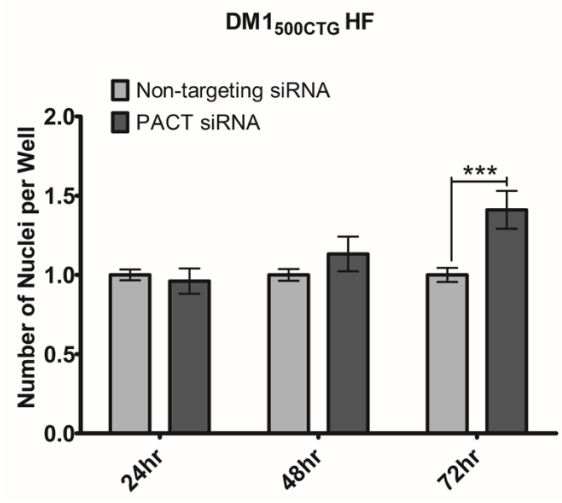

(B)

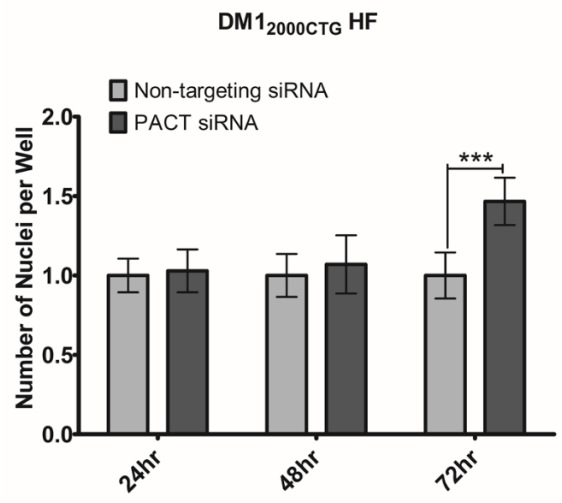

Supplementary Figure 3.4. PACT knockdown is not toxic to DM1 fibroblasts. Effect of PACT siRNA treatment on number of cells in (A) $DM1_{500\ CTG}$ and (B) $DM1_{2000\ CTG}$ HF. Cells were stained with Hoechst to visualize the nuclei. Quantification was done using the Columbus software (n=4; two-way ANOVA; error bars represent SD). For statistical analysis, each trial consisted of mean data from 3-9 replicate wells per sample with corresponding SD. The data was converted to fold change relative to non-targeting siRNA to accommodate plate-to-plate variability and the SD was adjusted to the same ratio. The fold change and SD data were averaged across all trials.

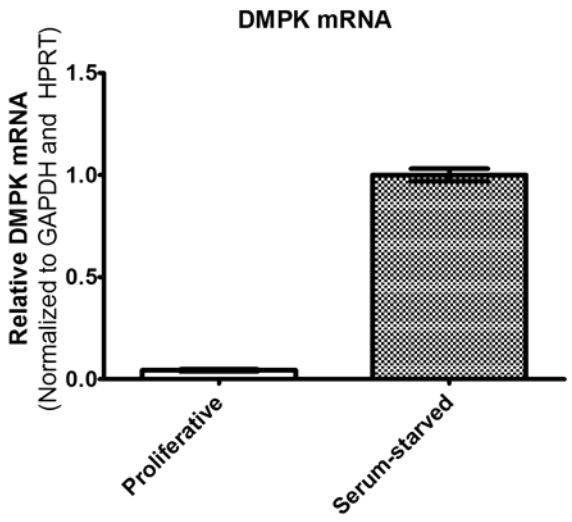

Supplementary Figure 4.1. DMPK mRNA expression is greater in serum-starved (differentiated) than proliferative DM1$_{3600CTG}$ immortalized myoblasts. Cells were grown in complete media (proliferative) or additionally serum-starved in differentiation media for 7, RNA was extracted and converted to cDNA, and DMPK mRNA was quantified using qPCR to compare expression between proliferative and serum-starved DM1$_{3600CTG}$ myoblast, normalized to GAPDH and HPRT.

Supplementary Table 4.1. Summary of FDA small-molecule screen in differentiated $DM1_{3600CTG}$ myoblasts. $DM1_{3600CTG}$ myoblasts were serum-starved in 384-well plates for 7 days and treated with 2uM of drugs for 24hrs. Post-treatment, cells were fixed with 4% PFA, DNA was stained with Hoechst and CUG RNA foci were probed by Alexa555-$(CAG)_{10}$. Foci area per nuclear area and number of nuclei per well were quantified using Columbus and normalized to DMSO control data per plate. Data is presented as the average fold-change relative to DMSO treatment (n=3).

Plate ID	Drug #	Drug Name	Well Name	Fold change based on DMSO mean (nuclei)		Fold change based on DMSO mean (foci)	
				AVERAGE	STDEV	AVERAGE	STDEV
cFDA800_3	1	Clindamycin·HCl	K3	1.063	0.188	0.858	0.231
cFDA800_3	2	Felbamate	K5	0.910	0.196	1.007	0.066
cFDA800_3	3	Cyclosporine A	K7	1.060	0.124	1.000	0.039
cFDA800_3	4	Donepezil·HCl	K9	0.914	0.094	1.018	0.035
cFDA800_3	5	Lincomycin·HCl	K11	1.007	0.108	0.993	0.036
cFDA800_3	6	Mycophenolic Acid	K13	1.054	0.218	0.901	0.069
cFDA800_3	7	Sirolimus (Rapamycin)	K15	1.134	0.227	0.904	0.091
cFDA800_3	8	Spectinomycin·HCl Pentahydrate	K17	1.104	0.285	1.028	0.026
cFDA800_3	9	Amiodarone·HCl	K19	0.865	0.142	0.990	0.047
cFDA800_3	10	Nicardipine·HCl	K21	1.071	0.193	1.049	0.055
cFDA800_1	11	Pimozide	B3	1.100	0.001	0.990	0.038
cFDA800_1	12	Loperamide·HCl	B5	1.097	0.074	1.003	0.030
cFDA800_1	13	Tolbutamide	B7	1.052	0.140	0.984	0.029
cFDA800_1	14	Glipizide	B9	0.992	0.120	0.995	0.025
cFDA800_1	15	Phentolamine·HCl	B11	1.103	0.133	1.033	0.040
cFDA800_1	16	Quinine·HCl·H2O	B13	1.052	0.136	0.972	0.020
cFDA800_1	17	Propafenone·HCl	B15	0.964	0.005	0.987	0.028
cFDA800_1	18	Phenytoin	B17	1.135	0.162	0.979	0.032
cFDA800_1	19	Procainamide·HCl	B19	1.108	0.139	0.982	0.013
cFDA800_1	20	Lidocaine·HCl·H2O	B21	0.941	0.068	0.994	0.042
cFDA800_1	21	Flecainide Acetate	C3	1.005	0.011	0.989	0.027
cFDA800_1	22	Rosiglitazone	C5	1.039	0.077	0.987	0.097
cFDA800_1	23	Amantadine·HCl	C7	1.009	0.080	1.011	0.030
cFDA800_1	24	Prazosin·HCl	C9	1.032	0.029	1.008	0.057
cFDA800_1	25	Clonidine·HCl	C11	0.947	0.022	0.977	0.046
cFDA800_1	26	Guanabenz Acetate	C13	0.976	0.047	0.982	0.026
cFDA800_1	27	Dihydroergotamine Mesylate	C15	1.001	0.044	0.982	0.086
cFDA800_1	28	Emtricitabine	C17	0.870	0.053	0.980	0.040
cFDA800_1	29	Betaxolol·HCl	C19	0.942	0.037	1.026	0.051
cFDA800_1	30	Caffeine	C21	1.000	0.051	1.001	0.007
cFDA800_1	31	(S)-Timolol Maleate	D3	1.034	0.104	0.980	0.017

cFDA800_1	32	Salbutamol Hemisulfate	D5	0.860	0.030	0.903	0.016
cFDA800_1	33	Pindolol	D7	0.878	0.022	1.002	0.042
cFDA800_1	34	Dobutamine·HCl	D9	0.997	0.061	0.923	0.013
cFDA800_1	35	Sotalol·HCl	D11	0.939	0.022	0.973	0.028
cFDA800_1	36	Maprotiline·HCl	D13	0.940	0.098	0.952	0.034
cFDA800_1	37	Pilocarpine·HCl	D15	0.976	0.089	0.991	0.005
cFDA800_1	38	Ipratropium·Br	D17	0.932	0.075	1.006	0.025
cFDA800_1	39	Tropicamide	D19	0.896	0.075	0.961	0.032
cFDA800_1	40	Pancuronium·2Br	D21	0.944	0.074	0.990	0.040
cFDA800_1	41	Ivermectin	E3	1.008	0.028	0.969	0.008
cFDA800_1	42	Haloperidol	E5	0.995	0.026	1.011	0.041
cFDA800_1	43	Cimetidine	E7	0.997	0.089	1.011	0.048
cFDA800_1	44	Zonisamide	E9	1.056	0.080	0.984	0.034
cFDA800_1	45	Zoledronic Acid Monohydrate	E11	0.973	0.017	0.991	0.039
cFDA800_1	46	Naltrexone·HCl	E13	0.987	0.019	1.013	0.016
cFDA800_1	47	Zolmitriptan	E15	0.935	0.103	0.986	0.013
cFDA800_1	48	Memantine·HCl	E17	0.977	0.087	0.994	0.019
cFDA800_1	49	Riluzole·HCl	E19	0.951	0.124	1.017	0.029
cFDA800_1	50	Propofol	E21	0.995	0.050	1.023	0.036
cFDA800_1	51	Aminophylline	F3	1.004	0.091	1.003	0.042
cFDA800_1	52	Nateglinide	F5	0.911	0.012	0.975	0.030
cFDA800_1	53	(±) Isoproterenol·HCl	F7	0.852	0.016	0.896	0.029
cFDA800_1	54	Acetylcholine Chloride	F9	0.996	0.076	1.062	0.044
cFDA800_1	55	Atropine Sulfate Monohydrate	F11	0.965	0.133	1.014	0.017
cFDA800_1	56	Apomorphine·HCl Hemihydrate	F13	0.928	0.061	1.017	0.164
cFDA800_1	57	Chlorpromazine·HCl	F15	0.900	0.042	1.016	0.041
cFDA800_1	58	Fluphenazine·HCl	F17	0.946	0.168	1.026	0.016
cFDA800_1	59	Risperidone	F19	0.965	0.065	0.927	0.060
cFDA800_1	60	Diphenhydramine·HCl	F21	0.929	0.096	0.965	0.032
cFDA800_1	61	Promethazine·HCl	G3	0.968	0.055	0.981	0.048
cFDA800_1	62	Ranitidine·HCl	G5	0.998	0.070	1.012	0.042
cFDA800_1	63	Epinephrine (L-(-)-Epinephrine-(+)-Bitartrate)	G7	0.856	0.073	0.902	0.019
cFDA800_1	64	Norepinephrine Bitartrate Monohydrate	G9	0.962	0.024	0.986	0.016
cFDA800_1	65	Quetiapine Fumarate	G11	0.936	0.060	1.039	0.030
cFDA800_1	66	Imipramine·HCl	G13	1.005	0.041	0.998	0.095
cFDA800_1	67	Amoxapine	G15	0.980	0.069	0.964	0.018
cFDA800_1	68	Metoclopramide·HCl	G17	1.005	0.054	0.983	0.036
cFDA800_1	69	Nalbuphine·HCl Dihydrate	G19	0.951	0.049	0.991	0.055
cFDA800_1	70	Carbachol (Carbamylcholine) Chloride	G21	1.008	0.054	1.023	0.025
cFDA800_1	71	Famotidine	H3	0.996	0.077	0.988	0.022

cFDA800_1	72	Isoniazid	H5	1.028	0.057	1.008	0.046
cFDA800_1	73	Ticlopidine·HCl	H7	1.013	0.071	1.023	0.011
cFDA800_1	74	Clemastine Fumarate	H9	0.948	0.040	0.964	0.045
cFDA800_1	75	Vardenafil	H11	1.012	0.092	1.033	0.055
cFDA800_1	76	Linezolid	H13	1.033	0.120	0.998	0.058
cFDA800_1	77	Docetaxel (Taxotere)	H15	0.813	0.017	0.926	0.021
cFDA800_1	78	Olopatadine	H17	0.958	0.087	1.019	0.066
cFDA800_1	79	Tolcapone	H19	0.997	0.084	0.970	0.045
cFDA800_1	80	Olmesartan	H21	0.891	0.095	0.989	0.064
cFDA800_3	81	Nisoldipine	K4	1.048	0.086	0.851	0.241
cFDA800_3	82	Olanzapine	K6	1.032	0.104	1.011	0.025
cFDA800_3	83	Lovastatin	K8	1.027	0.042	0.994	0.038
cFDA800_3	84	Lamotrigine	K10	1.016	0.212	0.999	0.036
cFDA800_3	85	Azathioprine	K12	0.961	0.093	0.956	0.057
cFDA800_3	86	Sildenafil Citrate	K14	0.970	0.076	0.983	0.067
cFDA800_3	87	Atovaquone	K16	0.914	0.074	1.011	0.021
cFDA800_3	88	Sertaconazole	K18	1.072	0.043	0.982	0.165
cFDA800_3	89	Cefepime·HCl Hydrate	K20	1.026	0.174	1.067	0.024
cFDA800_3	90	Aripiprazole	K22	1.052	0.150	1.004	0.013
cFDA800_1	91	Candesartan	B4	1.122	0.102	0.980	0.036
cFDA800_1	92	Butenafine·HCl	B6	1.066	0.048	1.010	0.011
cFDA800_1	93	Dorzolamide·HCl	B8	1.053	0.116	1.003	0.056
cFDA800_1	94	Escitalopram	B10	1.016	0.071	1.039	0.057
cFDA800_1	95	Eprosartan Mesylate	B12	1.028	0.113	0.996	0.054
cFDA800_1	96	Entacapone	B14	1.101	0.008	1.001	0.056
cFDA800_1	97	Bleomycin Sulfate	B16	0.873	0.076	0.921	0.060
cFDA800_1	98	Guanfacine·HCl	B18	0.985	0.040	0.992	0.032
cFDA800_1	99	Tizanidine·HCl	B20	0.989	0.020	0.962	0.035
cFDA800_1	100	Carvedilol	B22	1.062	0.098	1.053	0.066
cFDA800_1	101	Flumazenil	C4	1.012	0.079	0.992	0.056
cFDA800_1	102	Gefitinib	C6	0.872	0.048	0.995	0.050
cFDA800_1	103	Imatinib Mesylate	C8	0.960	0.072	1.077	0.114
cFDA800_1	104	Idarubicin·HCl	C10	0.807	0.040	0.953	0.050
cFDA800_1	105	Montelukast·Na	C12	0.955	0.127	1.018	0.053
cFDA800_1	106	Exemestane	C14	0.988	0.052	0.951	0.058
cFDA800_1	107	Dinoprostone	C16	0.948	0.076	0.849	0.041
cFDA800_1	108	Metformin·HCl	C18	0.925	0.062	0.998	0.078
cFDA800_1	109	Anagrelide	C20	0.919	0.030	0.968	0.031
cFDA800_1	110	Dofetilide	C22	1.064	0.059	0.937	0.079
cFDA800_1	111	Erlotinib	D4	0.993	0.052	0.974	0.053
cFDA800_1	112	Tacrine·HCl	D6	0.926	0.129	0.992	0.021
cFDA800_1	113	Galantamine·HBr	D8	1.049	0.082	1.020	0.067
cFDA800_1	114	Amiloride·HCl·2H2O	D10	0.997	0.083	0.994	0.012
cFDA800_1	115	Amlodipine	D12	0.934	0.108	1.022	0.027

cFDA800_1	116	Diltiazem·HCl	D14	0.944	0.043	0.987	0.023
cFDA800_1	117	Nifedipine	D16	0.978	0.052	0.993	0.034
cFDA800_1	118	Nimodipine	D18	0.935	0.057	0.981	0.050
cFDA800_1	119	Verapamil·HCl	D20	0.925	0.060	0.999	0.043
cFDA800_1	120	Gabapentin	D22	0.970	0.054	0.856	0.223
cFDA800_1	121	Felodipine	E4	0.944	0.049	1.005	0.019
cFDA800_1	122	Phenoxybenzamine·HCl	E6	0.982	0.109	1.030	0.010
cFDA800_1	123	Trifluoperazine·HCl	E8	0.944	0.035	0.999	0.047
cFDA800_1	124	Latanoprost	E10	1.066	0.027	0.983	0.045
cFDA800_1	125	Alfuzosin	E12	0.950	0.032	0.998	0.051
cFDA800_1	126	Bromocriptine Mesylate	E14	0.945	0.023	1.058	0.036
cFDA800_1	127	Clozapine	E16	0.956	0.016	0.991	0.022
cFDA800_1	128	Acitretin	E18	0.949	0.022	0.955	0.036
cFDA800_1	129	Calcitriol	E20	0.920	0.027	0.940	0.011
cFDA800_1	130	Ketoconazole	E22	0.926	0.035	0.999	0.051
cFDA800_1	131	Cromolyn·Na (Disodium Cromoglycate)	F4	0.989	0.137	0.982	0.046
cFDA800_1	132	Capsaicin	F6	0.931	0.059	1.014	0.034
cFDA800_1	133	Dexamethasone	F8	1.069	0.020	0.853	0.059
cFDA800_1	134	Dipyridamole	F10	0.941	0.051	1.014	0.033
cFDA800_1	135	Ethacrynic Acid	F12	0.937	0.060	0.851	0.020
cFDA800_1	136	Indomethacin	F14	0.903	0.071	1.086	0.093
cFDA800_1	137	Naproxen	F16	0.910	0.056	0.998	0.058
cFDA800_1	138	Ibuprofen	F18	1.020	0.076	1.004	0.025
cFDA800_1	139	Bumetanide	F20	0.977	0.144	0.971	0.032
cFDA800_1	140	Neomycin Sulfate	F22	0.951	0.088	1.000	0.058
cFDA800_1	141	Auranofin	G4	0.004	0.003	0.323	0.416
cFDA800_1	142	Captopril	G6	1.055	0.079	0.978	0.042
cFDA800_1	143	Tranylcypromine Hemisulfate	G8	0.939	0.080	0.977	0.046
cFDA800_1	144	Piroxicam	G10	0.960	0.064	1.027	0.028
cFDA800_1	145	Moxifloxacin·HCl	G12	0.961	0.096	0.999	0.046
cFDA800_1	146	Carbidopa	G14	1.006	0.093	1.050	0.038
cFDA800_1	147	Ketoprofen	G16	1.017	0.060	0.999	0.016
cFDA800_1	148	Meloxicam	G18	1.042	0.017	1.016	0.011
cFDA800_1	149	Terbinafine·HCl	G20	0.946	0.064	1.008	0.060
cFDA800_1	150	Sodium Phenylbutyrate	G22	0.963	0.093	0.979	0.012
cFDA800_1	151	Simvastatin	H4	0.884	0.105	0.958	0.007
cFDA800_1	152	Goserelin Acetate	H6	1.014	0.122	1.007	0.022
cFDA800_1	153	Raloxifene·HCl	H8	1.051	0.088	0.979	0.024
cFDA800_1	154	Rifampin (Rifampicin)	H10	0.939	0.066	0.973	0.025
cFDA800_1	155	Etoposide	H12	0.918	0.025	0.987	0.072
cFDA800_1	156	Mitomycin C	H14	0.922	0.096	0.755	0.015
cFDA800_1	157	Delavirdine Mesylate	H16	0.983	0.031	1.010	0.045
cFDA800_1	158	Daunorubicin·HCl	H18	0.599	0.009	3.832	0.249

cFDA800_1	159	Doxorubicin·HCl	H20	0.735	0.105	2.675	0.496
cFDA800_1	160	Cetirizine 2HCl	H22	0.922	0.109	0.986	0.031
cFDA800_1	161	Lapatinib Ditosylate	I3	0.992	0.044	1.006	0.017
cFDA800_1	162	Pioglitazone·HCl	I5	1.022	0.033	1.021	0.004
cFDA800_1	163	Rivastigmine Tartrate	I7	1.095	0.074	1.042	0.021
cFDA800_1	164	Ergotamine Tartrate	I9	1.033	0.030	1.011	0.007
cFDA800_1	165	Sulindac	I11	0.996	0.073	0.954	0.045
cFDA800_1	166	Valproic Acid	I13	0.974	0.047	1.018	0.019
cFDA800_1	167	Calcipotriene	I15	1.020	0.099	0.882	0.026
cFDA800_1	168	Zafirlukast	I17	0.999	0.089	0.957	0.020
cFDA800_1	169	Zileuton	I19	0.944	0.074	0.996	0.058
cFDA800_1	170	Bortezomib	I21	0.729	0.045	0.673	0.023
cFDA800_1	171	Diazoxide	J3	1.180	0.306	0.958	0.038
cFDA800_1	172	Glyburide	J5	1.022	0.091	1.021	0.047
cFDA800_1	173	Minoxidil	J7	1.138	0.223	1.023	0.030
cFDA800_1	174	Tolazamide	J9	1.149	0.053	1.017	0.046
cFDA800_1	175	Bexarotene	J11	0.932	0.126	0.938	0.046
cFDA800_1	176	Tranexamic Acid	J13	0.971	0.067	0.989	0.032
cFDA800_1	177	Celecoxib	J15	1.001	0.115	0.965	0.073
cFDA800_1	178	Levetiracetam	J17	0.968	0.070	0.967	0.017
cFDA800_1	179	Letrozole	J19	0.907	0.043	1.014	0.048
cFDA800_1	180	Anastrozole	J21	0.888	0.178	1.024	0.027
cFDA800_1	181	Bicalutamide	K3	1.069	0.120	0.994	0.019
cFDA800_1	182	Clindamycin Palmitate·HCl	K5	0.966	0.083	1.026	0.045
cFDA800_1	183	Vorinostat	K7	0.806	0.080	0.481	0.040
cFDA800_1	184	Didanosine	K9	0.961	0.024	0.992	0.028
cFDA800_1	185	Dolasetron	K11	0.929	0.021	1.040	0.038
cFDA800_1	186	Enalaprilat Maleate	K13	0.931	0.186	1.036	0.033
cFDA800_1	187	Fluvastatin·Na	K15	0.795	0.047	1.036	0.072
cFDA800_1	188	Fosinopril·Na	K17	0.896	0.106	1.019	0.034
cFDA800_1	189	Gemcitabine·HCl	K19	0.870	0.019	0.618	0.038
cFDA800_1	190	Granisetron·HCl	K21	0.907	0.096	1.038	0.043
cFDA800_1	191	Oxaliplatin	L3	1.013	0.033	1.108	0.071
cFDA800_1	192	Atazanavir	L5	0.969	0.069	1.058	0.070
cFDA800_1	193	Mycophenolate Mofetil	L7	0.917	0.055	0.921	0.021
cFDA800_1	194	Clofarabine	L9	0.933	0.018	0.726	0.012
cFDA800_1	195	Cabergoline	L11	1.040	0.041	1.046	0.052
cFDA800_1	196	Ibandronate·Na Monohydrate	L13	0.984	0.053	1.045	0.014
cFDA800_1	197	Imipenem	L15	0.919	0.034	1.014	0.064
cFDA800_1	198	Lomustine	L17	0.953	0.080	1.008	0.010
cFDA800_1	199	Adapalene	L19	0.868	0.036	0.880	0.035
cFDA800_1	200	Meropenem	L21	0.920	0.033	1.071	0.106
cFDA800_1	201	Oseltamivir Phosphate	M3	1.017	0.089	1.031	0.040

cFDA800_1	202	Pamidronate Disodium Pentahydrate (Pamidronic Acid)	M5	0.913	0.032	1.089	0.055
cFDA800_1	203	Pramipexole Dihydrochloride Monohydrate	M7	0.940	0.057	1.005	0.103
cFDA800_1	204	Triptorelin Acetate	M9	0.916	0.019	1.050	0.030
cFDA800_1	205	Risredonic Acid	M11	0.924	0.016	1.074	0.065
cFDA800_1	206	Rocuronium Bromide	M13	0.971	0.085	1.054	0.057
cFDA800_1	207	Vinorelbine	M15	0.880	0.033	0.934	0.073
cFDA800_1	208	Salmeterol	M17	0.890	0.081	0.935	0.064
cFDA800_1	209	Vincristine Sulfate	M19	0.858	0.009	0.849	0.072
cFDA800_1	210	Aspirin (Acetylsalicylic Acid)	M21	1.011	0.091	1.053	0.009
cFDA800_1	211	Acyclovir (Acycloguanosine) Zovirax	N3	1.025	0.038	1.035	0.087
cFDA800_1	212	Zidovudine (3'-Azido-3'-Deoxythymidine)	N5	0.966	0.069	1.110	0.119
cFDA800_1	213	Allopurinol	N7	0.925	0.051	1.085	0.021
cFDA800_1	214	Altretamine	N9	0.930	0.030	1.078	0.086
cFDA800_1	215	Alendronate·Na Trihydrate	N11	0.910	0.079	1.024	0.079
cFDA800_1	216	Albendazole	N13	0.916	0.074	1.107	0.096
cFDA800_1	217	Sumatriptan Succinate	N15	0.937	0.084	1.049	0.047
cFDA800_1	218	Amifostine	N17	0.926	0.085	0.989	0.039
cFDA800_1	219	4-Aminosalicylic Acid	N19	0.961	0.055	1.053	0.116
cFDA800_1	220	Mesalamine (5-Aminosalicylic Acid)	N21	0.934	0.043	1.067	0.049
cFDA800_1	221	Ampicillin Trihydrate	O3	1.029	0.060	1.018	0.095
cFDA800_1	222	(±)-Atenolol	O5	0.937	0.078	1.086	0.107
cFDA800_1	223	Atracurium Besylate	O7	0.927	0.004	1.013	0.064
cFDA800_1	224	Vinblastine Sulfate	O9	0.867	0.026	1.006	0.085
cFDA800_1	225	Azithromycin	O11	0.931	0.028	1.100	0.098
cFDA800_1	226	Aztreonam	O13	1.006	0.048	1.031	0.088
cFDA800_1	227	Betamethasone	O15	0.995	0.088	0.883	0.049
cFDA800_1	228	Bisacodyl	O17	0.728	0.057	0.947	0.082
cFDA800_1	229	Buspirone·HCl	O19	0.907	0.055	1.031	0.081
cFDA800_1	230	Carboplatin	O21	0.934	0.007	1.104	0.059
cFDA800_3	231	Carbamazepine	L3	0.796	0.403	0.973	0.026
cFDA800_3	232	Cefotaxime Acid	L5	1.027	0.133	1.066	0.181
cFDA800_3	233	Ceftazidime	L7	0.924	0.134	0.987	0.055
cFDA800_3	234	Chloramphenicol	L9	1.033	0.186	1.001	0.072
cFDA800_3	235	Chlorambucil	L11	0.936	0.131	1.035	0.077
cFDA800_3	236	Chlorpheniramine Maleate	L13	0.991	0.159	1.045	0.114
cFDA800_3	237	Chloroquine Diphosphate	L15	1.019	0.122	1.037	0.063
cFDA800_3	238	Thalidomide	L17	1.037	0.110	1.038	0.058
cFDA800_3	239	Ciprofloxacin	L19	0.964	0.036	1.067	0.015
cFDA800_3	240	Citalopram·HBr	L21	1.029	0.222	1.020	0.038

cFDA800_1	241	Clarithromycin	I4	1.133	0.049	0.973	0.034
cFDA800_1	242	Clomiphene Citrate	I6	1.016	0.062	0.989	0.061
cFDA800_1	243	Clopidogrel Hydrogen Sulfate	I8	0.986	0.080	0.989	0.028
cFDA800_1	244	Clobetasol Propionate	I10	1.070	0.035	0.788	0.033
cFDA800_1	245	Orphenadrine Citrate	I12	0.957	0.017	0.958	0.026
cFDA800_1	246	Crotamiton	I14	1.024	0.066	0.955	0.055
cFDA800_1	247	Cyclophosphamide (Free Base)	I16	0.945	0.047	1.031	0.052
cFDA800_1	248	Cytarabine	I18	0.911	0.032	0.763	0.041
cFDA800_1	249	Dacarbazine	I20	0.961	0.013	0.960	0.018
cFDA800_1	250	Danazol	I22	1.007	0.037	0.991	0.014
cFDA800_1	251	Desloratadine	J4	1.071	0.119	0.992	0.064
cFDA800_1	252	Dextromethorphan	J6	1.048	0.142	1.012	0.029
cFDA800_1	253	Diclofenac·Na Salt	J8	0.977	0.154	1.045	0.027
cFDA800_1	254	Zalcitabine (2',3'-Dideoxycytidine)	J10	0.910	0.117	1.014	0.022
cFDA800_1	255	Diflunisal	J12	1.018	0.035	1.036	0.071
cFDA800_1	256	Disulfiram	J14	0.552	0.168	0.730	0.099
cFDA800_1	257	Doxazosin Mesylate	J16	0.929	0.035	1.014	0.048
cFDA800_1	258	Doxycycline Monohydrate	J18	0.909	0.058	0.997	0.015
cFDA800_1	259	Enalapril	J20	0.934	0.113	1.025	0.037
cFDA800_1	260	Esomeprazole Potassium	J22	0.956	0.091	0.981	0.044
cFDA800_1	261	Estradiol	K4	0.991	0.059	0.992	0.043
cFDA800_1	262	Estrone	K6	1.015	0.024	1.052	0.049
cFDA800_1	263	Etidronate Disodium	K8	1.042	0.074	1.068	0.012
cFDA800_1	264	Famciclovir	K10	0.993	0.027	1.038	0.073
cFDA800_1	265	Fenoldopam Mesylate	K12	0.951	0.111	1.020	0.024
cFDA800_1	266	Fenoprofen Calcium	K14	0.958	0.024	1.034	0.099
cFDA800_1	267	Fenofibrate	K16	0.984	0.091	0.989	0.019
cFDA800_1	268	Finasteride	K18	0.932	0.048	0.996	0.053
cFDA800_1	269	Fluorouracil (5-Fluorouracil)	K20	0.982	0.037	1.015	0.063
cFDA800_1	270	Flurbiprofen	K22	0.905	0.085	1.055	0.007
cFDA800_1	271	Amitriptyline·HCl	L4	0.995	0.045	1.029	0.063
cFDA800_1	272	Floxuridine	L6	0.988	0.047	1.056	0.071
cFDA800_1	273	Fluocinolone Acetonide	L8	0.991	0.050	0.865	0.042
cFDA800_1	274	Flutamide	L10	1.004	0.035	1.035	0.105
cFDA800_1	275	Fluconazole	L12	0.955	0.055	1.001	0.061
cFDA800_1	276	Furosemide	L14	0.954	0.039	1.079	0.062
cFDA800_1	277	Ganciclovir	L16	0.932	0.054	1.034	0.064
cFDA800_1	278	Gatifloxacin	L18	0.992	0.056	1.042	0.010
cFDA800_1	279	Gentamycin Sulfate	L20	0.967	0.071	1.068	0.053
cFDA800_1	280	Gemfibrozil	L22	0.916	0.041	1.024	0.058
cFDA800_1	281	Glimepiride	M4	1.057	0.045	1.044	0.056
cFDA800_1	282	Hydrocortisone	M6	1.007	0.198	0.912	0.066

cFDA800_1	283	Hydrocortisone Acetate	M8	1.051	0.099	0.895	0.067
cFDA800_1	284	Idoxuridine	M10	0.975	0.046	1.006	0.040
cFDA800_1	285	Ifosfamide	M12	1.005	0.063	1.076	0.045
cFDA800_1	286	Imiquimod	M14	0.988	0.042	1.020	0.053
cFDA800_1	287	Indapamide	M16	0.974	0.100	1.032	0.035
cFDA800_1	288	Itraconazole	M18	0.956	0.055	1.113	0.086
cFDA800_1	289	Levonorgestrel	M20	0.979	0.063	1.030	0.048
cFDA800_1	290	Levofloxacin·HCl	M22	0.987	0.031	1.084	0.047
cFDA800_1	291	Leflunomide	N4	1.080	0.062	1.126	0.074
cFDA800_1	292	Lisinopril·2H2O	N6	0.959	0.058	1.063	0.108
cFDA800_1	293	Loratadine	N8	0.990	0.023	1.106	0.053
cFDA800_1	294	Losartan Potassium	N10	1.007	0.120	1.067	0.142
cFDA800_1	295	Mebendazole	N12	0.926	0.012	1.073	0.090
cFDA800_1	296	Medroxyprogesterone Acetate	N14	0.922	0.057	1.047	0.041
cFDA800_1	297	Mefenamic Acid	N16	0.925	0.078	1.064	0.114
cFDA800_1	298	Melphalan	N18	0.924	0.066	1.081	0.082
cFDA800_1	299	Methyldopa Sesquihydrate (L-A-Methyl-Dopa Sesquihyrate)	N20	0.967	0.065	1.044	0.055
cFDA800_1	300	Methylprednisolone	N22	1.024	0.084	0.864	0.038
cFDA800_1	301	Metoprolol Tartrate	O4	0.931	0.040	1.096	0.114
cFDA800_1	302	Methimazole	O6	1.044	0.085	1.054	0.042
cFDA800_1	303	Metronidazole	O8	1.019	0.070	1.059	0.043
cFDA800_1	304	Minocycline	O10	0.985	0.057	1.026	0.047
cFDA800_1	305	Mitoxantrone·HCl	O12	0.445	0.019	0.764	0.218
cFDA800_1	306	Paclitaxel (Taxol)	O14	0.982	0.036	1.071	0.054
cFDA800_1	307	Nabumetone	O16	1.048	0.063	1.121	0.078
cFDA800_1	308	Naphazoline·HCl	O18	1.044	0.033	1.042	0.058
cFDA800_1	309	Nefazodone·HCl	O20	1.085	0.085	1.073	0.087
cFDA800_1	310	Norethindrone	O22	0.973	0.040	1.094	0.057
cFDA800_3	311	Norfloxacin	L4	1.138	0.192	0.843	0.189
cFDA800_3	312	Nystatin	L6	1.047	0.162	1.005	0.009
cFDA800_3	313	Ofloxacin	L8	1.000	0.112	1.071	0.101
cFDA800_3	314	Omeprazole	L10	1.108	0.072	1.037	0.070
cFDA800_3	315	Oxcarbazepine	L12	0.979	0.156	1.002	0.028
cFDA800_3	316	Oxiconazole Nitrate	L14	1.119	0.111	1.008	0.026
cFDA800_3	317	Oxacillin·Na	L16	1.115	0.211	1.030	0.044
cFDA800_3	318	Pantoprazole	L18	1.040	0.188	1.051	0.059
cFDA800_3	319	Paroxetine·HCl	L20	1.016	0.151	0.998	0.093
cFDA800_3	320	Penciclovir	L22	1.171	0.349	0.973	0.033
cFDA800_3	321	Pentoxifylline	M3	0.722	0.499	0.920	0.230
cFDA800_3	322	Penicillin V Potassium	M5	1.007	0.048	0.800	0.420
cFDA800_3	323	Piperacillin	M7	0.983	0.185	1.080	0.072
cFDA800_3	324	Prednisolone	M9	1.101	0.253	0.945	0.075

cFDA800_3	325	Progesterone	M11	0.989	0.049	1.025	0.029
cFDA800_3	326	Procarbazine·HCl	M13	1.063	0.074	1.082	0.025
cFDA800_3	327	Prednisone	M15	1.040	0.156	1.021	0.070
cFDA800_3	328	Primaquine Phosphate	M17	1.020	0.116	1.034	0.011
cFDA800_3	329	Praziquantel	M19	1.047	0.157	1.049	0.030
cFDA800_3	330	Quinapril·HCl	M21	1.115	0.148	1.055	0.030
cFDA800_2	331	Ranolazine·2HCl	B3	1.039	0.042	0.968	0.028
cFDA800_2	332	Ramipril	B5	1.189	0.046	0.880	0.041
cFDA800_2	333	Ribavirin	B7	1.150	0.228	0.977	0.011
cFDA800_2	334	Nelfinavir Mesylate	B9	0.998	0.018	1.005	0.035
cFDA800_2	335	Rimantadine·HCl	B11	1.020	0.066	1.058	0.042
cFDA800_2	336	Propranolol·HCl	B13	0.979	0.056	0.962	0.063
cFDA800_2	337	Scopolamine·HBr	B15	0.957	0.043	0.973	0.037
cFDA800_2	338	Spironolactone	B17	1.064	0.037	0.979	0.070
cFDA800_2	339	Streptomycin Sulfate	B19	1.071	0.045	0.968	0.028
cFDA800_2	340	Sulfadiazine	B21	1.011	0.021	0.965	0.035
cFDA800_2	341	Sulfasalazine	C3	0.978	0.065	0.884	0.040
cFDA800_2	342	Tamsulosin·HCl	C5	0.957	0.022	0.989	0.089
cFDA800_2	343	Telmisartan	C7	1.006	0.040	1.008	0.060
cFDA800_2	344	Terazosin·HCl	C9	1.029	0.005	0.980	0.036
cFDA800_2	345	Tetracycline	C11	0.908	0.032	0.964	0.034
cFDA800_2	346	Temozolomide	C13	0.971	0.045	0.983	0.046
cFDA800_2	347	Tinidazole	C15	0.958	0.028	0.997	0.008
cFDA800_2	348	Tobramycin	C17	0.929	0.023	0.953	0.040
cFDA800_2	349	Topotecan·HCl	C19	0.959	0.031	0.994	0.016
cFDA800_2	350	Toremifene Base	C21	0.962	0.070	0.936	0.046
cFDA800_2	351	Tolmetin·Na	D3	0.945	0.057	0.992	0.035
cFDA800_2	352	Amoxicillin	D5	0.918	0.069	0.928	0.077
cFDA800_2	353	Tramadol·HCl	D7	0.856	0.058	0.975	0.031
cFDA800_2	354	Trimethoprim	D9	0.850	0.038	0.976	0.028
cFDA800_2	355	Valacyclovir·HCl	D11	0.846	0.060	1.055	0.064
cFDA800_2	356	Vecuronium Bromide	D13	0.907	0.054	0.961	0.044
cFDA800_2	357	Venlafaxine·HCl	D15	0.863	0.121	0.933	0.080
cFDA800_2	358	Bupivacaine·HCl	D17	0.932	0.081	1.005	0.048
cFDA800_2	359	Ketotifen Fumarate	D19	0.856	0.074	0.938	0.026
cFDA800_2	360	Naloxone·HCl	D21	0.862	0.093	0.984	0.017
cFDA800_2	361	Fluoxetine·HCl	E3	0.901	0.046	1.013	0.048
cFDA800_2	362	Ondansetron	E5	0.954	0.067	1.025	0.067
cFDA800_2	363	Tiotropium Bromide Monohydrate	E7	0.979	0.110	0.989	0.045
cFDA800_2	364	Thioridazine·HCl	E9	0.946	0.071	1.013	0.025
cFDA800_2	365	Amrinone	E11	0.977	0.084	0.966	0.063
cFDA800_2	366	Milrinone	E13	1.041	0.078	0.993	0.035
cFDA800_2	367	Alprostadil	E15	0.946	0.063	0.994	0.017

cFDA800_2	368	Misoprostol	E17	0.986	0.030	0.749	0.053
cFDA800_2	369	Argatroban	E19	0.961	0.085	0.965	0.037
cFDA800_2	370	Cilastatin·Na	E21	1.004	0.033	0.803	0.045
cFDA800_2	371	Butoconazole Nitrate	F3	0.943	0.047	0.989	0.029
cFDA800_2	372	Mifepristone	F5	0.952	0.042	1.019	0.037
cFDA800_2	373	Megestrol Acetate	F7	1.003	0.066	1.021	0.054
cFDA800_2	374	Tamoxifen Citrate	F9	0.942	0.031	1.003	0.021
cFDA800_2	375	Aprepitant	F11	1.044	0.201	0.979	0.041
cFDA800_2	376	Bosentan	F13	0.946	0.043	1.038	0.027
cFDA800_2	377	Efavirenz	F15	0.950	0.166	1.019	0.049
cFDA800_2	378	Miglustat (N-Butyldeoxynojirimycin·HCl)	F17	0.881	0.057	0.916	0.096
cFDA800_2	379	Fulvestrant	F19	0.930	0.059	1.006	0.046
cFDA800_2	380	Esmolol	F21	0.927	0.035	1.011	0.045
cFDA800_2	381	Capecitabine	G3	1.079	0.117	0.877	0.048
cFDA800_2	382	Succinylcholine Chloride·2H2O	G5	0.943	0.030	1.014	0.066
cFDA800_2	383	Cyproheptadine·HCl Sesquihydrate	G7	1.121	0.122	0.833	0.034
cFDA800_3	384	Abacavir Sulfate	M4	1.091	0.175	0.951	0.191
cFDA800_3	385	Acamprosate	M6	1.036	0.241	0.999	0.034
cFDA800_3	386	Acarbose	M8	0.908	0.142	1.046	0.040
cFDA800_3	387	Acebutolol·HCl	M10	0.986	0.076	0.979	0.050
cFDA800_3	388	Acetaminophen	M12	1.036	0.223	1.018	0.083
cFDA800_3	389	Acetazolamide	M14	0.703	0.580	1.023	0.037
cFDA800_3	390	Acetohexamide	M16	1.144	0.213	1.072	0.029
cFDA800_3	391	Acetohydroxamic Acid	M18	1.033	0.050	1.029	0.028
cFDA800_3	392	Acetylcysteine	M20	1.050	0.107	1.064	0.060
cFDA800_3	393	Acrivastine	M22	1.025	0.138	1.020	0.072
cFDA800_2	394	Adefovir Dipivoxil	B4	1.064	0.054	1.018	0.065
cFDA800_2	395	Adenosine	B6	1.192	0.049	0.983	0.022
cFDA800_2	396	Blank	B8	1.047	0.079	0.962	0.008
cFDA800_2	397	Alitretinoin	B10	1.054	0.052	0.964	0.035
cFDA800_2	398	Almotriptan	B12	1.069	0.049	0.949	0.045
cFDA800_2	399	Alosetron·HCl	B14	1.003	0.061	0.951	0.041
cFDA800_2	400	Blank	B16	1.041	0.015	0.953	0.011
cFDA800_2	401	Ambrisentan	B18	1.002	0.093	0.981	0.032
cFDA800_2	402	Amcinonide	B20	1.038	0.053	0.976	0.031
cFDA800_2	403	Amikacin Disulfate	B22	1.037	0.040	0.978	0.063
cFDA800_2	404	Aminocaproic Acid	C4	1.012	0.122	0.990	0.070
cFDA800_2	405	Aminohippurate·Na	C6	0.913	0.071	0.930	0.066
cFDA800_2	406	Aminolevulinic Acid·HCl	C8	0.988	0.102	0.993	0.098
cFDA800_2	407	Amlexanox	C10	0.965	0.134	0.932	0.068
cFDA800_2	408	Amphotericin B	C12	0.913	0.086	0.970	0.051
cFDA800_2	409	Arsenic Trioxide	C14	0.318	0.039	0.492	0.069

cFDA800_2	410	Artemether	C16	0.990	0.024	0.774	0.038
cFDA800_2	411	Articaine·HCl	C18	0.983	0.032	0.973	0.065
cFDA800_2	412	L-Ascorbic Acid	C20	0.961	0.104	0.978	0.044
cFDA800_2	413	Asenapine Maleate	C22	0.948	0.043	0.963	0.017
cFDA800_2	414	Atomoxetine·HCl	D4	0.936	0.097	1.006	0.056
cFDA800_2	415	Atorvastatin Calcium	D6	0.967	0.041	0.991	0.007
cFDA800_2	416	Azacitidine	D8	0.814	0.126	1.001	0.038
cFDA800_2	417	Azelaic Acid	D10	0.943	0.101	1.088	0.014
cFDA800_2	418	Azelastine·HCl	D12	0.928	0.034	0.988	0.027
cFDA800_2	419	Bacitracin	D14	0.909	0.075	0.980	0.049
cFDA800_2	420	Baclofen	D16	0.889	0.096	0.955	0.048
cFDA800_2	421	Balsalazide	D18	0.905	0.022	0.952	0.025
cFDA800_2	422	Beclomethasone Dipropionate	D20	0.965	0.112	0.827	0.077
cFDA800_2	423	Benazepril·HCl	D22	1.101	0.021	0.779	0.037
cFDA800_2	424	Bendamustine·HCl	E4	0.957	0.073	1.024	0.030
cFDA800_2	425	Bendroflumethiazide	E6	0.956	0.141	0.998	0.035
cFDA800_2	426	Benztropine Mesylate	E8	0.968	0.049	1.011	0.075
cFDA800_2	427	Betaine	E10	0.939	0.091	1.052	0.050
cFDA800_2	428	Bethanechol Chloride	E12	0.947	0.086	0.985	0.078
cFDA800_2	429	Bimatoprost	E14	0.928	0.071	0.962	0.054
cFDA800_2	430	Biperiden·HCl	E16	0.317	0.032	1.430	0.071
cFDA800_2	431	Bisoprolol Fumarate	E18	0.953	0.023	1.016	0.022
cFDA800_2	432	Brimonidine	E20	0.903	0.038	1.028	0.053
cFDA800_2	433	Bromfenac	E22	0.931	0.051	1.027	0.021
cFDA800_2	434	Brompheniramine Maleate	F4	0.922	0.101	0.989	0.050
cFDA800_2	435	Budesonide	F6	0.948	0.026	0.945	0.052
cFDA800_2	436	Bupropion	F8	0.957	0.027	1.031	0.080
cFDA800_2	437	Busulfan	F10	0.478	0.089	0.691	0.037
cFDA800_2	438	Butorphanol-(+)-Tartrate (Schedule Iv)	F12	0.936	0.073	0.983	0.081
cFDA800_2	439	Capreomycin Sulfate	F14	1.016	0.037	1.001	0.038
cFDA800_2	440	Carbinoxamine Maleate	F16	0.893	0.056	0.985	0.007
cFDA800_2	441	Carglumic Acid	F18	0.921	0.087	0.975	0.043
cFDA800_2	442	Blank	F20	0.882	0.081	0.988	0.022
cFDA800_2	443	Carmustine	F22	0.973	0.012	0.957	0.042
cFDA800_2	444	Cefaclor	G4	0.949	0.021	0.956	0.021
cFDA800_2	445	Cefadroxil	G6	0.921	0.058	0.810	0.016
cFDA800_2	446	Cefazolin·Na	G8	0.940	0.088	1.018	0.046
cFDA800_2	447	Cefdinir	G10	0.959	0.052	1.023	0.022
cFDA800_2	448	Cefditoren Pivoxil	G12	0.945	0.030	0.986	0.037
cFDA800_2	449	Cefixime	G14	0.915	0.105	1.008	0.058
cFDA800_2	450	Cefotetan Disodium	G16	0.932	0.125	1.021	0.013
cFDA800_2	451	Cefoxitin·Na	G18	1.011	0.135	1.015	0.016
cFDA800_2	452	Cefpodoxime Proxetil	G20	0.933	0.083	1.059	0.087

cFDA800_2	453	Cefprozil	G22	0.928	0.091	0.806	0.045
cFDA800_2	454	Ceftibuten	H4	1.019	0.033	0.969	0.044
cFDA800_2	455	Ceftizoxim·Na	H6	1.056	0.073	0.995	0.037
cFDA800_2	456	Ceftriaxone·Na	H8	1.001	0.037	1.030	0.023
cFDA800_2	457	Cefuroxime Axetil	H10	0.971	0.041	0.967	0.036
cFDA800_2	458	Cefuroxime·Na	H12	0.969	0.103	0.989	0.066
cFDA800_2	459	Cephalexin Monohydrate	H14	0.891	0.049	0.885	0.061
cFDA800_2	460	Chenodiol (Chenodeoxycholic Acid)	H16	1.032	0.104	1.052	0.059
cFDA800_2	461	Blank	H18	1.059	0.093	0.977	0.035
cFDA800_2	462	Chlorhexidine Dihydrochloride	H20	1.009	0.068	1.000	0.051
cFDA800_2	463	Chlorothiazide	H22	0.974	0.070	0.972	0.016
cFDA800_2	464	Chlorpropamide	I3	1.023	0.032	1.032	0.017
cFDA800_2	465	Chlorthalidone	I5	1.072	0.018	1.045	0.042
cFDA800_2	466	Chlorzoxazone	I7	0.992	0.101	1.027	0.048
cFDA800_2	467	Ciclesonide	I9	1.020	0.037	1.019	0.049
cFDA800_2	468	Ciclopirox	I11	0.919	0.073	1.063	0.016
cFDA800_2	469	Cidofovir	I13	0.979	0.062	0.998	0.063
cFDA800_2	470	Cilostazol	I15	1.055	0.012	1.058	0.009
cFDA800_2	471	Cinacalcet·HCl	I17	1.006	0.089	1.014	0.058
cFDA800_2	472	Cisatracurium Besylate	I19	0.996	0.059	0.993	0.017
cFDA800_2	473	Cisplatin (Cis-Diamineplatinum(Ii) Dichloride)	I21	1.003	0.133	0.985	0.072
cFDA800_2	474	Cladribine	J3	1.058	0.164	1.047	0.048
cFDA800_2	475	Clavulanate Potassium	J5	1.143	0.235	0.998	0.024
cFDA800_2	476	Clobazam	J7	0.944	0.058	1.015	0.004
cFDA800_2	477	Clofazimine	J9	1.026	0.109	1.047	0.014
cFDA800_2	478	Clomipramine·HCl	J11	1.130	0.130	1.065	0.046
cFDA800_2	479	Clonazepam	J13	0.949	0.078	1.056	0.015
cFDA800_2	480	Clotrimazole	J15	0.940	0.085	1.025	0.045
cFDA800_2	481	Cloxacillin·Na	J17	0.977	0.024	0.980	0.005
cFDA800_2	482	Colchicine	J19	1.030	0.180	1.039	0.036
cFDA800_2	483	Colistimethate·Na	J21	1.013	0.068	0.996	0.013
cFDA800_2	484	Colistin Sulfate	K3	0.981	0.114	1.004	0.024
cFDA800_2	485	Cortisone Acetate	K5	1.017	0.032	1.068	0.084
cFDA800_2	486	Cyclobenzaprine·HCl	K7	1.058	0.070	0.990	0.080
cFDA800_2	487	Cyclopentolate	K9	1.006	0.090	1.017	0.056
cFDA800_2	488	Cycloserine	K11	0.972	0.067	1.007	0.057
cFDA800_2	489	Cysteamine·HCl	K13	0.942	0.064	1.022	0.030
cFDA800_2	490	Dactinomycin (= Actinomycin D)	K15	0.962	0.116	0.983	0.054
cFDA800_2	491	Dalfampridine (4-Aminopyridine)	K17	0.968	0.052	1.053	0.032
cFDA800_2	492	Dantrolene·Na	K19	1.054	0.057	0.812	0.018

cFDA800_2	493	Dapsone	K21	1.003	0.068	1.038	0.040
cFDA800_2	494	Daptomycin	L3	1.084	0.030	1.088	0.028
cFDA800_2	495	Darifenacin·HBr	L5	0.970	0.122	1.065	0.044
cFDA800_2	496	Darunavir	L7	0.981	0.058	1.043	0.066
cFDA800_2	497	Dasatinib	L9	0.928	0.040	1.074	0.029
cFDA800_2	498	Decitabine	L11	1.008	0.028	1.067	0.065
cFDA800_2	499	Deferasirox	L13	1.005	0.065	1.048	0.095
cFDA800_2	500	Deferoxamine Mesylate	L15	0.938	0.074	1.030	0.069
cFDA800_2	501	Demeclocycline·HCl	L17	0.945	0.067	0.992	0.059
cFDA800_2	502	Desipramine·HCl	L19	0.956	0.059	1.061	0.047
cFDA800_2	503	Desogestrel	L21	0.877	0.069	1.083	0.045
cFDA800_2	504	Desonide	M3	0.985	0.079	1.088	0.037
cFDA800_2	505	Desoximetasone	M5	1.014	0.019	0.890	0.051
cFDA800_2	506	Desvenlafaxine Succinate Hydrate	M7	0.954	0.061	1.079	0.044
cFDA800_2	507	Dexchlorpheniramine Maleate	M9	0.971	0.070	1.093	0.048
cFDA800_2	508	Dexmedetomidine·HCl	M11	0.963	0.053	1.020	0.038
cFDA800_2	509	Blank	M13	0.971	0.041	1.100	0.053
cFDA800_2	510	Dexrazoxane	M15	0.959	0.030	1.100	0.050
cFDA800_2	511	Diatrizoate Meglumine	M17	0.960	0.031	0.986	0.017
cFDA800_2	512	Diazepam	M19	0.925	0.070	1.024	0.017
cFDA800_2	513	Dicloxacillin·Na Salt Monohydrate	M21	0.936	0.015	1.049	0.044
cFDA800_2	514	Dicyclomine·HCl	N3	0.922	0.044	1.036	0.039
cFDA800_2	515	Dienogest	N5	0.982	0.121	1.100	0.047
cFDA800_2	516	Blank	N7	0.880	0.052	1.092	0.039
cFDA800_2	517	Difluprednate	N9	1.016	0.060	1.052	0.056
cFDA800_2	518	Digoxin	N11	0.914	0.104	1.010	0.039
cFDA800_2	519	Dimenhydrinate	N13	1.028	0.120	1.095	0.014
cFDA800_2	520	Disopyramide	N15	0.917	0.047	1.052	0.003
cFDA800_2	521	Dopamine·HCl	N17	0.932	0.092	1.072	0.040
cFDA800_2	522	Doripenem	N19	1.008	0.074	1.068	0.052
cFDA800_2	523	Doxapram·HCl	N21	0.966	0.056	1.086	0.031
cFDA800_2	524	Doxepin·HCl	O3	1.001	0.048	1.078	0.056
cFDA800_2	525	Droperidol	O5	1.013	0.023	0.830	0.080
cFDA800_2	526	Drospirenone	O7	1.014	0.083	1.109	0.052
cFDA800_2	527	Duloxetine·HCl	O9	0.962	0.078	1.076	0.102
cFDA800_2	528	Dutasteride	O11	1.000	0.026	1.053	0.008
cFDA800_2	529	Dyphylline	O13	0.997	0.082	1.105	0.042
cFDA800_2	530	Econazole Nitrate	O15	1.026	0.083	0.978	0.044
cFDA800_2	531	Blank	O17	1.008	0.106	1.088	0.064
cFDA800_2	532	Eflornithine·HCl	O19	0.901	0.060	1.102	0.106
cFDA800_2	533	Epinastine·HCl	O21	0.923	0.128	1.067	0.055
cFDA800_3	534	Epirubicin·HCl	N3	1.020	0.246	1.061	0.077

cFDA800_3	535	Eplerenone	N5	1.085	0.149	0.932	0.238
cFDA800_3	536	Eptifibatide	N7	0.985	0.018	1.036	0.053
cFDA800_3	537	Erythromycin	N9	0.996	0.026	1.015	0.106
cFDA800_3	538	Estramustine Phosphate·Na	N11	1.023	0.123	1.076	0.028
cFDA800_3	539	Estropipate	N13	1.045	0.172	1.039	0.055
cFDA800_3	540	Eszopiclone	N15	1.048	0.179	0.994	0.062
cFDA800_3	541	Ethambutol Dihydrochloride	N17	0.967	0.153	1.068	0.024
cFDA800_3	542	Blank	N19	0.998	0.126	1.014	0.036
cFDA800_3	543	Ethinyl Estradiol	N21	0.603	0.520	1.011	0.037
cFDA800_2	544	Ethionamide	I4	1.034	0.124	1.033	0.003
cFDA800_2	545	Ethosuximide	I6	1.026	0.100	0.996	0.036
cFDA800_2	546	Etodolac	I8	0.979	0.054	1.054	0.031
cFDA800_2	547	Etomidate	I10	0.860	0.057	1.045	0.038
cFDA800_2	548	Etonogestrel	I12	0.980	0.080	1.019	0.019
cFDA800_2	549	Everolimus	I14	0.966	0.022	1.007	0.032
cFDA800_2	550	Ezetimibe	I16	0.992	0.059	1.013	0.025
cFDA800_2	551	Febuxostat	I18	0.987	0.100	1.037	0.006
cFDA800_2	552	Fexofenadine·HCl	I20	0.939	0.149	1.003	0.025
cFDA800_2	553	Fingolimod	I22	0.940	0.050	1.018	0.070
cFDA800_2	554	Flavoxate·HCl	J4	1.017	0.072	1.055	0.042
cFDA800_2	555	Flucytosine	J6	0.949	0.024	1.051	0.052
cFDA800_2	556	Fludarabine Phosphate	J8	1.014	0.021	1.006	0.009
cFDA800_2	557	Fludrocortisone Acetate	J10	0.949	0.046	1.056	0.026
cFDA800_2	558	Flunisolide	J12	1.021	0.080	1.012	0.035
cFDA800_2	559	Fluocinonide	J14	0.931	0.080	0.992	0.065
cFDA800_2	560	Fluorometholone	J16	0.993	0.054	1.039	0.042
cFDA800_2	561	Flurandrenolide	J18	0.948	0.074	1.027	0.035
cFDA800_2	562	Blank	J20	1.057	0.078	1.056	0.075
cFDA800_2	563	Fluticasone Propionate	J22	1.031	0.045	1.015	0.017
cFDA800_2	564	Fluvoxamine Maleate	K4	0.979	0.004	1.013	0.012
cFDA800_2	565	Fomepizole	K6	0.994	0.047	1.016	0.012
cFDA800_2	566	Formoterol	K8	0.953	0.111	0.979	0.062
cFDA800_2	567	Foscarnet·Na (Sodium Phosphonoformate Tribasic Hexahydrate)	K10	1.031	0.094	1.032	0.042
cFDA800_2	568	Fosfomycin Calcium	K12	0.903	0.030	1.015	0.010
cFDA800_2	569	Fosphenytoin·Na Pentahydrate	K14	1.009	0.043	1.053	0.018
cFDA800_2	570	Gemifloxacin	K16	0.945	0.123	1.085	0.056
cFDA800_2	571	Glycopyrrolate Iodide	K18	0.999	0.024	0.989	0.013
cFDA800_2	572	Griseofulvin	K20	0.866	0.039	1.049	0.045
cFDA800_2	573	Guanidine·HCl	K22	0.975	0.056	1.042	0.088
cFDA800_2	574	Halcinonide	L4	0.919	0.165	1.064	0.029
cFDA800_2	575	Halobetasol Propionate	L6	0.976	0.044	1.009	0.032
cFDA800_2	576	Hexachlorophene	L8	0.949	0.063	0.967	0.041

cFDA800_2	577	Homatropine Methylbromide	L10	0.968	0.050	0.869	0.016
cFDA800_2	578	Hydralazine·HCl	L12	0.947	0.005	1.041	0.081
cFDA800_2	579	Hydrochlorothiazide	L14	0.990	0.017	1.087	0.106
cFDA800_2	580	Hydroflumethiazide	L16	0.984	0.134	1.057	0.015
cFDA800_2	581	Hydroxocobalamin·HCl	L18	0.993	0.118	0.975	0.064
cFDA800_2	582	Hydroxychloroquine Sulfate	L20	0.951	0.048	1.042	0.016
cFDA800_2	583	Hydroxyurea	L22	0.925	0.062	1.058	0.051
cFDA800_2	584	Hydroxyzine Dihydrochloride	M4	1.011	0.038	1.057	0.051
cFDA800_2	585	Ibutilide Fumarate	M6	0.942	0.047	1.022	0.080
cFDA800_2	586	Iloperidone	M8	1.049	0.062	1.033	0.028
cFDA800_2	587	Indinavir	M10	1.029	0.096	1.047	0.062
cFDA800_2	588	Irbesartan	M12	0.957	0.077	1.107	0.018
cFDA800_2	589	Irinotecan·HCl	M14	0.876	0.044	1.080	0.050
cFDA800_2	590	Isocarboxazid	M16	1.040	0.048	1.081	0.026
cFDA800_2	591	Isosorbide Dinitrate	M18	0.999	0.112	1.023	0.024
cFDA800_2	592	Isotretinoin (13-Cis-Retinoic Acid)	M20	0.925	0.058	1.073	0.046
cFDA800_2	593	Isradipine	M22	0.974	0.058	1.086	0.088
cFDA800_2	594	Kanamycin Sulfate	N4	1.020	0.064	1.038	0.057
cFDA800_2	595	Ketorolac Tromethamine	N6	0.961	0.020	0.816	0.050
cFDA800_2	596	Labetalol·HCl	N8	0.919	0.075	1.066	0.039
cFDA800_2	597	Lacosamide	N10	0.950	0.075	1.080	0.038
cFDA800_2	598	Lactulose	N12	0.930	0.092	1.121	0.047
cFDA800_2	599	Lamivudine	N14	0.951	0.042	1.073	0.041
cFDA800_2	600	Lansoprazole	N16	0.963	0.055	1.056	0.053
cFDA800_2	601	Lenalidomide	N18	0.885	0.154	1.097	0.034
cFDA800_2	602	Leucovorin Calcium Pentahydrate	N20	1.041	0.023	1.085	0.047
cFDA800_2	603	Levalbuterol·HCl	N22	0.958	0.113	1.061	0.056
cFDA800_2	604	Levobunolol·HCl	O4	1.048	0.015	1.093	0.058
cFDA800_2	605	Levocarnitine	O6	0.980	0.077	1.041	0.040
cFDA800_2	606	Levocetirizine Dihydrochloride	O8	0.952	0.069	1.104	0.088
cFDA800_2	607	Levothyroxine·Na	O10	1.008	0.086	1.053	0.060
cFDA800_2	608	Lindane	O12	0.985	0.114	1.110	0.082
cFDA800_2	609	Liothyronine·Na	O14	0.924	0.076	1.075	0.081
cFDA800_2	610	Lopinavir	O16	1.044	0.073	1.093	0.091
cFDA800_2	611	Lorazepam	O18	0.972	0.067	1.064	0.079
cFDA800_2	612	Loteprednol Etabonate	O20	1.018	0.134	1.077	0.106
cFDA800_2	613	Loxapine Succinate	O22	1.030	0.082	1.064	0.042
cFDA800_3	614	Mafenide·HCl	N4	1.119	0.137	0.899	0.336
cFDA800_3	615	Malathion	N6	1.005	0.153	0.986	0.072
cFDA800_3	616	Mannitol	N8	1.087	0.203	1.033	0.030
cFDA800_3	617	Maraviroc	N10	1.015	0.135	1.078	0.057

cFDA800_3	618	Mechlorethamine·HCl	N12	1.022	0.132	1.008	0.027
cFDA800_3	619	Meclizine Dihydrochloride	N14	1.042	0.122	1.043	0.062
cFDA800_3	620	Meclofenamate·Na	N16	0.872	0.320	1.073	0.020
cFDA800_3	621	Mefloquine·HCl	N18	1.062	0.113	1.073	0.022
cFDA800_3	622	Mepenzolate Bromide	N20	1.061	0.070	1.104	0.073
cFDA800_3	623	Mepivacaine·HCl	N22	1.035	0.235	1.010	0.059
cFDA800_3	624	Meprobamate (Schedule Iv)	O3	1.065	0.101	1.066	0.047
cFDA800_3	625	Mequinol	O5	1.038	0.157	0.953	0.162
cFDA800_3	626	Mercaptopurine Hydrate	O7	0.846	0.210	1.089	0.038
cFDA800_3	627	Mesna	O9	0.882	0.064	1.100	0.064
cFDA800_3	628	Mestranol	O11	1.099	0.091	1.087	0.076
cFDA800_3	629	Metaproterenol Hemisulfate (Orciprenaline)	O13	0.991	0.167	1.024	0.066
cFDA800_3	630	Metaraminol Bitartrate	O15	1.033	0.051	1.020	0.028
cFDA800_3	631	Metaxalone	O17	1.105	0.247	1.094	0.017
cFDA800_3	632	Methacholine Chloride	O19	0.845	0.312	1.042	0.048
cFDA800_3	633	Methazolamide	O21	1.034	0.104	1.093	0.058
cFDA800_3	634	Methenamine Hippurate	B3	1.168	0.142	0.990	0.050
cFDA800_3	635	Methocarbamol	B5	0.906	0.221	0.961	0.109
cFDA800_3	636	Methotrexate	B7	1.059	0.166	1.005	0.096
cFDA800_3	637	Methoxsalen (Xanthotoxin)	B9	1.079	0.154	0.995	0.075
cFDA800_3	638	Methscopolamine Bromide ((−)-Scopolamine Methyl Bromide)	B11	1.105	0.094	1.018	0.067
cFDA800_3	639	Methsuximide	B13	1.044	0.129	0.995	0.084
cFDA800_3	640	Methyclothiazide	B15	1.118	0.114	0.997	0.045
cFDA800_3	641	Methyl Aminolevulinate·HCl	B17	1.062	0.184	1.001	0.022
cFDA800_3	642	Methylergonovine Maleate	B19	1.117	0.157	0.997	0.057
cFDA800_3	643	Metolazone	B21	1.159	0.153	0.975	0.072
cFDA800_3	644	Metyrapone	C3	1.047	0.042	1.025	0.038
cFDA800_3	645	Blank	C5	0.812	0.355	0.974	0.071
cFDA800_3	646	Mexiletine·HCl	C7	1.085	0.205	0.998	0.051
cFDA800_3	647	Micafungin	C9	1.053	0.260	1.047	0.079
cFDA800_3	648	Miconazole	C11	0.987	0.125	1.040	0.108
cFDA800_3	649	Blank	C13	1.030	0.120	1.012	0.050
cFDA800_3	650	Midodrine·HCl	C15	1.062	0.119	0.983	0.056
cFDA800_3	651	Miglitol	C17	1.017	0.150	0.980	0.053
cFDA800_3	652	Milnacipran·HCl	C19	1.083	0.153	1.005	0.090
cFDA800_3	653	Mirtazapine	C21	1.005	0.113	0.973	0.078
cFDA800_3	654	Mitotane	D3	1.075	0.063	1.017	0.019
cFDA800_3	655	Modafinil (Schedule Iv)	D5	1.051	0.129	0.973	0.037
cFDA800_3	656	Moexipril·HCl	D7	1.125	0.258	0.982	0.052
cFDA800_3	657	Mometasone Furoate	D9	0.982	0.104	0.827	0.095
cFDA800_3	658	Mupirocin	D11	1.068	0.190	1.034	0.090
cFDA800_3	659	Nadolol	D13	0.625	0.496	0.967	0.101

cFDA800_3	660	Nafcillin·Na	D15	1.054	0.204	0.986	0.067
cFDA800_3	661	Naftifine·HCl	D17	1.010	0.176	1.006	0.090
cFDA800_3	662	Naratriptan·HCl	D19	1.080	0.199	0.941	0.057
cFDA800_3	663	Natamycin	D21	0.914	0.150	0.972	0.052
cFDA800_3	664	Nebivolol·HCl	E3	1.037	0.191	1.021	0.026
cFDA800_3	665	Nelarabine	E5	1.036	0.161	0.979	0.040
cFDA800_3	666	Nepafenac	E7	1.006	0.092	1.027	0.060
cFDA800_3	667	Nevirapine	E9	1.105	0.234	1.010	0.041
cFDA800_3	668	Niacin (Known As Vitamin B3, Nicotinic Acid And Vitamin Pp)	E11	0.984	0.057	1.039	0.060
cFDA800_3	669	Nicotine	E13	1.054	0.269	1.014	0.081
cFDA800_3	670	Nilotinib	E15	0.836	0.248	1.024	0.077
cFDA800_3	671	Nilutamide	E17	0.966	0.056	0.926	0.108
cFDA800_3	672	Nitazoxanide	E19	0.942	0.082	0.927	0.006
cFDA800_3	673	Nitisinone	E21	1.059	0.133	0.966	0.080
cFDA800_3	674	Nitrofurantoin	F3	1.035	0.251	0.969	0.072
cFDA800_3	675	Nizatidine	F5	0.961	0.068	0.976	0.118
cFDA800_3	676	Nortriptyline·HCl	F7	0.982	0.201	0.968	0.069
cFDA800_3	677	Olsalazine·Na	F9	1.007	0.086	0.982	0.064
cFDA800_3	678	Orlistat (Tetrahydrolipstatin)	F11	0.647	0.549	1.023	0.062
cFDA800_3	679	Oxaprozin	F13	0.933	0.133	0.983	0.055
cFDA800_3	680	Oxazepam	F15	0.889	0.234	0.928	0.060
cFDA800_3	681	Oxtriphylline	F17	1.021	0.232	0.962	0.024
cFDA800_3	682	Oxybutynin Chloride	F19	0.812	0.233	0.960	0.106
cFDA800_3	683	Oxytetracycline·HCl	F21	0.960	0.128	0.963	0.027
cFDA800_3	684	Paliperidone	G3	1.118	0.175	0.977	0.042
cFDA800_3	685	Palonosetron·HCl	G5	0.865	0.114	1.057	0.021
cFDA800_3	686	Paromomycin Sulfate	G7	0.937	0.017	0.950	0.086
cFDA800_3	687	Pazopanib·HCl	G9	0.616	0.527	0.968	0.051
cFDA800_3	688	Pemetrexed Disodium	G11	1.073	0.096	0.947	0.088
cFDA800_3	689	Pemirolast Potassium	G13	1.016	0.132	0.965	0.033
cFDA800_3	690	Penicillamine (D-Penicillamine)	G15	0.972	0.091	0.962	0.091
cFDA800_3	691	Penicillin G Potassium (Benzylpenicillin)	G17	1.026	0.061	0.989	0.103
cFDA800_3	692	Pentamidine Isethionate	G19	0.975	0.020	0.928	0.063
cFDA800_3	693	Pentostatin	G21	0.977	0.053	0.982	0.017
cFDA800_3	694	Perindopril Erbumine	H3	1.027	0.051	0.945	0.054
cFDA800_3	695	Permethrin	H5	0.755	0.408	0.973	0.050
cFDA800_3	696	Perphenazine	H7	1.029	0.149	0.943	0.085
cFDA800_3	697	Phenelzine Sulfate	H9	1.008	0.238	1.005	0.057
cFDA800_3	698	Phenylephrine	H11	0.632	0.510	0.907	0.082
cFDA800_3	699	Phytonadione	H13	0.965	0.129	0.980	0.030
cFDA800_3	700	Pimecrolimus	H15	1.054	0.115	0.999	0.024

cFDA800_3	701	Pitavastatin Calcium	H17	0.836	0.267	1.049	0.082
cFDA800_3	702	Blank	H19	0.986	0.155	0.966	0.095
cFDA800_3	703	Podofilox	H21	0.960	0.121	0.766	0.047
cFDA800_3	704	Posaconazole	O4	1.018	0.118	1.178	0.133
cFDA800_3	705	Pralidoxime Chloride	O6	1.061	0.173	1.073	0.054
cFDA800_3	706	Prasugrel	O8	1.060	0.109	1.053	0.037
cFDA800_3	707	Pravastatin·Na	O10	0.671	0.550	1.071	0.070
cFDA800_3	708	Pregabalin	O12	0.797	0.396	1.074	0.029
cFDA800_3	709	Prilocaine·HCl	O14	1.061	0.049	1.126	0.058
cFDA800_3	710	Primidone	O16	0.777	0.429	1.080	0.010
cFDA800_3	711	Probenecid	O18	0.952	0.264	1.078	0.051
cFDA800_3	712	Blank	O20	1.006	0.075	1.058	0.098
cFDA800_3	713	Proparacaine·HCl	O22	0.863	0.040	1.039	0.023
cFDA800_3	714	Propylthiouracil	B4	1.064	0.082	1.015	0.052
cFDA800_3	715	Protriptyline·HCl	B6	0.932	0.113	0.983	0.040
cFDA800_3	716	Pyrazinamide	B8	1.104	0.142	0.999	0.093
cFDA800_3	717	Pyridostigmine Bromide	B10	0.652	0.541	1.008	0.068
cFDA800_3	718	Pyrimethamine	B12	1.036	0.078	0.983	0.064
cFDA800_3	719	Quinidine·HCl·H2O	B14	1.058	0.074	1.035	0.091
cFDA800_3	720	Rabeprazole·Na	B16	0.972	0.220	0.982	0.032
cFDA800_3	721	Raltegravir	B18	1.074	0.076	1.004	0.067
cFDA800_3	722	Ramelteon	B20	1.155	0.179	1.033	0.048
cFDA800_3	723	Rasagiline Mesylate	B22	1.116	0.139	1.020	0.090
cFDA800_3	724	Regadenoson	C4	1.065	0.152	0.965	0.050
cFDA800_3	725	Repaglinide	C6	0.988	0.165	0.928	0.064
cFDA800_3	726	Reserpine	C8	1.074	0.268	1.001	0.034
cFDA800_3	727	Rifabutin	C10	1.046	0.185	0.941	0.090
cFDA800_3	728	Rifapentine	C12	1.000	0.119	0.978	0.049
cFDA800_3	729	Rifaximin	C14	0.895	0.086	0.931	0.170
cFDA800_3	730	Ritonavir	C16	1.006	0.235	1.037	0.135
cFDA800_3	731	Rizatriptan Benzoate	C18	0.992	0.140	1.002	0.017
cFDA800_3	732	Ropinirole·HCl	C20	1.063	0.166	0.979	0.033
cFDA800_3	733	Ropivacaine·HCl Monohydrate	C22	1.023	0.149	0.987	0.057
cFDA800_3	734	Rosuvastatin Calcium	D4	1.004	0.161	0.970	0.028
cFDA800_3	735	Rufinamide	D6	0.976	0.164	1.007	0.112
cFDA800_3	736	Saquinavir Mesylate	D8	1.138	0.166	1.076	0.062
cFDA800_3	737	Selegiline·HCl	D10	1.027	0.133	1.002	0.050
cFDA800_3	738	Sertraline·HCl	D12	1.012	0.176	0.992	0.056
cFDA800_3	739	Silver Sulfadiazine	D14	1.084	0.219	0.989	0.080
cFDA800_3	740	Sitagliptin Phosphate	D16	1.089	0.130	0.916	0.058
cFDA800_3	741	Sorafenib Tosylate	D18	1.037	0.123	0.969	0.077
cFDA800_3	742	Stavudine	D20	0.657	0.505	0.964	0.063
cFDA800_3	743	Streptozocin	D22	1.075	0.153	0.955	0.066
cFDA800_3	744	Sulconazole Nitrate	E4	0.615	0.498	0.969	0.133

cFDA800_3	745	Sulfacetamide·Na	E6	1.018	0.143	0.984	0.073
cFDA800_3	746	Sulfamethoxazole	E8	0.958	0.098	0.950	0.051
cFDA800_3	747	Sulfanilamide	E10	0.978	0.076	1.048	0.090
cFDA800_3	748	Sunitinib Malate	E12	0.925	0.156	0.948	0.050
cFDA800_3	749	Tacrolimus (Fk506)	E14	1.007	0.211	0.966	0.077
cFDA800_3	750	Tadalafil	E16	0.873	0.104	1.048	0.200
cFDA800_3	751	Tazarotene	E18	1.034	0.142	0.986	0.061
cFDA800_3	752	Telbivudine	E20	1.013	0.182	1.004	0.057
cFDA800_3	753	Telithromycin	E22	0.992	0.236	0.930	0.071
cFDA800_3	754	Temazepam	F4	1.033	0.182	0.951	0.030
cFDA800_3	755	Temsirolimus	F6	0.906	0.198	0.992	0.077
cFDA800_3	756	Teniposide	F8	0.989	0.231	1.050	0.048
cFDA800_3	757	Tenofovir	F10	1.039	0.103	1.000	0.061
cFDA800_3	758	Terbutaline Hemisulfate	F12	0.839	0.074	0.927	0.031
cFDA800_3	759	Terconazole	F14	0.984	0.064	1.009	0.041
cFDA800_3	760	Testosterone Enanthate	F16	1.024	0.136	0.971	0.048
cFDA800_3	761	Tetrabenazine	F18	1.071	0.126	1.000	0.042
cFDA800_3	762	Tetrahydrozoline·HCl	F20	1.055	0.138	1.002	0.046
cFDA800_3	763	Theophylline	F22	1.032	0.125	0.942	0.065
cFDA800_3	764	Thioguanine (6-Thioguanine)	G4	1.056	0.120	0.993	0.053
cFDA800_3	765	Thiotepa	G6	1.056	0.138	0.984	0.078
cFDA800_3	766	Blank	G8	1.030	0.231	0.999	0.071
cFDA800_3	767	Tiagabine·HCl	G10	1.063	0.141	0.961	0.053
cFDA800_3	768	Tigecycline	G12	1.024	0.099	0.972	0.003
cFDA800_3	769	Tiludronate Disodium	G14	1.099	0.142	0.994	0.081
cFDA800_3	770	Tiopronin	G16	0.973	0.070	0.980	0.044
cFDA800_3	771	Tirofiban·HCl	G18	0.671	0.570	0.975	0.073
cFDA800_3	772	Tolterodine Tartrate	G20	0.974	0.149	0.999	0.046
cFDA800_3	773	Tolvaptan	G22	1.078	0.128	0.942	0.032
cFDA800_3	774	Topiramate	H4	1.021	0.036	0.972	0.050
cFDA800_3	775	Torsemide	H6	1.052	0.045	0.997	0.063
cFDA800_3	776	Trandolapril	H8	1.052	0.194	0.974	0.015
cFDA800_3	777	Travoprost	H10	1.083	0.112	1.021	0.025
cFDA800_3	778	Trazodone·HCl	H12	0.962	0.104	0.947	0.084
cFDA800_3	779	Tretinoin	H14	1.114	0.249	0.835	0.055
cFDA800_3	780	Triamcinolone Acetonide	H16	0.975	0.110	0.844	0.016
cFDA800_3	781	Triamterene	H18	0.917	0.297	1.046	0.071
cFDA800_3	782	Triazolam	H20	1.035	0.153	0.947	0.057
cFDA800_3	783	Trientine Dihydrochloride	H22	1.101	0.179	0.917	0.061
cFDA800_3	784	Trihexyphenidyl·HCl	I3	0.959	0.142	0.994	0.000
cFDA800_3	785	Trimethadione	I5	0.959	0.270	1.028	0.031
cFDA800_3	786	Trimethobenzamide·HCl	I7	0.998	0.052	0.976	0.043
cFDA800_3	787	Trimipramine Maleate	I9	1.069	0.251	0.977	0.055
cFDA800_3	788	Trospium Chloride	I11	1.049	0.132	1.022	0.060

cFDA800_3	789	Ursodiol	I13	1.047	0.107	0.816	0.204
cFDA800_3	790	Valganciclovir·HCl	I15	0.983	0.019	0.955	0.049
cFDA800_3	791	Valproate·Na	I17	1.079	0.139	0.992	0.058
cFDA800_3	792	Valsartan	I19	0.689	0.552	0.992	0.051
cFDA800_3	793	Vancomycin·HCl	I21	1.035	0.108	1.012	0.039
cFDA800_3	794	Varenicline Tartrate	J3	1.108	0.055	0.985	0.019
cFDA800_3	795	Vigabatrin	J5	1.027	0.104	1.020	0.042
cFDA800_3	796	Voriconazole	J7	1.048	0.080	0.977	0.013
cFDA800_3	797	Warfarin·Na	J9	0.966	0.173	0.976	0.035
cFDA800_3	798	Zaleplon	J11	1.077	0.174	1.021	0.072
cFDA800_3	799	Zanamivir	J13	0.981	0.028	1.033	0.049
cFDA800_3	800	Ziprasidone	J15	1.118	0.154	0.964	0.061

(A) (B)

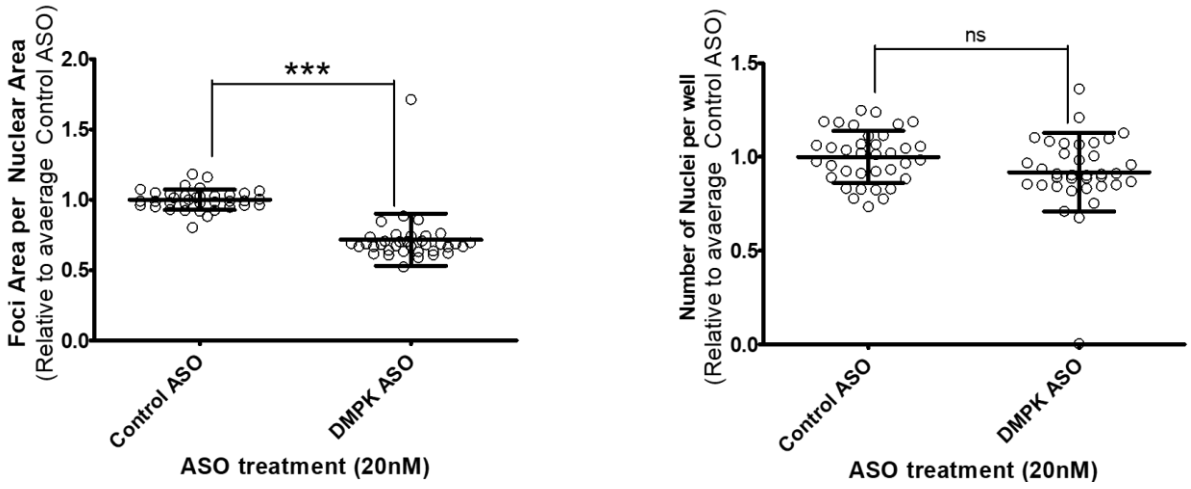

Supplementary Figure 4.2. DMPK ASO reduced foci by 30% in differentiated $DM1_{3600CTG}$ myoblasts. $DM1_{3600CTG}$ myoblasts were serum-starved in 384-well plates for 7 days and treated with 20nM of control or DMPK ASO (ISIS486178) for 24hrs (n=9, 6-wells per plate). Post-treatment, cells were fixed with 4% PFA, DNA was stained with Hoechst and CUG RNA foci were probed by Alexa555-(CAG)10 fluorescent oligo. (A) Foci area per nuclear area and (B) number of nuclei per well (to assess ASO-associated toxicity) were quantified using Columbus Software. DMPK ASO was used as a positive control to measure assay quality and resulted in a Z' score of 0.84 using foci area per nuclear area in panel A, indicating an "excellent" separation between positive and negative controls.

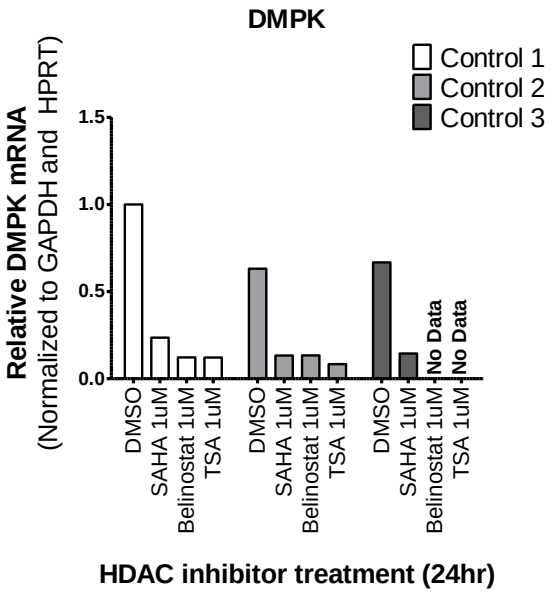

Supplementary Figure 4.3. Pan-HDAC inhibitors, vorinostat (SAHA), belinostat and TSA, all reduced DMPK mRNA levels in differentiated control myoblasts. Control myoblasts were serum-starved in 6-well plates for 7 days. Control cellls were treated with DMSO alone 1 of vorinostat (SAHA), belinostat and TSA. RNA was extracted (RNeasy micro kit, Qiagen) and reverse-transcribed to cDNA (iScript Advanced RT kit, Biorad). RT-qPCR was performed (iQ Sybr green supermix, Biorad) to assess mRNA levels of (A) DMPK and (B) SERCA1 splicing. (n=1)

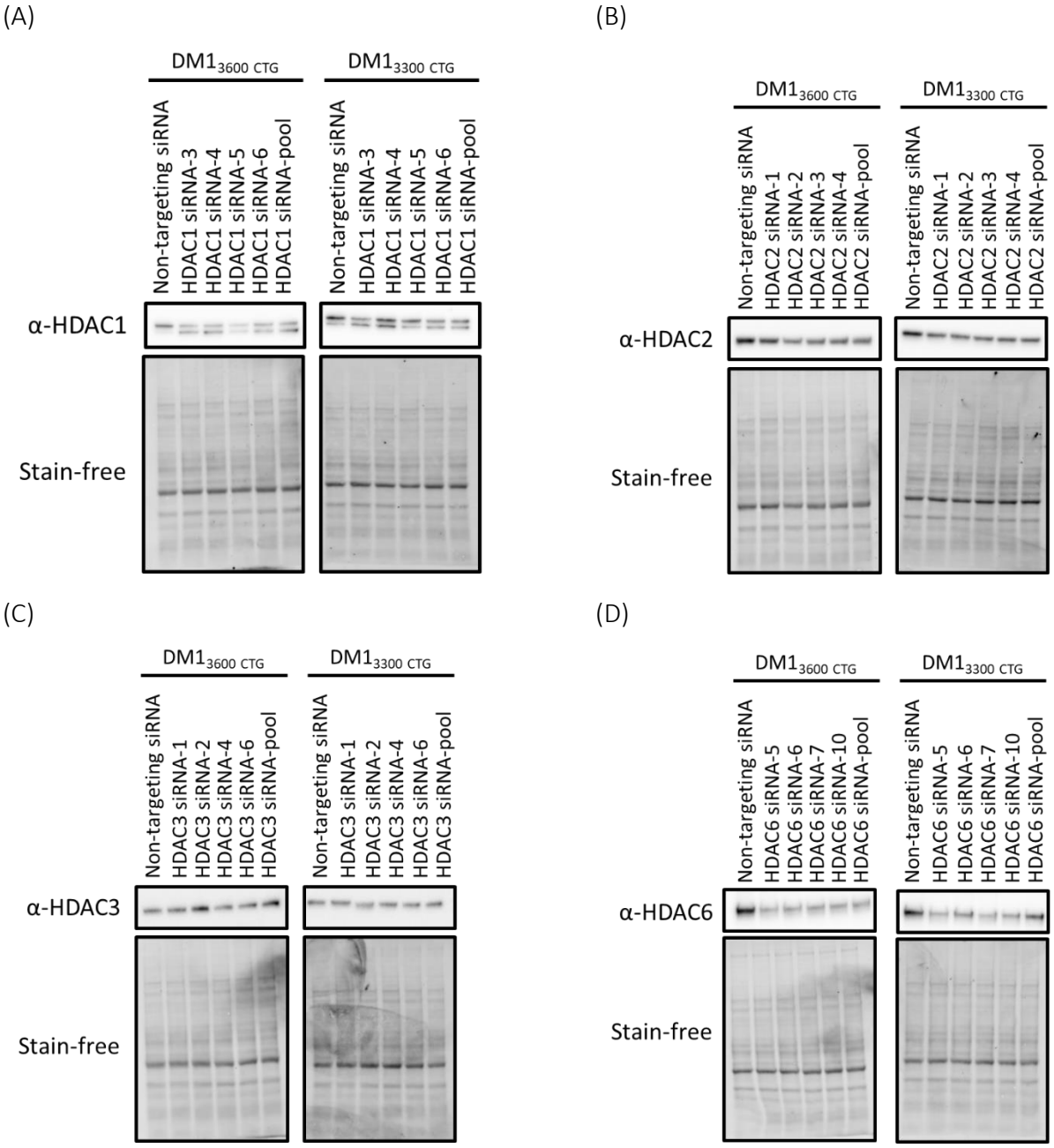

Supplementary Figure 4.4. HDAC-specific siRNA had variable knockdown effect on respective target HDAC proteins. $DM1_{3600CTG}$ and $DM1_{3300CTG}$ myoblasts were serum-starved in 6-well plates for 7 days and 10nM of non-targeting or HDAC siRNA for (A) HDAC 1, (B) HDAC 2, (C) HDAC 3 and (D) HDAC 6 were forward transfected using lipofectamine RNAi MAX. 72hr post-treatment, cells were harvested for western blot analysis.

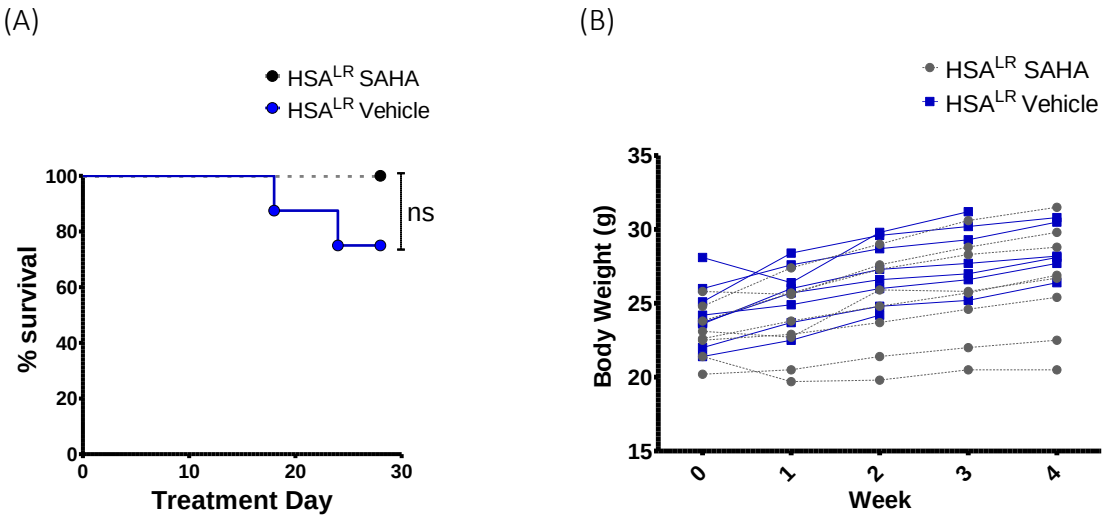

Supplementary Figure 4.5. Vorinostat (SAHA) is not toxic to DM1 HSA^{LR} mouse model. Mice at approximately 4 weeks of age were injected (IP) daily with vehicle or 50mg/kg vorinostat (SAHA) for 4 weeks. The mice were sacrifice by lethal injection and cervical dislocation. Skeletal muscle tissue from one hind leg was frozen in OCT for sectioning and imaging, and skeletal muscle tissue from the other hind leg was flash frozen in liquid nitrogen for RNA workup. (A) Survival plot and (B) body weight of the mice were used to assess toxicity of the drug.

REFERENCES

Aartsma-Rus, Annemieke and Arthur M. Krieg. 2017. "FDA Approves Eteplirsen for Duchenne Muscular Dystrophy: The Next Chapter in the Eteplirsen Saga." *Nucleic Acid Therapeutics* 27(1):1–3.

Antonini, Giovanni, Alessandro Clemenzi, Elisabetta Bucci, Stefania Morino, Matteo Garibaldi, Micaela Sepe-Monti, Franco Giubilei, and Giuseppe Novelli. 2009. "Erectile Dysfunction in Myotonic Dystrophy Type 1 (DM1)." *Journal of Neurology* 256(4):657–59.

Artero, Ruben, Andreas Prokop, Nuria Paricio, Gerrit Begemann, Ignacio Pueyo, Marek Mlodzik, Manuel Perez-Alonso, and Mary K. Baylies. 1998. "The Muscleblind Gene Participates in the Organization of Z-Bands and Epidermal Attachments of Drosophila Muscles and Is Regulated by Dmef2." *Developmental Biology* 195(2):131–43.

Ashizawa, Tetsuo, M. Anvret, M. Baiget, J. M. Barceló, H. Brunner, A. M. Cobo, B. Dallapiccola, R. G. Fenwick, U. Grandell, H. Harley, C. Junien, M. C. Koch, R. G. Korneluk, C. Lavedan, T. Miki, J. C. Mulley, A. De López Munain, G. Novelli, A. D. Roses, W. K. Seltzer, D. J. Shaw, H. Smeets, G. R. Sutherland, H. Yamagata, and P. S. Harper. 1994. "Characteristics of Intergenerational Contractions of the CTG Repeat in Myotonic Dystrophy." *American Journal of Human Genetics* 54(3):414–23.

Begemann, Gerrit, Nuria Paricio, Ruben Artero, Istvan Kiss, Manuel Pérez-Alonso, and Marek Mlodzik. 1997. "Muscleblind, a Gene Required for Photoreceptor Differentiation in Drosophila, Encodes Novel Nuclear Cys3His-Type Zinc-Finger-Containing Proteins." *Development* 124(21):4321–31.

Bennett, C. Frank. 2019. "Therapeutic Antisense Oligonucleotides Are Coming of Age." *Annual Review of Medicine* 70(1):307–21.

Bianco, F., E. Iacovelli, E. Tinelli, N. Locuratolo, F. Pauri, and F. Fattapposta. 2009. "CHARACTERISTIC BRAIN MRI APPEARANCE OF ERDHEIM-CHESTER DISEASE." *Neurology* 73:2120–29.

Boucher, C. A., S. K. King, N. Carey, R. Krahe, C. L. Winchester, S. Rahman, T. Creavin, P. Mehji, M. E. S. Bailey, F. L. Chartier, S. D. Brown, M. J. Siciliano, and K. J. Johnson. 1995. "A Novel Homeodomain-Encoding Gene Is Associated with a Large CPG Island Interrupted by the Myotonic Dystrophy Unstable (CTG)n Repeat." *Human Molecular Genetics* 4(10):1919–25.

Brady, Lauren I., Lauren G. MacNeil, and Mark A. Tarnopolsky. 2014. "Impact of Habitual Exercise on the Strength of Individuals with Myotonic Dystrophy Type 1." *American Journal of Physical Medicine & Rehabilitation / Association of Academic Physiatrists* 93(9):739–50.

Brook, J. David, Mila E. McCurrach, Helen G. Harley, Alan J. Buckler, Deanna Church, Hiroyuki Aburatani, Kent Hunter, Vincent P. Stanton, Jean Paul Thirion, Thomas Hudson, Robert Sohn, Boris Zemelman, Russell G. Snell, Shelley A. Rundle, Steve Crow, June Davies, Peggy Shelbourne, Jessica Buxton, Clare Jones, Vesa Juvonen, Keith Johnson, Peter S. Harper,

Duncan J. Shaw, and David E. Housman. 1992. “Molecular Basis of Myotonic Dystrophy: Expansion of a Trinucleotide (CTG) Repeat at the 3??? End of a Transcript Encoding a Protein Kinase Family Member.” *Cell* 68(4):799–808.

Burnstine, Michael A. and Allen Putterman. 2002. “Management of Myopathic Ptosis.” *Ophthalmology* 11(2):411–12.

Bustin, Stephen A., Vladimir Benes, Jeremy A. Garson, Jan Hellemans, Jim Huggett, Mikael Kubista, Reinhold Mueller, Tania Nolan, Michael W. Pfaffl, Gregory L. Shipley, Jo Vandesompele, and Carl T. Wittwer. 2009. “The MIQE Guidelines: Minimum Information for Publication of Quantitative Real-Time PCR Experiments.” *Clinical Chemistry* 55(4):611–22.

Carrell, Samuel T., Ellie M. Carrell, David Auerbach, Sanjay K. Pandey, C. Frank Bennett, Robert T. Dirksen, and Charles A. Thornton. 2016. “Dmpk Gene Deletion or Antisense Knockdown Does Not Compromise Cardiac or Skeletal Muscle Function in Mice.” *Human Molecular Genetics* 25(19):4328–38.

Caso, Francesca, Federica Agosta, Stojan Peric, Vidosava Rakočević-Stojanović, Massimiliano Copetti, Vladimir S. Kostic, and Massimo Filippi. 2014. “Cognitive Impairment in Myotonic Dystrophy Type 1 Is Associated with White Matter Damage.” *PLoS ONE* 9(8):1–8.

Chamberlain, Christopher M. and Laura P. W. Ranum. 2012. “Mouse Model of Muscleblind-like 1 Overexpression: Skeletal Muscle Effects and Therapeutic Promise.” *Human Molecular Genetics* 21(21):4645–54.

Charizanis, Konstantinos, Kuang Yung Lee, Ranjan Batra, Marianne Goodwin, Chaolin Zhang, Yuan Yuan, Lily Shiue, Melissa Cline, Marina M. Scotti, Guangbin Xia, Ashok Kumar, Tetsuo Ashizawa, H. Brent Clark, Takashi Kimura, Harutoshi Fujimura, Kenji Jinnai, Hiroo Yoshikawa, Mário Gomes-Pereira, Masanori P. Takahashi, Geneviève Gourdon, Noriaki Sakai, Seiji Nishino, Thomas C. Foster, Manuel Ares Jr, Robert B. Darnell, and Maurice S. Swanson. 2012. “Muscleblind-Like 2 Mediated Alternative Splicing in the Developing Brain and Dysregulation in Myotonic Dystrophy.” *Neuron* 75(3):437–50.

Charlet-B, N., R. S. Savkur, G. Singh, A. V Phillips, E. A. Grice, and T. A. Cooper. 2002. “Loss of the Muscle-Specific Chloride\rChannel in Type 1 Myotonic Dystrophy\rDue to Misregulated Alternative Splicing.” *Mol Cell* 10:45–53.

Chen, Hsin-Mei, Lulu Wang, and Santosh R. D’Mello. 2008. “A Chemical Compound Commonly Used to Inhibit PKR, {8- (Imidazol-4-Ylmethylene)-6H-Azolidino[5,4-g]Benzothiazol-7-One}, Protects Neurons by Inhibiting Cyclin-Dependent Kinase.” *European Journal of Neuroscience* 28(10):2003–16.

Cleary, John D. and Laura P. W. Ranum. 2013. “Repeat-Associated Non-ATG (RAN) Translation in Neurological Disease.” *Human Molecular Genetics* 22(R1):45–51.

Cleary, John Douglas, Amrutha Pattamatta, and Laura P. W. Ranum. 2018. “Repeat-Associated Non-ATG (RAN) Translation.” *Journal of Biological Chemistry* 293(42):16127–41.

Cohen, Philip. 2002. “Protein Kinases - The Major Drug Targets of the Twenty-First Century?” *Nature Reviews Drug Discovery* 1(4):309–15.

Cohen, Philip. 2009. “Targeting Protein Kinases for the Development of Anti-Inflammatory Drugs.” *Current Opinion in Cell Biology* 21(2):317–24.

Courtney, Kenneth R. 1981. “COMPARATIVE ACTIONS OF MEXILETINE ON SODIUM CHANNELS IN NERVE, SKELETAL AND CARDIAC MUSCLE.” *European Journal of Pharmacology* 74:9–18.

Dansithong, Warunee, Sharan Paul, Lucio Comai, and Sita Reddy. 2005. “MBNL1 Is the Primary Determinant of Focus Formation and Aberrant Insulin Receptor Splicing in DM1.” *The Journal of Biological Chemistry* 280(7):5773–80.

Davis, Brigid M., M. E. McCurrach, Krishan L. Taneja, Robert H. Singer, and David E. Housman. 1997. “Expansion of a CUG Trinucleotide Repeat in the 3’ Untranslated Region of Myotonic Dystrophy Protein Kinase Transcripts Results in Nuclear Retention of Transcripts.” *Proceedings of the National Academy of Sciences* 94(14):7388–93.

Debacker, Kim, Aisling Frizzell, Olive Gleeson, Lucy Kirkham-McCarthy, Tony Mertz, and Robert S. Lahue. 2012. “Histone Deacetylase Complexes Promote Trinucleotide Repeat Expansions.” *PLoS Biology* 10(2).

de Die-Smulders C.E., Höweler C.J., J. F. Mirandolle, H. G. Brunner, V. Hovers, H. Brüggenwirth, H. J. Smeets, and J. P. Geraedts. 1994. “Anticipation Resulting in Elimination of the Myotonic Dystrophy Gene: A Follow up Study of One Extended Family.” *Journal of Medical Genetics* 31:595–601.

Fardaei, M., Ken Larkin, J. David Brook, and Marion G. Hamshere. 2001. “In Vivo Co-Localisation of MBNL Protein with DMPK Expanded-Repeat Transcripts.” *Nucleic Acids Research* 29(13):2766–71.

Friedmann, T. 2017. “Gene Therapy for Spinomuscular Atrophy: A Biomedical Advance, a Missed Opportunity for More Equitable Drug Pricing.” *Gene Therapy* 24(9):503–5.

Fu, Author Ying-hui, David L. Friedman, Stephen Richards, Joel A. Pearlman, A. Richard, Antonio Pizzuti, Tetsuo Ashizawa, M. Benjamin Perryman, Guglielmo Scarlato, Raymond G. Fenwick, C. Thomas Caskey, Ying-hui Fu, David L. Friedman, Stephen Richards, Joel A. Pearlman, Richard A. Gibbs, Antonio Pizzuti, Tetsuo Ashizawa, M. Benjamin Perryman, Guglielmo Scarlato, Raymond G. Fenwick, and C. Thomas Caskeyt. 1993. “Decreased Expression of Myotonin-Protein Kinase Messenger RNA and Protein in Adult Form of Myotonic Dystrophy.” *Science* 260(5105):235–38.

Gagnon, Cynthia, Luc Noreau, Richard T. Moxley, Luc Laberge, Stéphane Jean, Louis Richer, Michel Perron, Suzanne Veillette, and Jean Mathieu. 2007. “Towards an Integrative Approach to the Management of Myotonic Dystrophy Type 1.” *Journal of Neurology, Neurosurgery and Psychiatry* 78(8):800–806.

Gourdon, Geneviève, François Radvanyi, Anne Sophie Lia, Chantal Duros, Martine Blanche, Marc Abitbol, Claudine Junien, and Hélène Hofmann-Radvanyi. 1997. “Moderate

Intergenerational and Somatic Instability of a 55-CTG Repeat in Transgenic Mice." *Nature Genetics* 15(2):190–92.

Groenen, P. J. T. A., Derick G. Wansink, M. Coerwinkel, Walther J. A. A. Van Den Broek, Gert Jansen, and Bé Wieringa. 2000. "Constitutive and Regulated Modes of Splicing Produce Six Major Myotonic Dystrophy Protein Kinase (DMPK) Isoforms with Distinct Properties." *Human Molecular Genetics* 9(4):605–16.

Hadwen, Jeremiah, Sarah Schock, Alan Mears, Robert Yang, Philippe Charron, Liying Zhang, Hualin S. Xi, and Alex MacKenzie. 2018. "Transcriptomic RNAseq Drug Screen in Cerebrocortical Cultures: Toward Novel Neurogenetic Disease Therapies." *Human Molecular Genetics* 27(18):3206–17.

Harley, H. G., S. A. Rundle, W. Reardon, J. Myring, S. Crow, P. S. Harper, D. J. Shaw, and J. D. Brook. 1992. "Unstable DNA Sequence in Myotonic Dystrophy." *The Lancet* 339(8802):1125–28.

Heath, C. M., P. D. Stahl, and M. A. Barbieri. 2003. "Lipid Kinases Play Crucial and Multiple Roles in Membrane Trafficking and Signaling." *Histology and Histopathology* 18(3):989–98.

Heatwole, Chad, Rita Bode, Nicholas Johnson, Christine Quinn, William Martens, Michael P. McDermott, Nan Rothrock, Charles Thornton, Barbara Vickrey, David Victorson, and Richard Moxley. 2012. "Patient-Reported Impact of Symptoms in Myotonic Dystrophy Type 1 (PRISM-1)." *Neurology* 79(4):348–57.

Hermans, Mieke C. E., Catharina G. Faber, Els K. Vanhoutte, Mayienne Bakkers, Marc H. De Baets, Christine E. M. De Die-Smulders, and Ingemar S. J. Merkies. 2011. "Peripheral Neuropathy in Myotonic Dystrophy Type 1." *Journal of the Peripheral Nervous System* 16(1):24–29.

Hilton-Jones, D., M. Bowler, H. Lochmueller, C. Longman, R. Petty, M. Roberts, M. Rogers, C. Turner, and D. Wilcox. 2012. "Modafinil for Excessive Daytime Sleepiness in Myotonic Dystrophy Type 1 - The Patients' Perspective." *Neuromuscular Disorders* 22(7):597–603.

Hino, Shin-Ichiro, Shinichi Kondo, Hiroshi Sekiya, Atsushi Saito, Soshi Kanemoto, Tomohiko Murakami, Kazuyasu Chihara, Yuri Aoki, Masayuki Nakamori, Masanori P. Takahashi, and Kazunori Imaizumi. 2007. "Molecular Mechanisms Responsible for Aberrant Splicing of SERCA1 in Myotonic Dystrophy Type 1." *Human Molecular Genetics* 16(23):2834–43.

Hodge, Rebecca D., Trygve E. Bakken, Jeremy A. Miller, Kimberly A. Smith, Eliza R. Barkan, Lucas T. Graybuck, Jennie L. Close, Brian Long, Nelson Johansen, Osnat Penn, Zizhen Yao, Jeroen Eggermont, Thomas Höllt, Boaz P. Levi, Soraya I. Shehata, Brian Aevermann, Allison Beller, Darren Bertagnolli, Krissy Brouner, Tamara Casper, Charles Cobbs, Rachel Dalley, Nick Dee, Song Lin Ding, Richard G. Ellenbogen, Olivia Fong, Emma Garren, Jeff Goldy, Ryder P. Gwinn, Daniel Hirschstein, C. Dirk Keene, Mohamed Keshk, Andrew L. Ko, Kanan Lathia, Ahmed Mahfouz, Zoe Maltzer, Medea McGraw, Thuc Nghi Nguyen, Julie Nyhus, Jeffrey G. Ojemann, Aaron Oldre, Sheana Parry, Shannon Reynolds, Christine Rimorin, Nadiya V. Shapovalova, Saroja Somasundaram, Aaron Szafer, Elliot R. Thomsen, Michael Tieu, Gerald

Quon, Richard H. Scheuermann, Rafael Yuste, Susan M. Sunkin, Boudewijn Lelieveldt, David Feng, Lydia Ng, Amy Bernard, Michael Hawrylycz, John W. Phillips, Bosiljka Tasic, Hongkui Zeng, Allan R. Jones, Christof Koch, and Ed S. Lein. 2019. "Conserved Cell Types with Divergent Features in Human versus Mouse Cortex." *Nature* 573(7772):61–68.

Hopkins, Andrew L. and Colin R. Groom. 2002. "The Druggable Genome." *Nature Reviews Drug Discovery* 1(9):727–30.

Hopkins, Philip M. 2006. "Skeletal Muscle Physiology." *Continuing Education in Anaesthesia, Critical Care and Pain* 6(1):1–6.

Hoy, Kim L. O., Catherine Tsilfidis, Mani S. Mahadevan, Catherine E. Neville, Juana Barceló, Alasdair G. W. Hunter, Robert G. Korneluk, Kim L. O. Hoy, Catherine Tsilfidis, Mani S. Mahadevan, Catherine E. Neville, Juana Barcelo, Alasdair G. W. Hunter, and Robert G. Korneluk. 1993. "Reduction in Size of the Myotonic Dystrophy Trinucleotide Repeat During Transmission." *Science* 259(5096):809–12.

Hrzenjak, Andelko, Farid Moinfar, Marie Luise Kremser, Bettina Strohmeier, Edgar Petru, Kurt Zatloukal, and Helmut Denk. 2010. "Histone Deacetylase Inhibitor Vorinostat Suppresses the Growth of Uterine Sarcomas in Vitro and in Vivo." *Molecular Cancer* 9:1–11.

Hu, Ye, Ryo Kunimoto, and Jürgen Bajorath. 2016. "Mapping of Inhibitors and Activity Data to the Human Kinome and Exploring Promiscuity from a Ligand and Target Perspective." *Chemical Biology and Drug Design* 89(6):834–45.

Huguet, Aline, Fadia Medja, Annie Nicole, Alban Vignaud, Céline Guiraud-Dogan, Arnaud Ferry, Valerie Decostre, Jean-yves Hogrel, Friedrich Metzger, Andreas Hoeflich, Martin Baraibar, Mario Gomes-pereira, Jack Puymirat, Guillaume Bassez, Denis Furling, Arnold Munnich, and Geneviève Gourdon. 2012. "Molecular , Physiological , and Motor Performance Defects in DMSXL Mice Carrying . 1 , 000 CTG Repeats from the Human DM1 Locus." 8(11):1–19.

Huichalaf, Claudia, Keiko Sakai, Bingwen Jin, Karlie Jones, Guo Li Wang, Benedikt Schoser, Christiane Schneider-Gold, Partha Sarkar, Olivia M. Pereira-Smith, Nikolai Timchenko, and Lubov Timchenko. 2010. "Expansion of CUG RNA Repeats Causes Stress and Inhibition of Translation in Myotonic Dystrophy 1 (DM1) Cells." *FASEB Journal* 24(10):3706–19.

Ikeda, Karin Suzete, Cristina Iwabe-Marchese, Marcondes Cavalcante França, Anamarli Nucci, and Keila Monteiro de Carvalho. 2016. "Myotonic Dystrophy Type 1: Frequency of Ophthalmologic Findings." *Arq Neuropsiquiatr* 74(3):183–88.

Jammi, Narasimham V., Landon R. Whitby, and Peter A. Beal. 2003. "Small Molecule Inhibitors of the RNA-Dependent Protein Kinase." *Biochemical and Biophysical Research Communications* 308(1):50–57.

Jansen, G., M. Mahadevan, C. Amemiya, N. Wormskamp, B. Segers, W. Hendriks, K. O'hoy, S. Baird, L. Sabourin, G. Lennon, P. L. Jap, D. Iles, M. Coerwinkel, M. Hofker, A. V. Carrano, P. J. de Jong, R. G. Korneluk, and B. Wieringa. 1992. "Characterization of the Myotonic

Dystrophy Region Predicts Multiple Protein Isoform–Encoding MRNAs." *Nature Genetics* 1(4):261–66.

Jansen, Gert, Patricia J. T. A. Groenen, Dietmar Bachner, Paul H. K. Jap, Frank Oerlemans, Walther Van Den Broek, Barbel Gohlsch, Jaap J. Plomp, Peter C. Molenaar, Marcel G. J. Nederhofl, Cees J. A. Van, Marleen Dekker, Anton Berns, Horst Hameister, and Be Wieringa. 1996. "Abnormal Myotonic Dystrophy Protein Kinase Levels Produce Only Mild Myopathy in Mice." *Nature* 13(July):316–24.

Jarvis, Blair and Allan J. Coukell. 1998. "Mexiletine A Review of Its Therapeutic Use in Painful Diabetic Neuropathy." *Adis Drug Evaluation* 56(4):691–707.

Jones, Lyn H. and Mark E. Bunnage. 2017. "Applications of Chemogenomic Library Screening in Drug Discovery." *Nature Reviews Drug Discovery* 16(4):285–96.

Kalsotra, Auinash, Xinshu Xiao, Amanda J. Ward, John C. Castle, Jason M. Johnson, Christopher B. Burge, and Thomas A. Cooper. 2008. "A Postnatal Switch of CELF and MBNL Proteins Reprograms Alternative Splicing in the Developing Heart." *Proceedings of the National Academy of Sciences of the United States of America* 105(51):20333–38.

Kanadia, Rahul N., Karen A. Johnstone, Ami Mankodi, Codrin Lungu, Charles A. Thornton, Douglas Esson, Adrian M. Timmers, William W. Hauswirth, and Maurice S. Swanson. 2003. "A Muscleblind Knockout Model for Myotonic Dystrophy." *Science* 302(5652):1978–80.

Kanadia, Rahul N., Jihae Shin, Yuan Yuan, Stuart G. Beattie, Thurman M. Wheeler, Charles a Thornton, and Maurice S. Swanson. 2006. "Reversal of RNA Missplicing and Myotonia after Muscleblind Overexpression in a Mouse Poly(CUG) Model for Myotonic Dystrophy." *Proceedings of the National Academy of Sciences of the United States of America* 103(31):11748–53.

Ketley, Ami, Catherine Z. Chen, Xin Li, Sukrat Arya, Thelma E. Robinson, Javier Granados-Riveron, Inyang Udosen, Glenn E. Morris, Ian Holt, Denis Furling, Soraya Chaouch, Ben Haworth, Noel Southall, Paul Shinn, Wei Zheng, Christopher P. Austin, Christopher J. Hayes, and J. David Brook. 2014. "High-Content Screening Identifies Small Molecules That Remove Nuclear Foci, Affect MBNL Distribution and CELF1 Protein Levels via a PKC-Independent Pathway in Myotonic Dystrophy Cell Lines." *Human Molecular Genetics* 23(6):1551–62.

Kim, Yun Kyoung, Mahua Mandal, Ramesh S. Yadava, Luc Paillard, and Mani S. Mahadevan. 2014. "Evaluating the Effects of CELF1 Deficiency Inamouse Model of RNA Toxicity." *Human Molecular Genetics* 23(2):293–302.

Kimura, Takashi, Masayuki Nakamori, John D. Lueck, Pierre Pouliquin, Futoshi Aoike, Harutoshi Fujimura, Robert T. Dirksen, Masanori P. Takahashi, Angela F. Dulhunty, and Saburo Sakoda. 2005. "Altered MRNA Splicing of the Skeletal Muscle Ryanodine Receptor and Sarcoplasmic/Endoplasmic Reticulum Ca2+-ATPase in Myotonic Dystrophy Type 1." *Human Molecular Genetics* 14(15):2189–2200.

Kino, Yoshihiro, Mori Daisuke, Yoko Oma, Yuya Takeshita, Noboru Sasagawa, and Shoichi Ishuira. 2004. “Muscleblind Protein, MBNL1/EXP, Binds Specifically to CHHG Repeats.” *Human Molecular Genetics* 13(5):495–507.

Klesert, Todd R., Diane H. Cho, John I. Clark, James Maylie, John Adelman, Lauren Snider, Eric C. Yuen, Philippe Soriano, and Stephen J. Tapscott. 2000. “Mice Deficient in Six5 Develop Cataracts: Implications for Myotonic Dystrophy.” *Nature Genetics* 25(1):105–9.

Klesert, Todd R., Anne D. Otten, Thomas D. Bird, and Stephen J. Tapscott. 1997. “Trinucleotide Repeat Expansion at the Myotonic Dystrophy Locus Reduces Expression of DMAHP.” *Nature* 16(august):402–6.

Koga, R., Y. Nakao, Y. Kurano, T. Tsukahara, A. Nakamura, S. Ishiura, I. Nonaka, and K. Arahata. 1994. “Decreased Myotonin-Protein Kinase in the Skeletal and Cardiac Muscles in Myotonic Dystrophy.” *Biochemical and Biophysical Research Communications* 202(1):577–85.

Korade-Mirnics, Zeljka, Jack Tarleton, Serenella Servidei, Renee R. Casey, Massimo Gennarelli, Elena Pegoraro, Corrado Angelini, and Eric P. Hoffman. 1999. “Myotonic Dystrophy: Tissue-Specific Effect of Somatic CTG Expansions on Allele-Specific DMAHP/SIX5 Expression.” *Human Molecular Genetics* 8(6):1017–23.

Kuyumcu-Martinez, N. Muge, Guey-Shin Wang, and Thomas A. Cooper. 2007. “Increased Steady State Levels of CUGBP1 in Myotonic Dystrophy 1 Are Due to PKC-Mediated Hyper-Phosphorylation.” *Mol Cell* 28(1):68–78.

Labayru, Garazi, Irati Arenzana, Jone Aliri, Miren Zulaica, Adolfo Lopez De Munain, and A. Andone Sistiaga. 2018. “Social Cognition in Myotonic Dystrophy Type 1: Specific or Secondary Impairment?” *PLoS ONE* 13(9):1–11.

Laberge, Luc, Cynthia Gagnon, and Yves Dauvilliers. 2013. “Daytime Sleepiness and Myotonic Dystrophy.” *Current Neurology and Neuroscience Reports* 13(4).

Ladd, A. N., N. Charlet-B., and T. A. Cooper. 2001. “The CELF Family of RNA Binding Proteins Is Implicated in Cell-Specific and Developmentally Regulated Alternative Splicing.” *Molecular and Cellular Biology* 21(4):1285–96.

Lahiry, Piya, Ali Torkamani, Nicholas J. Schork, and Robert A. Hegele. 2010. “Kinase Mutations in Human Disease: Interpreting Genotype-Phenotype Relationships.” *Nature Reviews Genetics* 11(1):60–74.

Landis, Story C., Susan G. Amara, Khusru Asadullah, Chris P. Austin, Robi Blumenstein, Eileen W. Bradley, Ronald G. Crystal, Robert B. Darnell, Robert J. Ferrante, Howard Fillit, Robert Finkelstein, Marc Fisher, Howard E. Gendelman, Robert M. Golub, John L. Goudreau, Robert A. Gross, Amelie K. Gubitz, Sharon E. Hesterlee, David W. Howells, John Huguenard, Katrina Kelner, Walter Koroshetz, Dimitri Krainc, Stanley E. Lazic, Michael S. Levine, Malcolm R. MacLeod, John M. McCall, Richard T. Moxle. Iii, Kalyani Narasimhan, Linda J. Noble, Steve Perrin, John D. Porter, Oswald Steward, Ellis Unger, Ursula Utz, and Shai D.

Silberberg. 2012. “A Call for Transparent Reporting to Optimize the Predictive Value of Preclinical Research.” *Nature* 490(7419):187–91.

Langlois, Marc André, Christelle Boniface, Gang Wang, Jessica Alluin, Paul M. Salvaterra, Jack Puymirat, John J. Rossi, and Nan Sook Lee. 2005. “Cytoplasmic and Nuclear Retained DMPK MRNAs Are Targets for RNA Interference in Myotonic Dystrophy Cells.” *Journal of Biological Chemistry* 280(17):16949–54.

Langlois, Marc André, Nan Sook Lee, John J. Rossi, and Jack Puymirat. 2003. “Hammerhead Ribozyme-Mediated Destruction of Nuclear Foci in Myotonic Dystrophy Myoblasts.” *Molecular Therapy* 7(5 I):670–80.

Larsen, Jan, Olof J. Pettersson, Maria Jakobsen, Rune Thomsen, Christina B. Pedersen, Jens M. Hertz, Niels Gregersen, Thomas J. Corydon, and Thomas G. Jensen. 2011. “Myoblasts Generated by Lentiviral Mediated MyoD Transduction of Myotonic Dystrophy Type 1 (DM1) Fibroblasts Can Be Used for Assays of Therapeutic Molecules.” *BMC Research Notes* 4(1):490.

Lin, Xiaoyan, Jill W. Miller, Ami Mankodi, Rahul N. Kanadia, Yuan Yuan, Richard T. Moxley, Maurice S. Swanson, and Charles A. Thornton. 2006. “Failure of MBNL1-Dependent Post-Natal Splicing Transitions in Myotonic Dystrophy.” *Human Molecular Genetics* 15(13):2087–97.

Liu, Yu Chi, Mark Wilkins, Terry Kim, Boris Malyugin, and Jodhbir S. Mehta. 2017. “Cataracts.” *The Lancet* 390(10094):600–612.

Lo, Yu Chen, Tianyun Liu, Kari M. Morrissey, Satoko Kakiuchi-Kiyota, Adam R. Johnson, Fabio Broccatelli, Yu Zhong, Amita Joshi, and Russ B. Altman. 2019. “Computational Analysis of Kinase Inhibitor Selectivity Using Structural Knowledge.” *Bioinformatics* 35(2):235–42.

Logigian, E. L., W. B. Martens, R. T. Moxley, M. P. McDermott, N. Dilek, A. W. Wiegner, A. T. Pearson, C. A. Barbieri, C. L. Annis, C. A. Thornton, and R. T. Moxley. 2010. “Mexiletine Is an Effective Antimyotonia Treatment in Myotonic Dystrophy Type 1.” *Neurology* 74(18):1441–48.

Magana, Jonathan J., Rocio Suarez-Sanchez, Norberto Leyva-Garcia, Bulmaro Cisneros, and Hernanded-Hernandez Oscar. 2012. “Myotonic Dystrophy Protein Kinase: Structure, Function and Its Possible Role in the Pathogenesis of Myotonic Dystrophy Type 1.” Pp. 213–42 in *Advances in Protein Kinases*.

Mahadevan, M., C. Tsilfidis, L. Sabourin, G. Shutler, C. Amemiya, G. Jansen, C. Neville, M. Narang, J. Barcelo, K. O’Hoy, and al. et. 1992. “Myotonic Dystrophy Mutation: An Unstable CTG Repeat in the 3’ Untranslated Region of the Gene.” *Science* 255(5049):1253–55.

Mankodi, A., E. Logigian, L. Callahan, C. McClain, R. White, D. Henderson, M. Krym, and C. A. Thornton. 2000. “Myotonic Dystrophy in Transgenic Mice Expressing an Expanded CUG Repeat.” *Science (New York, N.Y.)* 289(5485):1769–73.

Mankodi, Ami, Patana Teng-Umnuay, Matt Krym, Don Henderson, Maurice Swanson, and

Charles A. Thornton. 2003. “Ribonuclear Inclusions in Skeletal Muscle in Myotonic Dystrophy Types 1 and 2.” *Annals of Neurology* 54(6):760–68.

Mann, B. S., J. R. Johnson, M. H. Cohen, R. Justice, and R. Pazdur. 2007. “FDA Approval Summary: Vorinostat for Treatment of Advanced Primary Cutaneous T-Cell Lymphoma.” *The Oncologist* 12(10):1247–52.

Manning, Author G., D. B. Whyte, R. Martinez, T. Hunter, and S. Sudarsanam. 2002. “The Protein Kinase Complement of the Human Genome Author (s): G . Manning , D . B . Whyte , R . Martinez , T . Hunter , S . Sudarsanam Published by : American Association for the Advancement of Science Stable URL : Http://Www.Jstor.Org/Stable/3833111 .” 298(5600):1912–16.

Manta, Alexander, Derek W. Stouth, Donald Xhuti, Leon Chi, Irena A. Rebalka, Jayne M. Kalmar, Thomas J. Hawke, and Vladimir Ljubicic. 2019. “Chronic Exercise Mitigates Disease Mechanisms and Improves Muscle Function in Myotonic Dystrophy Type 1 Mice.” *Journal of Physiology* 597(5):1361–81.

Mathieu, J., P. Allard, L. Potvin, C. Prevost, and P. Begin. 1999. “A 10-Year Study of Mortality in a Cohort of Patients with Myotonic Dystrophy.” *Neurology* 52(8):1658–62.

Mathieu, Jean and Claude Prévost. 2012. “Epidemiological Surveillance of Myotonic Dystrophy Type 1: A 25-Year Population-Based Study.” *Neuromuscular Disorders* 22(11):974–79.

Matsumura, Tsuyoshi, Hiromi Iwahashi, Tohru Funahashi, Masanori P. Takahashi, Tomoko Saito, Kumiko Yasui, Toshio Saito, Akinori Iyama, Keiko Toyooka, Harutoshi Fujimura, and Susumu Shinno. 2009. “A Cross-Sectional Study for Glucose Intolerance of Myotonic Dystrophy.” *Journal of the Neurological Sciences* 276(1–2):60–65.

Matynia, Anna, Carina Hoi Ng, Warunee Dansithong, Andy Chiang, Alcino J. Silva, and Sita Reddy. 2010. “Muscleblind1, but Not Dmpk or Six5, Contributes to a Complex Phenotype of Muscular and Motivational Deficits in Mouse Models of Myotonic Dystrophy.” *PLoS ONE* 5(3):1–9.

De Mezer, Mateusz, Marzena Wojciechowska, Marek Napierala, Krzysztof Sobczak, and Wlodzimierz J. Krzyzosiak. 2011. “Mutant CAG Repeats of Huntingtin Transcript Fold into Hairpins, Form Nuclear Foci and Are Targets for RNA Interference.” *Nucleic Acids Research* 39(9):3852–63.

Michalowski, Susan, Jill W. Miller, Carl R. Urbinati, Miltiadis Paliouras, Maurice S. Swanson, and Jack Griffith. 1999. “Visualization of Double-Stranded RNAs from the Myotonic Dystrophy Protein Kinase Gene and Interactions with CUG-Binding Protein.” *Nucleic Acids Research* 27(17):3534–42.

Miller, J. W., C. R. Urbinati, P. Teng-Umnuay, M. G. Stenberg, B. J. Byrne, C. a Thornton, and M. S. Swanson. 2000. “Recruitment of Human Muscleblind Proteins to (CUG)(n) Expansions Associated with Myotonic Dystrophy.” *The EMBO Journal* 19(17):4439–48.

Mishra, Shri Kant, Sandeep Singh, Brian Lee, Shaweta Khosa, Negar Moheb, and Vishal A.

Tandon. 2018. "'Dystrophia Myotonica' and the Legacy of Hans Gustav Wilhelm Steinert." *Annals of Indian Academy of Neurology* 21(2):116–18.

Muth, Christopher C. 2018. "ASO Therapy: Hope for Genetic Neurological Diseases." *JAMA - Journal of the American Medical Association* 319(7):644–46.

Nakagawa, Hiroki, Tatsuo Munakata, and Akihiko Sunami. 2019. "Mexiletine Block of Voltage-Gated Sodium Channels: Isoform- And State-Dependent Drug–Pore Interactions." *Molecular Pharmacology* 95(3):236–44.

Napierała, Marek and Włodzimierz J. Krzyzosiak. 1997. "CUG Repeats Present in Myotonin Kinase RNA Form Metastable 'slippery' Hairpins." *Journal of Biological Chemistry* 272(49):31079–85.

Nguyen, Cam-Tu and Craig Campbell. 2016. "Myotonic Dystrophy Type 1." *CMAJ* 188(4):1033.

Nosengo, Nicola. 2016. "New Tricks for Old Drugs." *Nature* 534:314–16.

Ophuis, Ralph J. A. Oud., Susan A. M. Mulders, René E. M. A. Van Herpen, Rinske Van De Vorstenbosch, Bé Wieringa, and Derick G. Wansink. 2009. "DMPK Protein Isoforms Are Differentially Expressed in Myogenic and Neural Cell Lineages." *Muscle and Nerve* 40(4):545–55.

Pantic, Boris, Doriana Borgia, Silvia Giunco, Adriana Malena, Tohru Kiyono, Sergio Salvatori, Anita De Rossi, Emiliano Giardina, Federica Sangiuolo, Elena Pegoraro, Lodovica Vergani, and Annalisa Botta. 2016. "Reliable and Versatile Immortal Muscle Cell Models from Healthy and Myotonic Dystrophy Type 1 Primary Human Myoblasts." *Experimental Cell Research* 342(1):39–51.

Patel, Rekha C. and Ganes C. Sen. 1998. "PACT, a Protein Activator of the Interferon-Induced Protein Kinase, PKR." *EMBO Journal* 17(15):4379–90.

Paulson, Henry and Ann Arbor. 2006. *Repeat Expansion Diseases*.

Peric, Stojan, Tanja Nisic, Milena Milicev, Ivana Basta, Ivan Marjanovic, Marina Peric, Dragana Lavrnic, and Vidosava Rakocevic Stojanovic. 2013. "Hypogonadism and Erectile Dysfunction in Myotonic Dystrophy Type 1." *Acta Myologica* 32(2):106–9.

Philips, A. V., Lubov T. Timchenko, and Thomas A. Cooper. 1998. "Disruption of Splicing Regulated by a CUG-Binding Protein in Myotonic Dystrophy." *Science* 280(5364):737–41.

Pratap, J., J. Akech, J. J. Wixted, G. Szabo, S. Hussain, M. E. McGee-Lawrence, X. Li, K. Bedard, R. J. Dhillon, A. J. van Wijnen, J. L. Stein, G. S. Stein, J. J. Westendorf, and J. B. Lian. 2010. "The Histone Deacetylase Inhibitor, Vorinostat, Reduces Tumor Growth at the Metastatic Bone Site and Associated Osteolysis, but Promotes Normal Bone Loss." *Molecular Cancer Therapeutics* 9(12):3210–20.

Pushpakom, Sudeep, Francesco Iorio, Patrick A. Eyers, K. Jane Escott, Shirley Hopper, Andrew Wells, Andrew Doig, Tim Guilliams, Joanna Latimer, Christine McNamee, Alan Norris, Philippe Sanseau, David Cavalla, and Munir Pirmohamed. 2018. "Drug Repurposing:

Progress, Challenges and Recommendations." *Nature Reviews Drug Discovery* 18(1):41–58.

Ravel-Chapuis, Aymeric, Ali Al-Rewashdy, Guy Bélanger, and Bernard J. Jasmin. 2018. "Pharmacological and Physiological Activation of AMPK Improves the Spliceopathy in DM1 Mouse Muscles." *Human Molecular Genetics* 27(19):3361–76.

Reardon, W., J. C. MacMillan, J. Myring, H. G. Harley, S. A. Rundle, L. Beck, P. S. Harper, and D. J. Shaw. 1993. "Cataract and Myotonic Dystrophy: The Role of Molecular Diagnosis." *British Journal of Ophthalmology* 77(9):579–83.

Reddy, Sita, Daniel B. J. Smith, Mark M. Rich, John M. Leferovich, Patricia Reilly, Brigid M. Davis, Khoa Tran, Helen Rayburn, Roderick Bronson, Didier Cros, Rita J. Balice-gordon, and David Housman. 1996. "Mice Lacking the Myotonic Dystrophy Protein Kinase Develop a Late Onset Progressive Myopathy." *Nature* 13(July):325–35.

Rhodes, Jeremy D., Martin C. Lott, Sarah L. Russell, Vincent Moulton, Julie Sanderson, I. Michael Wormstone, and David C. Broadway. 2012. "Activation of the Innate Immune Response and Interferon Signalling in Myotonic Dystrophy Type 1 and Type 2 Cataracts." *Human Molecular Genetics* 21(4):852–62.

Richon, V. M. 2006. "Cancer Biology: Mechanism of Antitumour Action of Vorinostat (Suberoylanilide Hydroxamic Acid), a Novel Histone Deacetylase Inhibitor." *British Journal of Cancer* 95(SUPPL. 1):2–6.

Roberts, Robert, Nikolaj A. Timchenko, Jill W. Miller, Sita Reddy, C. Thomas Caskey, Maurice S. Swanson, and Lubov T. Timchenko. 1997. "Altered Phosphorylation and Intracellular Distribution of a (CUG) n Triplet Repeat RNA-Binding Protein in Patients with Myotonic Dystrophy and in Myotonin Protein Kinase." *Proc Natl Acad Sci U S A* 94:13221–26.

Roskoski, Robert. 2019. "Properties of FDA-Approved Small Molecule Protein Kinase Inhibitors." *Pharmacological Research* 144(March):19–50.

Sabourin, Luc A., Mani S. Mahadevan, Monica Narang, David S. C. Lee, Linda Surh, and Robert G. Korneluk. 1993. "Effect of the Myotonic Dystrophy (DM) Mutation on MRNA Levels of TheDMgene." *Nature* 4(july):233–38.

Salvatori, Sergio, M. Fanin, C. P. Trevisan, S. Furlan, S. Reddy, J. I. Nagy, and C. Angelini. 2005. "Decreased Expression of DMPK: Correlation with CTG Repeat Expansion and Fibre Type Composition in Myotonic Dystrophy Type 1." *Neurological Sciences* 26(4):235–42.

Sarkar, Partha S., Binoy Appukuttan, Jennifer Han, Yoshihiro Ito, Cuiwei Ai, Wenli Tsai, Yang Chai, J. Timothy Stout, and Sita Reddy. 2000. "Heterozygous Loss of Six5 in Mice Is Sufficient to Cause Ocular Cataracts." *Nature Genetics* 25(1):110–14.

Sarkar, Partha S., Jennifer Han, and Sita Reddy. 2004. "In Situ Hybridization Analysis of Dmpk MRNA in Adult Mouse Tissues." *Neuromuscular Disorders* 14(8–9):497–506.

Savkur, R. S., A. V Philips, and T. A. Cooper. 2001. "Aberrant Regulation of Insulin Receptor Alternative Splicing Is Associated with Insulin Resistance in Myotonic Dystrophy." *Nature*

Genetics 29(1):40–47.

Seznec, Herve, Onnik Agbulut, Nicolas Sergeant, Cedric Savouret, Antoine Ghestem, Nacira Tabti, Jean-Claude Willer, Lucie Ourth, Chantal Duros, Edith Brisson, Coralie Fouquet, Gillian S. Butler-Browne, Andre Delacourte, Claudine Junien, and Geneviève Gourdon. 2001. "Mice Transgenic for the Human Myotonic Dystrophy Region with Expanded CTG Repeats Display Muscular and Brain Abnormalities." *Human Molecular Genetics* 10(23):2717–26.

Seznec, Herve, Anee-Sophie Lia-Baldini, Chantal Duros, Coralie Fouquet, Celine Lacroix, Hélène Hofmann-Radvanyi, Claudine Junien, and Geneviève Gourdon. 2000. "Transgenic Mice Carrying Large Human Genomic Sequences with Expanded CTG Repeat Mimic Closely the DM CTG Repeat Intergenerational and Somatic Instability." *Human Molecular Genetics* 9(8):1185–94.

Singh, Madhurima and Rekha C. Patel. 2012. "Increased Interaction between PACT Molecules in Response to Stress Signals Is Required for PKR Activation." *Journal of Cellular Biochemistry* 113(8):2754–64.

De Sousa Cavalcante, Lucas and Gisele Monteiro. 2014. "Gemcitabine: Metabolism and Molecular Mechanisms of Action, Sensitivity and Chemoresistance in Pancreatic Cancer." *European Journal of Pharmacology* 741:8–16.

Sun, Chong and René Bernards. 2014. "Feedback and Redundancy in Receptor Tyrosine Kinase Signaling: Relevance to Cancer Therapies." *Trends in Biochemical Sciences* 39(10):465–74.

Takeshima, Ken, Hiroyuki Ariyasu, Tatsuya Ishibashi, Shintaro Kawai, Shinsuke Uraki, Jinsoo Koh, Hidefumi Ito, and Takashi Akamizu. 2018. "Myotonic Dystrophy Type 1 with Diabetes Mellitus, Mixed Hypogonadism and Adrenal Insufficiency." *Endocrinology, Diabetes & Metabolism Case Reports* 2018(January):1–6.

Tangalos, Eric G. and Barbara J. Zarowitz. 2005. "Combination Drug Therapy." *Journal of the American Medical Directors Association* 6(6):406–9.

Tarnopolsky, Mark A., Erin Pearce, Andre Matteliano, Cindy James, and David Armstrong. 2010. "Bacterial Overgrowth Syndrome in Myotonic Muscular Dystrophy Is Potentially Treatable." *Muscle and Nerve* 42(6):853–55.

Tian, B., R. J. White, T. Xia, S. Welle, D. H. Turner, M. B. Mathews, and C. A. Thornton. 2000. "Expanded CUG Repeat RNAs Form Hairpins That Activate the Double-Stranded RNA-Dependent Protein Kinase PKR." *RNA (New York, N.Y.)* 6(1):79–87.

Timchenko, L., W. Nastainczyk, T. Schneider, B. Patel, F. Hofmann, and C. T. Caskey. 1995. "Full-Length Myotonin Protein Kinase (72 KDa) Displays Serine Kinase Activity." *Proceedings of the National Academy of Sciences of the United States of America* 92(12):5366–70.

Tran, Kim, Renee Risingsong, Darlene B. Royce, Charlotte R. Williams, Michael B. Sporn, Patricia A. Pioli, Lalji K. Gediya, Vincent C. Njar, and Karen T. Liby. 2013. "The Combination of the Histone Deacetylase Inhibitor Vorinostat and Synthetic Triterpenoids Reduces

Tumorigenesis in Mouse Models of Cancer." *Carcinogenesis* 34(1):199–210.

Tsilfidis, C., a E. MacKenzie, G. Mettler, J. Barceló, and R. G. Korneluk. 1992. "Correlation between CTG Trinucleotide Repeat Length and Frequency of Severe Congenital Myotonic Dystrophy." *Nature Genetics* 1:192–95.

Verma, Ashok. 2018. "Recent Advances in Antisense Oligonucleotide Therapy in Genetic Neuromuscular Diseases." *Annals of Indian Academy of Neurology* 21(1):3–8.

Voermans, Nicol C., Corrie E. Erasmus, Charlotte W. Ockeloen, Baziel G. Van Engelen, and Catharina A. Eggink. 2015. "Primary Cataract as a Key to Recognition of Myotonic Dystrophy Type 1." *European Journal of Ophthalmology* 25(4):e46–49.

Vujnic, Milorad, Stojan Peric, Srdjan Popovic, Nela Raseta, Vesna Ralic, Valerija Dobricic, Ivana Novakovic, and Vidosava Rakocevic-Stojanovic. 2015. "Metabolic Syndrome in Patients with Myotonic Dystrophy Type 1." *Muscle and Nerve* 52(2):273–77.

Wagner, Florence F., Michel Weyiwer, Michael C. Lewis, and Edward B. Holson. 2013. "Small Molecule Inhibitors of Zinc-Dependent Histone Deacetylases." *Neurotherapeutics* 10(4):589–604.

Wang, Eric T., Amanda J. Ward, Jennifer M. Cherone, Jimena Giudice, Thomas T. Wang, Daniel J. Treacy, Nicole J. Lambert, Peter Freese, Tanvi Saxena, Thomas A. Cooper, and Christopher B. Burge. 2015. "Antagonistic Regulation of MRNA Expression and Splicing by CELF and MBNL Proteins." *Genome Research* 25(6):858–71.

Ward, Amanda J., Mendell Rimer, James M. Killian, James J. Dowling, and Thomas A. Cooper. 2010. "CUGBP1 Overexpression in Mouse Skeletal Muscle Reproduces Features of Myotonic Dystrophy Type 1." *Human Molecular Genetics* 19(18):3614–22.

Wheeler, Thurman M., Andrew J. Leger, Sanjay K. Pandey, a Robert MacLeod, Masayuki Nakamori, Seng H. Cheng, Bruce M. Wentworth, C. Frank Bennett, and Charles a Thornton. 2012. "Targeting Nuclear RNA for in Vivo Correction of Myotonic Dystrophy." *Nature* 488(7409):111–15.

Wheeler, Thurman M., Krzysztof Sobczak, John D. Lueck, Robert J. Osborne, Xiaoyan Lin, Robert T. Dirksen, and Charles A. Thornton. 2009. "Reversal of RNA Dominance by Displacement of Protein Sequestered on Triplet Repeat RNA." *Science* 325(5938):336–39.

Winchester, C. L., R. K. Ferrier, A. Sermoni, B. J. Clark, and K. J. Johnson. 1999. "Characterization of the Expression of DMPK and SIX5 in the Human Eye and Implications for Pathogenesis in Myotonic Dystrophy." *Human Molecular Genetics* 8(3):481–92.

Wojciechowska, Marzena, Katarzyna Taylor, Krzysztof Sobczak, Marek Napierala, and Wlodzimierz J. Krzyzosiak. 2014. "Small Molecule Kinase Inhibitors Alleviate Different Molecular Features of Myotonic Dystrophy Type 1." *RNA Biology* 11(6):1–13.

Wong, Vincent A., Peter S. Beckingsale, Christine A. Oley, and Timothy J. Sullivan. 2002. "Management of Myogenic Ptosis." *American Academy of Opthalmology* 109(5):1023–31.

Wu, Peng, Thomas E. Nielsen, and Mads H. Clausen. 2015. “FDA-Approved Small-Molecule Kinase Inhibitors.” *Trends in Pharmacological Sciences* 36(7):422–39.

Xia, Guangbin and Tetsuo Ashizawa. 2015. “Dynamic Changes of Nuclear RNA Foci in Proliferating DM1 Cells.” *Histochemistry and Cell Biology* 143(6):557–64.

Xia, Guangbin, Katherine E. Santostefano, Marianne Goodwin, Jilin Liu, S. H. Subramony, Maurice S. Swanson, Naohiro Terada, and Tetsuo Ashizawa. 2013. “Generation of Neural Cells from DM1 Induced Pluripotent Stem Cells as Cellular Model for the Study of Central Nervous System Neuropathogenesis.” *Cellular Reprogramming* 15(2):166–77.

Zhang, Fan, Nicole E. Bodycombe, Keith M. Haskell, Yumei L. Sun, Eric T. Wang, Carl A. Morris, Lyn H. Jones, Lauren D. Wood, and Mathew T. Pletcher. 2017. “A Flow Cytometry-Based Screen Identifies MBNL1 Modulators That Rescue Splicing Defects in Myotonic Dystrophy Type I.” *Human Molecular Genetics* 26(16):3056–68.

Zhang, Ji-Hu, Thomas D. Y. Chung, and Kevin R. Oldenburg. 1999. “A Simple Statistical Parameter for Use in Evaluation and Validation of High Throughput Screening Assays.” *Journal of Biomolecular Screening* 4(2):67–73.

Zhang, Nan and Tetsuo Ashizawa. 2017. “RNA Toxicity and Foci Formation in Microsatellite Expansion Diseases.” *Curr Opin Genet Dev* 44:17–29.